IN-26

127113

P- 124

Review of the Physical and Mechanical Properties and Potential Applications of the B2 Compound NiAl
(Unabridged Version of a Paper Published in International Materials Review)

Ronald D. Noebe, Randy R. Bowman,
and Michael V. Nathal
Lewis Research Center
Cleveland, Ohio

(NASA-TM-105598)   REVIEW OF THE   N93-11635
PHYSICAL AND MECHANICAL PROPERTIES
AND POTENTIAL APPLICATIONS OF THE
B2 COMPOUND NiAl: UNABRIDGED   Unclas
VERSION OF A PAPER PUBLISHED IN
INTERNATIONAL MATERIALS REVIEW
(NASA)   124 p   G3/26   0127113
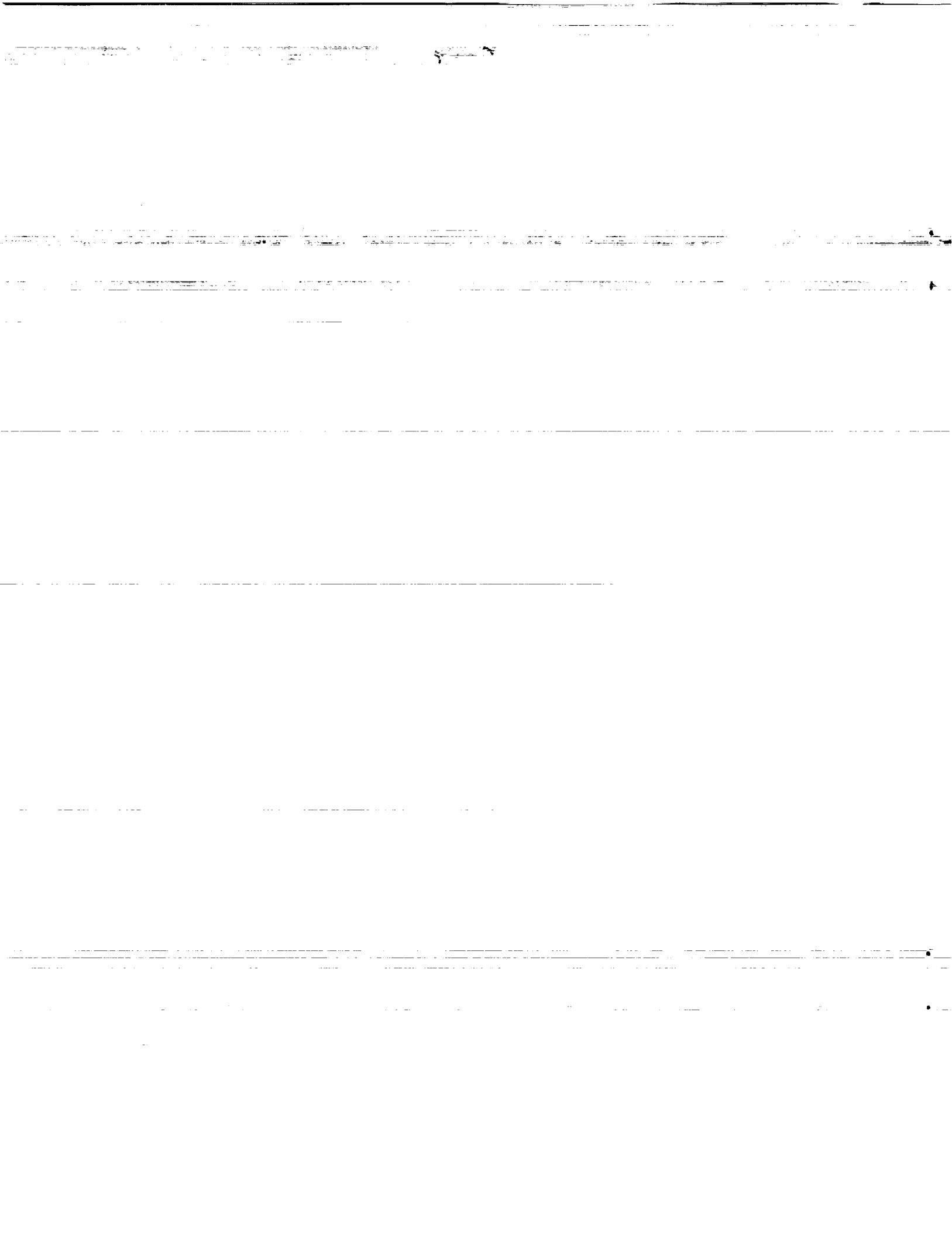
NASA

Review of the Physical and Mechanical Properties and
Potential Applications of the B2 Compound NiAl

1. Introduction

2. Physical Properties and Structure
    2.1 Crystal structure and bonding
    2.2 Thermodynamic properties and phase stability
    2.3 Thermophysical, electrical, magnetic and optical properties
    2.4 Elastic behavior
    2.5 Surface structure and properties

3. Crystal Defects
    3.1 Point defects
    3.2 Line defects
    3.3 Planar defects

4. Operative Slip Systems
    4.1 Slip in "soft" orientation single crystals
        4.1.1 Theoretical predictions
        4.1.2 Observed behavior
    4.2 Slip in "hard" orientation single crystals
        4.2.1 Theoretical predictions
        4.2.2 Observed behavior
    4.3 Bicrystals and polycrystalline material
    4.4 Effect of alloying additions on slip character

5. Yield Strength and Flow Behavior
    5.1 Factors that influence the strength of polycrystalline NiAl
        5.1.1 Temperature
        5.1.2 Grain size
        5.1.3 Stoichiometry
        5.1.4 Alloying additions
        5.1.5 Strain rate
        5.1.6 Cooling rate
        5.1.7 Texture
    5.2 Factors that influence the strength of single crystal NiAl
        5.2.1 Temperature and orientation
        5.2.2 Composition
        5.2.3 Strain rate

REVIEW OF THE PHYSICAL AND MECHANICAL PROPERTIES AND POTENTIAL

APPLICATIONS OF THE B2 COMPOUND NiAl

R.D. Noebe, R.R. Bowman, and M.V. Nathal
National Aeronautics and Space Administration
Lewis Research Center
Cleveland, Ohio 44135

SUMMARY

Considerable work has been performed on NiAl over the last three decades, with an extremely rapid growth in research on this intermetallic occurring in the last few years due to recent interest in this material for electronic and high temperature structural applications. However, many physical properties and the controlling fracture and deformation mechanisms over certain temperature regimes are still in question. Part of this problem lies in the incomplete characterization of many of the alloys previously investigated. Fragmentary data on processing conditions, chemistry, microstructure and the apparent difficulty in accurately measuring composition has made direct comparison between individual studies sometimes tenuous. Therefore, the purpose of this review is to summarize all available mechanical and pertinent physical properties on NiAl, stressing the most recent investigations, in an attempt to understand the behavior of NiAl and its alloys over a broad temperature range.

1. INTRODUCTION

The B2 ordered intermetallic phase NiAl exhibits a wide range of physical and mechanical characteristics which have sparked interest for applications ranging from high-pressure turbine blades to buried interconnects in electronic components. Furthermore, the high degree of structural stability exhibited by NiAl is retained on an atomic scale to its surface resulting in its use in a significant number of surface and catalytic studies. Consequently, NiAl has been the focus of numerous and diverse investigations with an abundance of data compiled on the basic physical and mechanical properties of this intermetallic. In spite of the large amount of data collected on NiAl during the last few decades, much of it generated in the last several years, a critical comprehensive review of this information has not been assembled. While a clear interpretation of the mechanisms responsible for many areas of behavior can be reached by analyzing the available data, divergent viewpoints still exist for a number of important issues. Therefore, the goal of this review is to critically assess the NiAl literature; presenting the acknowledged behavior of NiAl or describing obvious trends based on compilations of various studies, and finally recognizing areas where significant controversy remains or insufficient information still exists.

Since stoichiometry exerts such a profound influence on most physical and mechanical properties, the composition of each alloy is reported, where such information is known. All compositions are given in atomic percent and the term "NiAl" will be used to generically refer to any compound in the B2-NiAl phase field. However, it is important to note that even in the original references, compositions are often given as nominal or analysis techniques of unspecified precision were used, with no limits of error reported. In fact, the conclusions of some studies have been drawn into question due to the possibility of systematic errors in the bulk chemical analyses. Therefore, even reported compositions should be considered with some caution.

2. PHYSICAL PROPERTIES AND STRUCTURE

2.1 Crystal Structure and Bonding

NiAl is a Hume-Rothery β-phase electron compound with a valence electron to atom ratio of 3/2, which gives rise to the stability of a large family of intermetallics that crystallize in the primitive cubic CsCl structure (refs. 1 and 2). This crystal structure can be described by two interpenetrating primitive cubic cells where Al atoms occupy one sublattice and Ni atoms occupy the second sublattice (fig. 1). Thus, the symmetry of the structure is lowered from a body centered cubic, A2, in which the sites are equivalent, to simple cubic, B2. Stoichiometric Ni-50Al melts congruently at 1911 K (ref. 3), (though recent experiments indicate that the melting point could be 40° higher than this value (ref. 4)) and exists as a single phase, B2-ordered intermetallic over the composition range of 45 to almost 60 at % Ni (fig. 2).

The lattice constant for NiAl is a strong function of stoichiometry within the wide single phase region and has been determined by a number of investigators at room temperature (refs. 5 to 12) and at elevated temperatures (refs. 10 and 13). From these studies, a maximum in the lattice constant has been noted at the stoichiometric composition (refs. 5, 9, 11, and 12) as well as at slightly Al-rich levels (refs. 6 to 8 and 10).

The lattice parameter maximum at slightly Al-rich compositions in the older studies (refs. 6 to 8) is probably a consequence of inadequate chemistry control (ref. 9) and/or the inability to accurately measure composition when composition was determined at all. For example, Hughes et al. (ref. 10) also reported a peak in the lattice parameter at slightly Al-rich compositions but did not independently confirm the composition of their alloys. Instead they determined composition by fitting their lattice parameter measurements to the data of Guseva (ref. 7) and Cooper (ref. 8) which automatically biased the peak to Al-rich levels. It has also been suggested (ref. 14) that a loss of Al may have occurred in some of the x-ray powder samples due to the formation of $NiAl_2O_4$ surface films depleting the bulk of Al. Analysis of references 5 to 12 does indicate that the maximum in lattice parameter was found off stoichiometry, when longer and/or higher temperature anneals were utilized. Extreme care to ensure accurate chemical analysis of the alloys was only noted by Taylor and Doyle (ref. 5) who observed the peak in lattice parameter at the stoichiometric composition.

The data from the various lattice parameter studies are summarized in figure 3. The room temperature lattice constant of stoichiometric Ni-50Al determined from the best fit of the data in figure 3 is 0.2887 nm in agreement with the value reported by Taylor and Doyle for Ni-50Al (ref. 5). Assuming the peak does occur at Ni-50Al, the lattice parameter for NiAl on either side of stoichiometry can be described by a linear relationship of the form:

$$a_o(nm) = 0.299839 - 0.000222(at \% Ni) \quad \text{for 50 to 60 at \% Ni}$$

$$a_o(nm) = 0.266819 + 0.000438(at \% Ni) \quad \text{for 45 to 50 at \% Ni}$$

The variation of density with composition in the single phase region has also been determined (refs. 5, 6, 9, and 15). The density of NiAl decreases in a linear fashion with increasing Al content though a change in slope of the density versus composition dependence occurs at the stoichiometric composition which has a density of approximately 5.90 g/cm^3 (refs. 5, 6, and 9). On either side of stoichiometry the density data in figure 3 can be described by linear relationships where:

$$\rho(g/cm^3) = 3.15 + 0.055(at \% Ni) \quad \text{for 50 to 60 at \% Ni}$$

$$\rho(g/cm^3) = 0.118(at\ \%\ Ni) \quad \text{for 45 to 50 at } \%\ Ni$$

Both the lattice parameter data and the density measurements have been used to infer the type of defect structure which occurs in the NiAl lattice. Since Ni is a smaller atom than Al, increasing the Ni content above 50 atomic percent should cause the lattice parameter to decrease and the density to increase in the manner shown in figure 3. However, the behavior with increasing Al content does not follow this trend; rather the lattice spacing of NiAl falls and the decrease in density is more rapid than would be expected by the replacement of Ni atoms by aluminum. This behavior has been explained in terms of the creation of vacancies on Ni sites.

Despite the questionable accuracy of x-ray measurements for performing charge density studies (ref. 16), Cooper (ref. 17) was the first to generate a charge density distribution for NiAl based on powder x-ray diffraction results. He concluded that there was no ionic contribution to bonding, that d-band filling through Al-to-Ni charge transfer is the dominant feature of bonding in NiAl, and that the significant build-up of directional d-bonding charge along the nearest-neighbor Ni-Al direction is responsible for the high Ni-Al bond strength. Fox and Tabbernor (refs. 16, 18, and 19) have confirmed these findings from structure factor information deduced from electron diffraction data. All these studies (refs. 16 to 19) suggest that bonding in NiAl is a mixture of metallic and covalent types. Finally, because Al in NiAl acts as an electropositive element, there is also a strong repulsion between Al atoms as they are brought into nearest neighbor positions (refs. 19 and 20). Thus, order in NiAl can be explained in terms of charge donation and electrostatic effects (refs. 20 and 21).

An alternative mechanism for bonding in NiAl has been developed by Lui et al. (ref. 22). They measured the valence band structure of NiAl using angle-resolved photoemission with synchrotron radiation. Their experimental results agreed remarkably well with calculations based on a local density approximation. However, the findings differ from previous studies (refs. 16 to 19) since they predict that a large charge transfer occurs among the sp electrons in the opposite direction, i.e., from Ni to Al, leading to a net charge transfer from nickel to aluminum.

2.2 Thermodynamic Properties and Phase Stability

Properties of molten Ni-Al alloys can be found primarily in the Russian literature (refs. 23 and 24). The density for near equiatomic NiAl just above the melting point is approximately 4.75 g/cm^3 and the surface energy is 1486 mJ/m^2 (ref. 23). The temperature and concentration dependence of the kinematic viscosity and interatomic interaction energy for species in the melt have also been determined (ref. 24). For a given temperature, a sharp maximum in viscosity and a minimum in the interaction energy between similar atoms was observed for stoichiometric NiAl indicating that bonds between unlike atoms are the strongest. The strong attraction between dissimilar atoms also manifests itself as a large volume contraction (~17.9 percent) which occurs when pure liquid components are mixed (ref. 23). From these results it has been concluded that short range order corresponding to the structure of solid B2-NiAl is preserved in the melt (refs. 23 and 24).

Another indication of the relative thermodynamic stability of NiAl is its very large negative heat of formation. The heat of formation for near stoichiometric NiAl has been measured in the range of -59 to -72 kJ/mol and is a sharp maximum at the equiatomic composition (fig. 4) (refs. 25 to 29). Even within the lower end of this range, NiAl has one of the highest heats of formation for a B2 compound (refs. 30 and 31). It has been proposed (ref. 25) that the nearly 20 percent difference in reported values for ΔHf is a result of experimental techniques and the manner in which corrections were made for impurity effects.

A comparison of figures 2 and 4 indicates that stoichiometric NiAl is the most stable compound in the Ni-Al phase field with a corresponding maximum in melting point and heat of formation.

The high stability of NiAl is also reflected in the composition dependence of the activity of Ni and Al in NiAl. The activity of Al in NiAl has been experimentally determined at 1200 and 1400 K by Steiner and Komarek (ref. 32). They found that there was a large change in the activity of Al in the NiAl single phase field, from approximately 10^{-3} to 0.1, with a sharp increase in activity over the composition range of 48 to 50 at % Al. Such a drastic change in activities over a narrow concentration range is indicative of strong ordering in a system. Libowitz (ref. 33) and Neumann et al. (ref. 34) have analyzed the relationship between point defects and thermodynamic properties for NiAl and have suggested that a systematic error exists in the compositions of Steiner and Komarek's alloys. This same error is also inherent in the work of Hanneman and Seybolt (ref. 35) who performed Gibbs-Duhem integration of Steiner and Komarek's data to obtain activities of Ni in NiAl. Subsequently, Misra (ref. 36) has recalculated the activity of Ni in NiAl by Gibbs-Duhem integration and extrapolated these activities to 1573 K, assuming that the most rapid rise in Al activity occurs at 50 at % Al.

A qualitative assessment of the degree of order in NiAl at high temperatures has been made in an investigation of the x-ray intensity of {100} superlattice peaks in single crystals of NiAl (ref. 10). It was found that significant order existed in NiAl up to the melting temperature, which is consistent with the strong Ni-Al nearest neighbor bond in NiAl. However, Troshkina and Khomyakov (ref. 37) and Troshkina and Kucherenko (ref. 38) have suggested that an order-disorder transformation occurs in NiAl above approximately 800 K, but it is likely that the exothermic effect observed during their calorimetry experiments (refs. 37 and 38) resulted from the removal of supersaturated vacancies which were quenched in from the homogenization heat treatment and not due to an order-disorder reaction.

A quantitative measure of the degree of ordering in a compound can be obtained by calculating the degree of intrinsic disorder, α, which is the ratio of the number of disordered atoms of one kind to the total number of lattice sites in a stoichiometric crystal (ref. 39). A number of attempts have been made at calculating α for NiAl at 1273 K based on the activity data of Steiner and Komarek. The values obtained (refs. 32 and 40) when using the Wagner-Schottky theory and assuming anti-site defects are present on both sides of stoichiometry are probably too small, on the order of 4×10^{-4} to 9×10^{-5}. Starting with more realistic assumptions, e.g., correcting Steiner and Komarek's data for composition and using models based on the presence of triple defects, Libowitz (ref. 33) and Neumann et al. (ref. 34) calculated values for α in the range of 1.7×10^{-3} to 2×10^{-3}. Neumann et al. (ref. 34) also calculated an α of 2×10^{-3} using the enthalpy data of Henig and Lukas (ref. 28), which is in excellent agreement with the values determined from activity data. Finally, based on vacancy concentration measurements by Jacobi and Engell (ref. 12), Neumann et al. (ref. 34) also calculated an α of 4×10^{-3}. In terms of order, this means that only two to four Al atoms are out of position in a group of 500 unit cells in NiAl at 1273 K.

In practice, the high degree of stability exhibited by NiAl combined with the wide compositional range over which the B2 structure exits, means that NiAl is very difficult to disorder. Even under the most severe quenching conditions, quenching from the vapor phase with an effective quench rate of 10^8 K/sec, ordering in NiAl cannot be suppressed (refs. 41 and 42). NiAl is also very stable against radiation damage and bulk samples will not disorder even during heavy ion bombardment at temperatures as low as 15 K (refs. 43 to 46) or when thin films are irradiated by electrons between 10 and 810 K at doses as high as 3 dpa (refs. 47 to 50). This high degree of stability could possibly make NiAl a candidate for some nuclear applications.

Additional sources of thermodynamic data for NiAl include the compilation by Hultgren et al. (ref. 26), which contains data for heat of formation, free energy of formation, heat capacity and various

4

partial molar quantities. Furthermore, thermodynamic modeling of the Ni-Al system including the B2 phase regime has been undertaken by several investigators using various approaches (refs. 51 to 53). These references, while relying heavily on the data compiled by Hultgren et al. (ref. 26), contain semi-empirical analyses of various thermodynamic quantities of Ni-Al alloys as a function of temperature and composition and exist in a form which might be useful in many modeling applications. Additional properties which are very difficult to measure, including surface free energy and APB energy have been modeled on a "first principles" approach (refs. 54 and 55).

2.3 Thermophysical, Electrical, Magnetic, and Optical Properties

The heat capacity of NiAl has been determined at both very low temperatures (2.2 to 10 K) (ref. 56), and intermediate temperatures (300 to 1000 K) (refs. 37, 38, 57, and 58). From the low temperature data, the electronic specific heat coefficient, γ_{el}, has been determined (refs. 56 and 59) to fall between 1.26 and 2.64 mJ/mol K^2 with theoretical calculations of the electronic contribution to the specific heat (ref. 60) in agreement with the experimental values. The majority of the investigators who have measured the heat capacity of NiAl at intermediate temperatures have done so in an attempt to study point defects and order-disorder phenomenon (refs. 37, 38, and 57). During these studies, the heat capacity of Ni-50Al and a few nonstoichiometric compositions was determined as a function of temperature after various heat treatments and quenching conditions.

Taylor et al. (ref. 58) have determined the thermal diffusivity and thermal conductivity of polycrystalline β-Ni-45Al and Ni-45Al-1Mo alloys between room temperature and 1625 K. The thermal conductivity of polycrystalline (ref. 61) and single crystal Ni-50Al (ref. 62) also has been reported as a function of temperature. An important point to emphasize is that the thermal conductivity of NiAl and its alloys is four to eight times greater than that of Ni-base superalloys (fig. 5), which is one of the many property advantages driving the development of NiAl turbine blades (ref. 62).

The thermal expansion behavior for polycrystalline NiAl has been determined by a number of investigators and was found to be a strong function of temperature but not composition (refs. 61 and 63 to 65). The linear thermal expansion coefficient, α, can be adequately described as a function of temperature by fitting the thermal expansion data of Clark and Whittenberger (ref. 63). Therefore, between 300 and approximately 1300 K:

$$\alpha_{NiAl}(K^{-1}) = 1.16026 \times 10^{-5} + 4.08531 \times 10^{-9}(T) - 1.58368 \times 10^{-12}(T^2) + 4.18374 \times^{-16}(T^3)$$

The thermal expansion coefficient for NiAl is about 30 percent less than that for pure Ni (ref. 65) but is very similar to Ni-base superalloys (ref. 61). The thermal expansion coefficient of NiAl is a critical issue in the design of composite materials (refs. 66 and 67) where the α mismatch between the matrix and reinforcing material must be small. Unfortunately, most commonly available reinforcements for composite applications have an α approximately 2/3 to 1/4 that of NiAl (ref. 66).

The low-temperature electrical resistivity for NiAl has been determined by numerous investigators as a function of stoichiometry between 4.2 and 298 K (refs. 68 to 72). Independent of temperature, a sharp minimum in resistivity was observed at the stoichiometric composition for the majority of the studies (refs. 68 to 70), and at a slightly Al-rich composition (~Ni-50.4Al) in two other studies (refs. 71 and 72). This minimum was explained in terms of electron scattering from constitutional point defects, with the lowest defect concentration occurring at the same composition that the minimum in resistivity occurred. Jacobi et al. (ref. 68) also determined the shape of the Fermi surface at 298 K. It was determined that the Fermi energy rose rapidly between 46 and 50 at % Al, overlapping into higher Brillouin zones in the

<110> directions when the Al-concentration approached 50 at %. More recently, the valence band structure of NiAl was measured by use of angle-resolved photoemission using synchrotron radiation with the experimental results in agreement with calculations made using the local density approximation (ref. 22).

Unlike CoAl and FeAl which are strongly paramagnetic, NiAl is essentially nonmagnetic or Pauli paramagnetic, with an extremely low magnetic susceptibility, on the order of 2×10^{-5} to 6×10^{-5} emu/g (refs. 56, 71, 73, and 74). The most detailed study of magnetic susceptibility in NiAl was performed by Brodsky and Brittain (ref. 75) from 6 to 300 K on compounds ranging from 46.1 to 59.2 at % Ni. Using high-sensitivity apparatus they were able to observe that magnetic susceptibility was a slight function of temperature and composition. However, these dependencies were so small that they could not be resolved in previous studies (refs. 73 and 74). The electronic structure of vacancies (ref. 60) and antistructure defects (ref. 76) in NiAl have been calculated using ab-initio self-consistent techniques and the results used to explain the magnetic behavior of NiAl.

As with the majority of studies involved in measuring electrical and magnetic properties, the primary purpose for measuring the optical properties of NiAl has been to study the band structure of this intermetallic and to map Fermi surface and Brillouin-zone boundaries (refs. 77 to 79). In addition to information on bonding, the optical constants of NiAl have been measured as a function of composition between 45.2 and 61.6 at % Ni by Rechtien et al. (ref. 77) and as a function of alloying addition by Jacobi and Stahl (ref. 78). Rechtien et al. (ref. 77), also noted that the visible color of NiAl was very dependent on composition, appearing bright blue for near stoichiometric compositions to yellow or bronze for Ni-rich compositions and grey for Al-rich alloys. It has been suggested that these dramatic color changes with composition arise from the interband transitions associated with the Fermi surface (ref. 70).

2.4 Elastic Behavior

Good agreement exists between the various studies of the elastic properties of single crystal (refs. 80 to 83) and polycrystalline NiAl (refs. 15 and 84 to 86). The single crystal elastic constants have been determined as a function of temperature (refs. 80 and 81), cooling rate (thermal vacancy concentration) (ref. 82), and stoichiometry (ref. 81) and have been conveniently summarized by Rusovic and Warlimont (ref. 81). NiAl is elastically anisotropic, and at room temperature has an anisotropy factor, $A = 2C_{44}/(C_{11} - C_{12})$, of 3.74 for stoichiometric Ni-50Al (ref. 81). This value is comparable to FCC metals such as Cu (3.21) (ref. 87) and Ag (3.01) (ref. 87) and is significantly less than strongly anisotropic B2 compounds such as CuZn (8.63) (ref. 88) or AuCd (12.57) (ref. 89). The anisotropy factor for Ni-50Al is moderately dependent on temperature and decreases to a value of 2.94 at 873 K (ref. 81). However, the elastic anisotropy of NiAl is strongly dependent on composition, e.g., A = 1.85 for Ni-55Al and A = 5.67 for Ni-45Al at room temperature (ref. 81).

The elastic properties of polycrystalline NiAl have been determined for cast and homogenized alloys (ref. 84), and extruded (refs. 15, 86, and 90) and hot pressed (refs. 85 and 86) prealloyed powder materials. From these studies it is evident that Young's modulus, E, is very sensitive to processing technique and temperature but not composition. The room temperature elastic modulus determined by Rusovic and Warlimont (ref. 84) for cast and homogenized Ni-50Al was approximately 193 GPa and varied only slightly with composition for alloys containing 45 to 50 at % Ni. Young's modulus was more sensitive to temperature and was found to decrease almost linearly with increasing temperature according to the following relationship for stoichiometric material (ref. 84):

$$E(GPa) = 204.9 - 0.041(T)$$

where T is in Kelvin. Similarly, work performed by Harmouche and Wolfenden (ref. 15) on powder-extruded alloys determined that composition (between 47 and 56 at % Ni) had a minimal effect on modulus while temperature was the dominant factor affecting the elastic response of the material. However, they measured a room temperature modulus for Ni-50Al of 237 GPa and a temperature dependence described by the following nonlinear function:

$$E(GPa) = 259.3 - 0.072(T) + 3 \times 10^{-5}(T^2)$$

More recent work on a powder Ni-50.6 Al alloy has demonstrated that processing technique also plays a critical role in the resulting modulus of the material (refs. 85 and 86). When the powder is extruded the modulus can be described by the following equation:

$$E(GPa) = 249.3 - 0.031(T) + 1 \times 10^{-5}(T^2)$$

which is in agreement with Harmouche and Wolfenden's results (ref. 15). When the powder is hot pressed to full consolidation the modulus follows the relationship:

$$E(GPa) = 199.8 - 0.040(T)$$

which is similar to Rusovic and Warlimont's results (ref. 84). This difference in moduli depending on processing technique can be rationalized in terms crystallographic texture. The extruded stock most likely exhibits a <111> texture (ref. 91), while the other forms of material were not oriented.

Hellman et al. (ref. 85) have also determined the temperature dependence of the shear modulus, G, and Poisson's ratio, ν, for hot-pressed Ni-50.6 Al powder. The shear modulus depended on temperature as:

$$G(GPa) = 76.6 - 0.017(T)$$

Poisson's ratio was found to be almost independent of temperature and followed the relationship:

$$\nu = 0.307 + 2.15 \times 10^{-5}(T)$$

For very Ni-rich compositions, an anomalous temperature dependence of the elastic properties for both single crystal (refs. 81 and 83) and polycrystalline (ref. 84) material has been observed. In single crystal material of >55 at % Ni, the shear constant ($C_{11} - C_{12}$) becomes small at low temperatures while C_{11} is essentially independent of temperature (refs. 81 and 83). This results in a lattice instability such that shear of the lattice becomes very easy on {110} planes stacked along <110> directions. Similarly, an anomalous dependence of Young's modulus on temperature (i.e., $dE/dT > 0$) has been reported for polycrystalline Ni-rich NiAl (>60 at % Ni) (ref. 84). These elastic anomalies for Ni-rich NiAl are associated with a fully reversible martensitic transformation (refs. 81 to 83) in which the B2 structure transforms to an ordered tetragonal $L1_0$ lattice (refs. 92 to 94). Therefore, while NiAl is an extremely stable compound in thermodynamic terms, lattice instabilities manifested by changes in elastic behavior can lead to a diffusionless martensitic transformation in Ni-rich alloys.

2.5 Surface Structure and Properties

In recent years there has been a growing interest in the catalytic properties of metal and alloy surfaces and the properties of adsorbed gases on surfaces (ref. 95). In this regard, NiAl is unique because its

surface structure and composition varies as a function of orientation and because NiAl is presently one of the few alloy systems which is known to have a stable, well defined surface on an atomic level (ref. 96). Consequently, NiAl has been used as a substrate material in a number of catalytic investigations including the study of sulfur (ref. 96), carbon monoxide (refs. 96 and 97), oxygen (refs. 96 and 98) and xenon (refs. 95 and 99) adsorption.

The NiAl {100} surfaces have a simple structure and are ideally composed of either all Ni or Al atoms depending on where the lattice is truncated. However, the top atomic layer on a (100) surface is always predominantly composed of Al atoms with approximately 22 percent Ni also present on the surface while the second atomic layer is composed almost entirely of Ni (ref. 100).

NiAl {110} surfaces have been probed and analyzed by a number of sophisticated techniques (refs. 97, 99, and 101 to 105) and it has been determined that as in the ideal case, the {110} surfaces are composed of equal proportions of Ni and Al atoms which are ordered and aligned in alternating parallel rows. In addition, the top atomic layer is rippled with the rows of Al atoms protruding above the Ni rows by approximately 0.022 nm. This rippling effect then alternates in a decreasing sinusoidal fashion so that in the second atomic layer the rows of Ni atoms are higher than the Al atoms and vice versa until after about eight atomic layers, rows of Ni and Al atoms are no longer offset with respect to each other. This atomically rough surface and rippling effect has been modeled by Chen (ref. 106).

In the bulk, perfectly ordered NiAl consists of {111} planes composed only of Al alternating with planes composed only of Ni in an -A-B-A-B- stacking sequence (fig. 1). Consequently, the truncated bulk structure of a (111) surface should result in either a Ni or Al surface layer with atoms laterally arranged in an hexagonal structure. Consequently, NiAl {111} surfaces have been studied by a number of different investigators (refs. 107 to 110). From the majority of these studies (refs. 107, 108, and 110) it was concluded that NiAl {111} surfaces were actually stepped and terminated by an almost equal proportion of Al and Ni rich domains or terraces separated by single atomic layers. However, Niehus et al. (ref. 109) have concluded that NiAl {111} surfaces are Ni terminated followed by a second layer of Al atoms. They also proposed that the observations by previous investigators (refs. 107, 108, and 110) may have been skewed by oxygen contamination resulting in a stepped surface containing Al-rich domains on the Ni layer.

3. CRYSTAL DEFECTS

3.1 Point Defects

Compounds having a B2 structure can be divided into two groups depending on the type of lattice defects which are observed as a function of stoichiometry (ref. 34). In one group, the lattice defects consist of A atoms on β-sites and B atoms on α-sites. When this type of simple substitution occurs on both sides of stoichiometry the alloy is generally referred to as having an antistructure or substitutional defect structure. The other group of compounds exhibits lattice defects which consist of A atoms on β-sites and vacancies on α-sites. In other words, on one side of stoichiometry antistructure defects occur while on the other side of stoichiometry, vacancies occur. Materials with this second type of defect structure are considered to have a triple-defect structure because at the stoichiometric composition, three defects must exist simultaneously, two vacancies on α-sites and one A atom on a β-site (ref. 111).

NiAl falls into this second group of intermetallic compounds (refs. 5, 6, 8, and 111). The Al sublattice is always fully occupied, therefore, when an excess of Ni occurs, Ni substitutes on Al sites, Ni_{Al},

with no significant composition dependent vacancy concentration occurring on either sublattice (ref. 9). With excess Al, vacant sites or constitutional vacancies are formed in the Ni sublattice, V_{Ni}.

The one nagging question that persists is whether Al atoms can actually substitute to a limited extent on the Ni sublattice for Al-rich compositions. From analysis of the lattice parameter studies discussed in section 2.1, the majority of the resistivity investigations discussed in section 2.3, and the heat of formation data summarized in figure 4, a strong case can be made for no Al antistructure defects in NiAl. This viewpoint is also supported by the work of Wasilewski (ref. 111) on NiAl and Wasilewski et al. (ref. 112) on NiGa (which has the same type of triple-defect structure as NiAl). In both systems, they determined that antistructure defects on the Ni-sublattice are energetically unfavorable to the point of being extremely unlikely.

To the contrary, Georgopoulos and Cohen (ref. 9) have determined that up to 1 percent Al can substitute on Ni sites before Ni vacancies are formed. This conclusion was based on studies of integrated intensities from single crystals. This is about the only unrefuted evidence in support of Al antistructure defects. However, their x-ray analyses could have been biased by the planar defects which are observed to occur in Al-rich alloys. From the bulk of the data which exists today it would have to be concluded that no Al antistructure defects exist in NiAl. However, additional work in conclusively identifying the defect structure which exists for near stoichiometric Al-rich alloys is warranted.

In general, the constitutional defect structure in NiAl is consistent with the 3:2 valence electron to atom ratio which is essentially responsible for the ordered structure of the compound. Aluminum contributes three valence electrons to the conduction band while Ni contributes no electrons (ref. 113). Consequently, vacancies occur in Al-rich compositions because the high stability of the three valence electrons per unit cell is preserved by maintaining just one aluminum atom per unit cell. As a result, NiAl prefers to omit atoms from its structure rather than increase the number of electrons per unit cell above three.

Constitutional defects have been observed to display a type of ordered structure within the NiAl lattice such that there is a strong tendency to avoid the same species at the first neighbor distance of their sublattice (refs. 114 to 119). This defect ordering probably occurs to minimize the strain energy associated with the introduction of the defects, and has been suggested to form the precursor structure for phases adjacent to the NiAl phase (refs. 19 and 119). A manifestation of this ordering has been observed in Al-rich alloys in the form of diffuse scattering during diffraction (refs. 116, 120, and 121) that is similar to what is commonly observed in Ti and Zr alloys from the nucleation of metastable ω-phase nuclei (refs. 122 and 123). This diffuse scattering is more pronounced in Al-rich compositions and at low temperatures (ref. 121) and is probably due to localized atomic displacements in the vicinity of the constitutional vacancies (ref. 123) leading to local instability in the NiAl structure.

In addition to constitutional vacancies, a high concentration of thermal vacancies can be quenched into NiAl. For example, up to 2 percent thermal vacancies can be introduced in NiAl near its melting point (ref. 124) and the stoichiometric compound can retain from 0.5 to 1 percent thermal vacancies after quenching from moderate temperatures (refs. 57, 125, and 126). The presence of supersaturated thermal vacancies is reported to increase the hardness (ref. 127) and yield strength (ref. 128), without significantly affecting the elastic modulus of NiAl alloys (ref. 82).

Unlike constitutional vacancies which become incorporated in an ordered fashion within the NiAl lattice, thermal vacancies tend to agglomerate and form faceted voids when samples are rapidly quenched from the melt (ref. 129) or after further annealing of samples rapidly quenched from high temperatures (refs. 124, 126, and 130 to 132). The morphology of these voids is rhombic dodecahedra, consisting pri-

marily of {110} facets with occasional facets along {100} planes (refs. 126 and 130). An example of these faceted voids in a sample of as-melt spun NiAl ribbon is shown in figure 6.

Fan and Collins (ref. 133) have demonstrated that the thermal point defects retained in NiAl, before they are annihilated or form voids, can exist as both monovacancies or divacancy complexes which anneal out at approximately 773 K. Temperature dependence of the heat capacity (refs. 37, 38, and 57) of NiAl also exhibits an exothermic change beginning at temperatures near 800 K where this vacancy annihilation occurs. Subsequent annealing of quenched NiAl samples at these or higher temperatures will eventually cause the voids to shrink and disappear leaving behind vacancy dislocation loops and spiral dislocations which form as a consequence of the vacancy annihilation process (refs. 124, 132, 134, and 135).

While thermal vacancies form individually in disordered materials, in NiAl it has been suggested that either a vacancy must form on each sublattice in a balanced manner, or that two vacancies form on one sublattice with an associated antistructure defect on the second sublattice (ref. 111). While constitutional vacancies are accounted for by this latter defect structure, thermal vacancies probably occur by the former mechanism though the results of Fan and Collins (ref. 133) indicate that both defect structures may be possible for thermal vacancies. Assuming that the balanced divacancy mechanism is the dominant mode of thermal vacancy generation, Wasilewski (ref. 64) determined that the energy required to form a divacancy was 155 kJ/mol. This value agrees reasonably well with the 134 kJ/mol inferred from diffusion experiments (ref. 136), 140±19 kJ/mol reported by Parthasarathi and Fraser (ref. 124) and 148 kJ/mol determined by Kucherenko et al. (ref. 57) from heat capacity measurements.

The migration energy, E_m, for vacancies in NiAl has also been determined by several techniques. Based on diffusion measurements (ref. 136), E_m was estimated to be 180 kJ/mol and is assumed to be independent of stoichiometry. This agrees favorably with a value of 164 kJ/mol determined from positron annihilation experiments (ref. 137) but is slightly greater than the value of 138 kJ/mol estimated by Wasilewski (ref. 64). All three of these values are significantly less than a value of 369 kJ/mol determined for the migration energy of a vacancy at 1273 K by true heat capacity measurements (ref. 57). Presently, the discrepancy between these various values has not been resolved. In general, the relatively low formation energy and the slightly to significantly higher migration energy for vacancies in NiAl would explain the high densities of vacancies which can be quenched into this intermetallic.

3.2 Line Defects

A number of line defects are possible in NiAl, however, slip vectors which result in "wrong" nearest neighbor atoms are not favored due to the large ordering energy of NiAl. The three basic translation vectors which do not disrupt the order of the lattice are a_o<100>, a_o<110>, and a_o<111>, where a_o is the lattice constant of NiAl (fig. 1). Each of these slip vectors has been observed in NiAl though non-<001> slip vectors generally occur under very specific circumstances.

The line energy for dislocations in stoichiometric NiAl at room temperature has been calculated using fully anisotropic elasticity analysis (refs. 138 to 140), and the results are summarized by the plot of Lloyd and Loretto (ref. 140), which is reproduced in figure 7. Dislocations with <100> Burgers vectors have the lowest energy of the three unit vectors shown in figure 1, and the edge orientation for $\bar{b}$ = <100> has a slightly lower energy than the screw orientation. <100> dislocations within ±25° of the screw orientation are elastically unstable on {100} planes, and might also be expected to be elastically unstable on {110} planes based on the similarity of the line energy versus θ plot from $\theta = 0°$ to 45° (ref. 141). The energy of <110> dislocations on (110) planes (Fig. 7(a)) is sufficiently low so that dissociation into two <100> dislocations is not expected. However, dislocations near the <110>{100} edge orientation

10

(Fig. 7(b)) are expected to dissociate into two <100>{100} dislocations of appropriate line directions. Dislocations with <111> Burgers vectors of near-edge orientation are elastically unstable in their {110} slip plane (refs. 20 and 141) but no instability for a dislocation loop with <111> Burgers vector is expected on {112} planes (ref. 142). Therefore, <111> edge dislocations on {110} planes are unstable with respect to dissociation into <100> + <110> dislocations or into three <100> type dislocations at room temperature. Conversely, near edge <111> type dislocations on {112} planes are observed in NiAl after room temperature deformation, as expected (ref. 142). At elevated temperatures (greater than ~700 K) all <111> dislocations in NiAl tend to dissociate into <100> + <110> and eventually into three <100> type dislocations (refs. 143 to 145). These latter observations indicate that dislocation core energy may also be an important factor when determining the stability of dislocations (refs. 143 and 144).

Several types of sessile dislocation loops are commonly observed in the substructure of NiAl (refs. 132 and 146 to 150). These dislocation loops are edge in character, and lie in {001} planes with <100> Burgers vectors. There are two distinct forms of these loops as demonstrated in figure 8. The most common is a square loop, with rounded corners, with segments parallel to <100> (refs. 146 to 150). The other type of square loop consists of segments aligned strictly along <110> with extremely sharp corners (refs. 149 and 150). The former type of loop corresponds to the equilibrium shape calculated on the basis of elastic anisotropy (refs. 146 and 150). The sharp rectangular loops, which lie along <110> directions are composed of what should be elastically unstable segments (refs. 146 and 150). It has been proposed (ref. 150) that this type of loop is stabilized by the dissociation of the perfect dislocations into partial dislocations by the following reaction:

$$<001> \rightarrow 1/4<\overline{1}11> + 1/2<001> + 1/4<1\overline{1}1>$$
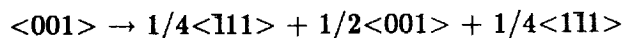
It has also been proposed (ref. 150) that this dissociation promotes <001>{110} slip over <001>{100} slip by significantly reducing the energy barriers associated with dislocation motion. This is consistent with experimental observations (section 4) that indicate <001>{110} slip is preferred over <001>{100} slip. However, the dissociation of <001> dislocations on {110} planes has yet to be confirmed by high resolution electron microscopy (HREM).

To date, no observations on the core structure or dissociation of any dislocations in NiAl by HREM have been published, though work is ongoing in this area. At present, the core structure of various dislocations in NiAl and thus an indication of dislocation mobility are inferred from theoretical calculations. Some of the earlier work in this area has been reviewed in detail by Yamaguchi (ref. 151) and Vitek and Yamaguchi (ref. 152). Core structure calculations of <001> screw dislocations in a "model" CsCl lattice using central force potentials has been conducted by Yamaguchi and Umakoshi (refs. 153 and 154). Their work predicts {110} as the operative slip plane at low temperatures while thermally activated cross-slip of <001> screw dislocations onto orthogonal {110} planes can occur at elevated temperatures. Also, the Peierls stress to move screw dislocations on {110} was determined to be quite low, 0.007 G, where G is the shear modulus. This low stress level was a consequence of the already quite planar core structure of the screw dislocation under stress free conditions. Therefore, no complex core transformations are necessary before <001> screw dislocations can begin to move.

Benhaddane and Beauchamp (ref. 155) have also performed a similar analysis for <100>{001} edge dislocations using two different sets of interatomic potentials. When they used the same potentials as were used by Yamaguchi and Umakoshi (refs. 153 and 154), they calculated an antiphase boundary (APB) energy on (110) of 107 mJ/m^2 and determined that the dislocation core was narrow. They also performed the analysis using potentials which lead to an APB energy on (110) of 700 mJ/m^2 (ref. 155), which is probably closer to the actual value for NiAl (section 3.3). In this case the dislocation core was predicted to be wider but extended in the {010} glide plane.

The core structure of <111> screw dislocations in a "model" CsCl lattice have been calculated for the case of a unit dislocation (ref. 156) and a dissociated dislocation (ref. 157). In either case, the deformation of CsCl-type crystals at low temperatures by <111> slip is governed by the movement of screw dislocations with their complex, nonplanar core structures, similar to the case of simple BCC metals (refs. 151 and 152).

More recent work specifically addressing the potential slip systems in NiAl as been performed by Farkas et al. (ref. 158) using embedded atom potentials. Their calculations indicated that <100>, <110>, and <111> dislocations all possess components of a nonplanar core configuration and that a large stress ($>3\times10^{-2}$ G) would be necessary before any of these dislocations became mobile. It was also determined that the lowest energy configuration for a <111> dislocation was as an undissociated unit dislocation. This prediction is consistent with reported observations of <111> dislocations in NiAl (refs. 141 and 142).

3.3 Planar Defects

Theoretical analyses of the possible planar faults resulting from the movement of partial dislocations in B2 crystals, have been performed with varying degrees of sophistication (refs. 159 and 160). From these studies it is apparent that the only stable faults likely to occur in NiAl are $1/2a_0$<111> APB on {110} and {112} planes. However, deformation-induced planar faults generally have not been observed in NiAl alloys (refs. 141 and 142). The only exception was the observation of a segment of a <111> dislocation of near edge orientation that was reported to be dissociated into two $1/2$<111> dislocations after annealing at 673 K (ref. 161). However, this observation can be rationalized as an artefact due to double diffraction at the core of the <111> superlattice dislocation (ref. 142).

The inability to differentiate splitting in superlattice dislocations strongly suggests that a high fault energy exists in NiAl, though values for APB energies in the literature vary significantly. Original (ref. 139) estimates of APB energy, γ, in NiAl were based on an Ising model and resulted in $\gamma = 223$ mJ/m^2 for $1/2a_0$<111>{110}, but estimates of interaction energies used in the formulation were probably too low for NiAl. This value did agree with the observation by Campany et al. (ref. 161) of a <111> dislocation dissociated 4.5 nm on a {110} plane after annealing at 673 K. This separation width is equivalent to an APB energy of approximately 200 ± 40 mJ/m^2 (ref. 161). The agreement between these results, however, is fortuitous and due to double diffraction effects during the TEM investigation (ref. 142).

The $1/2$<111> APB energy for NiAl was also calculated from molecular dynamics simulations at 240 mJ/m^2 on the (110) plane and 380 mJ/m^2 on the (112) plane, respectively, and were found to be independent of temperature (ref. 55). These values are also too low and imply a stable dissociation into $1/2$<111> edge companion superpartials over about 2.7 nm in a {112} plane. This separation distance would have been detected in the weak beam TEM study by Veyssiere and Noebe (ref. 142) in which a resolution of 1 to 1.5 nm was attained but in which no dissociation of <111> superlattice dislocations was observed. Therefore, estimating the maximum dissociation distance at 1.5 nm would correspond to antiphase boundary energies of at least 500 and 750 mJ/m^2 in the {110} and {112} planes, respectively (ref. 142). This much higher value for the APB energy in NiAl is consistent with all-electron self-consistent total energy LMTO calculations by Hong and Freeman (refs. 54 and 162) and the first principle total energy calculations of Fu and Yoo (ref. 20) which predict that $1/2$<111> APB energies on either {110} or {112} planes are on the order of 800 mJ/m^2.

Planar faults have been observed in Al-rich NiAl alloys (refs. 163 and 164). The exact nature of these faults remains uncertain, but they have been observed to form parallel to {001} NiAl planes (refs. 163 and 164), increase in density as the composition of the alloy becomes more Al-rich (ref. 164) and act as

heterogeneous nucleation sites for Ni_2Al_3 in alloys which are close to the $NiAl/Ni_2Al_3$ phase boundary (ref. 164). These planar faults are suggested to form by the nucleation of excess vacancies and Al atoms on {100} planes (ref. 163). While it has not been experimentally determined that the ω-like defects (discussed in section 3.1) are related to or are possible nuclei for these planar faults and for the eventual nucleation of the Ni_2Al_3 phase, the relationship is intriguing and could be the basis of an interesting HREM study.

4. OPERATIVE SLIP SYSTEMS

Investigation of operative slip systems has been one of the more active areas of research concerning NiAl. Considerable effort has been expended by numerous investigators to experimentally determine the operative slip systems in near-stoichiometric NiAl single crystals (refs. 138, 141 to 145, and 165 to 176) and polycrystalline alloys (refs. 128, 177, and 178) and to justify slip behavior on a theoretical basis (refs. 20, 138, 139, 179, and 180). The general consensus of these studies is that NiAl exhibits two significantly different types of slip behavior, with the dominate slip vector, $\overline{b}$, either <001> for "soft" orientations or a combination of <111>, <110>, and <100>, depending upon temperature, for "hard" orientations (table I). Soft orientations include all non-<001> loading directions where $\overline{b}$ = <100> slip dominates; and test orientations close to <001> are the "hard" orientations because <001> Burgers vectors have a zero or near-zero resolved shear stress.

4.1 Slip In "Soft" Orientation Single Crystals

4.1.1 Theoretical predictions.—Rachinger and Cottrell (ref. 179) were the first to theoretically approach the problem of predicting slip directions in ordered B2 structures and did so on the basis of ordering energy. They deduced a critical bond strength of 0.06 eV/atomic bond (5.79 kJ/mol), above which a_0<001>(110) slip would be preferred for deformation and below which formation of a superdislocation of two a/2<111> imperfect dislocations joined by a ribbon of APB would occur. Since the formation energy for NiAl has been measured between 59 and 72 kJ/mol (refs. 25 and 28) which corresponds to an ordering energy of between 0.076 and 0.093 eV/atomic bond, the slip system predicted according to Rachinger and Cottrell should be <001>{110}.

Lautenschlager et al. (ref. 159) analyzed slip modes in B2 alloys in terms of a hard sphere model. They concluded that the usual BCC slip systems, (e.g., <111> on {123}, {112}, and {110} slip planes), as well as <110>{110}, <100>{110}, and <100>{100} are all highly probable in CsCl-type materials. The preference for a particular slip system was determined to depend on the atom size ratio, the type of bonding, crystal orientation, and the tendency for dislocations to dissociate and form antiphase boundaries. In a material like NiAl, which has metallic bonding strongly reinforced with a covalent component, Lautenschlager et al. (ref. 159) concluded that the atomic radius ratio is the most important criteria for determining operative slip systems. In the case of NiAl, with a radius ratio of 0.847 they concluded that <100>{110} and <100>{100} slip should be the primary systems.

Predictions of slip systems in NiAl have also been made by Ball and Smallman (ref. 138) and Potter (ref. 139) using anisotropic elasticity theory to calculate dislocation line energies and mobilities (glide parameter) for various types of dislocations. Similar calculations were later performed by Mendiratta and Law (ref. 180) for Fe-Al alloys and NiAl except that the mobility parameter was modified to take into account the displacement normal to the slip plane through the radius ratio. Based on all three studies, a_0<100> dislocations have the lowest energy and based on both dislocation energies and glide considerations, the operative slip system predicted would be <100>{011}. Yet, cube slip (<100>{001}) cannot

be ruled out because it is predicted to occur at stresses only slightly higher than for <100>{011} slip (refs. 138 and 139).

Finally, Yoo et al. (ref. 181) and Fu and Yoo (ref. 20) have reviewed the slip processes in B2-type compounds including NiAl, on the basis of energetic and kinetic aspects of dislocation motion. They concluded that <001> slip in NiAl was a consequence of the relatively high APB energy and weak repulsive elastic force between partial dislocations that makes dissociation of <111> superdislocations into partial dislocations unlikely.

In summary, it appears that all techniques used to predict the general slip behavior of NiAl, regardless of complexity and based on criteria as different as ordering energies, constituent radius ratios, dislocation energies and mobilities and first principal calculations all arrive at the same result. NiAl should have a <100> slip vector and {011} slip plane with the possibility for slip also occurring on {001} type planes.

4.1.2 Observed behavior.—Table I contains a compendium of observed slip systems as a function of orientation and temperature for NiAl. From this table it is apparent that experimental investigation of the operative slip systems in soft orientation single crystals confirms the analyses of the previous section. The only observed slip systems responsible for deformation of single crystals of non-<001> orientated NiAl identified by numerous TEM and slip trace studies have been <001>{110} and <001>{100}, independent of deformation temperature (refs. 141, 144, 165 to 167, 169, 172, 173, 175, and 176).

An <001> slip vector was first confirmed by Pascoe and Newey (ref. 167) by surface slip trace analyses on single crystals deformed at room temperature and later substantiated by Loretto and Wasilewski (ref. 141) who performed a TEM study on deformed [112] oriented single crystals. Ball and Smallman (refs. 138 and 182) identified the operation of <001>{110} slip in NiAl by TEM and concluded that NiAl slipped on {110} planes in all soft orientations and at all temperatures investigated (300 to 1273 K). They also observed cross slip or pencil glide on orthogonal {110} planes. Wasilewski et al. (ref. 165) utilized optical microscopy, replica electron microscopy and x-ray diffraction techniques to investigate slip in NiAl. In addition to observing <001>{110} slip, they observed duplex cube slip, <010>{100}, in [110] oriented single crystals. In agreement with anisotropic elasticity theory (refs. 138 and 139), cube slip was observed at higher resolved stresses than for <001>{110} slip. For orientations other than [100] and [110], only single slip of the type <001>{110} was observed by Wasilewski et al. (ref. 165). However, <001> slip on cube planes was also observed by Loretto et al. (refs. 141 and 172) in [112] crystals deformed between 77 and 1053 K. More recent experiments by Kim et al. (refs. 144 and 175) and Field et al. (ref. 173) have also confirmed the operation of a <001> slip vector at low and intermediate temperatures in soft orientation single crystals. TEM analyses of high temperature creep samples have also confirmed the almost exclusive existence of <001> dislocations in as-deformed non-[001] samples (refs. 166, 176, and 183).

4.2 Slip In "Hard" Orientation Single Crystals

4.2.1 Theoretical predictions.—The only attempts to predict operative slip systems during deformation of [001] oriented NiAl crystals were made by Ball and Smallman (ref. 138) and Potter (ref. 139) using anisotropic elasticity theory to calculate dislocation line energies and glide parameters. Based on these criteria, room temperature slip is predicted to occur by dislocations with <110> Burgers vectors, which is the one slip vector that is not observed at low temperatures in deformed [001] NiAl (table I). For this reason, Potter (ref. 139) suggested that ordering energy should also be considered when predicting slip behavior. This is a reasonable suggestion since movement of dislocations with different Burgers vectors leads to a different closest distance of approach for the involved atoms. For example, the movement of dislocations of $\overline{b} = a_0<110>$ involves forcing like atoms to become nearest neighbors at the half-

14

slipped position. This is an energetically unfavorable situation in a material like NiAl that has a high ordering energy and directional bonding.

4.2.1 Observed behavior.—In the special case of [001] oriented NiAl single crystals, the resolved shear stress for <100> slip approaches zero and the stress necessary for deformation is several times greater than that for any other orientations at low and intermediate temperatures (refs. 144, 165, and 174). Consequently, deformation of [001] NiAl single crystals is unique compared to soft orientations and therefore, a significant amount of work has been spent on analyzing and understanding the operative slip systems in "hard" crystals through experimental means.

At liquid nitrogen temperatures (77 K), the observed slip direction is <111> on either {123} planes (ref. 167), {112} planes (refs. 141, 144, and 167) or {110} planes (ref. 141). Between room temperature and approximately 600 K both kinking (refs. 14, 167, 170, 175, 182, 184, and 185) and uniform deformation by <111> slip on {112} and {110} planes has been observed (refs. 141 to 144, 174, and 184). At higher temperatures (>600 K), where tensile ductility can be achieved in [001] crystals, deformation has been reported to be the result of <110> dislocations (refs. 166, 167, and 169) <001> dislocations (refs. 145, 170, 171, and 185) or a combination of glide and climb of both <001> and <011> type dislocations (refs. 143, 144, and 184). Finally, at elevated temperatures, both <100> and <110> dislocations have been observed after creep deformation of [001] single crystals (refs. 166 and 176). The observation of <110> dislocations have included both segments of dislocations that are contained within subgrain boundaries which formed during creep as well as dislocations within the subgrains.

It was first postulated by Bowman et al. (ref. 174), that sample geometry played an important role in determining the deformation behavior of [001] single crystals in compression at low and intermediate temperatures. Thus explaining some of the conflicting observations described above. In studies where kinking was observed at or above room temperature (refs. 167, 170, 182, and 185), the compression specimen length to diameter (l:d) ratio was 2.4 to 3 which is an elastically unstable geometry, whereas those studies where uniform slip occurred (refs. 141, 149, and 174), the l:d ratio was about 2. These sample geometry effects were verified in a recent study by Field et al. (ref. 184).

Figure 9 demonstrates the microstructure which results when a [001] Ni-50Al single crystal with a l:d ratio of 2 is deformed uniformly without kinking at room temperature. The slip systems identified in the micrograph are [111](112) and [111](112). For larger l:d ratios, room and intermediate temperature observation of <001> dislocations in [001] NiAl samples can be attributed to a kinking mechanism similar to that which occurs in HCP metals (ref. 186). For NiAl single crystals stressed close to [001], the resolved shear stress on <001> dislocations is a very small fraction of the applied stress and elastic bending of {110} planes would be necessary before dislocations of $\overline{b} = a_0<001>$ could accommodate any plastic deformation (ref. 171). This bending, and therefore kinking, would be very dependent on specimen orientation, specimen alignment, discontinuities in the sample and would have a higher probability of occurrence in samples with a greater l:d ratio. At higher temperatures where deformation can be accommodated by climb processes, kinking would also be rate dependent as demonstrated by Fraser et al. (refs. 170 and 171).

Uniform deformation of near [001] crystals at low temperatures can occur by <001> slip (without macrokinking) only by increasing the number of dislocation sources present in the crystal (ref. 175). This can be accomplished through the incorporation of an adherent oxide film on the sample surface by pre-oxidation. Then through a "microkinking" mechanism, uniform deformation of the crystal can occur by <001> slip at stresses significantly below those required for macroscopic kinking or <111> slip (ref. 175). Conversely, Field et al. (ref. 187) as well as Miracle et al. (ref. 188) have found that alloying additions of Cr to NiAl promoted the activation of <111> slip over deformation by kinking for a constant l:d ratio.

This was believed to result from differential proportional hardening of the <100> versus <111> slip systems (ref. 187).

When kinking is suppressed in [001] single crystal NiAl, a change in deformation behavior with temperature occurs at intermediate temperatures as amply demonstrated by Kim (refs. 143 and 144) and summarized in figure 10. This change in deformation behavior has been attributed to the instability of <111> dislocations at elevated temperatures and decomposition of these dislocations into a <100> and <110> dislocations (refs. 143 and 144).

The behavior that can be deduced from studies concerned with the deformation of [001] NiAl can be summarized in the following manner. Kinking is an artifact of an unstable testing geometry, which proceeds by movement of <001> dislocations. When kinking is suppressed, deformation occurs by slip of <111> dislocations below about 600 K. Above 600 K, which corresponds to the tensile brittle-to-ductile transition temperature (BDTT) for [001] oriented Ni-50Al, deformation occurs by glide and climb of <001> and <110> dislocations, as <111> dislocations become thermally unstable.

4.3 Bicrystals and Polycrystalline Material

Consistent with previous deformation studies on soft orientation single crystals, a recent study on the brittle-to-ductile transition temperature of polycrystalline NiAl (ref. 128) reports the observation of only <001> dislocations in samples uniaxially deformed between 300 to 900 K. Room temperature deformation of polycrystalline NiAl by <001> slip has also been reported by Lautenschlager et al. (ref. 177), Vedula et al. (ref. 178), and Cotton (ref. 189).

Isolated dislocation segments with Burgers vectors other than <001> have been observed in as-extruded NiAl alloys (refs. 140, 190, and 191). However, the presence of non-<001> dislocations in these studies do not constitute an alternative deformation mechanism but are probably formed as a result of dislocation interactions between gliding a_0<001> dislocations (refs. 145 and 190) and are observed only in dynamically recrystallized materials after extrusion.

Only a few substantial reports of deformation by non-<001> slip in polycrystalline NiAl exist. These include the observation by Lasalmonie (ref. 192) of limited <011> slip in near stoichiometric polycrystalline NiAl deformed between 850 to 900 K to very small strains. Under all other conditions, including lower and higher deformation temperatures and at larger strains at 850 to 900 K, <001> dislocations were exclusively observed. Dollar et al. (refs. 193 and 194) have also reported <110>{110} type dislocations after room temperature deformation of mechanically alloyed and extruded NiAl containing small additions of Ti and Mo, however, the predominant Burgers vector was still <100>.

Dislocations with <011> slip vectors have also been observed in special orientations of bicrystals deformed at room temperature and 933 K (refs. 195 and 196). But, the <011> dislocations were only observed in those halves of the bicrystals which had an [001] orientation while <001> slip was observed in all other bicrystal orientations. The observation of non-<001> slip in [001] oriented halves of bicrystals is not surprising since [001] single crystals tend to deform by non-<001> slip, as discussed in the previous section.

Until more conclusive work is performed, the observation of dislocations with non-<001> slip vectors in deformed polycrystalline material should not be taken as a general behavior for NiAl. The limited observations of <011> slip (refs. 192, 193, 195, and 196) appear to be exceptions that only occur under very specific conditions. Therefore, as in soft orientation single crystals and consistent with all theoreti-

cal results, it can be concluded that deformation of polycrystalline NiAl occurs by the operation of <001> dislocations. It is also recommended that future studies examining the relevance of non-<100> slip in the deformation of NiAl should analyze multiple samples and provide adequate statistical evidence as to the percentage of each type of dislocation present in the material, as in the study by Cotton (ref. 189).

4.4 Effect Of Alloying Additions On Slip Character

One common approach in attempting to improve the ductility and toughness of NiAl has been the addition of ternary macroalloying elements in an effort to enhance or modify slip processes (refs. 197 to 199). The primary criteria for alloying has been the identification of elements which may lower the ordering energy of NiAl thus making <111> slip easier. This idea is summarized in figure 11, which illustrates the relationship between thermodynamic properties and slip behavior of various B2 compounds. This figure qualitatively indicates that Cr, Mn, and V are reasonable choices for promoting <111> slip in NiAl in agreement with calculations based on interatomic potential models (refs. 54 and 162). These models have demonstrated that up to 70 percent reductions in APB energy are possible with alloying additions of at least 17 at %. In reality, such large alloying additions are not possible, as the solubility of Cr and V in NiAl is much lower. For example, the solubility of Cr in NiAl is approximately 1 to 2 at % on either sublattice (ref. 189 and 200); while the solubility of V is on the order of 5 to 12 at % when substituted for Al (refs. 201 and 202) and essentially zero when substituted for Ni (ref. 201).

In spite of the low solubility for Cr in NiAl, but in apparent agreement with the ideas presented above, <111> slip has been reported in polycrystalline NiAl alloyed with approximately 5 percent Cr or Mn (refs. 197 and 198). Although operation of <111> slip satisfies the requirement for generalized polycrystalline plasticity (ref. 203), no tensile ductility was reported in these materials at low temperatures but a change in fracture mode from intergranular to transgranular cleavage was observed (ref. 197). These results were a very small part of a much larger survey program by Law and Blackburn (refs. 197 and 198) and therefore a detailed understanding of the behavior of these materials was not attempted.

More recent and thorough work on NiAl(Cr) alloys by Cotton et al. (refs. 189 and 199) has not been able to verify Law and Blackburn's observations. Dislocation analysis of deformed NiAl(Cr) alloys, which included 34 different ternary alloy compositions and over 2000 dislocations, failed to observe any significant <111> activity. To eliminate any chance that processing or chemistry effects could influence the above observations, a piece of the original alloy studied in references 197 and 198 was also examined. Again no significant presence of <111> slip was observed in the as-cast or deformed material (refs. 189 and 199). While all of the alloys studied by Cotton et al. (refs. 189 and 199) contained almost exclusively <001> dislocations, in materials processed by extrusion, approximately 4 percent of the dislocations had <110> Burgers vectors. These segments were thought to be sessile dislocation reaction products from the extrusion process and had no effect on room temperature deformation.

Other studies (refs. 185, 187, and 188) which are often referenced to support the operation of <111> slip in NiAl due to Cr or V additions were performed on [001] oriented single crystals. Since <111> would be the preferred slip vector in this orientation even in the binary alloy, no conclusion about the effect of alloying on slip can be obtained from these studies. The slip behavior of polycrystalline Ni-Fe-Al alloys has also been studied (refs. 204 and 205) and again the observation of <100> slip was almost exclusive in the B2 phase NiAl(Fe) alloys.

It appears that alloying of NiAl with the intention of altering the operative slip vector has to date been unsuccessful, especially in generating <111> dislocations. However, little effort has been expended on Mn, which is the third potentially beneficial alloying addition. Due to the much greater solubility for

Mn (ref. 206) in NiAl compared to either Cr or V, more extensive investigation of Mn on the slip behavior of NiAl would be warranted. Unfortunately, very preliminary results indicate that Mn and Cr co-segregation may be responsible for embrittling grain boundaries in NiAl leading to very low strength intergranular fracture in Cr+ Mn-doped alloys (ref. 199).

Finally, the infrequent observation of <110>{011} dislocations in extruded alloys are thought to be dislocation reaction products with little potential for enhancing plasticity, however, this type of slip could be beneficial if glissile dislocations could be nucleated readily. The operation of <110>{110} slip alone supplies only two independent slip systems, as demonstrated in table II, however these slip systems are independent of <100>{110} slip common to NiAl. Therefore, the simultaneous operation of both families of slip systems would meet the von Mises criterion for polycrystalline ductility (ref. 207).

5. YIELD STRENGTH AND FLOW BEHAVIOR

Although yield stress is one of the most commonly reported mechanical properties for NiAl, a consistent description of all factors that can influence yielding and plastic flow behavior in this material does not exist. Inconsistencies in reported flow behavior for NiAl alloys are evident in the literature, in part because the flow properties of NiAl are highly sensitive to variables such as composition, strain rate, grain size, cooling rate, surface finish and specimen fabrication. Since most studies neglected to report all of these variables, meaningful comparisons of individual studies are difficult. In particular, the presence of impurities or slight deviations from stoichiometry, which can be very difficult to measure, can drastically influence the flow properties of NiAl alloys. Nevertheless, factors which influence the flow behavior of NiAl are reviewed in the following sections and trends in behavior have been identified.

5.1 Factors That Influence the Strength of Polycrystalline NiAl

5.1.1 Temperature.—At room temperature, Nagpal et al. (ref. 208) have reported an asymmetry in yield stress, on the order of 50 MPa, with the compressive yield stress being higher than that in tension. Since the flow properties of NiAl are extremely sensitive to many metallurgical properties, confirmation of this observation is possible only by comparing identical materials. Subsequently, work (ref. 209) on electropolished tension and compression specimens taken from the same extrusion rod has failed to show a statistically significant difference in the yield values in tension versus compression for polycrystalline NiAl. In addition, <111> oriented single crystals with different surface finishes were also tested and it was found that yield values in compression using as-machined finishes were approximately 20 MPa higher than that of identical material tested with an electropolished surface. Differences in surface finish could possibly explain the observation by Nagpal et al. (ref. 208) of an anisotropic yield stress since most investigators electropolish tensile samples before testing but generally not compression specimens. Finally, when electropolished Ni-50Al specimens were compared, the <111> single crystal yield stresses were close to that of the polycrystalline material which had a <111> extrusion texture (ref. 209).

Similar to BCC metals, the flow stress of NiAl exhibits a strong temperature dependence at low absolute temperatures (refs. 128, 182, and 212 to 222) which is attributed to a large Peierls stress. Although yield stress is highly sensitive to metallurgical properties, all studies agree that yield stress either decreases or remains constant with increasing temperature. Several studies have observed that the tensile strength of NiAl increases with temperature up to approximately 1000 K (refs. 212, 217, 219, and 221). Unfortunately, the generic term "strength" is often used loosely, denoting either a yield strength or a fracture strength. As a result, reports of increased tensile strength as a function of temperature have on occasion been incorrectly referenced as demonstrating an increase in yield stress with temperature. Due to the

limited ductility of most NiAl alloys, low temperature yield strength values are usually measured in compression because fracture often occurs prior to yielding.

In figure 12 the results of Pascoe and Newey (ref. 216) are reproduced and serve as an example of typical NiAl yield stress behavior as a function of temperature. In this figure the compressive yield stress for numerous extruded NiAl compositions and two strain rates is presented. Although the values of the yield stress, σ_y, and the shape of the σ_y versus temperature, T, curves are seen to depend on composition and strain rate, in all cases the yield stress basically decreases with increasing temperature.

Many studies have been conducted since the work of Pascoe and Newey (ref. 216), but because of differences in other metallurgical variables, the values of σ_y can be either higher or lower than those reported in figure 12. However, most studies agree that if tested over a sufficiently large temperature range three regions are typically observed in a σ_y versus T plot of high strength NiAl alloys, whereas in lower yield strength NiAl alloys the σ_y versus T curve appears essentially parabolic. In the high yield strength alloys, from the lowest temperatures tested to approximately 500 K, σ_y decreases with increasing temperature. With further increases in temperature a plateau or discontinuity in the σ_y versus T curve is observed. This athermal plateau can span anywhere from a few degrees to over 300 K. At temperatures beyond this plateau σ_y once again decreases with increasing temperature. While three regions of deformation are pronounced in the higher strength materials, the athermal region is in some cases completely absent, with strength continuously decreasing with temperature in lower strength materials.

Since σ_y is dependent on temperature, it is also possible to represent the data in an Arrhenius form. Consequently, when $\log \sigma_y$ is plotted versus $1/T$ for NiAl alloys, three distinct deformation regimes are observed and a change in slope (i.e., activation energy) is always noted at the BDTT of the alloy (refs. 128, 215, and 222) as demonstrated in figure 13. It has been suggested that the observed changes in slope or activation energy in figure 13, correspond to activation of alternate deformation mechanisms. At low temperatures (region I), dislocation glide controls deformation whereas at high temperatures (region III) dislocation climb and other creep mechanisms dominate (ref. 215).

In many studies discontinuous yielding has been observed, either in the form of serrated stress-strain curves or the presence of yield points. Serrated yielding has been observed at elevated temperatures (~1000 K) in an Al-rich alloy (53.3 at % Al) (ref. 210) and in a Ni-rich alloy (55 at % Ni) (ref. 211). It was suggested that the presence of vacancies in the Al-rich material was responsible for the serrated yielding (ref. 210) while dynamic recrystallization was the suspected mechanism in the Ni-rich material (ref. 211). Yield points have been reported both in tension (refs. 213, 217, and 221) and compression (ref. 216) testing of polycrystalline NiAl alloys. In each of these studies the magnitude of the yield point diminished with temperature disappearing above approximately 800 K except for reference 213 where the yield point was not observed above 500 K. As yet no investigation has been conducted to isolate the mechanics of the yield point phenomenon in NiAl.

5.1.2 Grain size.—While a few investigations have analyzed the effect of grain size on mechanical properties, only by analyzing all available data can the complicated effect of grain size on yield strength of NiAl be understood. As shown in figure 14, the yield stress of NiAl at room temperature can be independent, increase, or possibly decrease with decreasing grain size, or show a combination of these behaviors. The reason for the diverse range of behaviors can begin to be understood by examining figure 15. In figure 15 the Hall-Petch slope is plotted as a function of composition and the data (refs. 128, 208, 223, and 224) clearly indicate that the influence of grain size on yield stress increases with increasing deviation from stoichiometry. Consequently, yield stress is relatively independent of grain size for NiAl alloys very close to stoichiometry, whereas the yield stress of non-stoichiometric alloys is strongly influenced by grain

size. The effect of grain size on yield strength is further complicated when alloying additions are included, as demonstrated in figure 14. When NiAl is alloyed with 0.05 at % Zr, the yield stress is independent of grain size for grain sizes between 15 and 280 μm, but becomes strongly dependent on grain size for grains less than 16 μm in size (ref. 128). Figure 16 demonstrates that temperature also influences the sensitivity of yield stress to grain size. At elevated temperatures, the yield stress of nonstoichiometric NiAl alloys is influenced to a lesser degree by grain size than at lower temperatures (refs. 209 and 251).

No satisfactory explanation has been offered to explain the dependence of k_y on composition. Since k_y is a measure of the grain boundaries resistance to slip transmittal, it can be postulated that in the nonstoichiometric alloys slip transferal across the boundaries is more difficult than in stoichiometric alloys. Recent work by Chen et al. (ref. 225) using many body potentials has suggested that the grain boundary structure in NiAl is affected by compositional deviations from stoichiometry as is the bulk material. Specifically, their calculations show that unlike the bulk material, vacancies are the most stable defect at grain boundaries for both Ni- and Al-rich alloys. It is reasonable to assume that the presence of vacancies at the grain boundaries of nonstoichiometric alloys can hinder slip transmittal across the boundary resulting in an increase in the Hall-Petch slope. Further work is obviously needed in this area to fully understand this phenomena.

5.1.3 Stoichiometry.—NiAl exists as a B2 ordered compound over a very wide compositional range (fig. 2). Therefore, significant deviations are possible from the stoichiometric composition without altering the basic crystallography of the material. In general, stoichiometric Ni-50Al possesses a minimum in flow stress and hardness and a corresponding maximum in ductility. Westbrook (ref. 218) first noted the effect of stoichiometry during microhardness testing of arc-melted buttons, which was followed by one of the most complete studies of the effect of composition on the flow behavior of NiAl by Pascoe and Newey (ref. 216). This later work demonstrated that deviations from stoichiometry can significantly increase the flow stress as well as alter the shape of the σ_y versus T plot (fig. 12). If room temperature yield stress is plotted as a function of Ni content, as in figure 17, a linear dependence with composition is observed on either side of stoichiometry. Although the absolute values of yield stress varies when comparing individual studies due to differences in other metallurgical variables, the rate of hardening with deviation from stoichiometry is similar.

Although an increase in yield stress is observed for both Ni- and Al-rich alloys at lower temperatures, the magnitude of the strengthening effect is not equivalent. Most studies have found a greater hardening rate in the Al-rich alloys suggesting that vacancies provide a greater resistance to dislocation motion than that produced by substitutional atoms. Pascoe and Newey (ref. 216) found that hardening due to vacancies (dσ/dc) was approximately twice that for substitutional Ni atoms. Likewise, Nieh et al. (ref. 226) found the hardening coefficient to be 990 MPa/at % for vacancy defects and 100 MPa/at % for substitutional defects. From the compilation of data in figure 17 an average hardening rate for Ni-rich alloys is 120 MPa/at % while that for Al-rich NiAl is approximately 350 MPa/at %.

Only two studies (refs. 210 and 213) have reported greater hardening in Ni-rich alloys than in Al-rich. Lautenschlager et al. (ref. 210) reported greater strengthening in Ni-rich materials because a decrease in flow stress was observed as the limits of the β-phase field was approached for Al-rich alloys. It is possible that the compositions studied by Lautenschlager et al. (ref. 210) which were close to the ends of the single phase field were so brittle that compressive fracture was mistaken for yielding. Consequently, if these alloys are ignored, the remaining alloys in this study (ref. 210) also show a greater degree of strengthening for Al-rich compositions. The results of Hahn and Vedula (ref. 213) at present cannot be reconciled with the other studies. In their work, the hardening rate for Al-rich alloys was approximately 40 MPa/at % while that of Ni-rich alloys was 70 MPa/at %.

This apparent contradiction in results again illustrates the difficulty in comparing various studies and isolating mechanisms based on limited data. In this case, however, the majority of evidence indicates that hardening is more effective in Al-rich alloys than in Ni-rich alloys. If the increase in yield stress due to the presence of defects is analogous to a solid solution strengthening mechanism then it would be expected that greater hardening would occur in Al-rich alloys due to the greater dilatation of the lattice around the vacancy.

At low and intermediate temperatures the minimum yield stress occurs in the stoichiometric alloy (refs. 216 and 218) due to constitutional defect hardening on either side of stoichiometry. Ball and Smallman (ref. 182) found a reversal of this trend at temperatures above approximately 850 K (fig. 18) where the near-stoichiometric material has a higher initial flow stress than nonstoichiometric alloys. They also report a decrease in the activation energy required for self-diffusion with deviation from stoichiometry. Therefore, climb mechanisms are easier in the nonstoichiometric compositions and thus have a lower flow stress at elevated temperatures.

5.1.4 Alloying additions.—Solid solution alloying of NiAl has been explored in a number of studies (refs. 128, 189, 198, 219, 221, and 227 to 229) and typical of BCC materials (ref. 230), the flow strength of NiAl is greatly increased in the presence of solutes. Ternary additions to NiAl have included beryllium (ref. 227) boron (refs. 198, 227, and 228), carbon (ref. 227), chromium (ref. 189 and 198), lanthanum (ref. 220), molybdenum (refs. 220 and 229), yttrium (ref. 220), and zirconium (refs. 128 and 221). Table III lists the room temperature hardening rate for these ternary additions in NiAl. While these were all deliberate additions, it should be realized that the unknown presence of impurities such as carbon and oxygen or trace elements can also act as potent solid solution strengtheners with dramatic affects on mechanical properties. Furthermore, with this rapid rise in flow stress, improved ductility by alloying has been unsuccessful in NiAl because the yield stress is usually increased above the fracture stress. It is clear that the mechanical properties of NiAl are dramatically increased with alloying but as noted by Dimiduk and Rao (ref. 231), no accepted theory of solid solution strengthening has been successfully applied to intermetallic compounds such as NiAl.

George and Liu (ref. 227) rationalize the solid solution strengthening of NiAl by B, Be, and C in terms of the relative size of the atom compared to the resident site of the atom in the NiAl matrix. The interstitial site radius in NiAl was calculated to be approximately 0.036 nm. Based on an atomic radius argument and using the Goldschmidt radii (ref. 232) listed in table III it is predicted that B and C are likely to occupy the interstitial tetrahedral sites. Conversely, beryllium is more likely to substitute for either Ni or Al because of its larger radius. For elements which dissolve interstitially, the larger the radius the larger the associated strain field and the greater the resistance to dislocation motion, thus resulting in a greater hardening effect (fig. 19).

At some critical value, the radius becomes large enough that rather than dissolving interstitially, the element substitutes for Ni or Al. Qualitatively, from figure 19 it appears that the critical radius for interstitial dissolution is approximately 0.1 nm. Likewise, with increasing radius size, an increasing flow stress is observed with substitutional elements. This argument can also be used to explain increases in flow stress with deviations from stoichiometry for Ni-rich alloys. As seen in figure 17, the average results of several studies indicate that the strengthening of NiAl due to excess Ni is approximately 120 MPa/at % Ni. When plotted on figure 19 this value agrees well with the strengthening trends observed for other elements. Therefore, the increase in flow stress associated with deviations from stoichiometry for Ni-rich alloys can be explained in terms of a solid solution strengthening mechanism with Ni atoms substituting on Al sites.

One final note concerning alloying is that often there is little attention given to the specific site substitution in the B2 lattice and the resulting formation of point defects due to changes in alloy

stoichiometry (refs. 114 and 199). For example, it has been demonstrated that substituting a particular ternary addition such as Cu for Ni will result in different hardening characteristics than if the element were substituted for Al (ref. 199). A further complication occurs if the alloying addition causes a change in the overall stoichiometry of the intermetallic. For example, additions of a particular ternary element which substitutes readily for Al may cause the alloy to become Al-rich and result in the formation of excess constitutional vacancies. Therefore, hardening would result due to both substitutional effects and vacancy hardening. Any solid solution hardening models developed for ordered alloys will have take these effects into account.

5.1.5 Strain rate.—Strain rate is another variable which significantly affects the mechanical properties of most materials including NiAl. The majority of investigators that report tensile (or compression) properties for NiAl at intermediate or low temperatures have performed their tests in the range of 10^{-3} to 10^{-4} s^{-1} though data exits for strain rates ranging from 10^{-6} to 10^{-1} s^{-1} (refs. 128, 216, 217, 220, and 233 to 235). Strain rate effects at elevated temperatures (creep) are discussed in section 9.

One of the earliest studies of strain rate effects in polycrystalline NiAl was by Rozner and Wasilewski (ref. 217). In that study, an approximately 30 percent increase in flow stress was observed by increasing the strain rate from 10^{-4} to 10^{-3} s^{-1} over the temperature range of 750 to 1350 K, while only a slight increase in yield stress was observed at room temperature between 10^{-2} and 10^{-5} s^{-1}. The most complete set of strain rate—yield stress data for a single NiAl alloy covers almost 6 orders of magnitude strain rate from 500 to 1300 K (ref. 128) and is reproduced in figure 20. From this data it is evident that strain rate has almost no effect on yield strength at 500 K, has a moderate affect at intermediate temperatures and a significant affect in the creep regime at elevated temperatures. It has also been observed that the fracture stress at intermediate temperatures and the DBTT are significantly affected by strain rate (refs. 233 and 236).

5.1.6 Cooling rate.—The presence of vacancies in NiAl significantly influences the flow properties of this material. These vacancies can be introduced by compositional means (constitutional vacancies) and their affect on flow properties were discussed in section 5.1.3. The other type of vacancy defect which can exist in NiAl is a thermal vacancy which is introduced by rapid quenching from elevated temperatures. Consequently, cooling rate becomes another important variable which needs to be considered when processing and testing NiAl.

Nagpal and Baker (ref. 127) have studied the influence of thermal vacancies and stoichiometry on the hardness of NiAl. They found that air-cooled and water-quenched specimens exhibited relatively little difference in hardness compared to slow-cooled samples for nonstoichiometric alloys. But a small (~15 percent) difference in hardness was observed between slow-cooled and water-quenched Ni-50Al. The effect of thermally generated defects on the compressive yield stress of NiAl and NiAl(Zr) alloys subjected to post-extrusion heat treatments over a range of temperatures and cooling rates has also been investigated (ref. 128). The results of these experiments are summarized in table IV. It is apparent that the 0.2 percent compressive yield stress for binary NiAl is affected by cooling rate, annealing temperature, and composition. For example, NiAl specimens with d ≈ 22 μm and cooled at 1.33 K/s exhibit a yield stress of approximately 325 MPa in comparison to specimens cooled at about 0.025 K/s for which $\sigma_y \approx$ 255 MPa. Conversely, the yield stress of NiAl(Zr) specimens was relatively insensitive to post-extrusion heat treatments and cooling rate. Differences in the yield strength of binary NiAl resulting from these heat treatments cannot be attributed to grain size effects since none of the post-extrusion heat treatments resulted in significant grain growth. Therefore, while reference 127 saw only modest changes in hardness, which is a measure of strain hardening as well as flow stress, significant increases in yield stress do occur with rapid quenching for binary NiAl alloys of near-stoichiometric composition (ref. 128).

Consequently, the cooling rate after the final processing or heat treatment step is another very important parameter that needs to be controlled and should be accurately recorded in all future studies.

5.1.7 Texture.—Almost all mechanical property studies on NiAl have been performed on extruded material, consequently, few properties of a truly random polycrystalline NiAl alloy exist. When NiAl is processed by hot extrusion, a <111> or <110> texture is generally observed along the extrusion axis (refs. 91, 237, and 238). A <111> texture is commonly observed after 1100 K or higher extrusion and occurs in materials with a recrystallized grain structure (refs. 91, 237, and 238). A <110> texture has been found in materials extruded below 1100 K or in materials which have not had a chance to fully recrystallize (ref. 237). A <113> texture has been observed in a highly worked, particle strengthened NiAl alloy (ref. 237).

It follows that the tensile properties of extruded NiAl polycrystals will depend on the orientation of the tensile axis with respect to the extrusion axis. For a <111> texture, specimens prepared with the tensile axis oriented 45° to the extrusion direction will have the highest density of [001] directions parallel to the loading direction and therefore the lowest resolved shear stress on the primary <001>{110} slip system. Conversely, other orientations which will contain a lower density of [001] directions should have a lower flow stress. In figure 21 the flow properties of extruded NiAl specimens taken from various orientations relative to the extrusion axis are shown (ref. 178). Specimens tested in the 45° orientation exhibited the highest flow strengths while specimens oriented longitudinally or transverse to the extrusion direction have lower flow stresses, however, the actual differences in strength were relatively small. The reason that these orientation effects were relatively minor compared to what is observed in single crystals is that the textures observed in extruded NiAl are fairly weak, being only three to five times random (refs. 237 and 238).

5.2 Factors That Influence the Strength of Single Crystal NiAl

5.2.1 Temperature and orientation.—As with polycrystalline material NiAl single crystals exhibit a generally decreasing yield stress with increasing temperature. However, due to the very strong orientation dependence of the yield strength it is difficult to discuss temperature dependence without regard for the orientation of the specimens. In figure 22, yield stress as a function of temperature is shown for several different crystal orientations (refs. 174, 182, 216, and 239). Single crystals oriented in soft orientations exhibit a σ_y versus T curve which is distinct from the [001] material but very similar to low yield strength polycrystalline NiAl. In soft orientations the flow stress is initially lower than that in hard orientations and continually decreases with temperature with deformation occurring by movement of <100> dislocations over the entire temperature regime.

In the case of [001] oriented crystals the σ_y versus T response appears to be more complex. At lower temperatures, single crystals of NiAl loaded along [001] directions exhibit yield stresses several times higher than that for other orientations because [001] orientations have no resolved shear stress on the primary <001>{110} slip system and because the critical resolved shear stress (CRSS) for <111> and <110> slip is very high. Also at low temperatures (77 to 300 K), yield stress is strongly dependent on temperature while a plateau is observed between 300 and 600 K. At temperatures above 600 K the yield strength again becomes very dependent on temperature and a significant reduction in σ_y occurs over a relatively narrow temperature regime. It is also within this temperature regime that slip in hard crystals begins to change from <111> to <001> and <110> (fig. 10). Above 900 K where bulk diffusional process begin to dominate, hard single crystals have strengths similar to soft single crystals and polycrystals.

The σ_y of hard and soft oriented crystals can also be represented in Arrhenius plots as in figure 23. When the data is represented in this fashion, two distinct regions are clearly observed in the deformation of [001] crystals. It has been postulated that diffusional processes contribute to deformation in the later regime and are responsible for the change in activation energy of yielding observed above 600 K. The behavior of non-[001] single crystals is more complicated and the deformation mechanisms operating at intermediate temperatures are presently unknown but under investigation since they apparently lead to the low BDTT for soft orientation crystals.

As with so many other properties for NiAl, a wide range of CRSS values have been reported at room temperature. These are reviewed in table V. Wasilewski et al. (ref. 165) were the first to study flow properties of NiAl as a function of orientation and their results are presented in figure 24. For the soft orientations the slip vector was <001> in all cases. The active slip planes at room temperature in the "soft" orientations were {110} for the [111] and [112] oriented specimens and {100} for the [110] orientation. These slip systems correspond to the most highly stressed slip system of the type <001>{100} or <001>{110}. Based on these results, the CRSS of <001>{110} slip is in the range of 60 to 100 MPa and that of <001>{100} is approximately 150 MPa.

In the study by Field et al. (ref. 173), <001> slip on {110} planes was observed at room temperature in <111> oriented specimens resulting in a CRSS of 124 MPa. This is at least 25 percent greater than the 60 to 100 MPa measured by Wasilewski et al. (ref. 165), but not completely unexpected in light of the sensitivity of flow behavior to other properties. Field et al. (ref. 173) also tested <110> specimens but were unable to unambiguously determine the operative slip plane. If they assumed that the slip plane was {110} in the <110> oriented specimens, the calculated value for the CRSS was 77 MPa, which is inconsistent with the value they determined from measurements on <111> crystals (124 MPa). If, however, they assumed that the slip plane was {100}, as observed by Wasilewski (ref. 165) for <110> orientations, then the CRSS calculated for <100>{100} slip is 109 MPa. Since this value is lower than the CRSS calculated for <100>{110} slip, Field et al. (ref. 173) concluded that slip on {100} planes is favored at room temperature in <110> oriented crystals due to the slightly lower CRSS on these planes. Although the two studies (refs. 165 and 173) differ in concluding which system has the lowest CRSS, both agree that the CRSS for <001> slip on {100} and {110} is very similar. The advantage of the study performed by Field et al. (ref. 173) is that all of the specimens were taken from the same casting eliminating the possibility of differences in stoichiometry and impurity levels. The fact that unambiguous determination of the operative slip plane(s) is often not possible or is not reported, greatly hinders efforts to understand yielding in these materials. It is likely that slip is not dominated by a single system for some orientations, but that <100> slip is possible on multiple {100} and {110} planes, which could account for the difficulty that Field et al. (ref. 173) had in unambiguously determining the operative slip plane in <110> crystals.

Miracle (ref. 195) has compiled the results for both hard and soft orientations and calculated the CRSS as a function of temperature (fig. 25). The CRSS was calculated by resolving the flow stress onto either the observed slip system or the most highly stressed <001>{110} slip system when no slip system was reported. For [001] specimens, the CRSS was calculated for <111>{110} slip. The latter assumption is not strictly correct because slip in "hard" orientations is most likely to occur on {112} planes (ref. 142 and 174). However, this figure does serve to illustrate the difficulty in initiating <111> slip and explain the high flow strengths observed in [001] specimens.

Several studies have noted discontinuous yielding in NiAl single crystals tested in compression. Kinking is often observed in [001] oriented single crystals because of the high stresses required to produce slip (refs. 171, 182, 185, and 216). However, not all discontinuous yielding in [001] crystals has been attributed to kinking. Rozner and Wasilewski (ref. 217) observed that the load drops in room temperature

[001] NiAl single crystals were associated with the formation of a deformation band in the plane of the maximum shear stress. However, it is most likely that kinking and the deformation bands observed by Rozner and Wasilewski (ref. 217) are manifestations of the same deformation mechanism, but on different scales. Discontinuous yielding was also noted by Wasilewski et al. (ref. 165) in <123> oriented crystals. As in the [001] crystals, the load drops were observed to correspond to the formation of visible deformation bands during compression testing.

Tensile stress-strain data for single crystal NiAl is much more scarce than compression test results. This is due in part to the limited ductility generally achieved at low temperatures. For example, kinking has not been duplicated in [001] tensile samples since fracture occurs prior to yielding over the temperature range where kinking is observed in compression (ref. 185). In soft orientations, however, Field (ref. 173) has reported the presence of a yield point behavior in both <111> and <110> oriented tensile samples. The presence of a yield point in the single crystals is similar to that observed in polycrystalline NiAl (ref. 178) but has not been thoroughly studied in either type of material and no mechanism has been proposed.

5.2.2 Composition.—Single crystals of NiAl are subject to hardening due to the presence of defects in the lattice similar to that observed in polycrystals. In figure 26 (ref. 149), results for two nickel-rich and a stoichiometric NiAl alloy tested in compression in the hard orientation are compared. Deviations in stoichiometry result in an increase in flow stress below 1000 K and an extension of the athermal plateau to higher temperatures. Beyond the athermal plateau all materials exhibit a drop in flow stress associated with the change from <111> to non-<111> slip (ref. 144). Once the temperature exceeds 1000 K the effects of stoichiometry on flow stress are diminished and all compositions exhibit similar strengths. The effect of stoichiometry on the yield stress of soft orientation single crystals has not been reported but it is expected that they would behave similarly to polycrystalline material.

Similarly, only a few studies of ternary additions in single crystals have been performed and again the work has been on [001] oriented crystals. Both Cr (ref. 187) and V (ref. 185) have been observed to strengthen NiAl from room temperature to at least 1150 K. The ternary additions appear to affect the CRSS for both <111> and <100> slip, although interpretation of the results for these two studies is difficult because of the limited amount data and because the solubility limit was exceeded and precipitation hardening cannot be neglected. The effects of Zr also have been studied (ref. 240), where it was found that significant strengthening only occurred above the BDTT where a change in slip occurs. Consequently, it was concluded that the strengthening effect of Zr was dependent on the operative slip system and was more effective at preventing deformation by <001> than <111> dislocations.

It has been determined that the core structure of <111> dislocations is significantly different than that of <001> dislocations in BCC and BCC derivative materials (refs. 151, 152, 156, and 157). Consequently, these two types of dislocations would be influenced differently by short-range stress fields such as those around substitutional solute atoms. Therefore, it is conceivable that Cr, Zr, and V can influence <001> and <111> slip in significantly different degrees. Further testing of alloyed specimens under conditions of <111> and <001> slip is required to resolve this issue. It is also preferred that more single crystal alloying studies be performed on soft orientation single crystals since their behavior can be directly related to polycrystalline deformation mechanisms.

5.2.3 Strain rate.—One of the earliest studies concerned with strain rate effects in single crystal NiAl was by Wasilewski et al. (ref. 165). In this study an anisotropic behavior in strain rate sensitivity was observed at intermediate temperatures (T > 473 K) with cube oriented crystals showing the largest sensitivity to strain rate although the increase in flow stress was only about 10 percent for a change in strain rate from 10^{-4} to 10^{-3} s^{-1}. Pascoe and Newey (refs. 216 and 234) also found that [001] crystals were more

susceptible to strain rate effects than the soft orientations but for all orientations the strain rate sensitivity was greatest where the flow stress was strongly dependent on temperature.

A more recent study (ref. 239) also observed only a slight sensitivity of yield stress to strain rate in <110> as well as <111> samples in the temperature range of 400 to 800 K. Also in agreement with previous investigators (refs. 165, 216, and 234) [100] specimens exhibited a greater sensitivity to strain rate than soft orientations with the effect decreasing with increasing temperature (below the creep regime). The reason that [100] crystals are more sensitive to strain rate is unclear but must be related to the change in deformation by <111> to non-<111> dislocations since it is over this same temperature range that hard crystals are most affected by strain rate.

6. DUCTILITY AND FRACTURE

6.1 Polycrystals

6.1.1 Origins of low temperature fracture.—By now it is clear from this review that all non-[001] single crystal orientations and polycrystalline NiAl deform predominantly by <100> slip on {011} and occasionally {001} type planes. As a consequence, only three independent deformation mechanisms are available for polycrystalline deformation by <100> slip (ref. 203). Even with slip on all planes of the <001> zone, i.e., {hk0}<001>, only three independent slip systems are available, therefore, no extra independent systems are provided by cross slip (ref. 138). Because this is less than the five independent deformation modes considered necessary for extensive, uniform, crack-free deformation of a polycrystalline aggregate (refs. 203 and 241), NiAl is considered to have little potential for exhibiting significant room temperature ductility. Experimental evidence to date supports this view.

In room temperature studies of NiAl (refs. 213, 215, 217, 222, 223, 227, and 233) the reported tensile ductilities have been small, ranging from zero to a maximum of about 4 percent. Furthermore, observations (refs. 213, 215, 217, 222, and 227) of grain boundary fracture in both tensile and compression specimens at low temperatures appear to confirm that limited ductility arises from the incompatibility in the shape changes of neighboring grains due to an insufficient number of slip systems. This is demonstrated in figure 27, which is an example of the magnitude of the intergranular cracking that occurs in NiAl after compression testing at room temperature. In tension these intergranular cracks would provide an easy path for intergranular fracture in binary NiAl.

Intergranular fracture in metals can also result from impurity contamination of the grain boundaries and this was originally thought to be the case in NiAl (refs. 242 and 243) Westbrook and Wood (ref. 242) and Seybolt and Westbrook (ref. 243) investigated the effect of oxygen on the grain boundary hardness of NiAl. They concluded that because the grain boundaries were harder than the matrix material, oxygen embrittlement was responsible for the intergranular fracture of NiAl. Because the grain boundary hardening occurred only after high temperature heat treatments followed by slow cooling or quenching and intermediate annealing, this behavior was explained in terms of oxygen-vacancy interactions (ref. 244). However, these same results can also be explained in terms of vacancy or point defect gradients near the grain boundaries without the necessity for the presence of oxygen since grain boundaries are very strong sources and sinks for vacancies. Furthermore, it has been concluded from recent in-situ Auger electron spectroscopy studies of cast and extruded alloys (refs. 227 and 228) and powder extruded materials after various heat treatments (ref. 245) that the grain boundaries in NiAl are clean and free from measurable impurity contamination including oxygen. These results conclusively demonstrate that intergranular fracture in binary stoichiometric Ni-50Al is not due to any form of impurity induced intergranular embrittlement.

26

Intergranular fracture can also arise because grain boundaries are intrinsically weak due to their structure, as is true of Ni_3Al (refs. 246 to 248). However, grain boundary structure simulations for NiAl indicate that there are no periodic structural defects present at the grain boundaries in near-stoichiometric NiAl which would cause the grain boundaries to be inherently weak (refs. 225, 247, and 249). This suggests that only grain boundary incompatibility due to an insufficient number of independent slip systems is the primary factor responsible for the observed intergranular fracture of near-stoichiometric NiAl.

6.1.2 Effect of composition on ductility and fracture.—George et al. (refs. 227 and 228) have observed that B both segregates to the grain boundaries in NiAl and affects a change in fracture mode from predominantly intergranular to transgranular in nature. Consequently, they concluded that the grain boundaries in NiAl are intrinsically weak and that B must strengthen the grain boundaries. It has also been suggested (refs. 233 and 209) that the major affect of B was to suppress plastic deformation, eliminating the opportunity for intergranular fracture to initiate, rather than actually strengthening the boundaries. In fact, the fracture mode for NiAl alloys is predominantly transgranular any time fracture occurs significantly before yielding as in the case of Zr-doped alloys (refs. 128 and 221) as well as Re-, Hf-, Y-, WC-, and Cr-doped alloys (ref. 250). This point is demonstrated in figure 28, which is a plot of yield stress versus fracture stress for a number of different NiAl alloys. A detailed description of the alloys represented in figure 28 and their room temperature properties are summarized in table VI. From figure 28 and table VI it is evident that all low yield strength NiAl alloys, that exhibit at least some ductility, fail in a predominantly intergranular manner and that all brittle, high strength alloys fail in a predominantly transgranular fashion.

Similarly, nonstoichiometric binary NiAl alloys, which are not known to exhibit room temperature ductility, also fail in a predominantly transgranular manner (refs. 198, 220, 251, and 252). This behavior is demonstrated in figure 29 and argues against the weak grain boundary hypothesis since grain boundary strength would be expected to be even worse in nonstoichiometric compositions (refs. 225 and 247).

Thus, it appears that grain boundaries in NiAl must be at least as strong as the bulk. Consequently, grain boundaries in NiAl are not intrinsically (structurally) weak, but become the site of Griffith defects when slip is activated in low strength alloys. Since only relatively pure NiAl and (Be-doped alloys (ref. 227)) actually yield before fracture at room temperature they are the only alloys which experience intergranular failure. All other NiAl-based materials fail in a transgranular manner consistent with the calculations by Yoo and Fu (ref. 253) which indicate that the cleavage strength of NiAl is relatively low.

6.1.3 The Brittle-to-ductile-transition temperature and effects of processing, composition, and strain rate.—Over 20 years had past before Vedula et al. (refs. 178 and 213) had reproduced the original observations of Rozner and Wasilewski (ref. 217) for room temperature ductility of NiAl. Now limited room temperature ductility in NiAl has been verified repeatedly in cast and extruded alloys (refs. 223, 227, and 233) as well as in powder-extruded material (ref. 215). While limited ductility can be achieved in low yield strength NiAl alloys at room temperature, this does not constitute the brittle-to-ductile transition temperature (BDTT) for this intermetallic. Instead, a more significant increase in ductility corresponding to the BDTT is observed in the range of 550 to 700 K (table VII). Not only is the BDTT defined by a dramatic increase in ductility, but a significant and concurrent increase in fracture strength is also observed (fig. 30).

Overall, the data in table VII (refs. 197, 213, 215, 217, 221, 222, 233, 236, 254, and 255) suggests that as long as extrusion is the final processing step the processing route for the precursor material has no significant affect on the BDTT. For example, the product form before extrusion has included cast ingots (refs. 213, 217, 233, and 255), prealloyed powders (refs. 128, 197, 215, and 221), and even chopped melt spun ribbons (ref. 254). Grain size appears to have only a secondary effect on the brittle ductile transition as

evident from studies on a Ni-49Al-0.01 Zr (refs. 220, 236, and 251) alloy and on Ni-50.6Al (refs. 128, 215, and 221). The effect of a reduced grain size is to shift the BDTT to lower temperatures within the BDTT window of 550 to 700 K.

Strain rate has a significant effect on the BDTT (refs. 233 and 236) with a three order of magnitude increase in strain rate resulting in an approximately 200 K increase in transition temperature for cast and extruded NiAl, as shown in figure 31 (ref. 233). Alloy composition also has a very significant effect on the BDTT of NiAl. It is apparent from the data in table VII that even small alloying additions (refs. 128, 197, 221, 222, and 254) or slight deviations from stoichiometry (refs. 197 and 256) tend to shift the BDTT for NiAl to significantly higher temperatures.

The one anomaly to the typically reported BDTT range for near stoichiometric binary NiAl was reported by Grala (ref. 219) who determined the BDTT for cast NiAl to be almost 1000 K. In addition to possible differences in composition, a likely explanation can be related to the fact that his tests were run under constant loading rate conditions as opposed to a constant crosshead velocity as in all the other studies. Therefore, with increasing test temperature resulting in a sharp decrease in work hardening rate (refs. 128 and 216), the strain rate on the NiAl samples tested by Grala would have been significantly increased to maintain the constant loading rate.

6.1.4 Effect of grain size.—Schulson has suggested that grain refinement can be used to increase the ductility of brittle intermetallics such as NiAl (ref. 257) and performed tensile tests on NiAl as a function of grain size and temperature to support this view, figure 32 (refs. 236 and 255). However, grain size only had a critical effect on the ductility of NiAl within the 550 to 750 K BDTT window. Even though no tensile ductility was achieved at room temperature in these studies the results are often incorrectly quoted in support of a critical grain size for room temperature ductility of NiAl. Further testing of the effect of grain size on the room temperature ductility of cast and extruded NiAl by Nagpal and Baker (ref. 223) showed that room temperature ductility was essentially independent of grain size.

A quantitative model based on a critical J-integral approach has been developed by Chan (ref. 258) which very accurately predicts the dependence of tensile ductility on grain size for semibrittle materials when the mechanical properties listed in table VIII are known. Chan's model has been verified for NiAl (refs. 215 and 222) and the theoretical and actual test results are shown in figure 33, for the alloy described in table VIII. It is clear from figure 33 that grain size affects ductility in markedly different ways depending on the temperature range. There is strong dependence of tensile ductility on grain size at 700 K, when the grain size is less than about 20 μm. In contrast there is very little grain size dependence of ductility at 300 K for grain sizes greater than 1 μm. Although ductility is predicted by Chan's model to increase with decreasing grain size below 1 μm, only about 5 percent tensile ductility is expected at grain sizes of approximately 0.1 μm. Furthermore, it will be extremely difficult to stabilize such a fine grain size, due to grain growth during processing and service exposure, without introducing extrinsic defects in the material which are greater in size than the maximum allowed grain size.

Consequently, grain size refinement alone is not a practical method for achieving significant improvements in the ductility of NiAl at room temperature. A more pragmatic approach would be to increase the number of independent slip systems without substantially altering the yield strength of the alloy and/or increase the fracture toughness of the material. The implicit relationship between fracture toughness and ductility is apparent when examining figure 33 and table VIII. The higher ductility of NiAl at 700 K in comparison to room temperature is for the most part due to the higher fracture toughness exhibited by NiAl at elevated temperatures.

6.2 Single Crystals

Some confusion exists within the literature concerning the tensile ductility of single crystal NiAl. This is due in part to an incorrect interpretation of the work by Ball and Smallman (ref. 182) which is often quoted in support of extensive tensile ductility of NiAl single crystals at room temperature. In fact, Ball and Smallman (182) actually tested NiAl single crystal specimens in compression. To eliminate confusion as to the mode of testing being discussed, ductility in compression and tensile ductility are described in separate sections.

6.2.1 Compression ductility.—Until very recently, compressive ductility or yield strength were nearly the only mechanical properties reported for NiAl single crystals tested at room temperature and these results are summarized in table IX. It was found that room temperature compressive ductility for NiAl single crystals is very dependent on orientation (refs. 165 and 182) and material quality (refs. 149 and 259). For example, in compression at room temperature, 3 to 16 percent strain to fracture has been reported for [001] single crystals (refs. 165, 260, and 261), 6 to 36 percent strain to fracture for [123] single crystals (refs. 165, 260, and 262) and 10 to 50 percent strain to failure has been observed in [110] crystals (refs. 165 and 182). The failure of specimens exhibiting low ductility in compression, appears to be due to the resolved tensile stresses resulting from the deformation process acting on defects in the crystal and resulting in axial fracture (refs. 149 and 259).

6.2.2 Tensile ductility.—Tensile data for NiAl single crystals has been growing rapidly in recent years. However, before about 1989 the only tensile data available was a single reported room temperature tensile ductility of 4.5 percent for a Ni-48Al single crystal from a 1965 air force report (ref. 263). This is also the largest reported value for tensile ductility of a binary NiAl alloy to date, though ternary alloys can exhibit slightly greater ductilities. In 1967, Wasilewski et al. (ref. 165) also reported on the tensile properties of single crystal NiAl but only at 673 K and above. Recently, more complete room and intermediate temperature tensile test results have been generated due mainly to the research efforts at General Electric (refs. 62, 185, 239, and 264), and NASA Lewis (refs. 174, 265, and 266).

Consistent with the behavior of polycrystalline NiAl, single crystals exhibit very limited room temperature ductility in tension. Cube oriented, Ni-50Al single crystals exhibit essentially zero plastic strain to failure at room temperature but undergo a sharp brittle-to-ductile transition at approximately 600 K (fig. 34) (refs. 174 and 185). This corresponds to the same temperature at which [001] crystals begin to undergo a change in deformation mechanism (fig. 10) and where the steep decrease in yield strength with temperature begins (figs. 23 and 26). Ni-rich Ni-40Al cube oriented crystals undergo a similar brittle-to-ductile transition but at approximately 1000 K (fig. 34) (ref. 265).

Soft orientation single crystals, of near-stoichiometric composition, exhibit room temperature ductility on the order of 0.5 to 2 percent (refs. 174 and 239). These crystals also undergo a dramatic brittle-to-ductile transition but at the relatively low temperature of 473 K or 0.25 T_m. Soft orientation Ni-40Al single crystals do not exhibit any tensile ductility at room temperature and undergo an even sharper brittle-to-ductile transition than the binary alloys, though at a much greater temperature, 900 to 1000 K (ref. 266).

The effects of composition other than stoichiometry, on the tensile properties of single crystal nickel aluminides are quite interesting. It was recently discovered (refs. 62 and 264) that when near-stoichiometric [110] single crystals were doped with approximately 1000 ppm of Fe, Mo, or Ga the room temperature tensile ductility increased from approximately 1 percent to upwards of 6 percent (fig. 35). From this figure it is obvious that the peak in ductility occurs at very small alloying additions but as the level of dopant exceeds 0.5 at % the benefits in ductility become lost. It has been speculated that this ductilizing effect could be

due to a gettering phenomenon or arise from some type of slip homogenization process, though the actual mechanism remains unknown.

The effect of strain rate on the BDTT of soft orientation single crystals has been performed by Lahrman et al. (ref. 239) and it was found that no more than a 50 K increase in BDTT occurs for a two order of magnitude increase in strain rate. This is less than the approximately 130 K increase in BDTT which has been observed in polycrystalline NiAl for the same change in strain rate (ref. 233). However, a similar effect of strain rate on the BDTT has been found in [001] oriented crystals (ref. 264), where a 2-order-of-magnitude increase in strain rate results in approximately a 120 K increase in BDTT.

6.2.3 Analytical modeling of fracture processes.—An increasing effort has been underway to try to understand the fracture behavior of NiAl from an atomic standpoint and to model fracture processes in NiAl crystals using embedded atom method calculations (refs. 267 to 270). During computer simulations it was observed that [001] oriented NiAl was brittle at 10 K (ref. 268), meaning that fracture preceded most dislocation motion at the crack tip, and that a brittle-to-ductile transition occurred between the 300 and 800 K (ref. 267). These results agree reasonably well with the experimentally determined BDTT of approximately 600 K for [001] oriented crystals (fig. 34). It was also observed that at low temperatures martensite was formed in the vicinity of the crack which impeded further dislocation motion near the crack tip (refs. 269 and 270). If this occurred in practice it might explain the poor cleavage strength of NiAl at low and intermediate temperatures and could even be used as a possible explanation for the brittle-ductile-transition in soft orientation single crystals. Corroboration of this effect experimentally would be the next step in understanding the fracture processes in NiAl and should be made a high priority.

6.3 Mechanism(s) Responsible For The Brittle-To-Ductile Transition

A dramatic change in deformation behavior including a sharp increase in ductility and fracture strength takes place at intermediate temperatures for NiAl. The range of temperatures over which this behavior occurs for polycrystalline NiAl and [001] oriented single crystals is approximately 550 to 700 K. For soft orientation single crystals this change in behavior occurs as low as 475 K.

For polycrystalline material, these changes in behavior have been attributed to either initiation of new or secondary slip systems (ref. 140 and 195) or to the onset of thermally activated deformation processes such as dislocation climb (refs. 128, 138, 222, and 233). The former mechanism does not adequately describe the rate dependent deformation behavior of NiAl near the BDTT (refs. 128 and 233) the change in activation energy for deformation at the BDTT (fig. 13) or the change in stress exponent observed in the temperature range where the BDTT occurs (fig. 20). All these behaviors are the consequence of thermally activated deformation processes. In situ annealing studies also have verified significant dislocation climb activity near grain boundaries beginning at the BDTT (ref. 128). In addition to changes in flow behavior, that support the theory of a BDTT due to thermally activated deformation processes is one key observation; that alternate slip systems are not generally observed in monotonically deformed NiAl, at or above the BDTT (ref. 128).

Consequently, for polycrystalline NiAl, dramatic changes in mechanical behavior at the BDTT are due to the onset of thermally activated deformation processes. The significance of dislocation climb occurring in a material such as NiAl has been demonstrated by Groves and Kelly (ref. 271), who have determined that the combination of both glide and climb of dislocations with <100> Burgers vectors will result in five independent deformation mechanisms. This condition would satisfy the von Mises criterion

30

allowing for extensive plasticity in polycrystalline NiAl by relieving stresses at the grain boundaries and other sites of extensive stress concentration.

The lowest temperature at which the BDTT occurs in polycrystalline NiAl, approximately 0.30 T_m, is still within the temperature regime for which thermally activated deformation mechanisms occur primarily by short circuit diffusion (refs. 272 and 273). For example, climb could be restricted to grain boundary regions and yet be very influential in relieving compatibility stresses. Typical dislocation glide processes would still dominate the deformation behavior of the grain interiors until temperatures of approximately 0.5 T_m are reached. This description is consistent with in situ TEM annealing studies on NiAl that have qualitatively determined the operative temperatures for dislocation climb by short circuit and bulk diffusion processes (ref. 128).

Dislocation climb processes could also be used to explain the brittle-to-ductile transition in [001] oriented single crystals, as the BDTT varies in the same manner with strain rate as polycrystalline NiAl. Furthermore, the temperature range over which this change in behavior occurs corresponds to the change in deformation from <111> slip to deformation by <100> and <110> dislocations. Because of the orientation of hard crystals, <001> slip would be almost impossible because of a zero resolved shear stress. Consequently, these dislocations would have to move by a climb process.

The mechanism for the brittle-to-ductile transition in soft orientation single crystals, however, is not clear. For soft single crystal orientations the BDTT occurs at lower temperatures, approximately 0.25 T_m, and the dependence of the BDTT on strain rate is small. It has been proposed that the BDTT could arise because of enhanced cross-slip, or unlocking of dislocations from impurities or point defects. However, observed deformation behaviors and TEM observations have failed to make a strong case for either mechanism. It is even possible that the BDTT arises because the temperature is sufficiently high to prevent stress induced martensite formation at the crack tip, a phenomenon revealed by computer simulations refs. 269 and 270). With understanding of the mechanism responsible for the BDTT in soft single crystals could come the development of more ductile alloys. Consequently, this is starting to become an area of increased research effort.

7. FRACTURE MECHANICS AND FATIGUE

7.1 Fracture Toughness

Fracture toughness evaluation of NiAl-based materials has been a topic of recent emphasis. Consequently, room temperature data now exists for: single phase polycrystalline NiAl alloys processed by a number of techniques (refs. 274 to 279), two-phase and/or ternary alloys based on NiAl (refs. 276, 279, and 280), single crystal NiAl (refs. 62, 280, and 281), NiAl composites (refs. 275 and 276), and NiAl-based eutectic alloys (refs. 264 and 282). Typical room temperature toughness values for NiAl and NiAl-based alloys and composites are summarized in table X.

The plane strain fracture toughness for binary, single phase polycrystalline NiAl at room temperature has been measured between approximately 4 and 6 MPa√m and is essentially independent of grain size, stoichiometry or processing technique (refs. 274, 275, 277 to 279, and 283). These values are relatively low, and similar to those for dense polycrystalline ceramics, i.e., 5 to 6 MPa√m for polycrystalline Al_2O_3 and about 7 MPa√m for polycrystalline Al_2O_3-ZrO_2 of eutectic composition (ref. 284). Furthermore, room temperature fracture in NiAl occurs without any stable crack growth (ref. 274) and the fracture mode during toughness testing has been reported to be transgranular (refs. 276 and 278) as opposed to intergranular, which is observed during monotonic tensile tests of binary Ni-50Al. However, due to the

extreme dependence of fracture morphology on composition and the lack of compositional characterization in these studies (refs. 276 and 278) it is not possible to conclude whether the test technique or some compositional effect was the cause of the transgranular fracture.

The fracture toughness of polycrystalline NiAl can be increased by going to very Ni-rich compositions, >60 at % Ni, while smaller deviations from stoichiometry have no apparent affect on toughness (fig. 36). There are probably two different toughening mechanisms responsible for this increased toughness. First, a peak in toughness of approximately 9 MPa√m has been reported for single phase β-alloys at 61.5 percent Ni, possibly due to martensitic transformation toughening (ref. 276). However, due to the small volume increase during the NiAl to martensite transformation (ref. 285), only a very small increase in toughness would be expected by this mechanism (ref. 265). The toughness of Ni-rich NiAl can also be increased with the formation of a two-phase microstructure consisting of a Ni_3Al necklace structure surrounding β-grains (refs. 276 and 277). This increased toughness, demonstrated in figure 36, can be attributed to typical ductile phase toughening mechanisms. However, the toughness of a two-phase NiAl-based alloy decreases if the second phase has less toughness than NiAl as in the case of NiAl/NiAlNb alloys (ref. 280). A several fold increase in the toughness of NiAl has also been observed after alloying with additions of 5 at % Nb or Ti (ref. 279). This result is surprising considering the brittleness of the second phase particles that would be present, especially in the case of the Nb-doped alloy (ref. 280), and the mechanism behind this increase in toughness is presently unknown.

The fracture toughness of single-crystal NiAl is similar to or greater than single-phase polycrystalline material but is anisotropic. It varies between 4 to 6 MPa√m when the notch is parallel to {110} and 8 to 10 MPa√m when the plane of the notch is parallel to {100} (refs. 280 and 281). It was observed that cracks tend to initiate along higher index planes such as {115} or {117} and then transition to {110} planes as demonstrated in figure 37 (ref. 281). The reason for this transient behavior is unknown. It has also been reported (ref. 62) that alloying elements that tend to ductilize single crystals such as Fe, Mo, and Ga tend to increase the fracture toughness of single crystal NiAl. The room temperature fracture toughness of NiAl also has been successfully modeled from a first principles total energy approach by Yoo and Fu (ref. 253). They not only predict a K_{IC} fracture toughness of 5 to 6 MPa√m for NiAl but predict a (110) cleavage plane as well.

The fracture toughness of powder-processed, NiAl-based composites has been investigated by Kumar et al. (ref. 276). They found that 1-μm diameter TiB_2 particulates had essentially no effect on the room temperature fracture toughness of NiAl but that Al_2O_3 whisker reinforcement resulted in a 50 percent increase in toughness when present at volume fractions of 15 to 25 percent. Initial results on a FP Al_2O_3 fiber-reinforced NiAl composite that had a fracture toughness of 14.3 MPa√m (ref. 286) indicate that continuous fiber reinforcement has potential for increasing toughness. Composite-like materials also can be produced by eutectic solidification processing. When a NiAl-9Mo eutectic is arc melted it has a fracture toughness of approximately 9 MPa√m (ref. 282), but after directional solidification the eutectic composite consists of approximately 11 vol % 1-μm diameter rods in a single-crystal NiAl matrix and has a fracture toughness of 15 MPa√m (ref. 264). Directionally solidified NiAl-Cr eutectics have a toughness of approximately 18 MPa√m but the volume fraction of α-Cr in this eutectic alloy is on the order of 34 vol % (ref. 264).

Fracture toughness investigations of NiAl at elevated temperatures have been primarily limited to the work of Reuss and Vehoff (refs. 278, 280, and 283). They found that the fracture toughness of polycrystalline NiAl increases with temperature with the transition to ductile behavior and high toughness values occurring between 550 and 650 K (fig. 38). In this intermediate temperature regime the fracture toughness of NiAl ranges from 20 to nearly 50 MPa√m depending on the microstructure and grain size (refs. 278 and 283). The increasing toughness of NiAl with temperature corresponds to the observed increase in tensile fracture strength with temperature (fig. 30), and would be expected considering the

linear dependence between K_{IC} and fracture stress for a constant flaw size. Thus, the same mechanisms responsible for the BDTT in NiAl would be responsible for this increase in toughness since both properties would be manifestations of the same change in deformation behavior.

7.2 Cyclic Deformation

Reports on fatigue behavior of B2 compounds have been limited to cyclic hardening behavior and fatigue crack initiation of FeCo-2%V alloys (refs. 287 to 289) and limited room temperature testing of Fe-40Al and Ni-20Fe-30Al alloys (refs. 290 and 291). However, several fatigue programs on single-crystal (ref. 292) and polycrystalline NiAl (ref. 293 and 294) are presently underway.

Initial results (ref. 293) of plastic strain controlled, low cycle fatigue of polycrystalline Ni-50Al at 1000 K indicate that the fatigue life of NiAl is only mildly sensitive to processing technique (fig. 39). The fatigue life of Ni-50Al samples produced by HIP'ing prealloyed powders is about a factor of 3 lower than that for cast and extruded material. It was observed that the fatigue crack growth path in either material was intergranular but fast fracture always occurred in a transgranular manner. It was determined that fatigue life also could be increased slightly by testing in vacuum as opposed to air (ref. 293). Low cycle fatigue failure at lower temperatures (600 to 700 K) was mixed mode in nature, however, the regions of stable crack growth prior to failure are difficult to resolve from the region of fast fracture and lives were fairly low (ref. 294). Finally, cyclic failure at room temperature is preceded by continuous hardening and is predominantly intergranular in morphology (ref. 293).

At elevated temperatures, 1033 K, [001] Ni-49.9Al-0.1Mo single crystals follow the expected Manson-Coffin strain life behavior, typical of conventional nickel-base superalloys (ref. 292), and lives were very similar to polycrystalline material (fig. 39). The lives of the NiAl were longer compared to RENE'N4 at high strain ranges because of the higher ductility of the nickel aluminide. The lives of the intermetallic were much shorter than the superalloy at low strain ranges reflecting the lower yield strength of NiAl at elevated temperatures.

8. DIFFUSION

Using various techniques a number of different investigators have examined the diffusion behavior of NiAl as a function of temperature and intermetallic stoichiometry. Tracer diffusion (refs. 136 and 295 to 297) of Ni^{63}, In^{114}, or Co^{60}, and interdiffusion in Ni-Al alloys using diffusion couples of various compositions, with (refs. 298 to 300) and without (ref. 301) inert markers has been investigated. The reaction diffusion and interfacial stability of Ni-50Al with various Ni-Cr-Al alloys (ref. 302) and interdiffusion in the Ni-rich section of the Ni-Cr-Al phase diagram including the NiAl phase (refs. 303 to 305) have also been extensively studied.

The diffusion coefficients for NiAl determined by various investigators tend to agree within an order of magnitude for most studies, as demonstrated in figure 40. The measured diffusion coefficients for Ni^{63} determined by Hancock and McDonnell (ref. 136) compare reasonably well with earlier data for the diffusion of Co^{60} in NiAl (ref. 297), and self-diffusion of Ni in NiAl (refs. 298 and 299), while diffusion for In^{114} was found to be about an order of magnitude slower at Al-rich compositions (ref. 295). This is probably due to the larger atomic mass and volume of the In^{144} isotope which can result in a low pre-exponential term, D_0. Nevertheless, these are the only experiments (ref. 295) that have examined the tracer diffusion of a specie that resides on the Al sublattice. Values of the pre-exponential term were also unusually low for Ni^{63} diffusion in Al-rich compositions (ref. 136), but generally fell within the range

typical for B2 compounds (ref. 306) otherwise. The interdiffusion data of Shankar and Seigle (ref. 298) are higher than the tracer diffusion coefficients by about a factor of 10.

A minimum in the diffusion coefficient occurs near stoichiometric NiAl (refs. 136, 295, 297, and 298) as demonstrated in figure 40. From the data available, the minimum in the diffusion coefficient occurs either at stoichiometry (ref. 297), or within a percent of stoichiometry at slightly Ni-rich (ref. 298) or Al-rich (refs. 136 and 295) compositions. Again, the main problem appears to be in the accurate measurement of composition and not alloy behavior. With obvious deviation from stoichiometry, small excesses of Al increase the diffusion coefficient significantly, which is due to the presence of a high concentration of structural vacancies in addition to the thermal vacancies present. A much smaller increase in the diffusion coefficient is observed as the composition moves to the Ni-rich side of stoichiometry.

The activation energy for diffusion of various species in NiAl is summarized in figure 41. It is evident from the plot that there is fairly significant scatter between the various studies. From the data in figure 41, the average activation energy for diffusion in NiAl, independent of composition, is 225±39 kJ/mol. However, average independent measurements for the energies of formation and migration of vacancies discussed in section 3.1, are approximately 140 and 160 kJ/mol, respectively. The sum of these two values indicates that the activation energy for diffusion in NiAl should be closer to 300 kJ/mol, which is in agreement with the results of Hancock and McDonnell (ref. 136). For studies investigating activation energies as a function of composition (refs. 136, 295, 297, and 298) it was observed that a change in activation energy occurred near stoichiometric compositions and three studies (refs. 136, 295, and 297 reported a peak in activation energy near Ni-50Al. At Ni-rich compositions the activation energy either decreases or reaches a plateau with further increases in Ni-content (refs. 136, 295, 297, and 298). The decrease in activation energy for Al-rich NiAl is proposed to result from the formation of constitutional vacancies, and the activation energy reflects the energy of motion of a vacancy, while the higher activation energy for Ni-rich NiAl reflects the energy required to form and to move a vacancy (ref. 136). This behavior has been interpreted as evidence for diffusion by a vacancy mechanism (ref. 136).

Although diffusion data for NiAl has been analyzed with respect to the standard Arrhenius equation, a measurable deviation from linearity was noted at lower temperatures (ref. 136), which is probably due to the onset of short-circuit diffusion mechanisms. Additional work on determining the activation energy and mechanisms of diffusion at lower temperatures is needed since almost no diffusion data exits for NiAl below approximately 1200 K.

9. CREEP OF NiAl AND NiAl-BASED MATERIALS

9.1 Introduction

Creep resistance of NiAl is one of the most important properties required for its extended use at high temperatures. Consequently, the review of creep properties is divided into two main parts. First, the creep behavior of the binary, single phase intermetallic is presented, and the basic creep mechanisms discussed. The second half of this section will describe strategies and attempts at improving the creep strength of NiAl-based intermetallics.

9.2 Creep of Binary NiAl

Creep behavior in B2 aluminides follows that for metals and alloys and can be divided into primary, secondary and tertiary stages. The shape of the primary creep curve provides an important clue for

determining the deformation mechanisms, although the secondary stage is usually of more interest because it tends to comprise the majority of the creep life. The tertiary stage has rarely been examined in NiAl-based materials, primarily because most testing to date has been in compression, where tertiary creep is suppressed or eliminated.

The second stage or steady-state creep rate $\dot{\varepsilon}$ is usually expressed as a form of the Dorn equation (ref. 307):

$$\dot{\varepsilon} = A \ \sigma^n \ \exp(-Q/RT)$$

where σ is the applied stress, n is the stress exponent, Q is the activation energy for creep, R is the gas constant, T is the absolute temperature, and A is a constant which takes into account such variables as microstructure and stacking fault or anti-phase boundary energy. The values for n and Q are dependent on the operative deformation mechanisms within a given temperature and stress regime. An important point implied by the above creep relationship is that the steady-state creep rate is independent of test mode. Although creep tests have traditionally been performed under constant load or constant stress conditions, with the steady state strain rate measured as the dependent variable, it is equally valid to impose a constant strain rate and measure the steady state flow stress as the dependent variable. This has been experimentally verified for a number of systems (refs. 308 and 309) with known exceptions that can be traced to microstructural instabilities (ref. 310).

9.2.1 Dislocation creep.—Dislocation creep mechanisms are well described by the above semi-empirical equation, although the details of the mechanisms themselves are being continuously refined (ref. 311). For single-phase metals and alloys, dislocation creep can be classified as either of two main types, known as Class M, or pure metal type, and Class A, or alloy type (refs. 311 to 313). Class M creep is characterized by glide being much faster than climb, and thus creep becomes controlled by the rate of climb past substructural obstacles. Class A creep is often called viscous glide controlled creep, since the glide of dislocations is restricted by solute atoms or perhaps by a high lattice friction stress due to long range order. This reduced glide mobility is the limiting creep process, while climb can occur readily. These two types of behavior can be distinguished by several criteria including the stress exponent, the shape of the primary creep curve, dislocation substructure and the response of the material to stress or strain rate transients (refs. 307 and 311 to 315).

A summary of the stress exponents and activation energies determined by various authors (refs. 169, 235, and 316 to 322) for creep of NiAl is presented in table XI. For NiAl, the average value for the activation energy of creep is approximately 314 kJ/mol. This value is reasonably close to the higher end of the range of activation energies determined in diffusion experiments (refs. 136, 295, 297, and 298). Correction for the temperature dependence of the elastic modulus, using dynamic moduli (refs. 15 and 90) results in reductions in Q ranging from 20 to 30 kJ/mol, thus bringing the value for Q within the range of data for diffusion displayed in figure 41.

Figure 42 presents a summary of measured and interpolated creep data for binary NiAl at 1175 K (refs. 235, 317, 319 to 321, and 323). Most of the data fall within reasonable agreement, with no more than about a factor of 5 difference in creep rate at a given stress level, and similar stress exponents that are on the order of 4.5 to 6. The strengths reported by Vandervoort et al. (ref. 235) appear to be abnormally weak for no known reason. Figure 43 is a compilation of stress exponents as a function of temperature and includes studies (refs. 166, 170, 235, and 316 to 319, 321, and 322) on materials having a wide variety of grain sizes, including single crystals. Below about 1000 to 1100 K, the stress exponent rises significantly, indicating a transition between high temperature creep and lower temperature behavior. Discounting the abnormally weak material of Vandervoort et al. (ref. 235), this figure reveals that

between approximately 1100 to 1400 K, the values for n cluster between 5 and 7. Although a stress exponent of 7 is higher than typical, such high values have been observed in several Class M materials (refs. 324 and 325). Observations of subgrain formation after high temperature deformation have been made by numerous workers (refs. 138, 166, 168, 177, and 316 to 320) and normal primary creep behavior, under both constant load and constant crosshead speed conditions, has also been observed (refs. 166, 316 to 318, and 326). Additionally, the strain rate transient tests performed by Yaney and Nix (ref. 326) are consistent with Class M behavior. So in summary, the vast majority of results from a wide variety of sources indicate that high temperature creep in NiAl is climb controlled.

Figure 44 is a plot of steady state creep rate as a function of Al content for NiAl for three different temperature and stress conditions. Unlike most properties for NiAl, there is a broad range in composition between about 45 and 52 at % Al, where the creep rate is roughly independent of stoichiometry (refs. 235, 317, 319, and 327). The largest difference in creep rates within this range of compositions is about a factor of 5. Only at very low Al contents is NiAl noticeably weaker (refs. 183 and 327). This is most easily explained by the lower melting points of these compositions, which in turn implies a higher diffusivity, although the diffusivity data summarized in figure 40 would imply a more significant effect. These trends as a function of stoichiometry are reversed from those observed at lower temperatures (ref. 216), where defect hardening predominates over the effects of diffusion.

Although dislocation creep mechanisms are generally considered to be independent of grain size, studies of NiAl and FeAl (ref. 328) have demonstrated that elevated temperature creep strength can sometimes be improved by decreasing the grain size. In the case of NiAl, the data in figure 45 (refs. 316 and 322) illustrate that material with a grain size below $\simeq$10 μm is capable of improved creep resistance. Since NiAl is a Class M material which exhibits subgrain boundaries that act as obstacles to dislocation motion, this behavior can be expected when the grain size is finer than the equilibrium subgrain size (ref. 316). Unfortunately, the effectiveness of fine grain size is restricted to lower temperatures and/or higher stresses, where diffusional creep mechanisms have less influence.

9.1.2 Diffusional creep.—Time dependent deformation can occur by stress-assisted vacancy flow at stresses which are too low for dislocation processes to be significant. Creep by these diffusional mechanisms such as Nabarro-Herring or Coble creep is attributed solely to movement of vacancies from sources to sinks, which are usually grain boundaries of different orientations with respect to the applied stress. These mechanisms are characterized by stress exponents of n = 1 and a clear dependence of creep strength on grain size, with large grained materials being more creep resistant. Rudy and Sauthoff (ref. 320) provided the most convincing evidence for diffusional mechanisms in a B2 Ni-20Fe-50Al alloy, namely a stress exponent of 1. Additionally, there is some evidence in binary NiAl at temperatures above 1300 K and at low strain rates, where grain growth during the creep test resulted in coarser grained material having higher strengths (ref. 317). Figure 42 displays some recent data (ref. 323) showing a low stress exponent that may indicate some grain boundary assisted mechanism operating at low stresses. In addition, figure 45 illustrates that the fine grained material begins to lose its advantage at stresses below approximately 30 MPa, as indicated by the change in slope. Therefore, the limited data generated to date on high temperature ($\geq$1300 K) creep in polycrystalline NiAl indicates that diffusional creep is possible.

9.3 Strategies for Improving Creep Resistance

There is a decrease of about 8 orders of magnitude in creep rate as progressive alloying changes are made from pure Ni to a Ni-base superalloy, and the formation of a second phase is one of the major reasons for this improvement (ref. 308). Similar improvements will be necessary for nickel aluminides to

compete with current superalloys. As a measure of progress to date, creep properties of NiAl-based alloys, which were generated primarily in compression, will be compared to the tensile creep response of NASAIR 100, a first generation single crystal superalloy (ref. 330).

9.3.1 Solid solution strengthening.—The role of solid solution hardening in NiAl at 1200 K is summarized in figure 46 (refs. 317, 320, 322, 329, and 330 to 332). Two data sets for binary NiAl are shown which cover the range in creep strength seen in the numerous studies, with both having a stress exponent of $\simeq 5$. All of the solid solution alloys show some improvements in strength, but they also exhibit a change in n to a value near 3 or 4. Thus it appears that these solute additions have changed creep to a viscous drag mechanism, in a manner very similar to that which occurs when alloying elements are added to pure metals. In fact, in one recent study (ref. 333), a transition from Class M to Class A behavior was observed in the B2 compound Ni-20Fe-30Al as a function of applied stress, and the transition appeared to be well described by current theories developed for disordered solid solutions (refs. 312 and 313). However, because of this new stress exponent, the strength improvements over binary NiAl were only large at high stresses, and in the lower stress regime the advantage was reduced or eliminated. Finally, it is of interest to note in figure 46 that one of the largest strengthening effects was produced by an addition of only 0.05 at % Zr (ref. 322). This sensitivity to small differences in composition might be the main reason for discrepancies in mechanical properties among various published results for nominally "binary" NiAl. While it appears that solid solution hardening does provide some creep strength improvements over the binary alloy, this concept is inadequate by itself and must be used in combination with other strengthening mechanisms to compete with superalloys.

9.3.2 Precipitation strengthening.—Significant improvements in creep strength of NiAl by precipitation hardening were first demonstrated by Polvani et al. (ref. 334) by adding Ti to form a two-phase mixture of NiAl and Heusler phase Ni_2AlTi. Additional Heusler phases and other intermetallic compounds such as Laves (e.g., NiAlTa) can be formed with ternary additions such as Nb, Ta, Hf, Zr, and V. The creep properties of some Ti- and Ta-containing alloys are presented in figure 47. It is evident that these materials are reasonably strong, but again, extrapolation to low stresses shows the advantage diminishing. The reasons for the low stress exponent in these alloys is not entirely clear, since most creep resistant, two-phase alloys exhibit significantly higher stress exponents than the matrix phase. In most cases, the microstructures of the ternary alloys were probably not optimized. For example, if the second phase is not fine enough, effective strengthening would not be expected. Equally valid explanations may be that the observed n values represent a superposition of several deformation mechanisms, including diffusional creep, and/or that coarsening of the precipitate phase results in less strengthening in the low stress/long life regime. By analogy to the superalloys, optimizing the creep strength requires a balance of the compositions of the two phases, the precipitate volume fraction and the size and distribution of the precipitates.

A further example of the sensitivity of creep strength to microstructure in NiAl-based alloys is shown in figure 48 (refs. 317, 330, 332, 335, and 336). The alloys with Nb-rich Laves phase behave similarly to the other alloys in figure 47, but it is also evident that by changing the processing of the alloy from casting plus extrusion to directional solidification, both the creep strength and the stress exponent were changed even when the second phase was only partially aligned (ref. 336).

Darolia (ref. 62) has recently reported promising tensile creep-rupture properties for single crystals containing Heusler precipitates. A comparison of the creep response of NiAl+1Hf in both polycrystalline (ref. 337) and single-crystal (ref. 338) form is exhibited in figure 49. The polycrystalline material, which is strengthened by Heusler precipitates, shows behavior similar to the other ternary alloys in figure 47. However, the single-crystal version is not only stronger but displays a significantly different stress dependence. This implies that the polycrystalline version is deforming by a superposition of dislocation

37

and grain boundary mechanisms. However, one complicating factor was the presence of approximately 200 wt % ppm Si in the single crystal that resulted in the formation of a significant quantity of G-phase precipitates (refs. 339 and 340). The influence of Si pickup and the presence of the G-phase on creep of single-crystal NiAl has not been determined.

Anisotropy in creep strength is another important effect that must be considered with single crystals. Certain orientations may possess higher creep strength, which could be exploited in applications such as turbine blades. For creep of single phase binary compounds at temperatures above approximately 1050 K, some research has found significantly higher strength for the hard orientation (refs. 166 and 176) whereas a significant anisotropy has not been observed in other work (ref. 183 and 216). A probable reason for these discrepancies lies in differences in sample geometry and the use of tension versus compression testing. Subgrain formation, which has been shown to be an important factor in the creep response of NiAl, might be delayed when single crystals are tested. In single crystal form, the limited number of slip systems in NiAl would prevent or delay the onset of intersecting slip which is necessary for subgrain formation. In fact, Strutt and Dodd (ref. 341) have reported that subgrain formation was not observed in single crystals unless short aspect ratio compression specimens were used. In any case, the degree of anisotropy would be expected to be quite different in precipitation-strengthened alloys, where the dislocation structure would be on a much finer scale.

9.3.3 Dispersion strengthening.—By rapid solidification, very fine dispersions of second phases, with diameters on the order of 20 to 50 nm, can be formed. These particles are generally resistant to coarsening due to their very low solubility in the matrix. For NiAl, both pure elements such as W and Mo and various carbides or borides are candidates for this type of strategy. These dispersoids also tend to pin grain boundaries and result in significant grain refinement (refs. 129, 342, and 343). Figure 50 reveals that the additions of W (ref. 129) and TiC (ref. 342) had very little strengthening effect, and TiB_2 (ref. 342) showed about an order of magnitude improvement over binary NiAl. However, this degree of strengthening can be achieved simply due to grain refinement similar to that shown in figure 45, or due to solid solution strengthening by B. Consequently, significant dispersoid/dislocation interactions are not expected in these alloys.

More interesting are the improvements achieved with HfB_2 (ref. 344) and HfC (refs. 342 and 343), dispersions, which are considerably stronger than binary NiAl. In the case of HfC-strengthened NiAl, there was some indication of a threshold stress at approximately 50 MPa below which no creep occurred (ref. 343). However, more recent work has shown that this apparent threshold stress is the result of dynamic grain growth which is a function of testing conditions (refs. 310 and 345). These new data indicate that for HfC-strengthened NiAl, coarse-grained material is more creep resistant than the finer grained product, which is opposite of the trend observed in the binary alloy. In the case of the HfC strengthened material, it is possible the grain interiors have been strengthened sufficiently such that diffusional creep mechanisms were occurring at similar rates. The mechanism for the improved strength is related primarily to the interaction of the dispersoids with mobile dislocations (refs. 342 and 343) and subgrain boundaries (ref. 344). However, it is probably not a coincidence that the two most effective dispersoids contained Hf, which by itself is a very potent solid solution strengthening agent (ref. 337).

To date, the use of rapid solidification to dispersion strengthen NiAl has not yet provided sufficient strengthening to compete effectively with superalloys. The potential for improvement exists, primarily in the areas of optimizing the dispersoid volume fractions, and in devising the thermomechanical processing schedules needed to produce the desired grain structures that have proven more successful in the oxide dispersion-strengthened Ni-base alloys (ref. 346).

9.3.4 Reaction milled composites.—An unusual but effective example of a composite is the AlN dispersoid-reinforced NiAl which can be produced by milling NiAl powder in liquid nitrogen (refs. 347 to 350). This process produces very fine dispersoids, on the order of 50 nm, at relatively high volume fractions of approximately 10 percent. The particles are not uniformly distributed, but are clustered along prior particle boundaries. As can be observed in figure 51, 1300 K creep strengths approaching that of NASAIR 100 were obtained. After correcting for density, the deformation resistance of the superalloy and NiAl/AlN are nearly equivalent. Also of interest is that the properties of extruded material, where the particle-rich regions are strung out along the extrusion direction, were roughly equivalent to HIP-consolidated material, where the particles are not aligned but still segregated. The reasons for the exceptional properties of this type of second phase reinforcement are not currently understood although the promising results in compression certainly warrant more extensive testing in tension. Furthermore, the oxidation resistance of this material is superior to superalloys and almost equivalent to that of reactive-element doped NiAl (ref. 351), making this one of the first truly promising NiAl-based structural alloys.

9.3.5 Discontinuous reinforced composites.—Another approach to strengthening is through the use of composites containing discontinuous reinforcements. These reinforcements are typically larger in size and present in higher concentrations than that found in dispersion-strengthened materials. One example is TiB_2 particulate reinforced NiAl containing 1-μm diameter particles produced by an exothermic reaction process (refs. 318, 352, and 353). Figure 52 demonstrates that such composites do show improvements in strength that scale with the amount of reinforcement (refs. 317, 318, and 330). It is important to note that the stress exponents are all high, which indicates that the dislocation substructure is refined and stabilized by the second phase when compared to the same matrix without the reinforcement. Evidence for this contention has been provided by TEM (ref. 318), where the creep deformation structure was characterized by subgrain boundaries pinned by the particles, in combination with a much higher dislocation content within the subgrains.

Another type of discontinuous reinforcement which has been examined in NiAl is Al_2O_3 whiskers (refs. 354 and 355). The whiskers, which had an average aspect ratio of approximately 7.5, were added by mechanical blending at volume fractions ranging from 0 to 25 percent. Some improvements in creep resistance are seen in figure 53, but the whiskers are not as effective as TiB_2 particles (fig. 52) in increasing strength. Also, the stress exponents of the NiAl-Al_2O_3 composites were about the same as that of the matrix, which indicates that deformation is controlled by flow in the matrix, as predicted by several models of composite strengthening (ref. 356). These models would predict further improvements in creep strength by increasing the aspect ratio of the whiskers. However, because some whisker breakage after testing was observed (ref. 354), higher strength whiskers will also be needed. Control of whisker distribution and alignment, and whisker damage during processing, are major concerns with this type of composite.

Finally, hybrid composites containing both TiB_2 particulates and Al_2O_3 whiskers have been made and have demonstrated that these strengthening concepts were additive (ref. 354). It should be noted, however, that combining creep-strengthening mechanisms is not always effective. For example, there is no additional benefit in creep strength from adding TiB_2 particles to a Heusler phase (Ni_2AlTi) reinforced NiAl alloy (refs. 357 and 358). In fact the TiB_2-reinforced material was weaker under creep conditions than the unreinforced NiAl-Ni_2AlTi alloy.

9.3.6 Continuous reinforced composites.—A final strategy is the reinforcement of NiAl with continuous fibers. Such composites can either be natural, such as directionally solidified eutectics, or artificially fabricated, using fiber-matrix combinations not achievable through eutectic solidification. The early work by Walter and Cline (ref. 359) has shown that a eutectic consisting of α-Cr rods in a NiAl matrix possessed some promising creep properties, as indicated in figure 54. However, good creep strength is only maintained as long as the Cr rods are continuous in nature, and not just short fibers aligned parallel

to the growth direction (ref. 360). Rod-type and lamellar eutectic microstructures can also be produced in NiAl by directional solidification with Mo (ref. 361), W (refs. 129 and 229), Re (ref. 362), V (ref. 363), and NiAlNb (ref. 336) phases, and these may also prove to be advantageous.

Artificial composites have been made by a powder metallurgy approach (ref. 364) where either W, Mo, or Al_2O_3 fibers have been incased in an intermetallic matrix by hot pressing. These composites have been tested in bending (refs. 365 to 367) and substantial strength improvements in the NiAl/W and NiAl/Mo systems over the matrix have been observed, whereas the NiAl/Al_2O_3 composites did not show any strengthening. The differences in strength were traceable to degrees of bonding, where load could be transferred to the strongly bonded refractory metal fibers but not to the weakly bonded Al_2O_3. However, the composite with weakly bonded fibers did show evidence of toughening, and thus a hybrid concept of using two types of reinforcement is one way to achieve a balance of properties (ref. 366). Further testing of these composites is required to ascertain whether the high strengths will be maintained in creep tests, and whether they can survive in an environment involving thermal cycling.

9.4 Summary

High temperature creep deformation in NiAl appears to be satisfactorily described by type M, or dislocation climb controlled creep, as all of the major defining characteristics of this class of creep have been observed. Stoichiometry variations appear to be relatively unimportant, especially between 45 and 52 at % Al, a fact which is surprising based on the relatively large effect of stoichiometry on diffusion characteristics and many other properties. Diffusional creep mechanisms appear to become important at low stresses and above about 0.7 T_m, although they appear to be more prominent in ternary alloys and in materials which have been strengthened against dislocation creep.

A general observation concerning NiAl creep literature is the heavy reliance on compression testing. Compression tests are very valuable in isolating deformation mechanisms and for providing an indication of the maximum creep strength achievable in a given material. However, several technologically important topics such as grain boundary cavitation, necking, and tertiary creep can best be examined in tension creep experiments.

Various strategies to improve the creep resistance of NiAl have been attempted although none have been fully optimized. Of these attempts, both solid solution and precipitation hardening have shown progress, but the low stress exponents of these materials result in less attractive properties at lower stresses and creep rates. However, recent advances using precipitate strengthening in single crystals have shown promise. Rapid solidification has shown only small improvements in strength, whereas TiB_2 particulates and Al_2O_3 whiskers showed larger but still insufficient advances. The NiAl/AlN composite has some of the best creep properties to date, comparable to the Cr containing directionally solidified eutectic. Finally, the strengthening which can be achieved with continuous fibers is dependent on the choice of reinforcing fiber as well as the matrix/fiber bond strength.

10. ENVIRONMENTAL RESISTANCE

10.1 Isothermal and Cyclic Oxidation

The excellent oxidation resistance of NiAl based materials is well known and has been exploited for many years in the form of coatings for Ni-base superalloys (refs. 368 and 369). This behavior stems from the easy formation and slow growth rate of a protective Al_2O_3 scale. Under isothermal conditions, scale

formation often involves a transient growth stage followed by a steady-state regime. The transient stage involves the formation of transition oxides, including NiO, $NiAl_2O_4$, and metastable γ- and θ-Al_2O_3 (refs. 370 to 372). Observations of NiO are usually found only in alloys with lower Al content (ref. 371), and $NiAl_2O_4$ is favored at very low temperatures where the slower growth rates of Al_2O_3 allows for the less thermodynamically stable phase to form. Mature scales typically follow a parabolic growth law but the form of the scale is dependent on temperature. At temperatures near 1200 K, θ-Al_2O_3 appears to be the predominant oxide in mature scales (refs. 370, 373, and 374), but at higher temperatures α-Al_2O_3 is formed. The growth rate of θ-Al_2O_3 is higher than that of α-Al_2O_3, such that oxidation at approximately 1200 K is faster than at higher temperatures as demonstrated in figure 55 (refs. 373 and 374). Transformation from the transition oxides to the mature α-Al_2O_3 scale involves a volume change of 13 percent, which results in cracking of the oxide, which is healed by new α-Al_2O_3 formation (refs. 370 and 373). Evidence in the form of ^{18}O tracer diffusion studies (refs. 375 and 376) and scale morphologies (refs. 370 and 373) indicate that the transition oxides grow primarily by outward cation diffusion, whereas the mature oxide grows by a combination of both outward cation and inward oxygen diffusion, with a strong influence from short circuit diffusion paths. This is in contrast to MCrAl alloys, where primarily inward-growing scales are found (refs. 377 and 378).

Alloy stoichiometry appears to have only minor effects on isothermal oxidation rates. Hutchings and Lorretto (ref. 379) found that increasing the Al level from 42 to 50 percent resulted in an order of magnitude reduction in oxidation rate. More recent work (ref. 380) has shown that, although differences on the order of a factor of 10 are observed, the oxidation rates did not vary monotonically with Al level (fig. 56). Instead, the oxidation rate increases by close to an order of magnitude after as little as a 3-percent drop in Al content from the stoichiometric composition and then is relatively constant over a very broad range of Al levels. Other factors can also affect oxidation; for example polished surface finish and the use of single crystals can each lower oxidation rates by about a factor of 2 (refs. 381 and 382).

The accelerated oxidation rates at intermediate temperatures which are due to transient oxide growth, are still relatively low and are not considered as problematic. However, some indications of "pest" attack at intermediate temperatures have been observed in the past. Defined as a disintegration into powder due to exposure to oxygen, pesting in air has been observed in Al-rich compounds (ref. 383). However, these compositions are very brittle and therefore of limited engineering interest. Mild pesting reactions have also been induced in the laboratory in other compositions of NiAl by testing at very low partial pressures of oxygen (ref. 374).

Cyclic oxidation testing is significantly more severe than isothermal oxidation and more closely approximates actual service conditions. During the cooling portion of the cycle, the difference in thermal expansion coefficients between metal and oxide results in high stresses at the oxide/metal interface that can lead to scale spallation. Figure 57 has several examples of some weight versus time curves for different metallic materials and various NiAl alloys under cyclic oxidation conditions. Examples of materials which experience weight gains due to oxide growth and weight losses due to spalling are exhibited. This figure also demonstrates that the excellent performance of NiAl compared to conventional oxidation resistant alloys is only achieved when reactive elements such as Zr are added. The damage due to spalling usually accelerates as the number of cycles accumulates, such that lifetimes can be very short compared to isothermal conditions. NiAl alloys are also more sensitive to stoichiometry under cyclic conditions compared to isothermal tests (ref. 384). For long-term cyclic conditions it is best to have a NiAl alloy containing at least 45 percent Al and for even a few cycles it is best to stay above 40 percent Al to avoid significant oxide spalling.

The behavior of NiAl alloys under cyclic oxidation conditions are sufficiently understood that life prediction can now be made with reasonable accuracy (refs. 384 to 387). Useful lives are usually defined as

time needed to obtain a given amount of metal recession, a given amount of weight change (typically 5 to 10 mg/cm^2), or a transition to a less protective oxide (ref. 384). In the case of NiAl, severe cyclic oxidation exposure eventually leads to Al depletion and subsequent formation of NiO and NiAl$_2$O$_4$, which can be used as a criteria to define life. This Al depletion also implies that Ni-rich aluminides fail sooner, which has been confirmed experimentally (refs. 381 and 384).

Finally, it is well known that rare-earth or oxygen-active dopants have a very large beneficial effect on the oxidation resistance of MCrAl, NiAl, and superalloy materials. Y, Hf, and Zr are the main additions that have been studied, although other elements such as Ce and La are expected to behave similarly. Beneficial effects in NiAl are observed when elemental additions are made to the melt at about the 0.1 at % level (refs. 373, 380, and 384 to 386), when present as dispersed Y-rich oxides (refs. 351 and 385), or when incorporated in the surface by ion implantation (ref. 382). These additions decrease the isothermal oxide growth rate (refs. 373, 382, and 385), apparently through a decrease in diffusion through the scale. However, the main benefit of these additions is observed under cyclic conditions, where they dramatically increase scale adherence (refs. 380 and 384 to 386). This has been attributed to several causes (refs. 382 and 388 to 390): oxide "pegging," elimination of voids at the interface, increased scale plasticity, and changes in the chemical bond between the oxide and metal. Although a complete answer probably involves a combination of several factors, it has been shown that one major effect is the role of these elements in preventing S segregation to the interface (refs. 388 to 390) or to interfacial voids (ref. 374) which can degrade bonding.

10.2 Hot Corrosion Resistance

Hot corrosion due to molten sulfate deposits has been studied because of the importance of this type of attack in marine, industrial, and aircraft gas turbine materials. This attack is most prominent at intermediate temperatures (900 to 1300 K), and can occur by a number of mechanisms (ref. 391). For example, molten deposits containing Na$_2$SO$_4$ can cause fluxing reactions that dissolve the protective oxides. Additionally, the formation of sulfides beneath the deposits, and subsequent oxidation of these sulfides, can be quite detrimental to surface integrity (refs. 391 and 392).

Binary NiAl is not particularly resistant to hot corrosion, as the rate of corrosion can far exceed the oxidation rate at equivalent temperatures (refs. 392 to 394). This occurs because the level of Al depletion from the specimen is much faster causing the less resistant γ' phase to form early during exposure. Chromium was found to increase the hot corrosion resistance of NiAl and Y added to Cr-doped NiAl resulted in marginal but additional improvements in corrosion resistance (ref. 395). However, Cr additions were found to be detrimental to sulphidation resistance of the NiAl phase when the test environment consisted of He-S$_2$ gas mixtures with very low partial pressures of oxygen (ref. 394). When alloyed with Cr in sufficient quantity to form MCrAl-based alloys in the $\gamma + \gamma' + \beta$ phase field, these materials can result in very good performance in both laboratory and burner rig tests (refs. 391, 392, and 394).

11. APPLICATIONS

A brief description of potential applications for NiAl is presented below with the main purpose of reviewing those combinations of properties which are responsible for raising interest in NiAl for future utilization. Our hope is that by reviewing those properties that make NiAl unique compared to other materials, new and totally unrelated applications may become apparent.

11.1 Coatings

Primarily because of lack of ductility, aluminide intermetallic compounds, including NiAl, have not been used in the past for load bearing applications. But because of their excellent oxidation resistance they have been used as coatings over a ductile base material (ref. 396). Additionally, the high melting point and especially a high thermal conductivity were original motivating factors in the use of NiAl based coatings (ref. 61). A high thermal conductivity was considered particularly important since this meant that hot spots on the coating were eliminated, significantly increasing the potential use temperature of the coated component (ref. 61). The most common example of this application is the use of NiAl-base coatings on virtually all superalloy turbine blades and vanes (refs. 62, 368, and 369). Also, NiAl has shown resistance to liquid metal corrosion, particularly alkali metals, and may someday see use as the base for a protective coating for steel components operating in contact with molten low-melting metals (ref. 397). However, results in this particular area, while promising, are still very preliminary.

11.2 High Temperature Structures

The demand for new structural materials to replace superalloys in advanced jet engines and other high performance aerospace applications has been one of the strongest driving forces behind the development of intermetallic, ceramic and composite materials. These efforts have been necessitated primarily by the need for greater engine operating efficiencies. However, this goal can only be met by materials that possess a balanced range of properties. NiAl offers a number of distinct advantages over conventional superalloys including: (1) significantly higher melting point, (2) density which is about two-thirds that of a typical superalloy (ref. 58), (3) specific modulus which is about 35 percent greater than the stiffest superalloys (refs. 15 and 86), (4) a three- to eight-fold advantage in thermal conductivity (refs. 58 and 61), and (5) cyclic oxidation resistance that is superior to any existing high temperature alloy (refs. 351, 380, and 386).

The immediate benefits that would be derived from using NiAl in engine applications would include reduced cooling requirements, reduced weight, and higher operating temperatures. Together these benefits would lead to increased engine thermodynamic efficiency and an increased thrust-to-weight ratio. The weight savings alone would be significant. For example, design studies have shown that the replacement of superalloy turbine blades with NiAl could lead to a 40 percent reduction in the weight of the rotor system (blade and disk) (ref. 62).

Presently, an extensive program is underway at General Electric to develop single crystal NiAl alloys specifically for use as a high-pressure turbine blade material (refs. 62, 264, and 398). Two possible routes for producing the turbine blades have been proposed. One route involves the casting of single crystal ingots from which solid blades can be machined by conventional machining processes such as electrical-discharge machining, electrochemical machining and grinding processes. An example of a high pressure turbine blade manufactured by this process is shown in figure 58. The other technique for producing turbine blades involves casting a blade to near net shape, splitting the blade into two halves so that intricate cooling passages can be machined into the component and bonding the two halves back together.

11.3 Electronics

The most recent group to take interest in NiAl is the electronics industry. The incorporation of metallic (NiAl) films embedded in semiconductor device structures is being pursued by several research laboratories as evident from the recent flurry of publications in this area (refs. 399 to 415). With the use

of NiAl, it is hoped that unique metal-semiconductor heterostructures can be fabricated with the goal of utilizing the combined transport properties of metals and semiconductors (ref. 403). For example, (Al,Ga)As/NiAl/(Al,Ga)As heterostructures have been fabricated by molecular beam epitaxy (refs. 404 to 408). These heterostructures pave the way for the fabrication of a host of new electronic and photonic devices such as buried metal-base transistors, buried-metal interconnects and buried ground planes (refs. 399, 406, and 409). The interface structure and stability of these heterostructures has been theoretically modeled by Joo et al. (ref. 410).

One of the primary properties that has driven the development of NiAl as a high temperature structural material is also important to the development of this intermetallic as an electronic material. Namely, stability at elevated temperatures which is required for semiconductor overgrowth processes (ref. 411). Also critically important is a close lattice match with semiconductor materials to allow epitaxial growth at both metal-on-semiconductor and semiconductor-on-metal heterojunctions. Serendipitously, stoichiometric NiAl has a close lattice parameter match with (Al,Ga)As (refs. 399 and 412), and (In,Ga)As (ref. 412) compounds and can be further modified through changes in stoichiometry (fig. 3). Also, NiAl is a very promising candidate for a low-leakage rectifying contact to GaAs because NiAl overlayers form Schottky barrier heights on the order of 0.9 to 1.0 eV which is significantly higher than most metals on GaAs (refs. 413 and 414). The barrier height can be increased to 1.15 to 1.35 eV when an AlAs layer is deposited between NiAl and GaAs creating a NiAl/AlAs/GaAs system (ref. 415). This later value is nearly a factor of two larger than exhibited by most metal/GaAs interfaces.

12. CONCLUDING REMARKS

Almost all the physical and mechanical properties of β-phase NiAl are dependent on stoichiometry within the single phase regime, with most properties exhibiting a minimum or maximum at (or very near) the stoichiometric composition. Differences in properties as a function of composition exist because of the defect structure necessary to maintain the B2 crystal structure. What is generally not appreciated is that many properties determined on nonstoichiometric compositions might not be any more representative of the inherent properties of the stoichiometric compound Ni-50Al than those of a solid solution alloy are representative of the pure solvent metal.

It would also appear that most discrepancies in composition-dependent properties can be attributed to errors in measuring the composition of the alloy rather than the measurement of the specific properties. Compositional measurement is probably the most under appreciated problem affecting the materials scientist today and is one area in which researchers need to be aware of the limitations imposed by the various methods. In fact, analyzing composition of alloys to any high degree of accuracy is probably the least discussed problem affecting NiAl research today.

ACKNOWLEDGMENTS

REFERENCES

1. Barrett, C.; and Massalski, T.B.: Structure of Metals: Third ed., Chap. 10. Pergamon Press, New York, 1980.

2. Westbrook, J.H.: Intermetallic Compounds. Chap. 10. Krieger Pub. Co., Inc., Huntington, New York, 1977.

3. Singleton, M.F.; Murray, J.L.; and Nash, P.: Al-Ni (Aluminum-Nickel). Binary Alloy Phase Diagrams. T.B. Massalski, ed., American Society for Metals, Metals Park, OH, 1986, pp. 140-143.

4. Dobbs, J.: General Electric Aircraft Engine Group and M.V. Nathal and R.D. Noebe: NASA Lewis Research Center, unpublished research (1990).

5. Taylor, A.; and Doyle, N.J.: Further Studies on the Nickel-Aluminum System. I. The β-NiAl and δ-Ni$_2$Al$_3$ Phase Fields. J. Appl. Cryst., vol. 5, 1972, pp. 201-209.

6. Bradley, A.J.; and Taylor, A.: An X-ray Analysis of the Nickel-Aluminum System. Proc. R. Soc. (London), vol. A159, 1937, pp. 56-72.

7. Guseva, L.N.: On the Nature of the β-phase in the System Ni-Al. Dokaldy Akad. Nauk. S.S.S.R., vol. 77, 1951, pp. 415-418.

8. Cooper, M.J.: An Investigation of the Ordering of the Phases CoAl and NiAl. Philos. Mag., vol. 8, 1963, pp. 805-810.

9. Georgopoulos, P.; and Cohen, J.B.: The Defect Structure and Debye Waller Factors vs. Composition in β Ni$_{1\pm x}$Al$_{1\pm x}$. Scripta Metall., vol. 11, 1977, pp. 147-150.

10. Hughes, T., et al.: X-ray Diffraction Investigation of β-NiAI Alloys. J. Appl. Phys., vol. 42, 1971, pp. 3705-3716.

11. West, G.W.: Nuclear Magnetic Resonance and Lattice Parameter Measurements in β-NiAl. Phys. Status Solidi. (A), vol. 20, 1973, pp. 647-651.

12. Jacobi, H.; and Engell, H.J.: Defect Structure in Non-Stoichiometric β-(Ni,Cu)Al. Acta Metall, vol. 19, 1971, pp. 701-711.

13. Taylor, A.; and Doyle, N.J.: Further Studies on the Nickel-Aluminum System. II. Vacancy Filling in β and δ-Phase Alloys by Compression at High Temperatures. J. Appl. Cryst., vol. 5, 1972, pp. 210-215.

14. Fraser, H.L., et al.: Oxidation-induced defects in NiAl. Philos. Mag., vol. 28, 1973, pp. 639-650.

15. Harmouche, M.R.; and Wolfenden, A.: Temperature and Composition Dependence of Young's Modulus in Polycrystalline B2 Ni-Al. J. Test. Eval., vol. 15, 1987, pp. 101-104.

16. Fox, A.G.; and Tabbernor, M.A.: Bonding and the Physical and Mechanical Properties of β-NiAl. High Temperature Intermetallics, The Institute of Metals, London, England, 1991, pp. 219-221.

17. Cooper, M.J.: The Electron Distribution in the Phases CoAl and NiAl. Philos. Mag., vol. 8, 1963, pp. 811-821.

18. Fox, A.G.: The Electron Charge Distribution of β'-NiAl. Electron Microscopy and Analysis, G.J. Tatlock, ed., Adam Hilger Ltd., Bristol, England, 1985, pp. 379-382.

19. Fox, A.G.; and Tabbernor, M.A.: The Bonding Charge Density of β'-NiAl. Acta Metall. Mater., vol. 39, 1991, pp. 669-678.

20. Fu, C.L.; and Yoo, M.H.: First-Principles Investigation of Mechanical Behavior of B2 Type Aluminides: FeAl and NiAl. High Temperature Ordered Intermetallic Alloys IV, L.A. Johnson, D.P. Pope, and T.O. Steigler, eds., MRS, Pittsburgh, PA., 1991, pp. 667-672.

21. Fu, C.L.: The Role of Electronic Structure in the Mechanical Behavior of Aluminides. Proceedings of the International Symposium on Intermetallic Compounds: Structure and Mechanical Properties, O. Izumi, ed., Japan Institute of Metals, Sendai, Japan, 1991, pp. 387-396.

22. Lui, S.-C., et al.: Electronic Structure of NiAl. Phys. Rev. B, vol. 42, 1990, pp. 1582-1597.

23. Ayushina, G.D.; Levin, E.S.; and Gel'd, P.V.: The Density and Surface Energy of Liquid Alloys of Aluminum with Cobalt and Nickel. Russ. J. Phys. Chem., vol. 43, 1969, pp. 1548-1551.

24. Petrushevskii, M.S.; Levin, E.S.; and Gel'd, P.V.: Viscosity and Interatomic Interaction Energy in Nickel-Aluminum Melts. Russ. J. Phys. Chem., vol. 45, 1971, pp. 1719-1721.

25. Kubaschewski, O.: The Heats of Formation in the System Aluminum+Nickel+Titanium. Faraday Soc. Trans., vol. 54, 1958, pp. 814-820.

26. Hultgren, R., et al.: Al-Ni. Selected Values of Thermodynamic Properties of Binary Alloys, American Society For Metals, Metals Park, OH, 1973, pp. 191-195.

27. Oelsen, W.; and Middel, W.: The Thermochemistry of Alloys. I. Direct Determination of the Heats of Formation of the Alloy Series Cobalt-Silicon, Iron-Aluminum, Cobalt-Aluminum, Nickel-Aluminum, Copper-Aluminum and Antimony-Zinc for the Cast State. Mitt. Kaiser Wilhelm Inst. Eisenforsch., vol. 19, 1937, pp. 1-26.

28. Henig, E.-T.; and Lukas, H.L.: Kalorimetrische Bestimmung der Bildungsenthalpie und die Beschreibung der Fehlordnung der Geordneten β-Phase $(Ni,Cu)_{1-x}Al_x$. Z. Metallk, vol. 66, 1975, pp. 98-106.

29. Dannohl, H.D.; and Lukas, H.L.: Kalorimetrische Bestimmung der Bildungsenthalpien Einiger Intermetallischer Phasen. Z. Metallk., vol. 65, 1974, pp. 642-649.

30. Kubaschewski, O.; and Heymer. G.: Heats of Formation of Transition-Metal Aluminides. Faraday Soc. Trans., vol. 56, 1960, pp. 473-478.

31. Neumann, J.P.; Austin, Y.; and Ipser, H.: On the Relationship Between the Enthalpy of Formation and the Disorder Parameter of Intermetallic Phases with the B2 Structure. Scripta Metall., vol. 10, 1976, pp. 917-922.

32. Steiner, A.; and Komarek, K.L.: Thermodynamic Activities of Solid Nickel-Aluminum Alloys. Trans. Metall. Soc. AIME, vol. 230, 1964, pp. 786-790.

33. Libowitz, G.G.: Point Defects and Thermodynamic Properties in CsCl-type Intermetallic Compounds. Metall. Trans., vol. 2, 1971, pp. 85-93.

34. Neumann, J.P.; Chang, Y.A.; and Lee, C.M.: Thermodynamics of Intermetallic Phases with the Triple-Defect B2 Structure. Acta Metall., vol. 24, 1976, pp. 593-604.

35. Hanneman, R.E.; and Seybolt, A.U.: Nickel Activity Data in the Nickel-Aluminum System at 1000 °C. Trans. Metall. Soc. AIME, vol. 245, 1969, pp. 434-435.

36. Misra, A.K.: Thermodynamic Analysis of Compatibility of Several Reinforcement Materials with Beta Phase NiAl Alloys. NASA CR-4171, 1988.

37. Troshkina, V.A.; and Khomyakov, K.G.: Heat Capacity of the Intermetallic Compound NiAl After Various Heat Treatments. Russ. J. Inorg. Chem., vol. 6, 1961, pp. 1233-1234.

38. Kucherenko, L.A.; and Troshkina, V.A.: Transformations in the Compound NiAl. Russ. Metall., vol. 1, 1971, pp. 115-118.

39. Wagner, C.; and Schottky, W.: Theorie der Geordneten Mischphasen. Z. Phys. Chem., vol. 11, 1930, pp. 163-210.

40. Ettenberg, M.; Komarek, K.L.; and Miller, E.: Thermodynamic Properties and Ordering in PdAl. Metall. Trans., vol. 2, 1971, pp. 1173-1181.

41. Bashev, V.F.; Miroshnichenko, I.S.; and Dotsenko, F.F.: Crystallization of Al-Ni Alloys During Rapid Cooling. Izv. Akad. Nauk SSSR, Met., no. 6, 1989, pp. 55-58.

42. Sumiyama, K.; Hirose, Y.; Nakamura, Y.: Magnetic and Electrical Properties of Nonequilibrium Ni-Al Alloys Produced by Vapor Quenching. Phys. Status Solidi. (A), vol. 114, 1989, pp. 693-704.

43. Nastasi, M., et al.: Phase Transformation of Ni_2Al_3 to NiAl. I. Ion Irradiation Induced. J. Appl. Phys., vol. 57, 1985, pp. 1050-1054.

44. Nastasi, M.; and Mayer, J.W.: Thermodynamics and Kinetics of Phase Transformations Induced by Ion Irradiation. Mater. Sci. Rep., vol. 6, 1991, pp. 1-51.

45. Eridon, J.; Was, G.S.; and Rehn, L.: A Thermodynamic and Kinetic Basis for Understanding Metastable Phase Formation During Ion-Beam Mixing of Nickel-Aluminum Alloys. J. Mater. Res., vol. 3, 1988, pp. 626-639.

46. Hung, L.S., et al.: Ion-Induced Amorphous and Crystalline Phase Formation in Al/Ni, Al/Pd, and Al/Pt Thin Films. Appl. Phys. Lett., vol. 42, 1983, pp. 672-674.

47. Mori, H., et al.: Amorphous Transition in Intermetallic Compounds Induced by Electron Irradiation, Scripta Metall., vol. 18, 1984, pp. 783-788.

48. Liu, H.C.: Radiation Damage in Ordered Alloys. Ph.D. Thesis, Case Western Reserve University, Cleveland, OH., 1981.

49. Liu, H.C.; and Mitchell, T.E.: Irradiation Induced Order-Disorder in Ni_3Al and NiAl. Acta Metall., vol. 31, 1983, pp. 863-872.

50. Liu, H.C.; and Mitchell, T.E.: Defect Aggregation in Irradiated Ni_3Al and NiAl. J. Nucl. Mater., vol. 107, 1982, pp. 318-326.

51. Kaufman, L.; and Nesor, H.: Calculation of Superalloy Phase Diagrams: Part II. Metall. Trans., vol. 5, 1974, pp. 1623-1629.

52. Sigli, C.; and Sanchez, J.M.: Theoretical Description of Phase Equilibrium in Binary Alloys. Acta Metall., vol. 33, 1985, pp. 1097-1104.

53. Ansara, I.; Sundman, B.; and Willemin, P.: Thermodynamic Modeling of Ordered Phases in the Ni-Al System. Acta Metall., vol. 36, 1988, pp. 977-982.

54. Hong, T.; and Freeman, A.J.: Electronic Structure and Mechanical Properties of Intermetallics: APB Energies in Ni-Al-Based Systems. High Temperature Ordered Intermetallic Alloys III, C.T. Liu, ed., MRS, Pittsburgh, PA., 1989, pp. 75-80.

55. Clapp, P.C., et al.: Some Thermodynamic Properties of NiAl Calculated by Molecular Dynamics Simulations. High Temperature Ordered Intermetallic Alloys III, C.T. Liu, ed., MRS, Pittsburgh, PA., 1989, pp. 29-35.

56. Seitchik, J.A.; and Walmsley, R.H.: Nuclear Magnetic Resonance Study of Al^{27} in NiAl. Phys. Rev., vol. 131, 1963, pp. 1473-1477.

57. Kucherenko, L.A.; Aristova, N.M.; and Troshkina, V.A.: Use of Heat Capacities to Determine Energies of Formation and Activation of Movement of Defects in the Nickel-Aluminum Compound NiAl. Russ. J. Phys. Chem., vol. 49, 1975, pp. 14-15.

58. Taylor, R.E.; Groot, H.; and Larimore, J.: Thermophysical Properties of Aluminides. TPRL 506, Purdue University, West Lafayette, IN, 1986.

59. Begot, J.J., et al.: Chaleur Specifique a Basse Temperature de la Famille $Ni_{1-x}Co_xAl$: Observations en Relation Avec la Structure de Bandes de Ce Composes et la Transformation Martensitique de $Ni_{1+y}Al_{1-y}$. J. Phys.—Lett., vol. 35, 1974, pp. L225-L228.

60. Koch, J.M.; and Koenig, C.: Electronic Structure of Vacancies in Ordered Metallic "CsCl" Compounds. Philos. Mag. B, vol. 54, 1986, pp. 177-197.

61. Singleton, R.H.; Wallace, A.V.; and Miller, D.G.: Nickel Aluminide Leading Edge for a Turbine Vane. Summary of the Eleventh Refractory Composites Working Group Meeting. E.H. Beardslee and D.R. James, eds., AFML-TR-66-179, 1966, pp. 717-738.

62. Darolia, R.: NiAl Alloys for High-Temperature Structural Applications. J. Met., vol. 43, no. 3, 1991, pp. 44-49.

63. Clark, R.W.; and Whittenberger, J.D.: Thermal Expansion of Binary CoAl, FeAl, and NiAl Alloys. Thermal Expansion 8, T.A. Hahn, ed., Plenum Press, New York, 1984, pp. 189-196.

64. Wasilewski, R.J.: Thermal Vacancies in NiAl. Acta Metall., vol. 15, 1967, pp. 1757-1759.

65. Ivanov, E.G.: The Temperature Coefficient of Linear Expansion of Iron, Nickel and Chromium Aluminides. Izv. Akad. Nauk SSSR, Met., no. 2, 1986, pp. 168-169.

66. Misra, A.K.: Theoretical Analysis of Compatibility of Several Reinforcement Materials With NiAl and FeAl Matrices. NASA CR-182291, 1989.

67. Misra, A.K.: Reaction of Beta-Phase Ni-Al Alloys with CrB_2. J. Mater. Res., vol. 6, 1991, pp. 1664-1672.

68. Jacobi, H.; Vassos, B.; and Engell, H.-J.: Electrical Properties of β-Phase NiAl. J. Phys. Chem. Solids, vol. 30, 1969, pp. 1261-1271.

69. Yamaguchi, Y., et al.: Electrical Resistivity of NiAl, CoAl, NiGa, and CoGa. J. Appl. Phys., vol. 39, 1968, pp. 231-232.

70. Yamaguchi, Y.; Aoki, T.; and Brittain, J.O.: Electronic Structure of β'-NiAl. J. Phys. Chem. Solids, vol. 31, 1970, pp. 1325-1343.

71. Butler, S.R., Hanlon, J.E.; and Wasilewski, R.J.: Electric and Magnetic Properties of B2 Structure Compounds: NiAl, CoAl. J. Phys. Chem. Solids, vol. 30, 1969, pp. 1929-1934.

72. Caskey, G.R.; Franz, J.M.; and Sellmyer, D.J.: Electronic and Magnetic States in Metallic Compounds—II: Electron Transport and Magnetic Susceptibility in NiAl and FeAl. J. Phys. Chem. Solids, vol. 34, 1973, pp. 1179-1198.

73. Hohl, M.: Magnetische Untersuchungen an Binaren und Ternaren Kubisch Raumzentrierten Phasen des Aluminiums Mit Den Elementen der Eisengruppe. Z. Metall., vol. 51, 1960, pp. 85-95.

74. West, G.W.: Nuclear Magnetic Resonance and Susceptibility Measurements in Intermetallic Compounds. Philos. Mag., vol. 15, 1967, 855-866.

75. Brodsky, M.D.; and Brittain, J.O.: Magnetic Susceptibility of β'-NiAl. J. Appl. Phys., vol. 40, 1969, pp. 3615-3617.

76. Koch, J.M.; and Koenig, C.: Antistructure Defects in Transition-Metal Aluminides. Philos. Mag. B, vol. 55, 1987, pp. 359-375.

77. Rechtien, J.J.; Kannewurf, C.R.; and Brittain, J.O.: Optical Constants of β-Phase NiAl. J. Appl. Phys., vol. 38, 1967, pp. 3045-3050.

78. Jacobi, H.; and Stahl, R.: Optical Properties of Ternary β Electronphases Based on NiAl. J. Phys. Chem. Solids, vol. 34, 1973, pp. 1737-1748.

79. Kim, K.J.; Harmon, B.N.; and Lynch, D.W.: Calculation of the Optical Spectra of β-NiAl and CoAl. Phys. Rev. B, vol. 43, 1991, pp. 1948-1953.

80. Wasilewski, R.J.: Elastic Constants and Young's Modulus of NiAl. Trans. Metall. Soc. AIME, vol. 236, 1966, pp. 455-457.

81. Rusovic, N.; and Warlimont, H.: The Elastic Behavior of β_2-NiAl. Phys. Stat. Sol. (A), vol. 44, 1977, pp. 609-619.

82. Rusovic, N.; and Henig, E.-Th.: Influence of Supersaturated Thermal Vacancies on the Elastic Constants of β_2-NiAl. Phys. Status Solidi. (A), vol. 57, 1980, pp. 529-540.

83. Enami, K., et al.: Elastic Softening and Electron-Diffraction Anomalies Prior to the Martensitic Transformation in a Ni-Alβ_1 Alloy. Scripta Metall., vol. 10, 1976, pp. 879-884.

84. Rusovic, N.; and Warlimont, H.: Young's Modulus of β_2-NiAl Alloys. Phys. Status Solidi. (A), vol. 53, 1979, pp. 283-288.

85. Hellmann, J.R., et al.: Interfacial Shear Studies in Sapphire Fiber-Reinforced Niobium and Nickel Aluminide Composites. HITEMP Review—1990: Advanced High Temperature Engine Materials Technology Program, NASA CP-10051, 1990, pp. 41-1 - 41-11.

86. Tressler, R.E.; Hellman, J.R.; and Hahn, H.T.: Advanced High Temperature Composite Materials For Engine Applications. Annual Report. Contract NAGW-1381. Center for Advanced Materials, The Pennsylvania State University, University Park, 1991, pp. 141-151.

87. Hirth, J.P.; and Lothe, J.: Theory of Dislocations. Second ed., John Wiley & Sons, Inc., New York, 1982, p. 837.

88. Lazarus, D.: The Variation of the Adiabatic Elastic Constants of KCl, NaCl, CuZn, Cu, and Al with Pressure to 10,000 Bars. Phys. Rev., vol. 76, 1949, pp. 545-533.

89. Zirinsky, S.: The Temperature Dependence of the Elastic Constants of Gold-Cadmium Alloys. Acta Metall., vol. 4, 1956, pp. 164-171.

90. Harmouche, M.R.; and Wolfenden, A.: Modulus Measurements in Ordered Co-Al, Fe-Al, and Ni-Al Alloys. J. Test. Eval., vol. 13, 1985, pp. 424-428.

91. Khadkikar, P.S.; Michal, G.M.; and Vedula, K.: Preferred Orientations in Extruded Nickel and Iron Aluminides. Metall. Trans., vol. 21A, 1990, pp. 279-288.

92. Rosen, S.; and Goebel, J.A.: The Crystal Structure of Nickel-Rich NiAl and Martensitic NiAl. Trans. Metall. Soc. AIME, vol. 42, 1968, pp. 722-724.

93. Nagasawa, A., et al.: Reversible Shape Memory Effect. Scripta Metall., vol. 8, 1974, pp. 1055-1060.

94. Enami, K.; and Nenno, S.: Memory Effect in Ni-36.8 at. pct. Al Martensite. Metall. Trans., vol. 2, 1971, pp. 1487-1489.

95. Castro, G.R.; Isern, H.; Schneider, U.; Stocker, M.; and Wandelt, K.: Two-Dimensional Phase Transition of Adsorbed Xenon on NiAl(110) and Al(110). J. Vac. Sci. Technol. A, vol. 9, 1991, pp. 1676-1679.

96. Franchy, R.; Wuttig, M.; and Ibach, H.: The Adsorption of Sulfur, Carbon Monoxide and Oxygen on NiAl(111). Surf. Sci., vol. 189-190, 1987, pp. 438-447.

97. Patterson, C.H.; and Buck, T.M.: The Binding Site of CO on NiAl(110) Determined by Low Energy Ion Scattering. Surf. Sci., vol. 218, 1989, pp. 431-451.

98. Isern, H.; and Castro, G.R.: The Initial Interaction of Oxygen with a NiAl(110) Single Crystal: A LEED and AES Study. Surf. Sci., vol. 211/212, 1989, pp. 865-871.

99. Castro, G.R., et al.: Xenon Adsorption on NiAl(110). Vacuum, vol. 41, 1990, pp. 393-395.

100. Mullins, D.R.; and Overbury, S.H.: The Structure and Composition of the NiAl(110) and NiAl(100) Surfaces. Surf. Sci., vol. 199, 1988, pp. 141-153.

101. Davis, H.L.; and Noonan, J.R.: Atomic Rippling of a Metallic Ordered Alloy Surface-NiAl(110). J. Vac. Sci. Technol. A, vol. A3, 1985, pp. 1507-1510.

102. Yalisove, S.M.; and Graham, W.R.: Multilayer Rippled Structure of the NiAl(110) Surface: A Medium Energy Ion Scattering Study. Surf. Sci., vol. 183, 1987, pp. 556-564.

103. Wuttig, M., et al.: Surface-Phonon Dispersion of NiAl(110). Phys. Rev. B, vol. 42, 1990, pp. 5443-5450.

104. Wuttig, M., et al.: Structure and Dynamics of NiAl(110). Vacuum, vol. 41, 1990, pp. 433-436.

105. Lui, S.-C., et al.: Surface States on NiAl(110). Phys. Rev. B, vol. 39, 1989, pp. 13149-13159.

106. Chen, S.P.: Theoretical Studies of Metallic Interfaces. Mater. Sci. Eng., vol. B6, 1990, pp. 113-121.

107. Noonan, J.R.; and Davis, H.L.: Domain Mixtures in the NiAl(111) Surface. J. Vac. Sci. Technol. A, vol. 6, 1988, pp. 722-725.

108. Overbury, S.H.; Mullins, D.R.; and Wendelken, J.F.: Surface Structure of Stepped NiAl(111) by Low Energy Li$^+$ Ion Scattering. Surf. Sci., vol. 36, 1990, pp. 122-134.

109. Niehus, H., et al.: Surface Structure of NiAl(111) Determined by Ion Scattering and Scanning Tunneling Microscopy. Surf. Sci. Lett., vol. 225, 1990, pp. L8-L14.

110. Kang, M.H., et al.: Atomic and Electronic Structure of the NiAl(111) Surface. Phys. Rev. B, vol. 41, 1990, pp. 4920-4929.

111. Wasilewski, R.J.: Structure Defects in CsCl Intermetallic Compounds—I. Theory. J. Phys. Chem. Solids, vol. 29, 1968, pp. 39-49.

112. Wasilewski, R.J.; Butler, S.R.; and Hanlon, J.E.: Constitutional and Thermal Structure Defects in NiGa. J. Appl. Phys., vol. 39, 1968, pp. 4234-4241.

113. Raynor, G.: Progress in the Theory of Alloys. Prog. Met. Phys., vol. 1, 1949, pp. 1-77.

114. Georgopoulos, P.: The Defect Structure in Beta-Nickel-Aluminum. Ph.D. Thesis, Northwestern University, Evanston, IL, 1979.

115. Liu, H.C.; Mukai, T.; and Mitchell, T.E.: Defect Structures in β-NiAl and Their Response to Electron Irradiation. Point Defects and Defect Interactions in Metals, J.-I. Takamura, M. Doyama and M. Diritani, eds., University of Tokyo Press, Tokyo, Japan, 1982, pp. 635-638.

116. Georgopoulos, P.; and Cohen, J.B.: The Defect Arrangement in (Non-Stoichiometric) β'-NiAl. Acta Metall., vol. 29, 1981, pp. 1535-1551.

117. Delavignette, P.; Richel, H.; and Amelinckx, S.: The Ordering of Vacancies in $Ni_{1-x}Al$. Phys. Status Solidi. (A), vol. 13, 1972, pp. 545-555.

118. de Ridder, R.; Van Tendeloo, G.; and Amelinckx, S.: The Ordering of Vacancies in $Ni_{1-x}Al$. Phys. Status Solidi. (A), vol. 43, 1977, pp. 133-139.

119. West, G.W.: Nuclear Magnetic Resonance in Intermetallic Compounds. Philos. Mag., vol. 9, 1964, pp. 979-991.

120. Ortiz, C.; and Epperson, J.E.: On the ω-Like Diffraction Effects from β'-NiAl. Scripta Metall., vol. 13, 1979, pp. 237-239.

121. Georgopoulos, P.; and Cohen, J.B.: Omega-Like Structural Defects in β-NiAl. Modulated Structures—1979, J.M. Cowley et al., eds., American Institute of Physics, New York, 1979 (AIP Conference Proceedings No. 53), pp. 279-281.

122. Kuan, T.S.; and Sass, S.L.: The Structure of a Linear Omega-Like Vacancy Defect in Zr-Nb B.C.C. Solid Solutions. Acta Metall., vol. 24, 1976, pp. 1053-1059.

123. Sikka, S.K.; Vohra, Y.K.; and Chidambaram, R.: Omega Phase in Materials. Prog. Mater. Sci., vol. 27, 1982, pp. 245-310.

124. Parthasarathi, A.; and Fraser, H.L.: The Annealing of Vacancy Defects in β-NiAl: I. Vacancy Loop Growth in As-Grown Single Crystals Annealed in Ultra-High Vacuum. Philos. Mag. A, vol. 50, 1984, pp. 89-100.

125. Fraser, H.L., et al.: Annealing of Point Defects in Quenched NiAl. Philos. Mag., vol. 32, 1975, pp. 873-875.

126. Yang, W.J.; and Dodd, R.A.: The Effect of Carbon Content on Void Formation in Quenched and Aged Near Stoichiometric NiAl. Scripta Metall., vol. 8, 1974, pp. 237-242.

127. Nagpal, P.; and Baker, I.: Effect of Cooling Rate on Hardness of FeAl and NiAl. Metall. Trans., vol. 21A, 1990, pp. 2281-2282.

128. Bowman, R.R.; Noebe, R.D.; Raj, S.V.; and Locci, I.E.: Correlation of Deformation Mechanisms with the Tensile and Compressive Behavior of NiAl and NiAl(Zr) Intermetallic Alloys. Metall. Trans. A, vol. 23A, 1992, pp. 1493-1508.

129. Locci, I.E.; Noebe, R.D.; Moser, J.A.; Lee, D.S.; and Nathal, M.: Processing and Microstructure of Melt Spun NiAl Alloys. High Temperature Ordered Intermetallic Alloys III, C.T. Liu et al., eds., MRS, Pittsburgh, PA., 1989, pp. 639-646.

130. Epperson, J.E., et al.: Voids Formed in Quenched and Annealed NiAl. Philos. Mag. A, vol. 38, 1978, pp. 529-541.

131. Eibner, J.E., et al.: Annealing of Point Defects in Quenched NiAl. Philos. Mag., vol. 31, 1975, pp. 739-742.

132. Yang, W.; Dodd, R.A.; and Strutt, P.R.: Formation of Voids and Dislocation Loops in Near-Stoichiometric NiAl by Aging at 700° to 900 °C, and Some Effects on Alloy Properties. Metall. Trans., vol. 3, 1972, pp. 2049-2054.

133. Fan, J.; and Collins, G.S.: Point Defects in NiAl Near the Equiatomic Composition. Hyperfine Struct., vol. 60, 1990, pp. 655-658.

134. Parthasarathi, A.; and Fraser, H.L.: The Annealing of Vacancy Defects in β-NiAl: II. The Role of Surface Oxidation in Vacancy Loop Growth in Slowly Cooled Crystals. Philos. Mag. A, vol. 50, 1984, pp. 101-115.

135. Ball, A.; and Smallman, R.E.: Vacancy Defects in the Ordered Compound NiAl. Acta Metall., vol. 16, 1968, pp. 233-241.

136. Hancock, G.F.; and McDonnell, B.R.: Diffusion in the Intermetallic Compound NiAl. Phys. Status Solidi., vol. 4, 1971, pp. 143-150.

137. Shimotomai, M.; Wang, T.-M.; and Doyama, M.: Mobilities of Radiation-Induced Vacancies in Ni_3Al and NiAl Studied by Positron Techniques. J. Nucl. Mater., vol. 116, 1983, pp. 347-348.

138. Ball, A.; and Smallman, R.E.: The Operative Slip System and General Plasticity of NiAl—II. Acta Metall., vol. 14, 1966, pp. 1517-1526.

139. Potter, D.I.: Prediction of the Operative Slip System in CsCl Type Compounds Using Anisotropic Elasticity Theory. Mater. Sci. Eng., vol. 5, 1969, pp. 201-209.

140. Lloyd, C.H.; and Loretto, M.H.: Dislocations in Extruded β'-NiAl. Phys. Status Solidi., vol. 39, 1970, pp. 163-170.

141. Loretto, M.H.; and Wasilewski, R.J.: Slip Systems in NiAl Single Crystals at 300 °K and 770 °K. Philos. Mag., vol. 23, 1971, pp. 1311-1328.

142. Veyssiere, P.; and Noebe, R.: Weak-Beam Study of <111> Superlattice Dislocations in NiAl. Philos. Mag. (A), vol. 65, 1992, pp. 1-13.

143. Kim, J.T.; and Gibala, R.: Slip Transition in [001] Oriented NiAl at High Temperatures. High Temperature Ordered Intermetallic Alloys IV, L.A. Johnson, D.P. Pope, and J.O. Stiegler, eds., MRS, Pittsburgh, PA, 1991, pp. 261-266.

144. Kim, J.-T.: On the Slip Behavior and Surface Film Effects In B2 Ordered NiAl Single Crystals. Ph.D. Thesis, The University of Michigan, 1990.

145. Zaluzec, N.J.; and Fraser, H.L.: The Origin of Dislocations with b = <110> in Single Crystals of β-NiAl Compressed Along <001> at Elevated Temperatures. Scripta Metall., vol. 8, 1974, pp. 1049-1054.

146. Tisone, T.C.; Marshall, G.W.; and Brittain, J.O.: Prismatic Dislocations in β'NiAl. J. Appl. Phys., vol. 39, 1968, pp. 3714-3717.

147. Marshall, G.W.; and Brittain, J.O.: Climb Sources in β'-NiAl. Metall. Trans. A, vol. 6, 1975, pp. 921-926.

148. Marshall, G.W.; and Brittain, J.O.: Hot Stage TEM Investigations of Dislocation Climb in NiAl. Metall. Trans. A, vol. 7, 1976, pp. 1013-1020.

149. Noebe, R.D., et al.: The Potential for Ductility Enhancement from Surface and Interface Dislocation Sources in NiAl. High Temperature Aluminides and Intermetallics, S.H. Whang, C.T. Liu, and J.O. Steigler, eds., The Minerals, Metals & Materials Society, Warrendale, PA, 1990, pp. 271-300.

150. Aindow, M.; Parthasarathi, A.; and Fraser, H.L.: On the Shape of Edge-Dislocation Loops in β-NiAl. Philos. Mag., vol. 62, 1990, pp. 317-322.

151. Yamaguchi, M.: Atomistic Studies of Dislocations in BCC and BCC-Based Ordered Alloys. Mechanical Properties of BCC Metals, M. Meshii, ed., The Metallurgical Society of AIME, Warrendale, PA, 1982, pp. 31-40.

152. Vitek, V.; and Yamaguchi, M.: Atomistic Studies of Dislocations. Interatomic Potentials and Crystalline Defects, J.K. Lee, ed., The Metallurgical Society of AIME, Warrendale, PA, 1981, pp. 223-248.

153. Yamaguchi, M.; and Umakoshi, Y.: Core Structure of <100> Dislocation in B.C.C. and B.C.C. Ordered (CsCl) Crystals. Proceedings of the 1976 International Conference on Computer Simulation for Materials Applications, R.J. Arsenault, J.R. Beeler, and J.A. Simmons, eds., National Bureau of Standards, Gaithersburg, MD, 1976, pp. 763-774.

154. Yamaguchi, M.; and Umakoshi, Y.: The Core Structure of <100> Screw Dislocations in a Model CsCl Type Ordered Lattice. Scripta Metall., vol. 9, 1975, pp. 637-640.

155. Benhaddane, K.; and Beauchamp, P.: Core Structure of the a<100><001> Edge Dislocation in a B2 Ordered Alloy. Phys. Status Solidi. (A), vol. 98, 1986, pp. 195-202.

156. Takeuchi, S.: An Interpretation of <111> Slip Behavior in B2 Compounds in Terms of the Peierls Mechanism of a Screw Dislocation. Strength of Metals and Alloys, Vol. 1, P. Haasen, V. Gerold, and G. Kostorz, eds., Pergamon Press, New York, 1979, pp. 53-58.

157. Takeuchi, S.: Computer Simulation of Motion of <111> Superlattice Screw Dislocation in the CsCl-Type Lattice. Philos. Mag. A, vol. 41, 1980, pp. 541-553.

158. Farkas, D., et al.: Correlation of TEM Observations with Dislocation Core Structure Calculations in B2 Ordered Alloys. High Temperature Ordered Intermetallic Alloys IV, L.A. Johnson, D.P. Pope, and J.O. Steigler, eds., MRS, Pittsburgh, PA, 1991, pp. 223-228.

159. Lautenschlager, E.P.; Hughes, T.; and Brittain, J.O.: Slip in Hard-Sphere CsCl Models. Acta Metall., vol. 15, 1967, pp. 1347-1357.

160. Yamaguchi, M., et al.: Planar Faults and Dislocation Dissociations in Body-Centered-Cubic-Derivative Ordered Structures. Philos. Mag. A, vol. 43, 1981, pp. 1265-1275.

161. Campany, R.G.; Loretto, M.H.; and Smallman, R.E.: The Determination of the 1/2 <110> {110} Antiphase Boundary Energy of NiAl. J. Microsc., vol. 98, 1973, pp. 174-179.

162. Hong, T.; and Freeman, A.J.: Effect of Antiphase Boundaries on the Electronic Structure and Bonding Character of Intermetallic Systems: NiAl. Phys. Rev. B, vol. 43, 1991, pp. 6446-6458.

163. Ball, A.: Unusual Lattice Defects in Non-Stoichiometric NiAl. Philos. Mag., vol. 20, 1969, pp. 113-124.

164. Yang, W.J.; Lin, F.; Dodd, R.A.: Structure of Vacancy—Defective NiAl. Scripta Metall., vol. 12, 1978, pp. 237-241.

165. Wasilewski, R.J.; Butler, S.R.; and Hanlon, J.E.: Plastic Deformation of Single-Crystal NiAl. Trans. Metall. Soc. AIME, vol. 239, 1967, pp. 1357-1364.

166. Strutt, P.R.; Dodd, R.A.; and Rowe, G.M.: Creep in Stoichiometric Beta-NiAl. Strength of Metals and Alloys. Proceedings of the 2nd International Conference, Vol. III, ASM International, Metals Park, OH, 1970, pp. 1057-1061.

167. Pascoe, R.T.; and Newey, C.W.A.: Deformation Modes of the Intermediate Phase NiAl. Phys. Status Solidi., vol. 29, 1968, pp. 357-366.

168. Kanne, W.R.; Strutt, P.R.; and Dodd, R.A.: Nature of Slip Line and Substructure Formation During Creep in Stoichiometric NiAl at Temperatures Between 475° and 775 °C. Trans. Metall. Soc. AIME, vol. 245, 1969, pp. 1259-1267.

169. Bevk, J.; Dodd, R.A.; and Strutt, P.R.: The Orientation Dependence of Deformation Mode and Structure in Stoichiometric NiAl Single Crystals Deformed by High Temperature Steady-State Creep. Metall. Trans., vol. 4, 1973, pp. 159-166.

170. Fraser, H.L.; Smallman, R.E.; and Loretto, M.H.: The Plastic Deformation of NiAl Single Crystals Between 300 °K and 1050 °K: I. Experimental Evidence on the Role of Kinking and Uniform Deformation in Crystals Compressed Along <001>. Philos. Mag., vol. 28, 1973, pp. 651-665.

171. Fraser, H.L.; Loretto, M.H.; and Smallman, R.E.: The Plastic Deformation of NiAl Single Crystals Between 300 °K and 1050 °K: II. The Mechanism of Kinking and Uniform Deformation. Philos. Mag., vol. 28, 1973, pp. 667-677.

172. Loretto, M.H.; and Wasilewski, R.J.: Transmission Electron Microscopy of Plastically Deformed <100> Single Crystals of NiAl. Strength of Metals and Alloys. Proceedings of the 2nd International Conference, Vol. I, ASM International, Metals Park, OH, 1970, pp. 113-117.

173. Field, R.D.; Lahrman, D.F.; and Darolia, R.: Room Temperature Deformation in "Soft" Orientation NiAl Single Crystals. High Temperature Ordered Intermetallic Alloys IV, L.A. Johnson, D.P. Pope, and J.O. Stiegler, eds., MRS, Pittsburgh, PA, 1991, pp. 255-260.

174. Bowman, R.R.; Noebe, R.D.; and Darolia, R.: Mechanical Properties and Deformation Mechanisms of NiAl. HITEMP Review—1989: Advanced High Temperature Engine Materials Technology Program, NASA CP-10039, 1989, pp. 47-1 - 47-15.

175. Kim, J.T.; Noebe, R.D.; and Gibala, R.: Observation of Dislocation Substructures in Surface Oxide Softened Single Crystals of NiAl. Proceedings of the International Symposium on Intermetallic Compounds—Structure and Mechanical Properties, O. Izumi, ed., Japan Institute of Metals, Sendai, Japan, 1991, pp. 591-595.

176. Strutt, P.R., et al.: Creep in Ordered Binary and Ternary Ordered B.C.C. Alloys. Electron Microscopy and Structure of Materials, G. Thomas, ed., University of California Press, Berkeley, CA, 1972, pp. 722-731.

177. Lautenschlager, E.P.; Tisone, T.C.; and Brittain, J.O.: Electron Transmission Microscopy of NiAl. Phys. Status Solidi., vol. 20, 1967, pp. 443-450.

178. Vedula, K.; Hahn, K.H.; and Boulogne, B.: Room Temperature Tensile Ductility in Polycrystalline B2 NiAl. High Temperature Ordered Intermetallic Alloys III, C.T. Liu, ed., MRS, Pittsburgh, PA., 1989, pp. 299-304.

179. Rachinger, W.A.; and Cottrell, A.H.: Slip in Crystals of the Caesium Chloride Type. Acta Metall., vol. 4, 1956, pp. 109-113.

180. Mendiratta, M.G.; and Law, C.C.: Dislocation Energies and Mobilities in B2-Ordered Fe-Al Alloys. J. Mat. Sci, vol. 22, 1987, pp. 607-611.

181. Yoo, M.H., et al.: Slip Modes in B2-Type Intermetallic Alloys. Mater. Trans., J.I.M., vol. 31, 1990, pp. 435-442.

182. Ball, A.; and Smallman, R.E.: The Deformation Properties and Electron Microscopy Studies of the Intermetallic Compound NiAl. Acta Metall., vol. 14, 1966, pp. 1349-1355.

183. Whittenberger, J.D.; Noebe, R.D.; Cullers, C.L.; Kumar, K.S.; and Mannan, S.K.: 1000 to 1200 K Time-Dependent Compressive Deformation of Single-Crystalline and Polycrystalline B2 Ni-40Al. Metall. Trans. A, vol. 22, 1991, pp. 1595-1607.

184. Field, R.D.; Lahrman, D.F.; and Darolia, R.: Slip Systems in <001> Oriented NiAl Single Crystals. Acta Metall. Mater., vol. 39, 1991, pp. 2951-2959.

185. Darolia, R., et al.: Alloy Modeling and Experimental Correlation for Ductility Enhancement in NiAl. High Temperature Ordered Intermetallic Alloys III, C.T. Liu, ed., MRS, Pittsburgh, PA, 1989, pp. 113-189.

186. Hess, J.B.; and Barrett, C.S.: Structure and Nature of Kink Bands in Zinc. Trans. Met. Soc. AIME, vol. 185, 1949, pp. 599-606.

187. Field, R.D.; Lahrman, D.F.; and Darolia, R.: The Effect of Alloying on Slip Systems in <001> Oriented NiAl Single Crystals. Acta Metall. Mater., vol. 39, 1991, pp. 2961-2969.

188. Miracle, D.B.; Russell, S.; and Law, C.C.: Slip System Modification in NiAl. High Temperature Ordered Intermetallic Alloys III, C.T. Liu, ed., MRS, Pittsburgh, PA, 1989, pp. 225-230.

189. Cotton, J.D.: The Influence of Chromium on Structure and Mechanical Properties of B2 Nickel Aluminide Alloys. Ph.D. Thesis, The University of Florida, Gainesville, FL, 1991. (Also available as NASA CR-189124, 1992.)

190. Baker, I.; and Schulson, E.M.: The Structure of Extruded NiAl. Metall. Trans. A, vol. 15, 1984, pp. 1129-1136.

191. Munroe, P.R.; and Baker, I.: Observation of <111> Slip in NiAl. Scripta Metall., vol. 23, 1989, pp. 495-499.

192. Lasalmonie, A.: Deformation of Ni-Al at High Temperature. J. Mater. Sci., vol. 17, 1989, pp. 2419-2423.

193. Dollar, M., et al.: The Occurrence of <110> Slip in NiAl. Scripta Metall. Mater., vol. 26, 1992, pp. 29-34.

194. Dymek, S., et al.: Deformation Mechanisms and Ductility of Mechanically Alloyed NiAl. To be published in Mater. Sci. Eng., 1992.

195. Miracle, D.B.: Deformation in NiAl Bicrystals. Acta Metall. Mater., vol. 39, 1991, pp. 1457-1468.

196. Miracle, D.B.: The Deformation of Nickel Aluminide Bicrystals. Ph.D. Thesis, Ohio State University, Columbus, OH, 1990.

197. Law, C.C.; and Blackburn, M.J.: Rapidly Solidified Lightweight Durable Disk Material. Final Technical Report, AFWAL-TR-87-4102, 1987.

198. Law, C.C.; and Blackburn, M.J.: Rapidly Solidified Lightweight Durable Disk Material. Report No. ED/GPD FR-18674-4, United Technologies Corp., Pratt and Whitney Group, Sept. 17, 1985.

199. Cotton, J.D.; Kaufman, M.J.; Noebe, R.D.; and Behbehani, M.: The Potential for Room Temperature Ductility in Polycrystalline NiAl Through Slip System Modification by Macroalloying. HITEMP Review, 1991: Advanced High Temperature Engine Materials Technology Program, NASA CP-10082, 1991, pp. 23-1 to 23-18.

200. Merchant, S.M.; and Notis, M.R.: A Review: Constitution of the Al-Cr-Ni System. Mater. Sci. Eng., vol. 66, 1984, pp. 47-60.

201. Cotton, J.D.; Kaufman, M.J.; and Noebe, R.D.: Constitution of Pseudobinary Hypoeutectic β-NiAl + α-V Alloys. Scripta Metall. Mater., vol. 25, 1991, pp. 1827-1832.

202. Jayanth, C.S.: Phase Equilibria in the Ni-Al-Zr and Ni-Al-V Systems. M.S. Thesis, Illinois Institute of Technology, Chicago, IL, 1983.

203. Groves, G.W.; and Kelly, A.: Independent Slip Systems in Crystals. Philos. Mag., vol. 8, 1963, pp. 877-887.

204. Patrick, D.K., et al.: Burgers Vector Transition in Fe-Al-Ni Alloys. High Temperature Ordered Intermetallic Alloys IV, L.A. Johnson, D.P. Pope, and J.O. Steigler, eds., MRS, Pittsburgh, PA, 1991, pp. 267-272.

205. Guha, S.; Munroe, P.R.; and Baker, I.: Room Temperature Deformation Behavior of Multiphase Ni-20at.%Al-30at.%Fe and Its Constituent Phases. Mater. Sci. Eng, vol. A131, 1991, pp. 27-37.

206. Chakrabarti, D.J.: Phase Stability in Ternary Systems of Transition Elements with Aluminum. Metall. Trans. B, vol. 8, 1977, pp. 121-123.

207. Cotton, J.D.; Kaufman, M.J.; and Noebe, R.D.: A Simplified Method for Determining the Number of Independent Slip Systems in Crystals. Scripta Metall. Mater., vol. 25, 1991, pp. 2395-2398.

208. Nagpal, P., et al.: Room Temperature Strength and Fracture of FeAl and NiAl. High Temperature Ordered Intermetallic Alloys IV, L.A. Johnson, D.P. Pope, and J.O. Steigler, eds., MRS, Pittsburgh, PA, 1991, pp. 533-538.

209. Noebe, R.D.: The Effect of Temperature, Strain Rate and Composition on the Flow and Fracture Behavior of the Intermetallic Compound NiAl. Ph.D. Thesis, The University of Michigan, Ann Arbor, MI, in progress.

210. Lautenschlager, E.P.; Kiewit, D.A.; and Brittain, J.O.: The Influence of Point Defects Upon the Compressive Strength of Ni-Al. Trans. Metall. Soc. AIME, vol. 233, 1965, pp. 1297-1302.

211. Vedula, K.; and Stephens, J.R.: B2 Aluminides for High Temperature Applications. High Temperature Ordered Intermetallic Alloys II, N.S. Stoloff, C.C. Koch, and C.T. Liu, eds., MRS, Pittsburgh, PA, 1987, pp. 381-391.

212. Barinov, S.M.; and Kotenev, V.I.: Anomaly of the Plasticity of Nickel Aluminides. Izv. Akad. Nauk SSSR, Met., No. 1, 1986, pp. 94-97.

213. Hahn, K.H.; and Vedula, K.: Room Temperature Tensile Ductility in Polycrystalline B2 NiAl. Scripta Metall., vol. 23, 1989, pp. 7-12.

214. Hwang, S.J., et al.: Microstructure and Mechanical Properties of Mechanically Alloyed NiAl. High Temperature Ordered Intermetallic Alloys IV, L.A. Johnson, D.P. Pope, and J.O. Steigler, eds., MRS, Pittsburgh, PA, 1991, pp. 661-666.

215. Noebe, R.D., et al.: Flow and Fracture Behavior of NiAl in Relation to the Brittle-to-Ductile Transition Temperature. High Temperature Ordered Intermetallic Alloys IV, L.A. Johnson, D.P. Pope, and J.O. Steigler, eds., MRS, Pittsburgh, PA, 1991, pp. 589-596.

216. Pascoe, R.T.; and Newey, C.W.A.: The Mechanical Behavior of the Intermediate Phase NiAl. Met. Sci. J., vol. 2, 1968, pp. 138-143.

217. Rozner, A.G.; and Wasilewski, R.J.: Tensile Properties of NiAl and NiTi. J. Inst. Met., vol. 94, 1966, pp. 169-175.

218. Westbrook, J.H.: Temperature Dependence of Hardness of the Equi-Atomic Iron Group Aluminides. J. Electrochem. Soc., vol. 103, 1956, pp. 54-63.

219. Grala, E.M.: Investigations of NiAl and Ni_3Al. Mechanical Properties of Intermetallic Compounds, J.H. Westbrook, ed., John Wiley & Sons, Inc., New York, 1960, pp. 358-402.

220. Graham, R.B.: The Effect of Temperature, Composition and Grain Size on the Mechanical Properties of NiAl. M.E. Thesis, Dartmouth College, Hanover, NH., 1984.

221. Raj, S.V.; Noebe, R.D.; and Bowman, R.: Observations on the Brittle to Ductile Transition Temperatures of B2 Nickel Aluminides with and without Zirconium. Scripta Metall., vol. 23, 1989, pp. 2049-2054.

222. Noebe, R.D., et al.: Flow and Fracture Behavior of Binary NiAl with Prospects for Future Alloy Development. HITEMP Review, 1990: Advanced High Temperature Engine Materials Technology Program, NASA CP-10051, 1990, pp. 20-1 to 20-19.

223. Nagpal, P.; and Baker, I.: The Effect of Grain Size on the Room-Temperature Ductility of NiAl. Scripta Metall. Mater., vol. 24, 1990, pp. 2381-2384.

224. George, E.: Oak Ridge National Laboratory, unpublished research, 1991.

225. Chen, S.P., et al.: Theoretical Studies of Ni_3Al and NiAl with Impurities. High Temperature Ordered Intermetallic Alloys III, C.T. Liu, ed., MRS, Pittsburgh, PA, 1989, pp. 149-154.

226. Nieh, T.G.; Wadsworth, J.; and Liu, C.T.: Hardening Behavior of Nickel Beryllides. Scripta Metall., vol. 22, 1988, pp. 1409-1413.

227. George, E.P.; and Liu, C.T.: Brittle Fracture and Grain Boundary Chemistry of Micro-alloyed NiAl. J. Mater. Res., vol. 5, 1990, pp. 754-762.

228. George, E.P.; Liu, C.T.; and Liao, J.J.: Mechanical Properties, Fracture Behavior, and Grain Boundary Chemistry of B-Doped NiAl. Alloy Phase Stability and Design, G.M. Stocks, et al., eds., MRS, Pittsburgh, PA, 1991, pp. 375-380.

229. Stover, E.R.: Effects of Alloying and Deformation Processing on Mechanical Behavior of NiAl. WADC-TDR-60-184, Part VII, Vol. II, 1966. (Avail. NTIS, AD-810645).

230. Kubin, L.P.: The Low Temperature Plastic Deformation of BCC Metals. Rev. Deform. Behav. Mater., vol. 1, 1976, pp. 244-288.

231. Dimiduk, D.M.; and Rao, S.: Deformation Mechanisms and Solid-Solution Strengthening in Ordered Alloys. High Temperature Ordered Intermetallic Alloys IV, L.A. Johnson, D.P. Pope, and J.O. Steigler, eds., MRS, Pittsburgh, PA, 1991, pp. 499-513.

232. Laves, F.: Crystal Structure and Atomic Size. Theory of Alloy Phases, American Society for Metals, Cleveland, OH, 1956, pp. 124-198.

59

233. Noebe, R.D.; Cullers, C.L.; and Bowman, R.R.: The Effect of Strain Rate and Temperature on the Tensile Properties of NiAl. J. Mater. Res., vol. 7, 1992, pp. 605-612.

234. Pascoe, R.T.; and Newey, C.W.A.: Deformation Processes in the Intermediate Phase NiAl. Met. Sci. J., vol. 5, 1971, pp. 50-55.

235. Vandervoort, R.R.; Mukherjee, A.K.; and Dorn, J.E.: Elevated-Temperature Deformation Mechanisms in β'-NiAl. Trans. ASM, vol. 59, 1966, pp. 930-944.

236. Schulson, E.M.: The Effects of Grain Size on the Flow and Fracture of Long-Range Ordered Alloys. High Temperature Ordered Intermetallic Alloys, C.C. Koch, C.T. Liu, and N.S. Stoleff, eds., MRS, Pittsburgh, PA, 1985, pp. 193-204.

237. Bieler, T.R.; Noebe, R.D.; Whittenberger, J.D.; and Luton, M.J.: Extrusion Textures In NiAl and Reaction Milled NiAl/AlN Composites. In Intermetallic Matrix Composites II, D.B. Miracle and J.A. Graves, eds., MRS Symposia Proc., Vol. 273, 1992.

238. Bowman, K.J.; Noebe, R.D.; Jenny, J.; Kim, S.: Texture in Hot-Worked B2 Structure Aluminides. To be published in Mater. Sci. Eng., 1992.

239. Lahrman, D.F.; Field, R.D.; and Darolia, R.: The Effect of Strain Rate on the Mechanical Properties of Single Crystal NiAl. High Temperature Ordered Intermetallic Alloys IV, L.A. Johnson, D.P. Pope, and J.O. Steigler, eds., MRS, Pittsburgh, PA, 1991, pp. 603-607.

240. Noebe, R.D., et al.: Effect of Zr Additions on the Microstructure and Mechanical Behavior of NiAl. HITEMP Review, 1989: Advanced High Temperature Engine Materials Technology Program, 1989, NASA CP-10039, 1989, pp. 48-1 - 48-15.

241. von Mises, R.: Mechanics of Plastic Form Change of Crystals. Z. Angew. Math. Mech., vol. 8, 1928, pp. 161-185. (Available as NASA TT-20718, 1990.)

242. Westbrook, J.H.; and Wood, D.L.: A Source of Grain-Boundary Embrittlement in Intermetallics. J. Inst. Met., vol. 91, 1962, pp. 174-182.

243. Seybolt, A.U.; and Westbrook, J.H.: Oxygen-Induced Grain Boundary Hardening in the Intermetallic Compounds AgMg, NiGa and NiAl. Metals for the Space Age: Plansee Proceedings, F. Benesofsky, ed., Springer, New York, 1965, pp. 845-857.

244. Seybolt, A.U.; Westbrook, J.H.; and Turnbull, D.: Mechanism for Grain Boundary and Free Surface Hardening by Oxygen-Vacancy Interactions. Acta Metall., vol. 12, 1964, pp. 1456-1457.

245. Zeller, M.V.; Noebe, R.D.; and Locci, I.E.: Grain Boundary Segregation Studies of NiAl and NiAl(Zr) Using Auger Electron Spectroscopy. HITEMP Review, 1990: Advanced High Temperature Engine Materials Technology Program, NASA CP-10051, 1990, pp. 21-1 - 21-17.

246. Kruisman, J.; Vitek, V.; and DeHossan, J.Th M.: Atomic Structure of Stoichiometric and Non-Stoichiometric Grain Boundaries in A_3B Compounds with $L1_2$ Structure. Acta Metall., vol. 36, 1988, pp. 2729-2741.

247. Vitek, V.; and Chen, S.P.: Modeling of Grain Boundary Structures and Properties in Intermetallic Compounds. Scripta Metall. Mater., vol. 25, 1991, pp. 1237-1242.

248. Chaki, T.K.: Mechanism of Boron-Induced Strengthening of Grain Boundaries in Ni_3Al. Philos. Mag. Lett., vol. 63, 1991, pp. 123-126.

249. Petton, G.; and Farkas, D.: Grain Boundary Structure Simulations in B2 Ordered NiAl. Scripta Metall. Mater., vol. 25, 1991, pp. 55-60.

250. Noebe, R.D.; and Cotton, J.D.: NASA Lewis Research Center, Cleveland, OH, unpublished research, 1991.

251. Barker, D.R.: The Strength and Ductility of Polycrystalline NiAl. M.E. Thesis, Dartmouth College, Hanover, NH., 1982.

252. Nagpal, P.; and Baker, I.: Room Temperature Fracture of FeAl and NiAl. Mater. Character., vol. 27, 1991, pp. 167-173.

253. Yoo, M.H.; and Fu, C.L.: On the Theory of Cleavage Fracture in B2-Type Aluminides—FeAl and NiAl. Scripta Metall. Mater., vol. 25, 1991, pp. 2345-2350.

254. Mason, D.P.; Van Aken, D.C.; Noebe, R.D.; Locci, I.E.; and King, K.L.: Microstructure and Mechanical Properties of Near Eutectic β-NiAl and α-Re Alloys Produced by Rapid Solidification and Extrusion. High Temperature Ordered Intermetallic Alloys IV, L.A. Johnson, D.P. Pope, and J.O. Stiegler, eds., MRS, Pittsburgh, PA, 1991, pp. 1033-1038.

255. Schulson, E.M.; and Barker, D.R.: A Brittle to Ductile Transition in NiAl of a Critical Grain Size. Scripta Metall., vol. 17, 1983, pp. 519-522.

256. Westbrook, J.H.; Grenoble, H.E.; and Wood, D.L.: Effect of Basic Physical Parameters on Engineering Properties of Intermetallic Compounds. WADD-TR-60-184, Pt V, 1964, p. 22.

257. Schulson, E.M.: Comments on the Brittle to Ductile Transition of Long-Range Ordered Alloys. Res. Mech. Lett., vol. 1, 1981, pp. 111-114.

258. Chan, K.S.: Theoretical Analysis of Grain Size Effects on Tensile Ductility. Scripta Metall. Mater., vol. 24, 1990, pp. 1725-1730.

259. Noebe, R.D.; Kim, J.T.; and Gibala, R.: Structure-Property Relationships in Directionally Solidified Single Crystal NiAl. Interdisciplinary Issues in Materials Processing and Manufacturing, Vol. 1, S.K. Samanta, R. Komanduri, and R. McMeeking, eds., ASME, New York, 1988, pp. 223-231.

260. Noebe, R.D.; and Gibala, R.: Surface Oxide Softening of Single Crystal NiAl. Scripta Metall., vol. 20, 1986, pp. 1635-1639.

261. Noebe, R.D.; Kim, J.T.; and Gibala, R.: Temperature and Orientation Dependence of Surface Film Effects in Single Crystal NiAl. High Temperature Ordered Intermetallic Alloys II, N.S. Stoloff, ed., MRS, Pittsburgh, PA, 1987, pp. 473-480.

262. Savitskii, E.M.; Burkhanov, G.S.; and Zalivin, I.M.: Structure and Mechanical Properties of NiAl Compound in Polycrystalline and Monocrystalline States. Strength Mater., vol. 4, 1972, pp. 1406-1407.

263. Seybolt, A.U.; Stover, E.R.; and Westbrook, J.H.: Investigation of the Basic Parameters Affecting the Properties of Intermetallic Compounds. WADC-TR-60-184. Pt. VI, 1965.

264. Darolia, R., et al.: Overview of NiAl Alloys for High Temperature Structural Applications. Ordered Intermetallics—Physical Metallurgy and Mechanical Behavior, C.T. Liu et al., eds., Kluwer Academic Publishers, The Netherlands, 1992, pp. 679-698.

265. Noebe, R.D.; Misra, A.; and Gibala, R.: Plastic Flow and Fracture of B2 NiAl-Based Intermetallic Alloys Containing a Ductile Second Phase. Iron Steel Inst. J. Int., vol. 31, 1991, pp. 1172-1185.

266. Noebe, R.D.: NASA Lewis Research Center, 1991, unpublished research.

267. Charpenay, S., et al.: Molecular Dynamics Study of Crack Propagation in Ni-Al. High Temperature Ordered Intermetallic Alloys III, C.T. Liu, ed., MRS, Pittsburgh, PA, 1989, pp. 29-35.

268. Charpenay, S.; Clapp, P.C.; and Rifkin, J.A.: Fracture Simulation in NiAl. Advanced Materials, A. ul Hag, N. Ahmad, and A.Q. Khan, eds., University Grants Commission, Pakistan, 1990, pp. 282-287.

269. Moncevicz, A.; Clapp, P.C.; and Rifkin, J.A.: Dislocation Mobilies in NiAl from Molecular Dynamics Simulations. Defects in Materials, P.D. Bristowe, ed., MRS, Pittsburgh, PA, 1990, pp. 213-218.

270. Kim, D.; Clapp, P.C.; and Rifkin, J.A.: Stress Induced Martensitic (SIM) Transformations in B2 NiAl Observed in Crack Propagation Computer Simulations. High Temperature Ordered Intermetallic Alloys IV, L.A. Johnson, D.P. Pope, and J.O. Stiegler, eds., MRS, Pittsburgh, PA, 1991, pp. 249-254.

271. Groves, G.W.; and Kelly, A.: Change of Shape Due to Dislocation Climb. Philos. Mag., vol. 19, 1969, pp. 977-986.

272. Brophy, H.; Rose, R.M.; and Wulff, J.: Thermodynamics of Structure, John Wiley & Sons, Inc., 1967, pp. 80-83.

273. Shewmon, P.G.: Diffusion in Solids, McGraw-Hill, 1983, pp. 170-172.

274. Lewandowski, J.J., et al.: Fracture Toughness and the Effects of Stress State on Fracture of Nickel Aluminides. Alloy Phase Stability and Design, G.M. Stocks. et al., eds., MRS, Pittsburgh, PA, 1991, pp. 341-347.

275. Kumar, K.S., et al.: Nickel Aluminide/Titanium Diboride Composites Via XD^{TM} Synthesis. MML TR 89-102(C), 1989.

276. Kumar, K.S.; Mannan, S.K.; and Viswanadham, R.K.: Fracture Toughness of NiAl and NiAl-Based Composites. Acta Metall. Mater., vol. 40, 1992, pp. 1201-1222.

277. Russell, S.M., et al.: Lightweight Disk Alloy Development. PWA-FR-19577-8, Pratt & Whitney, 1989.

278. Reuss, S.; and Vehoff, H.: Temperature Dependence of the Fracture Toughness of Single Phase and Two Phase Intermetallics. Scripta Metall. Mat., vol. 24, 1990, pp. 1021-1026.

279. Kaysser, W.A., et al.: Improvement of P/M-NiAl by Ti and Nb Additions. Int. J. Powder Metall., vol. 27, no. 1, 1991, pp. 43-49.

280. Reuss, S.; and Vehoff, H.: Bruchzahigkeiten Intermetallischer Werkstoffe. Intermetallische Phasen als Strukurwerkstoffe fur hohe Temperaturen, F.J. Bremer, ed., Forschungszentrum Julich GmbH, 1991, pp. 65-73.

281. Chang, K.M.; Darolia, R.; and Lipsitt, H.A.: Fracture of B2 Aluminide Single Crystals. High Temperature Ordered Intermetallic Alloys IV, L.A. Johnson, D.P. Pope, and J.O. Steigler, eds., MRS, Pittsburgh, PA, 1991, pp. 597-602.

282. Subramanian, P.R., et al.: Microstructures and Mechanical Properties of NiAl + Mo In-Situ Eutectic Composites. Intermetallic Matrix Composites, D.L. Anton, ed., MRS, Pittsburgh, PA, 1990, pp. 147-154.

283. Reuss, S.; and Vehoff, H.: Mechanical Properties of Intermetallics at High Temperatures. High Temperature Aluminides and Intermetallics, S.H. Whang, ed., The Minerals, Metals & Materials Society. Warrendale, 1990, pp. 329-352.

284. Kazmin, V.I.; Mileiko, S.T.; and Tvardovsky, V.V.: Strength of Ceramic Matrix-Metal Fibre Composites. Comp. Sci. Technol., vol. 38, 1990, pp. 69-84.

285. Chakravorty, S.; and Wayman, C.M.: The Thermoelastic Martensitic Transformation in β'Ni-Al Alloys: I. Crystallography and Morphology. Metall. Trans., vol. 7A, 1976, pp. 555-568.

286. Shah, D.M.; Anton, D.L.; and Musson, C.W.: Intermetallic Composite Feasibility. FR 20410-10, Pratt & Whitney, 1990.

287. Hsiung, L.M.; and Stoloff, N.S.: Cyclic Hardening and Crack Initiation in Intermetallic Compounds. Strength of Metals and Alloys, Vol. 1, P.O. Kettunen, T.K. Lepisto, and M.E. Lehtonen, eds., Pergamon Press, 1989, pp. 683-688.

288. Boettner, R.C.; Stoloff, N.S.; and Davies, R.G.: Effect of Long-Range Order on Fatigue. Trans. Metall. Soc. AIME, vol. 236, 1966, pp. 131-133.

289. Kuruvilla, A.K.; and Stoloff, N.S.: Fatigue of Ordered Alloys. Strength of Metals and Alloys, H.J. McQueen, ed., Pergamon Press, 1986, pp. 1335-1342.

290. Hartfield-Wunsch, S.E.; and Gibala, R.: Cyclic Deformation of B2 Aluminides. High Temperature Ordered Intermetallic Alloys IV, L. Johnson, D.P. Pope, and J.O. Stiegler, eds., MRS, Pittsburgh, PA, 1991, pp. 575-580.

291. Hartfield-Wunsch, S.E.: Monotonic and Cyclic Deformation Behavior of B2 Aluminides. Ph.D. Thesis, The University of Michigan, Ann Arbor, MI, 1991.

292. Bain, K.R.; Field, R.D.; and Lahrman, D.F.: Fatigue Behavior of NiAl Single Crystals. Presented at the 1991 TMS Fall Meeting, Oct. 21, 1991, Cincinnati, OH.

293. Lerch, B.; and Noebe, R.D.: Fatigue Behavior of Polycrystalline NiAl. HITEMP Review, 1992: Advanced High Temperature Engine Materials Technology Program, NASA CP- , 1992.

294. Cullers, C.L.: Deformation Mechanisms in Cyclically Deformed NiAl. M.S. Thesis, Georgia Institute of Technology, Atlanta, Ga., in progress.

295. Lutze-Birk, A.; and Jacobi, H.: Diffusion of ^{114m}In in NiAl. Scripta Metall., vol. 9, 1975, pp. 761-765.

296. Smoluchowski, R.; and Burgess, H.: Vacancies and Diffusion in NiAl. Phys. Rev., vol. 76, 1949, pp. 309-310.

297. Berkowitz, A.E.; Jaumot, F.E.; and Nix, F.C.: Diffusion of Co^{60} in Some Ni-Al Alloys Containing Excess Vacancies. Phys. Rev., vol. 95, 1954, pp. 1185-1189.

298. Shankar, S.; and Seigle, L.L.: Interdiffusion and Intrinsic Diffusion in the NiAl(δ) Phase of the Al-Ni System. Metall. Trans., vol. 9A, 1978, pp. 1467-1476.

299. Janssen, M.M.P.: Diffusion in the Nickel-Rich Part of the Ni-Al System at 1000° to 1300 °C; Ni_3Al Layer Growth, Diffusion Coefficients, and Interface Concentrations. Metall. Trans., vol. 4, 1973, pp. 1623-1633.

300. Janssen, M.M.P.; and Rieck, G.D.: Reaction Diffusion and Kirkendall-Effect in the Nickel-Aluminum System. Trans. Metall. Soc., AIME, vol. 239, 1967, pp. 1372-1385.

301. Kainuma, R., et al.: Pseudo-Interface in B2 Phase Region in Diffusion Couples of Ni-Al and Co-Al Base Systems. Proceedings of the International Symposium on Intermetallic Compounds—Structure and Mechanical Properties. O. Izumi, ed., Japan Institute of Metals, Sendai, Japan, 1991, pp. 99-103.

302. Merchant, S.M.; Notis, M.R.; and Goldstein, J.I.: Interface Stability in the Ni-Cr-Al System: Part I. Morphological Stability of β-γ Diffusion Couple Interfaces at 1150 °C. Metall. Trans., vol. 21A, 1990, pp. 1901-1919.

303. Nesbitt, J.A.; and Heckel, R.W.: Interdiffusion in Ni-rich, Ni-Cr-Al Alloys at 1100 and 1200 °C: Part I. Diffusion Paths and Microstructures. Metall. Trans., vol. 18A, 1987, pp. 2061-2073.

304. Nesbitt, J.A.; and Heckel, R.W.: Interdiffusion in Ni-rich, Ni-Cr-Al Alloys at 1100 and 1200 °C: Part II. Diffusion Coefficients and Predicted Concentration Profiles. Metall. Trans., vol. 18A, 1987, pp. 2075-2086.

305. Nesbitt, J.A.; and Heckel, R.W.: Predicting Diffusion Paths and Interface Motion in $\gamma/\gamma + \beta$, Ni-Cr-Al Diffusion Couples. Metall. Trans. vol., 18A, 1987, pp. 2087-2094.

306. Gupta, D.; and Lieberman, D.S.: Self-Diffusion in CsCl-Type Ordered Alloys. Ordered Alloys: Structural Applications and Physical Metallurgy, B.H. Kear, ed., Claitor Press, Baton Rouge, LA, 1970, pp. 195-213.

307. Nix, W.D.; and Ilschner, B.: Mechanisms Controlling Creep of Single Phase Metals and Alloys. Strength of Metals and Alloys: Proceedings of the Fifth International Conference, Vol. 3, P. Hassen, V. Gerald, and G. Kostorz, eds., Pergamon, 1980, pp. 1503-1531.

308. Nathal, M.V.; Diaz, J.O.; and Miner, R.V.: High Temperature Creep Behavior of Single Crystal Gamma Prime and Gamma Alloys. High Temperature Ordered Intermetallic Alloys III, C.T. Liu, ed., MRS, Pittsburgh, PA, 1989, pp. 269-274.

309. Oliver, W.C.; and Nix, W.D.: High Temperature Deformation of Oxide Dispersion Strengthened Al and Al-Mg Solid Solutions. Acta Metall., vol. 30, 1982, pp. 1335-1347.

310. Whittenberger, J.D.; Ray, R.; and Jha, S.C.: Does a Threshold Stress for Creep Exist in HfC-Dispersed NiAl? High Temperature Ordered Intermetallic Alloys IV, L.A. Johnson, D.P. Pope, and J.O. Steigler, eds., MRS, Pittsburgh, PA, 1991, pp. 581-587.

311. Mills, M.J.; Gibeling, J.C.; and Nix, W.D.: Measurement of Anelastic Creep Strains in Al 5.5 at % Mg Using a New Technique: Implications for the Mechanism of Class I Creep. Acta Metall., vol. 34, 1986, pp. 915-925.

312. Mohamed, F.A.; and Langdon, T.G.: The Transition from Dislocation Climb to Viscous Glide in Creep of Solid Solution Alloys. Acta Metall., vol. 22, 1974, pp. 779-788.

313. Soliman, M.S.; and Mohamed, F.A.: Correlation Between Creep Behavior and Substructure in an Al-3at.%Mg Solid Solution Alloy. Maters. Sci. Eng., vol. 55, 1982, pp. 111-119.

314. Yaney, D.L.; Gibeling, J.C.; and Nix, W.D.: A New Strain Rate Change Technique for Distinguishing Between Pure Metal and Alloy Type Creep Behavior. Acta Metall., vol. 35, 1987, pp. 1391-1400.

315. Langdon, T.G.; and Yavari, P.: The Effect of Instantaneous Strain on Creep Measurements at Apparent Constant Structure. Creep and Fracture of Engineering Materials and Structure, B. Wilshire and D.R.J. Owen, eds., Pineridge Press, Swansea, UK, 1981, pp. 71-84.

316. Whittenberger, J.D.: The Influence of Grain Size and Composition on 1000 to 1400 K Slow Plastic Flow Properties of NiAl. J. Mater. Sci., vol. 23, 1988, pp. 235-240.

317. Whittenberger, J.D.: Effect of Composition and Grain Size on Slow Plastic Flow Properties of NiAl Between 1200 and 1400 K. J. Mater. Sci., vol. 22, 1987, pp. 394-402.

318. Whittenberger, J.D., et al.: Elevated Temperature Slow Plastic Deformation of NiAl-TiB$_2$ Particulate Composites at 1200 and 1300 K. J. Mater. Sci., vol. 25, 1990, pp. 35-44.

319. Yang, W.J.; and Dodd, R.A.: Steady-State Creep and Associated Microstructures in Stoichiometric and Non-Stoichiometric Polycrystalline NiAl. Met. Sci. J., vol. 7, 1973, pp. 41-47.

320. Rudy, M.; and Sauthoff, G.: Creep Behavior of the Ordered Intermetallic (Fe,Ni)Al Phase. High Temperature Ordered Intermetallic Alloys, C.C. Koch, C.T. Liu, and N.S. Stolotti, eds., MRS, Pittsburgh, PA, 1985, pp. 327-333.

321. Hocking, L.A.; Strutt, P.R.; and Dodd, R.A.: Comparison of Steady-State Compression Creep Behavior in Stoichiometric CoAl and NiAl Single Crystals Between 850 and 1050 °C. Inst. Met. J., vol. 99, 1971, pp. 98-101.

322. Noebe, R.D.; and Whittenberger, J.D.: Unpublished research. NASA Lewis Research Center, Cleveland, OH, 1991.

323. Raj, S.V.; and Farmer, S.: Unpublished research. NASA Lewis Research Center, Cleveland, OH, 1991.

324. Ashby, M.F.: A First Report on Deformation-Mechanism Maps. Acta Metall., vol. 20, 1972, pp. 887-897.

325. Bird, J.E.; Mukherjee, A.K.; and Dorn, J.E.: Correlations Between High-Temperature Creep Behavior and Structure. Quantitative Relation Between Properties and Microstructures, Proceedings of the International Conference, D.G. Brandon and A. Rosen, eds., Israel University Press, Jerusalem, Israel, 1969, pp. 255-342.

326. Yaney, D.L.; and Nix, W.D.: Mechanisms of Elevated-Temperature Deformation in the B2 Aluminides NiAl and CoAl. J. Mater. Sci., vol. 23, 1988, pp. 3088-3098.

327. Whittenberger, J.D.; Kumar, K.S.; and Mannan, S.K.: 1000 to 1300 K Slow Plastic Compression Properties of Al-Deficient NiAl. J. Mater. Sci., vol. 26, 1991, pp. 2015-2022.

328. Whittenberger, J.D.: The Influence of Grain Size and Composition on Slow Plastic Flow in FeAl Between 1100 and 1400 K. Mater. Sci. Eng., vol. 77, 1986, pp. 103-113. Also, Effect of Grain Size on the High Temperature Properties of B2 Aluminides. NASA TM-101382, 1987.

329. Jung, I.; Rudy, M.; and Sauthoff, G.: Creep in Ternary B2 Aluminides and Other Intermetallic Phases. High Temperature Ordered Intermetallic Alloys II, N.S. Stoloff, ed., MRS, Pittsburgh, PA, 1987, pp. 263-274.

330. Nathal, M.V.; and Ebert, L.J.: Elevated Temperature Creep-Rupture Behavior of the Single Crystal Nickel-Base Superalloy NASAIR 100. Metall. Trans., vol. 16A, 1985, pp. 427-439.

331. Whittenberger, J.D., et al.: 1200 to 1400 K Slow Strain Rate Compressive Behavior of Small Grain Size NiAl/Ni$_2$AlTi Alloys and NiAl/Ni$_2$AlTi-TiB$_2$ Composites. J. Mater. Res., vol. 4, 1989, pp. 1164-1171.

332. Pathare, V.M.: Processing, Physical Metallurgy and Creep of NiAl + Ta and NiAl + Nb Alloys. Ph.D. Thesis, Case Western Reserve University, Cleveland, OH, 1987. (Also, NASA CR-182113, 1988.)

333. Raj, S.V.; Locci, I.E.; and Noebe, R.D.: Deformation Behavior of a Ni-30Al-20Fe-0.05Zr Intermetallic Alloy. Metall. Trans. A., vol. 23A, 1992, pp. 1705-1718.

334. Polvani, R.S.; Tzeng, W.S.; and Strutt, P.R.: High Temperature Creep in a Semi-Coherent NiAl-Ni$_2$AlTi Alloy. Metall. Trans., vol. 7A, 1976, pp. 33-40.

335. Whittenberger, J.D.; Westfall, L.J.; and Nathal, M.V.: Compressive Strength of a B2 Matrix NiAl-Nb Intermetallic at 1200 and 1300 K. Scripta Metall., vol. 23, 1989, pp. 2127-2130.

336. Whittenberger, J.D.; Reviere, R.; Noebe, R.D.; Oliver, B.F.: Compressive Strength of Directionally Solidified NiAl-NiAlNb Intermetallics at 1200 and 1300 K. Scripta Metall. Mater., vol. 26, 1992, pp. 987-992.

337. Whittenberger, J.D., et al.: Slow Strain Rate 1200-1400 K Compressive Properties of NiAl-1Hf. Mater. Letters, vol. 11, 1991, pp. 267-272.

338. Bowman, R.R., et al.: Creep Behavior of [001] Oriented Ni-49Al-1Hf Single Crystals. Unpublished research.

339. Locci, I.E.; and Noebe, R.D.: Characterization of Second-Phase Particles in NiAl Containing Trace Additions of Zr. Proceedings of the 47th Annual Meeting of the Electron Microscopy Society of America, G.W. Bailey, ed., San Francisco Press, Inc., San Francisco, CA, 1989, pp. 308-309.

340. Locci, I.E.; Noebe, R.D.; Bowman, R.R.; Miner, R.V.; Nathal, M.V.; and Darolia, R.: Microstructure and Mechanical Properties of a Single Crystal NiAl Alloy with Zr or Hf Rich G-phase Precipitates. High Temperature Ordered Intermetallic Alloys IV, L.A. Johnson, D.P. Pope, J.O. Steigler, eds., MRS, Pittsburgh, PA, 1991, pp. 1013-1018.

341. See discussion following the paper by Strutt, P.R.; and Dodd, R.A.: Creep in Ordered Alloys. Ordered Alloys: Structural Applications and Physical Metallury, B.H. Kear, ed., Claitor's Publishing Division, Baton Rouge, LA, 1970, pp. 475-504.

342. Whittenberger, J.D.; Gaydosh, D.J.; Kumar, K.S.: 1300 K Compressive Properties of Several Dispersion Strengthened NiAl Materials. J. Mater. Sci., vol. 25, 1990, pp. 2771-2776.

343. Jha, S.C.; Ray, R.; and Whittenberger, J.D.: Carbide-Dispersion-Strengthened B2 NiAl. Mater. Sci. Eng., vol. A119, 1989, pp. 103-111.

344. Whittenberger, J.D., et al.: 1000-1300 K Slow Strain Rate Properties of NiAl Containing Dispersed TiB_2 and HfB_2. Mater. Sci. Eng., vol. A138, 1991, pp. 83-93.

345. Whittenberger, J.D.; Ray, R.; and Jha, S.: Influence of Grain Size on the Creep Behavior of HfC-Dispersed NiAl. Mater. Sci. Eng. A, vol. A151, 1992, pp. 137-146.

346. Benn, R.C.: Microstructure and Property Relationships in Oxide Dispersion Strengthened Alloys. MiCon 86: Optimization of Processing, Properties and Service Performance Through Microstructural Control: Proceedings of the Symposium, ASTM STP-979, B.L Bramfitt, R.C. Benn, and C.R. Brinkman, eds., ASTM, Philadelphia, PA, 1988, pp. 238-268.

347. Whittenberger, J.D.; Arzt, E.; and Luton, M.J.: Preliminary Investigation of a NiAl Composite Prepared by Cryomilling. J. Mater. Res., vol. 5, 1990, pp. 271-277.

348. Whittenberger, J.D.; Arzt, E.; and Luton, M.J.: 1300 K Compressive Properties of a Reaction Milled NiAl-AlN Composite. J. Mater. Res., vol. 5, 1990, pp. 2819-2827.

349. Whittenberger, J.D.; Arzt, E.; and Luton, M.J.: 1300 K Compressive Properties of a Reaction Milled NiAl-AlN Composite. Intermetallic Matrix Composites, D.L. Anton, ed., MRS, Pittsburgh, PA, 1990, pp. 211-218.

350. Whittenberger, J.D.: Solid State Processing for High Temperature Alloys and Composites. Solid State Processing, A.H. Clauer and J.J. deBarbadillo, eds., The Minerals, Metals and Materials Society, Warrendale, PA, 1990, pp. 137-155.

351. Lowell, C.E.; Barrett, C.A.; and Whittenberger, J.D.: Cyclic Oxidation Resistance of a Reaction Milled NiAl-AlN Composite. Intermetallic Matrix Composites, D.L. Anton, ed., MRS, Pittsburgh, PA, 1990, pp. 355-360.

352. Viswanadham, R.K., et al.: Elevated Temperature Slow Plastic Deformation of $NiAl/TiB_2$ Particulate Composites. High Temperature/High Performance Composites, F.D. Lemkey, ed., MRS, Pittsburgh, PA, 1988, pp. 89-94.

353. Whittenberger, J.D., et al.: Slow Plastic Deformation of Extruded $NiAl-10TiB_2$ Particulate Composites at 1200 and 1300 K. J. Mater. Sci. Lett., vol. 9, 1990, pp. 326-328.

354. Whittenberger, J.D.; Kumar, K.S.; and Mannan, S.K.: 1200 and 1300 K Slow Plastic Compression Properties of Ni-50Al Composites. Mater. High Temp., vol. 9, 1991, pp. 3-12.

355. Whittenberger, J.D.; Mannan, S.K.; and Kumar, K.S.: 1100 to 1300 K Slow Plastic Compression Properties of Ni-38.5Al Composites. Scripta Metall., vol. 23, 1989, pp. 2055-2060.

356. Kelly, A.; and Street, K.N.: Creep of Discontinuous Fibre Composites II. Theory for the Steady State. Proc. R. Soc. London A, vol. 328, no. 1573, 1972, pp. 283-293.

357. Kumar, K.S.; and Whittenberger, J.D.: Intermetallic Matrix Composites via XD^{TM} Synthesis. Proceedings of the International Symposium on Intermetallic Compounds—Structure and Mechanical Properties, O. Izumi, ed., Japan Institute of Metals, Sendai, Japan, 1991, pp. 927-934.

358. Whittenberger, J.D., et al.: 1200 to 1400 K Slow Strain Rate Compressive Properties of $NiAl/Ni_2AlTi$-Base Materials. High Temperature Ordered Intermetallic Alloys III, C.T. Liu, ed., MRS, Pittsburgh, PA, 1989, pp. 621-626.

359. Walter, J.L.; and Cline, H.E.: The Effect of Solidification Rate on Structure and High-Temperature Strength of the Eutectic NiAl-Cr. Metall. Trans., vol. 1, 1970, pp. 1221-1229.

360. Johnson, D.; Joslin, S.M.; Oliver, B.F.; Noebe, R.D.; and Whittenberger, J.D.: Intermetallic/ Metallic Polyphase In-Situ Composites. Intermetallic Matrix Composites II, D.B. Miracle and J.A. Graves, eds., MRS Symposia Proc., Vol. 273, 1992.

361. Walter, J.L.; and Cline, H.E.: Stability of the Directionally Solidified Eutectics NiAl-Cr and NiAl-Mo. Metall. Trans., vol. 4, 1973, pp. 33-38.

362. Webber, J.G.; and Van Aken, D.C.: Studies of a Quasi-Binary β-NiAl and α-Re Eutectic. Scripta Metall., vol. 23, 1989, pp. 193-196.

363. Pellegrini, P.W.; and Hutta, J.J.: Investigations of Phase Relations and Eutectic Directional Solidification of the NiAl-V Join. J. Cryst. Growth, vol. 42, 1977, pp. 536-539.

364. Pickens, J.W.; Noebe, R.D.; Watson, G.K.; Brindley, P.K.; and Draper, S.L.: Fabrication of Intermetallic Matrix Composites by the Powder Cloth Process. NASA TM-102060, 1989.

365. Noebe, R.D.; Bowman, R.R.; and Eldridge, J.: Initial Evaluation of Continuous Fiber Reinforced NiAl Composites. Intermetallic Matrix Composites, D.L. Anton, ed., MRS, Pittsburgh, PA, 1990, pp. 323-332.

366. Bowman, R.R.; and Noebe, R.D.: Processing and Mechanical Evaluation of Continuous Fiber Reinforced NiAl Composites. HITEMP Review—1990: Advanced High Temperature Engine Materials Technology Program, NASA CP-10051, 1990, pp. 40-1 to 40-14.

367. Bowman, R.R.; Noebe, R.D.; Doychak, J.; Crandall, K.S.; and Locci, I.E.: Effect of Interfacial Properties on the Mechanical Behavior of NiAl Based Composites. HITEMP Review—1991: Advanced High Temperature Engine Materials Technology Program, NASA CP-10082, 1991, pp. 43-1 to 43-14.

368. Wood, J.H.; and Goldman, E.: Protective Coatings. Superalloys II, C.T. Sims, N.S. Stoloff, and W.C. Hagel, eds., Wiley, 1987, pp. 359-384.

369. Rhys-Jones, T.N.: Coatings for Blade and Vane Applications in Gas Turbines. Corros. Sci., vol. 29, 1989, pp. 623-646.

370. Doychak, J.; Smialek, J.L.; and Mitchell, T.E.: Transient Oxidation of Single-Crystal β-NiAl. Metall. Trans., vol. A20, 1989, pp. 499-518.

371. Wood, G.C.; and Chattopadhyay, B.: Transient Oxidation of Ni-Base Alloys. Corros. Sci., vol. 10, 1970, pp. 471-480.

372. Hutchings, R.; Loretto, M.H.; and Smallman, R.E.: Oxidation of Intermetallic Compound NiAl. Met. Sci, vol. 15, 1981, pp. 7-13.

373. Rybicki, G.C.; and Smialek, J.L.: Effect of the θ-α-Al_2O_3 Transformation on the Oxidation Behavior of β-NiAl + Zr. Oxid. Met., vol. 31, 1989, pp. 275-304.

374. Grabke, H.J., et al.: Oxidation and Intergranular Disintegration of the Aluminides NiAl and $NbAl_3$ and Phases in the System Nb-Ni-Al. Oxid. Met., vol. 35, 1991, pp. 199-222.

375. Young, E.W.A.; and DeWit, J.H.W.: An [18]O Tracer Study on the Growth Mechanism of Alumina Scales on NiAl and NiAlY Alloys. Oxid. Met., vol. 26, 1986, pp. 351-361.

376. Young, E.W.A.; and DeWit, J.H.W.: The Use of a [18]O Tracer and Rutherford Backscattering Spectrometry to Study the Oxidation Mechanism of NiAl. Solid State Ionics, vol. 16, 1985, pp. 39-46.

377. Reddy, K.P.R.; Smialek, J.L.; and Cooper, A.R.: [18]O Tracer Studies of Al_2O_3 Scale Formation on NiCrAl Alloys. Oxid. Met., vol. 17, 1982, pp. 429-449.

378. Huntz, A.M.: Influence of Active Elements on the Oxidation Mechanism of M-Cr-Al Alloys. Mater. Sci. Eng., vol. 87, 1987, pp. 251-260.

379. Hutchings, R.; and Loretto, M.H.: Compositional Dependence of Oxidation Rates of NiAl and CoAl. Met. Sci., vol. 12, 1978, pp. 503-510.

380. Doychak, J.; Smialek, J.L.; and Barrett, C.A.: The Oxidation of Ni-Rich Ni-Al Intermetallics. Oxidation of High Temperature Intermetallics, T. Grobstein and J. Doychak, eds., The Minerals, Metals and Materials Society, Warrendale, PA, 1989, pp. 41-55.

381. Doychak, J.: The Evolution and Growth of Al_2O_3 Scales on β-NiAl. NASA CR-175097, 1986.

382. Jedlinski, J.; and Mrowec, S.: The Influence of Implanted Yttrium on the Oxidation Behavior of β-NiAl. Mater. Sci. Eng., vol. 87, 1987, pp. 281-287.

383. Westbrook, J.H.; and Wood, D.L.: "Pest" Degradation in Beryllides, Silicides, Aluminides and Related Compounds. J. Nucl. Mater., vol. 12, 1964, pp. 208-215.

384. Doychak, J.; Barrett, C.A.; and Smialek, J.L.: Oxidation Between 1000 °C and 1600 °C and Limiting Criteria for the Use of Zr-Doped β-NiAl and β/γ' Alloys. Corrosion and Particle Erosion at High Temperatures, V. Srinivasan and K. Vedula, eds., The Minerals, Metals and Materials Society, Warrendale, PA, 1989, pp. 487-514.

385. Smialek, J.L.; and Meier, G.H.: High-Temperature Oxidation. Superalloys II, C.T. Sims, N.S. Stoloff, and W.C. Hagel, eds., Wiley, 1987, pp. 293-326.

386. Barrett, C.A.: Effect of 0.1 at % Zirconium on the Cyclic Oxidation Resistance of β-NiAl. Oxid. Met., vol. 30, 1988, pp. 361-390.

387. Nesbitt, J.A., et al.: Predicting the Oxidative Lifetime of β NiAl-Zr Alloys. HITEMP Review—1991: Advanced High Temperature Engine Materials Technology Program, NASA CP-10082, 1991, pp. 19-1 to 19-12.

388. Smeggil, J.G.; Funkenbush, A.W.; and Bornstein, N.S.: A Relationship Between Indigenous Impurity Elements and Protective Oxide Scale Adherence Characteristics. Metall. Trans., vol. 17A, 1986, pp. 923-932.

389. Smeggil, J.G.: Some Comments on the Role of Yttrium in Protective Oxide Scale Adherence. Mater. Sci. Eng., vol. 87, 1987, pp. 261-265.

390. Smialek, J.L.: Adherent Al_2O_3 Scales Formed on Undoped NiCrAl Alloys. Metall. Trans., vol. 18A, 1987, pp. 164-167.

391. Pettit, F.S.; and Giggins, G.S.: Hot Corrosion. Superalloys II, C.T. Sims, N.S. Stoloff, and W.C. Hagel, eds., Wiley, 1987, pp. 327-358.

392. Kaufman, M.: Hot Corrosion Reactions in Nickel, Cobalt and Nickel-Aluminide-Base Alloys. Trans. ASM, Q., vol. 62, 1969, pp. 590-606.

393. Ellis, D.: Hot Corrosion of the B2 Nickel Aluminides. M.S. Thesis, Case Western Reserve University, Cleveland, OH, 1987.

394. Godlewski, K., et al.: Sulphide Corrosion of Pure and Chromium-Modified, β-NiAl Intermetallic Compound at High Temperatures. Mater. Sci. Eng., vol. A120, 1989, pp. 105-109.

395. McCarron, R.L.; Lindblad, N.R.; and Chatterji, D.: Environmental Resistance of Pure and Alloyed γ'Ni$_3$Al and β-NiAl. Corrosion, vol. 32, 1976, pp. 476-481.

396. Aitken, E.A.: Corrosion Behavior. Intermetallic Compounds, J.H. Westbrook, ed., R.E. Krieger Publishing Co., Huntington, NY, 1977, pp. 491-516.

397. Tsvikilevich, O.S.; Shirokov, V.V.; and Stepanishkin, V.I.: Structure and Properties of a Nickel-Aluminum Intermetallide Coating Obtained in a Medium of Low-Melting Metals on 08Kh16N11M3 Steel. Sov. Mater. Sci., vol. 26, 1990, pp. 692-694.

398. Darolia, R.; Field, R.D.; and Lahrman, D.F.: Alloy Modeling and Experimental Correlation for Ductility Enhancement in Near Stoichiometric Single Crystal Nickel Aluminide. High Temperature Ordered Intermetallic Alloys III; Proceedings of the Third Symposium, C.T. Liu, ed., MRS, Pittsburgh, PA, 1989, pp. 113-118.

399. Chambers, S.A.: Surface Termination of Epitaxial NiAl on GaAs(001) by High-Angular-Resolution X-Ray Photoelectron Diffraction. Phys. Rev. B, vol. 42, 1990, pp. 10865-10872.

400. Chambers, S.A.; and Loebs, V.A.: Structure, Chemistry, and Fermi-Level Movement at Interfaces of Epitaxial NiAl and GaAs(001). J. Vac. Sci. Technol., vol. B8, 1990, pp. 724-729.

401. Chambers, S.A.: Surface Termination of Epitaxial NiAl on GaAs(001) by X-Ray Photoelectron Diffraction. J. Vac. Sci. Technol., vol. A8, 1990, pp. 2062-2067.

402. Chambers, S.A.; and Loebs, V.A.: Schottky Barrier Height and Thermal Stability of the NiAl/ n-Ge/GaAs(001) Interface. J. Vac. Sci. Technol., vol. A8, 1990, pp. 2074-2078.

403. Tabatabaie, N., et al.: Negative Differential Resistance in AlAs/NiAl/AlAs Heterostructures: Evidence for Size Quantization in Metals. Appl. Phys. Lett., vol. 53, 1988, pp. 2528-2530.

404. Harbison, J.P., et al.: Molecular Beam Epitaxial Growth of Ultrathin Buried Metal Layers: (Al,Ga)As/ NiAl/(Al,Ga)As Heterostructures. Appl. Phys. Lett., vol. 53, 1988, pp. 1717-1719.

405. Kamigaki, K., et al.: High-Temperature Growth of Epitaxial NiAl Thin Films on AlAs by Molecular-Beam Epitaxy. J. Appl. Phys., vol. 69, 1991, pp. 2196-2200.

406. Sands, T., et al.: Epitaxial Growth of GaAs/NiAl/GaAs Heterostructures. Appl. Phys. Lett., vol. 52, 1988, pp. 1216-1218.

407. Harbison, J.P., et al.: MBE Growth of AlGaAs/NiAl/AlGaAs Heterostructures: A Novel Epitaxial III-V Semiconductor/Metal System. J. Cryst. Growth, vol. 95, 1989, pp. 425-426.

408. Tabatabaie, N., et al.: Electrical Resistivity of Thin Epitaxial NiAl Buried in (Al,Ga)As. Appl. Phys. Lett., vol. 54, 1989, pp. 2112-2114.

409. Cheeks, T.L., et al.: Electrical and Optical Characterization of Back-to-Back Schottky (Al,Ga)As/ NiAl/(Al,Ga)As Molecular Beam Epitaxially Grown Double-Heterostructure Diodes. Appl. Phys. Lett., vol. 56, 1990, pp. 1043-1045.

410. Joo, G.C.; Tsakalakos, T.; and Chen, S.P.: Modelling the Growth of NiAl Epilayer on Zinc-Blende Substrate. Philos. Mag. Lett., vol. 63, 1991, pp. 249-256.

411. Sands, T., et al: Interface Crystallography and Stability in Epitaxial Metal (NiAl,CoAl)/III-V Semiconductor Heterostructures. Mater. Sci. Eng., vol. B6, 1990, pp. 147-157.

412. Sands, T.: Stability and Epitaxy of NiAl and Related Intermetallic Films on III-V Compound Semiconductors. Appl. Phys. Lett., vol. 52, 1988, pp. 197-199.

413. Chambers, S.A.: Molecular-Beam Epitaxial Growth of NiAl on GaAs(001). J. Vac. Sci. Technol., vol. B7, 1989, pp. 737-741.

414. Sands, T., et al.: NiAl/n-GaAs Schottky Diodes: Barrier Height Enhancement by High Temperature Annealing. Appl. Phys. Lett., vol. 52, 1988, pp. 1338-1340.

415. Chambers, S.A.; Loebs, V.A.; and Doyle, D.H.: The Role of Ultrathin AlAs Interlayers in Determining the Interface Fermi Energy of the Epitaxial NiAl/AlAs/n-GaAs(001) System. J. Vac. Sci. Technol., vol. B8, 1990, pp. 985-989.

TABLE I.—OBSERVED SLIP SYSTEMS IN UNIAXIALLY DEFORMED NiAl

Material	Temperature range, K	Slip vector	Slip plane	Analysis technique[a,b]	References
Polycrystalline NiAl	300-900	<100>	{011}	TEM	128,177,178
Single crystal NiAl "soft" orientations:					
[111]	77-1373	<100>	{011}	SSTA/TEM	165,167,173,176
[122]	77-300	<100>	{011}	SSTA	167
[123]	77-873	<100>	{011}	TEM	144,175
[110]	77-300	<100>	{011}	SSTA/TEM	138,167
[110]	300-1373	<100>	{001}	SSTA/TEM	165,166,167,169,173,176
[227]	573	<100>	{011}	SSTA	165
[112]	77-873	<100>	{011} or {001}	SSTA/TEM	141,165,172
"Hard" orientation [001]	300-1300	<100>	{011}	SSTA/TEM	143-145,167,170-172
	600-1372	<110>	{011}	SSTA/TEM	143,144,166,167,169,176
	77-600	<111>	{112},{011}, or {123}	SSTA/TEM	141,144,167,172,174,175

[a]TEM - Transmission electron microscopy investigation.
[b]SSTA - Surface slip trace analysis.

TABLE II.—SLIP FAMILIES AND RESULTING NUMBER OF INDEPENDENT SLIP SYSTEMS (ref. 207)

Slip family(ies)	Number physically distinct	Number independent
{011}<100>	6	3
{011}<0Ī1>	6	2
{011}<100> + {011}<0Ī1>	12	5
{100}<011>	6	3
{011}<100> + {100}<011>	12	3
{011}<11Ī>	12	5
{112}<11Ī>	12	5

TABLE III.—SOLID SOLUTION STRENGTHENING IN NiAl

Dopant	Atomic %	$\Delta\sigma_y/\Delta c$, MPa/at %	Reference	Goldschmidt radii, nm	Atomic radii, nm
Boron	0.04	4500	227,228	0.093	0.117
Zirconium	.05	4000	128	.157	.216
Carbon	.11	>1700	227	.084	.0091
Chromium	1.00	258	189,199	.125	.185
Beryllium	.24	100	227	.111	.140

TABLE IV.—EFFECT OF POST EXTRUSION HEAT-TREATMENT ON THE ROOM TEMPERATURE 0.2 PERCENT YIELD STRENGTH OF NiAl AND NiAl + 0.05 at % Zr ALLOYS (ref. 128)

Alloy	Grain size, μm	Annealing temperature (K)/ annealing time (hr)	Cooling rate, K/s	Yield strength,[a] MPa
NiAl	11.0±1.0	As-extruded (1200 K)	0.33-0.833	333±6
		875/2	0.17	342±6
		975/2	0.17	334±2
		1075/2	0.17	284±12
		1180/2	0.17	288±8
NiAl	21.8±2.8	As-extruded (1400 K)	0.33-0.833	292±3
	22.0±3.0	1100/1	1.33 (air cool)	326
	22.2±2.6	1173/2	.017	257±5
	22.0±3.0	1073/2	.017	250±5
NiAl(Zr)	5.5±0.9	As-extruded (1200 K)	0.33-0.833	572±8
	5.5±1.0	1100/1	1.33 (air cool)	603
	5.5±1.0	1173/2	.017	567±5
	5.5±1.0	1073/2	.017	577±9
NiAl(Zr)	14.0±1.6	As-extruded (1200 K)	0.33-0.833	379±4
	14.0±2.0	1100/1	1.33 (air cool)	387
	14.0±1.6	1173/2	.017	378±6

[a]Average of at least four tests when standard deviation is reported.

TABLE V.—ROOM TEMPERATURE RESOLVED SHEAR
STRESS VALUES ON {110} AND {100} PLANES FOR
"SOFT" ORIENTED NiAl SINGLE CRYSTALS

Orientation	0.2%σ_y, MPa	Resolved shear stress, MPa		Reference
		{110}	{100}	
[110]	[a]95	34	48	138
[123]	347	158	149	174
[111]	[a]145	68	48	165
[110]	[a]296	105	148	165
[112]	[a]206	97	69	165
[111]	264±4.6	124±2.2	88±1.5	173
[110]	217±0.7	77±0.2	109±0.4	173
[111]	147	69	49	262
[110]	294	104	147	262

[a]Estimated from stress-strain curves.

TABLE VI.—ROOM TEMPERATURE PROPERTIES AND FRACTURE BEHAVIOR OF NiAl ALLOYS

Key for figure 28	Alloy, at %	Processing route	Grain size, μm	Yield strength, MPa	Tensile fracture strength, MPa	Fracture morphology[a]	Reference
a	Ni-50.6 Al	Powder ext.	10-11	[b]330-350	340-360	Mixed mode	128
b	Ni-50.6 Al	Powder ext.	33	[b]274	277	Mixed mode	128
c	NiAl (0.03 C)	Cast + ext.	29±3	211-213	232-252	Mostly int.	233
d	NiAl	Cast + ext.	18±2	172-192	252-264	Mostly int.	189,250
e	NiAl (0.004 B)	Cast + ext.	33±4	227-229	260-279	Mixed mode	250
f	NiAl (0.05 Zr)	Powder ext.	4-5	[b]620	630	Trans.	128
g	NiAl (0.05 Zr)	Powder ext.	13-19	[b]410-420	400-420	Mostly trans.	128
h	NiAl (3 Re)	Ext. MSR[c]	1-3	[b]660-668	497	Mostly trans.	250,254
i	NiAl (0.5W,0.1C)	Ext. MSR[c]	3	[b]704-715	635	Trans.	250
j	NiAl (0.5 W)	Ext. MSR[c]	8	[b]457-465	430	Trans.	250
k	NiAl (0.05 Hf)	Ext. MSR[c]	9-11	[b]380-390	415	Trans.	250
l	NiAl (0.05 Y)	Ext. MSR[c]	9-11	[b]265-273	146	Trans.	250
m	NiAl (1 Cr)	Cast + ext.	24±3	[b]430-444	266	Mostly trans.	189,250
n	Ni-48Al-2Cr	Cast + ext.	20±4	[b]520-540	325-481	Trans.	189,250
o	Ni-45Al-5Cr	Powder ext.	9-13	[b]808-830	500-632	Trans.	189,250
p	Ni-50.3 Al	Cast + ext.	11-16	240	320	[d]Mixed mode	213
q	NiAl	Cast + ext.	13-25	115	180-200	[e]Inter.	223,252
r	NiAl	Cast + ext.	25-35	154	229	[d]Mostly inter.	227,228
s	NiAl (0.12 B)[+]	Cast + ext.	25-35	[f]694	329	[d]Trans.	227,228
t	NiAl (0.11 C)[+]	Cast + ext.	25-35	[g]710	336	[d]Mostly trans.	227,228
u	NiAl (0.24 Be)[+]	Cast + ext.	25-35	178	307	[d]Mostly inter.	227,228

[a]The following scale was used in evaluating the fracture mode of NiAl alloys:

Description	Percent intergranular fracture
Trans(granular)	0-20
Mostly trans(granular)	20-40
Mixed mode	40-60
Mostly inter(granular)	60-80
Inter(granular)	80-100

[b]Yield stress determined in compression (no macro-yield in tension).
[c]MSR - chopped melt spun ribbon.
[d]Based on quantitative measurement of published micrograph.
[e]Based on qualitative description found in the reference (percent intergranular fracture was not quantitatively measured).
[f]Estimate based on data from reference 228.
[g]Estimate based on the strength of alloy (i) in this table.

TABLE VII.—BRITTLE-TO-DUCTILE TRANSITION TEMPERATURES[a] FOR NiAl ALLOYS

Alloy composition, at %	Processing technique	Grain size, μm	Strain rate, s^{-1}	BDTT,[a] K	Reference
Ni-50.5Al[b] (initial charge comp.)	Cast + extruded	(e)	1.4×10^{-3}	550	217
Ni-50.6Al (0.028 O + C + S)	Extruded powder	33±4 10 5	1.4×10^{-4} 1.4×10^{-4} 1.4×10^{-4}	715 615 550	128,215
Ni-50Al[b] (nominal comp.)	Extruded powder	20-40	1.4×10^{-4}	675	197
Ni-50.3Al (0.013 O + C)	Cast + extruded	≈16	1.4×10^{-4}	≈550	213
Ni-50Al[b] (nominal comp.)	Extruded melt-spun ribbon	8	1.4×10^{-4}	715	254
Ni-49Al-0.01Zr (0.010 O + C + S)	Cast + extruded	[c]30	1.4×10^{-4} 5×10^{-6}	690 600	236,255
Ni-49.7Al[b]	As cast	(e)	Variable[d]	1000	219
Ni-50.3Al-0.05Zr (0.027 O + C + S)	Extruded powder	19±2	1.4×10^{-4}	875	128,221
Ni-51Al-1.5Re (0.070 O + C)	Extruded melt-spun ribbon	2	1.4×10^{-4}	900	254
Ni-48.5Al-3Re (0.076 O + C)	Extruded melt-spun ribbon	2	1.4×10^{-4}	900	254
Ni-50Al-0.25B[b]	Extruded powder	(e)	3.3×10^{-4}	1000	197
Ni-47Al[b]	Hot rolled ingot	(e)	1.3×10^{-4}	≈1000	256
Ni-43Al[b]	Extruded powder	(e)	3.3×10^{-4}	925	197
Ni-50.3Al (0.0096 O + C)	Cast + extruded	29.3±3	1.4×10^{-1} 1.4×10^{-2} 1.4×10^{-4}	740 690 550	233

[a]Defined as the lowest temperature at which >5 percent tensile ductility can be achieved.
[b]Interstitial analysis not reported.
[c]Data are recorded as a function of grain size.
[d]Performed under constant displacement velocity.
[e]Not reported.

TABLE VIII.—INPUT PARAMETERS USED IN CHAN'S MODEL (ref. 258)

FOR PREDICTING TENSILE DUCTILITY OF NiAl

Input parameter	300 K	700 K	Reference
Yield strength (as a function of grain size), d (μm)	176 + 522 (1/$\sqrt{d}$)	78 + 261 (1/$\sqrt{d}$)	215
Strain hardening exponent	0.361	0.178	215
Fracture toughness, MPa$\sqrt{m}$	5	22	278
Young's modulus, GPa	231	203	15
Poisson's ratio	0.33	0.33	85

TABLE IX.—COMPRESSIVE PROPERTIES OF NEAR STOICHIOMETRIC NiAl SINGLE CRYSTALS AT OR BELOW ROOM TEMPERATURE

Composition	Orientation	Test temperature, K	Strain rate, s^{-1}	0.2 percent yield stress, MPa	Strain to failure	Reference
Ni-47.1Al-0.03Zr	<123>	298	2.0×10^{-4}	540	0.06	259,260
	<001>	298	2.0×10^{-4}	1370	.08	
Ni-47.5Al	<123>	298	2.0×10^{-4}	560	0.36	260,261
	<123>	210	2.0×10^{-4}	830	>.12	
	<001>	298	2.0×10^{-4}	1300	>.16	
	<001>	210	2.0×10^{-4}	1500	.08	
NiAl (nominal)	<001>	296	2.2×10^{-4}	1270	>0.04	216
	<001>	195	2.2×10^{-4}	1470	>.03	
	<001>	77	2.2×10^{-4}	1860	.03	
NiAl (nominal)	<001>	298	5.0×10^{-4}	980	0.05	262
	<011>	298	5.0×10^{-4}	294	.12	
	<111>	298	5.0×10^{-4}	147	.12	
NiAl (nominal)	<011>	293	Not reported	137	>0.50	182
Ni-50Al	<001>	298	1.7×10^{-3}	1030	0.03	165
	<011>	298	1.7×10^{-3}	296	.10	
	<111>	298	1.7×10^{-3}	145	.12	
	<112>	298	1.7×10^{-3}	200	.17	
	<123>	298	Not reported	290	.16	

TABLE X.—ROOM TEMPERATURE FRACTURE TOUGHNESS OF NiAl AND NiAl ALLOYS AND COMPOSITES

Material (processing technique)	Grain size, μm	Fracture toughness, MPa$\sqrt{m}$	Reference
Polycrystalline alloys:			
NiAl (hot pressed powder)	20	5.4 K_{IC}	274
NiAl (hot pressed and HIPped powder)	~20	6 K_{IC}	275,276
NiAl (extruded cast ingot)	~50	5.4-5.9 K_{IC}	277
NiAl (electron beam-zone melted)	4000 μm long by 2000 μm diam	$\simeq$5 K_{IC}	278
NiAl (powder processed)	8	2.7-3.8 K_{IC}	279
Ni-43Al (extruded cast ingot)	~50	4.3-6.9 K_{IC}	277
Ni-40Al (hot pressed and HIPped powder)	~20	6 K_{IC}	275,276
Ni-38.5Al (hot pressed and HIPped powder)	~20	9 K_{IC}	275,276
NiAl + 0.25B (extruded cast ingot)	~50	5.9-6.2 K_{IC}	277
NiAl + 5Nb (powder processed)	8	12.2-15.4 K_{IC}	279
NiAl + 5Ti (powder processed)	8	4.7-14.5 K_{IC}	279
Single crystals:			
NiAl (directionally solidified)	---	8 K_c Notched parallel to (001)	280
		4 K_c Notched parallel to (011)	280
NiAl (directionally solidified)	---	10 K_{IC} Notched parallel to (001)	281
		6 K_{IC} Notched parallel to (011)	281
Eutectics:			
NiAl-9Mo (arc melted and chill cast)	---	9.5 K_Q	282
NiAl-12Mo (arc melted and chill cast)		14 K_Q	282
NiAl-34Cr (directionally solidified)	---	18	264
NiAl-9Mo (directionally solidified)		15	264,360
NiAl-Cr/Mo (directionally solidified)		12	264
NiAl-40V (directionally solidified)	---	31	360
Composites:			
NiAl + 20 vol % TiB$_2$ (particulate)	---	~6 K_{IC}	275,276
NiAl + 15-25 vol % Al$_2$O$_3$ (whisker) (hot pressed and HIPped)	---	~9 K_{IC}	275,276
NiAl/NiAlNb (HIPped powder or cast and recrystallized)	---	2-4 K_{IC}	278,281

TABLE XI.—SUMMARY OF CREEP PARAMETERS FOR NiAl

Al, at %	Grain size, μm	T, K	n	Q, kJ/mol	Reference
48.25	5-9	1000-1400	6.0-7.5	313	316
44-50.6	15-20	1100-1400	5.75	314	317
50	12	1200-1300	6	350	318
50	450	1073-1318	10.2-4.6	283	319
50	500	1173	4.7	----	320
50.4	1000	1075-1750	7.0-3.3	230-290	235
50	SX[123]	1023-1223	7.7-5.4	----	321
50	SX	1023-1328	4.0-4.5	293	169
50	SX[001]	1000-1300	6	440	322
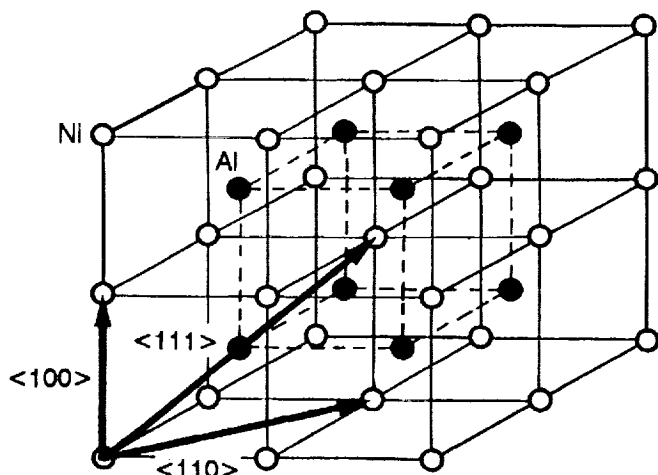
Figure 1.—The B2 crystal structure and unit lattice (slip) vectors for NiAl. Shown are eight unit cells illustrating the interpentrating simple cubic sublattices of Ni and Al atoms.
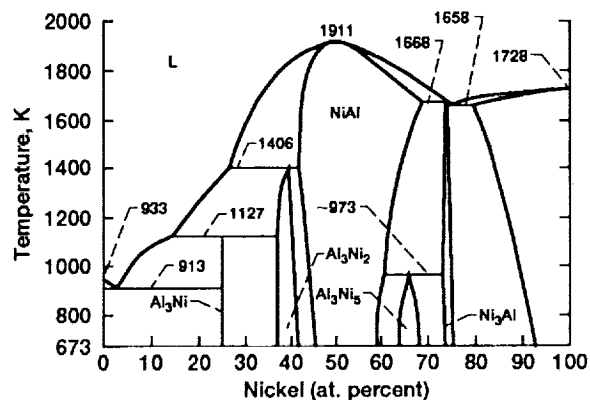
Figure 2.—The NiAl phase diagram (ref. 3).
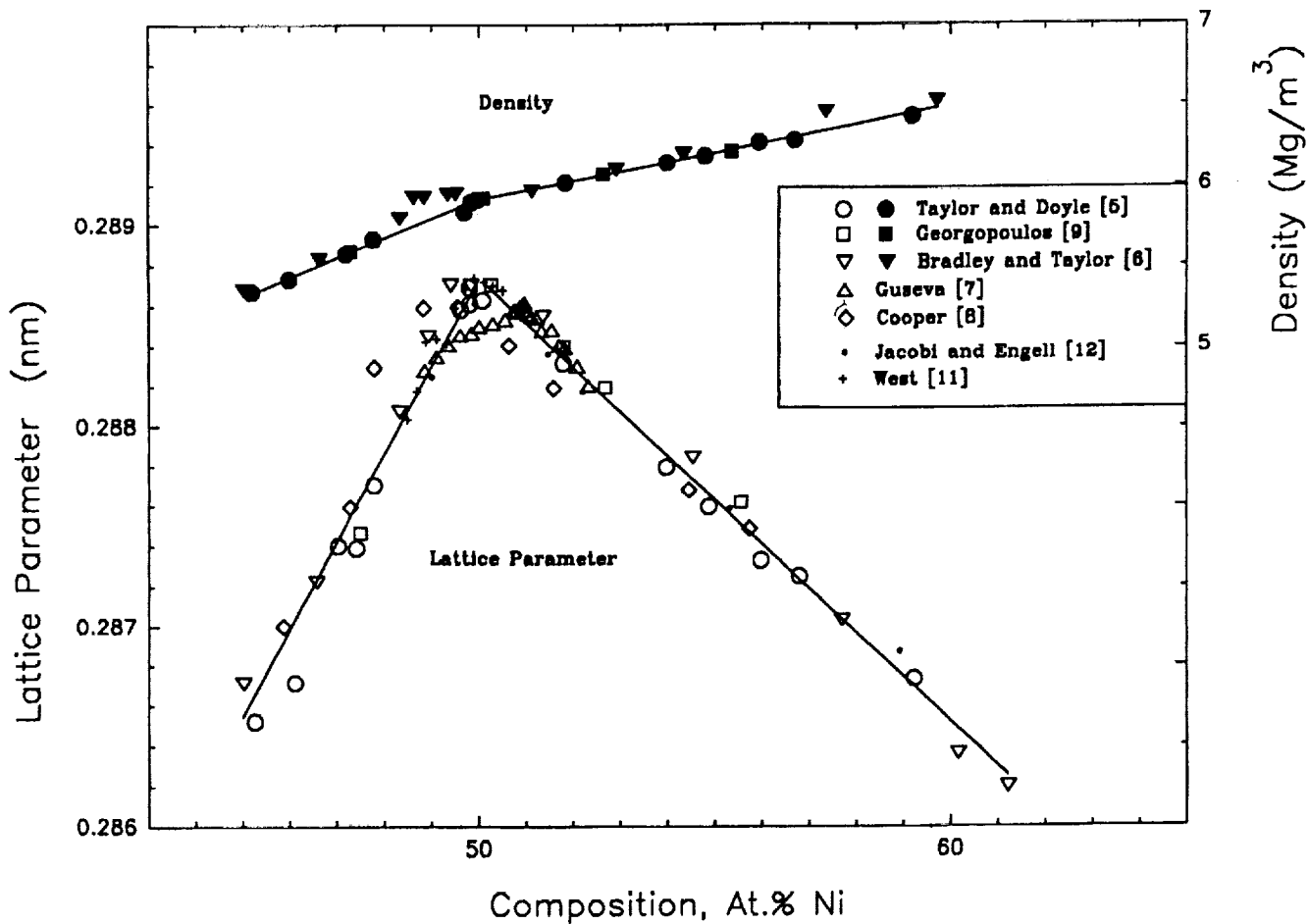
Figure 3.—Lattice parameter and density of NiAl as a function of stoichiometry at room temperature.

78

Figure 4.—Heats of formation for Ni-Al alloys.
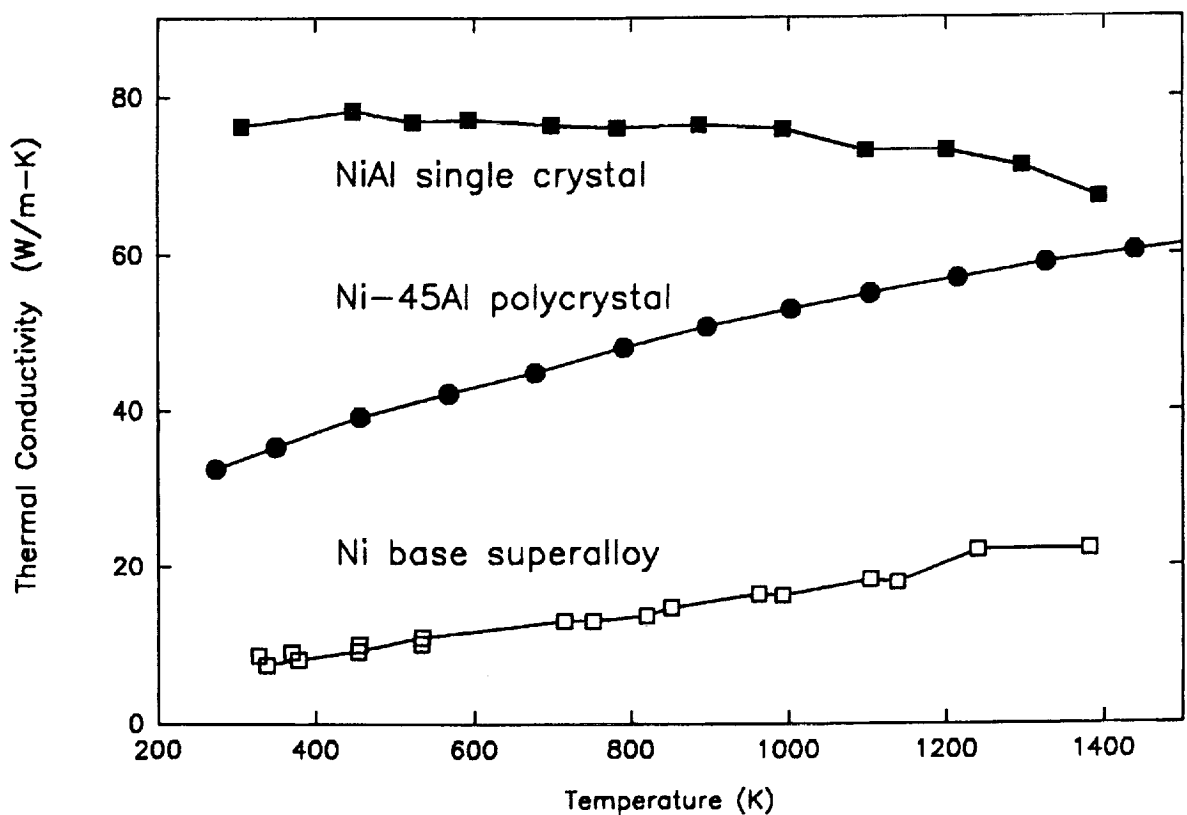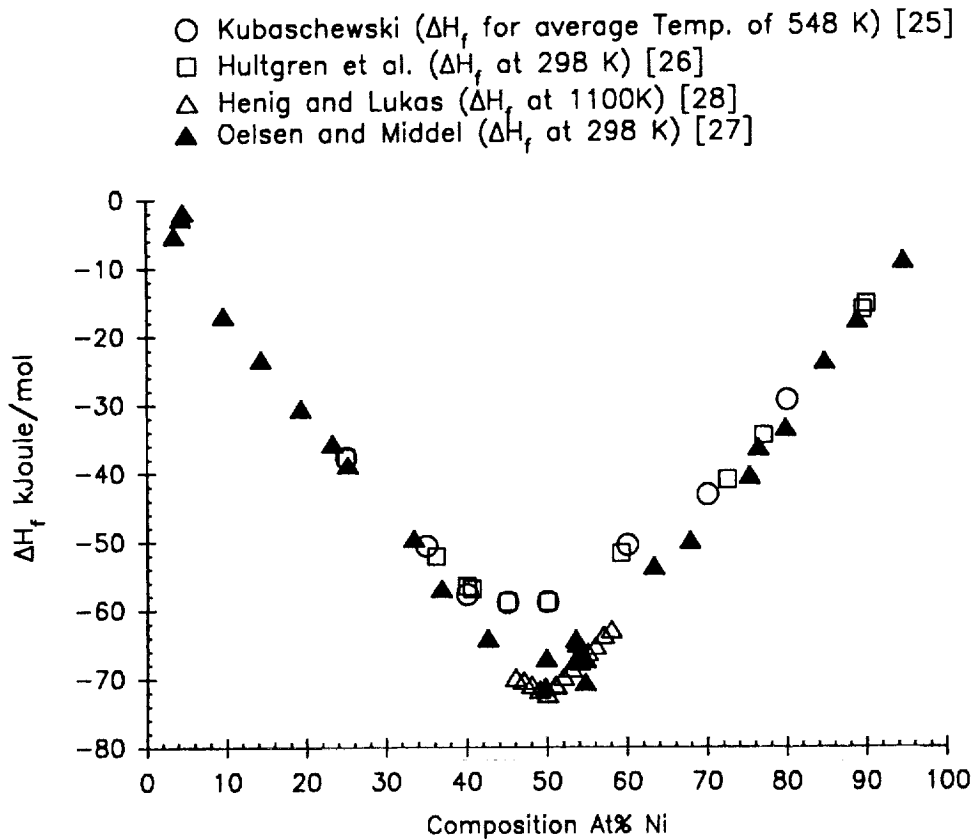
Figure 5.—Comparison of the thermal conductivity of single crystal NiAl (ref. 62), polycrystalline Ni-45Al (ref. 58), and a conventional nickel-base superalloy (ref. 62) as a function of temperature.

79
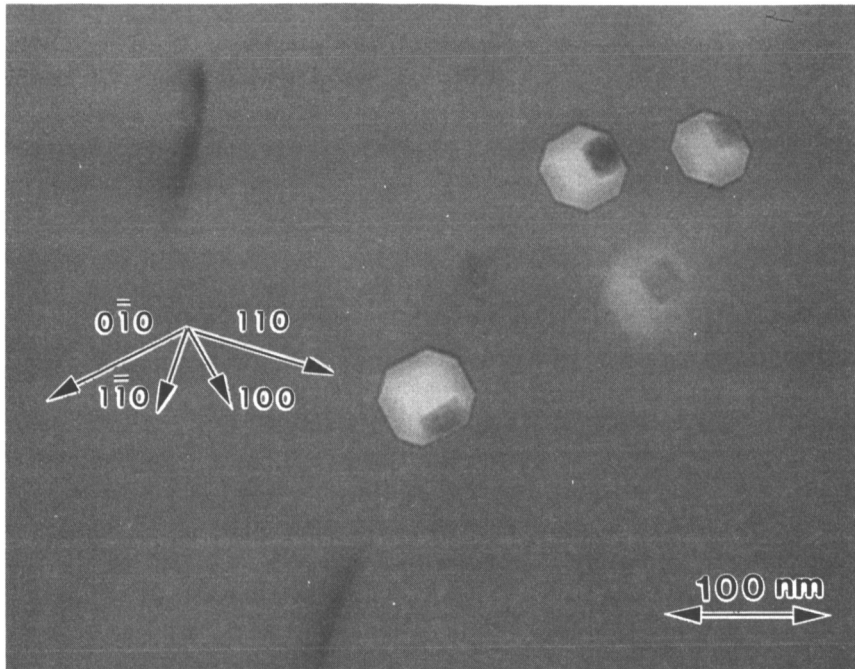
Figure 6.—Faceted voids in NiAl due to point defect agglomeration in melt spun Ni-50Al. (Figure courtesy of I. Locci, NASA Lewis Research Center.)
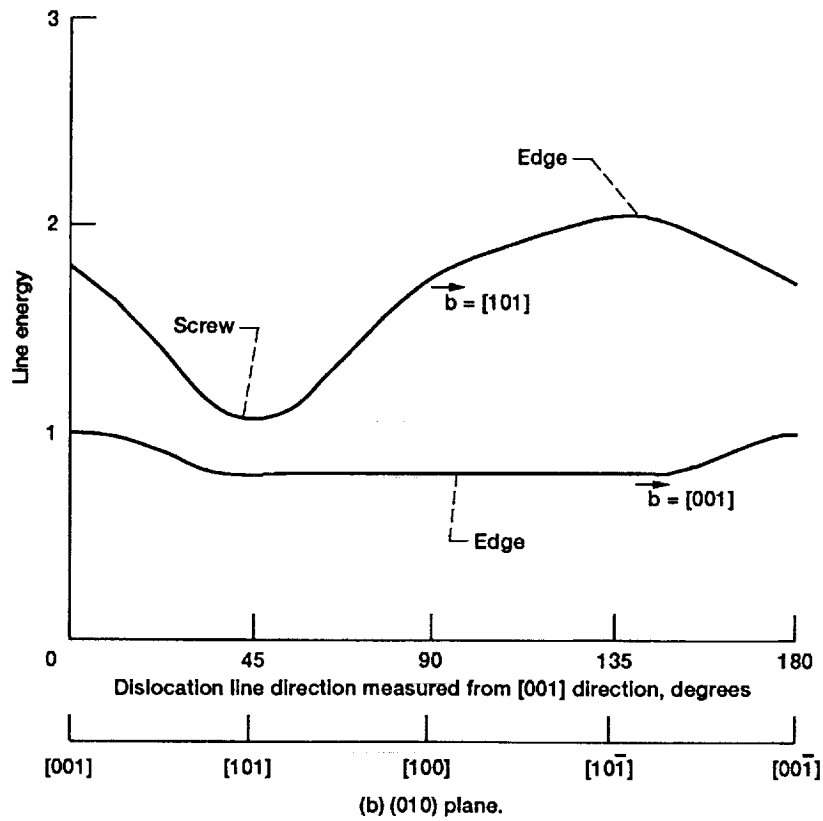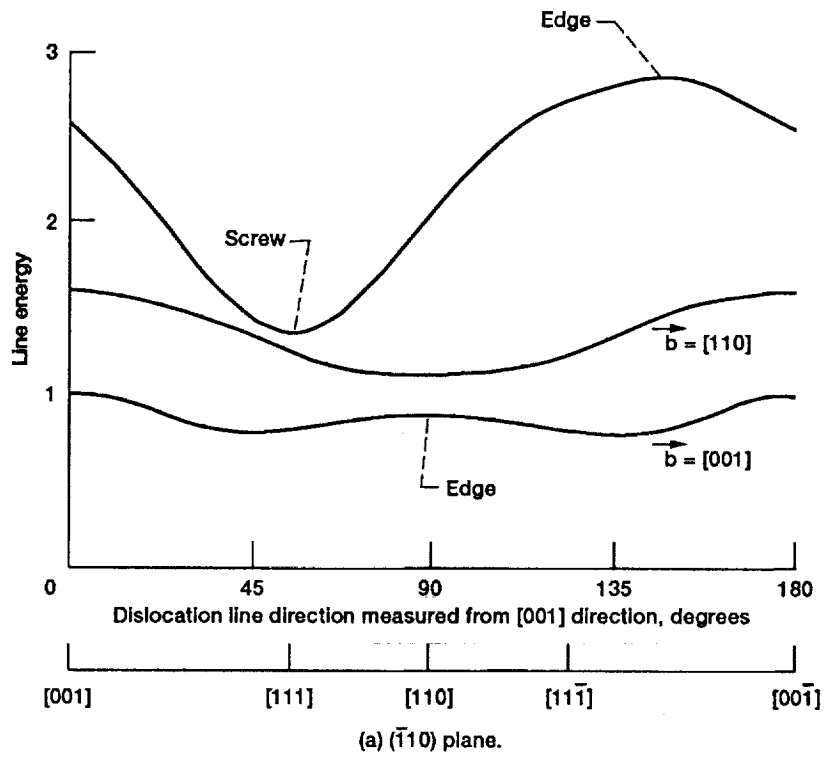
Figure 7.—Line energy for dislocations in stoichiometric NiAl at room temperature. (After Lloyd and Loretto ref. 140).

81
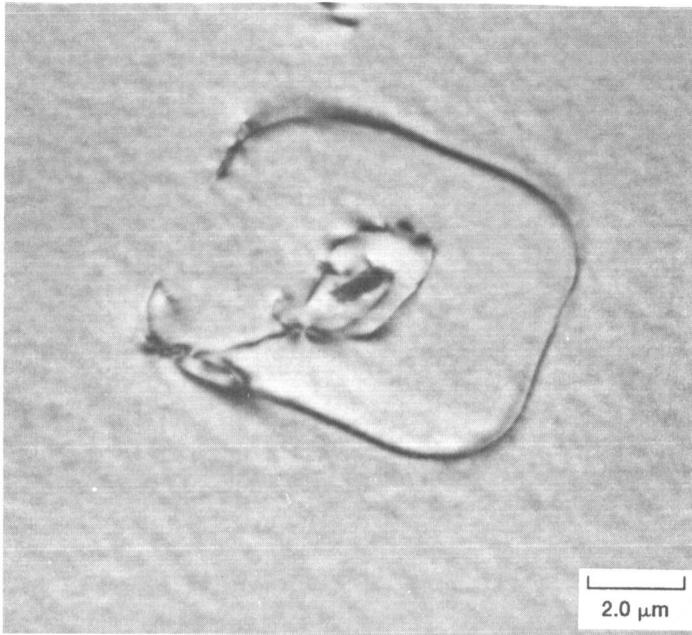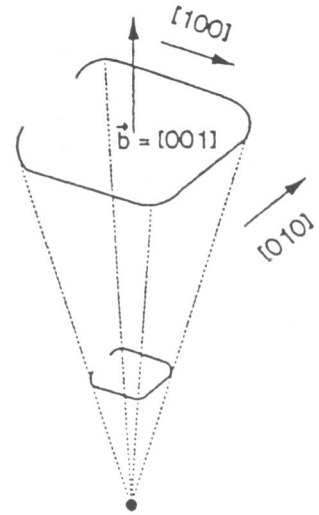
(a) Actual.

(b) Schematic illustration of rounded square loops with line directions along <001>.
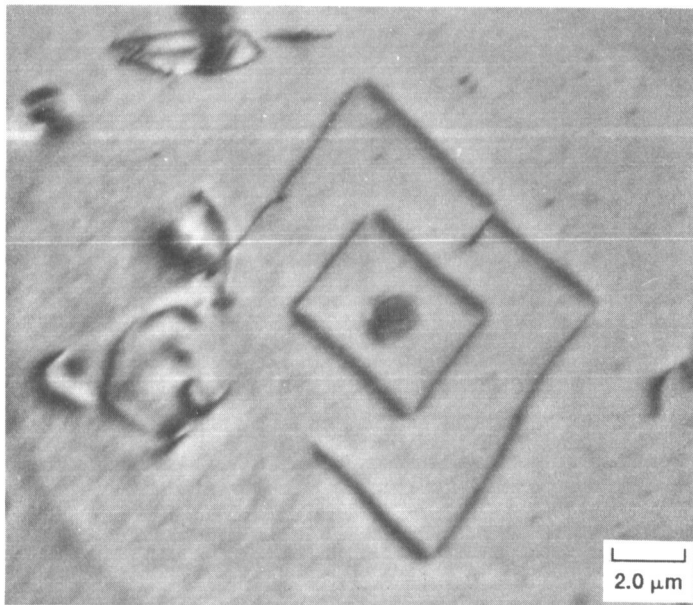
(c) Actual.
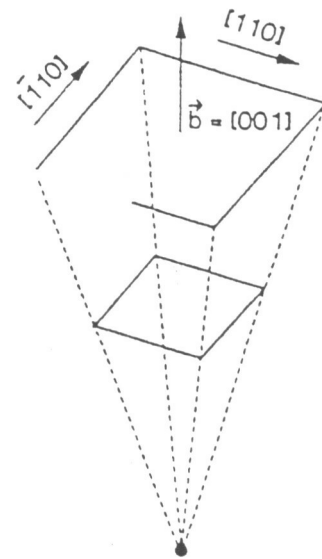
(d) Schematic illustration of sharp rectangular loops with line directions along <110>.

Figure 8.—Types of prismatic edge dislocation loops commonly observed in NiAl (after ref. 149).
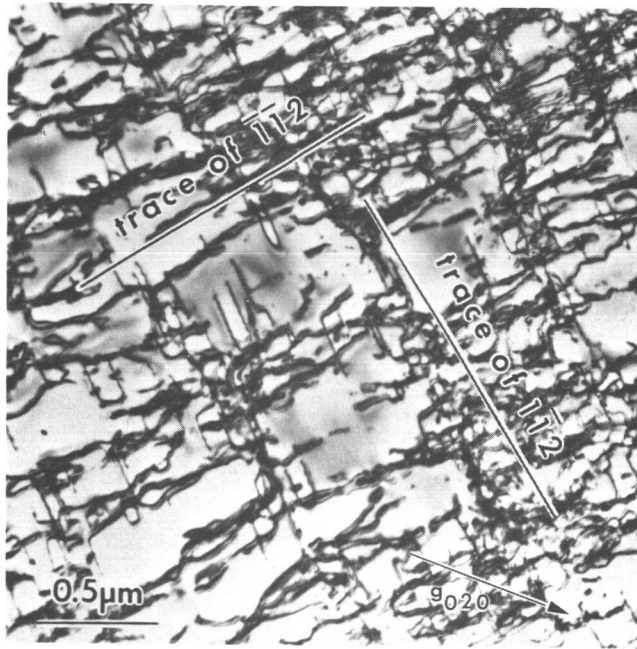
Figure 9.—Microstructure of a NiAl [001] single crystal deformed uniformly at room temperature. "A" dislocations are [111] ($1\bar{1}2$) and "B" dislocations are [$\bar{1}11$] ($1\bar{1}2$) (ref. 149).
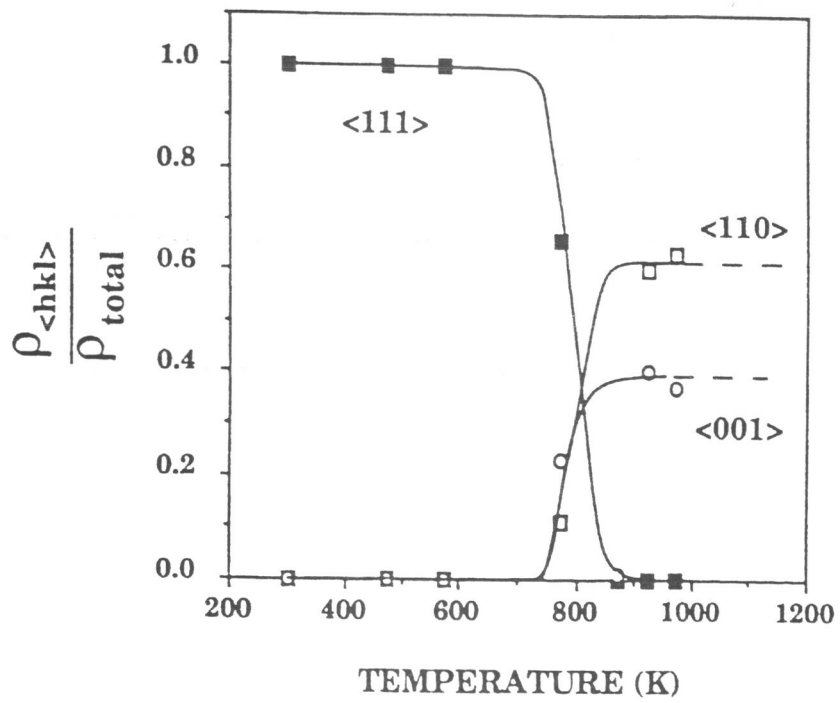
Figure 10.—The density ratio of various dislocations observed as a function of temperature in compressed [001] Ni-48Al single crystals (ref. 143).
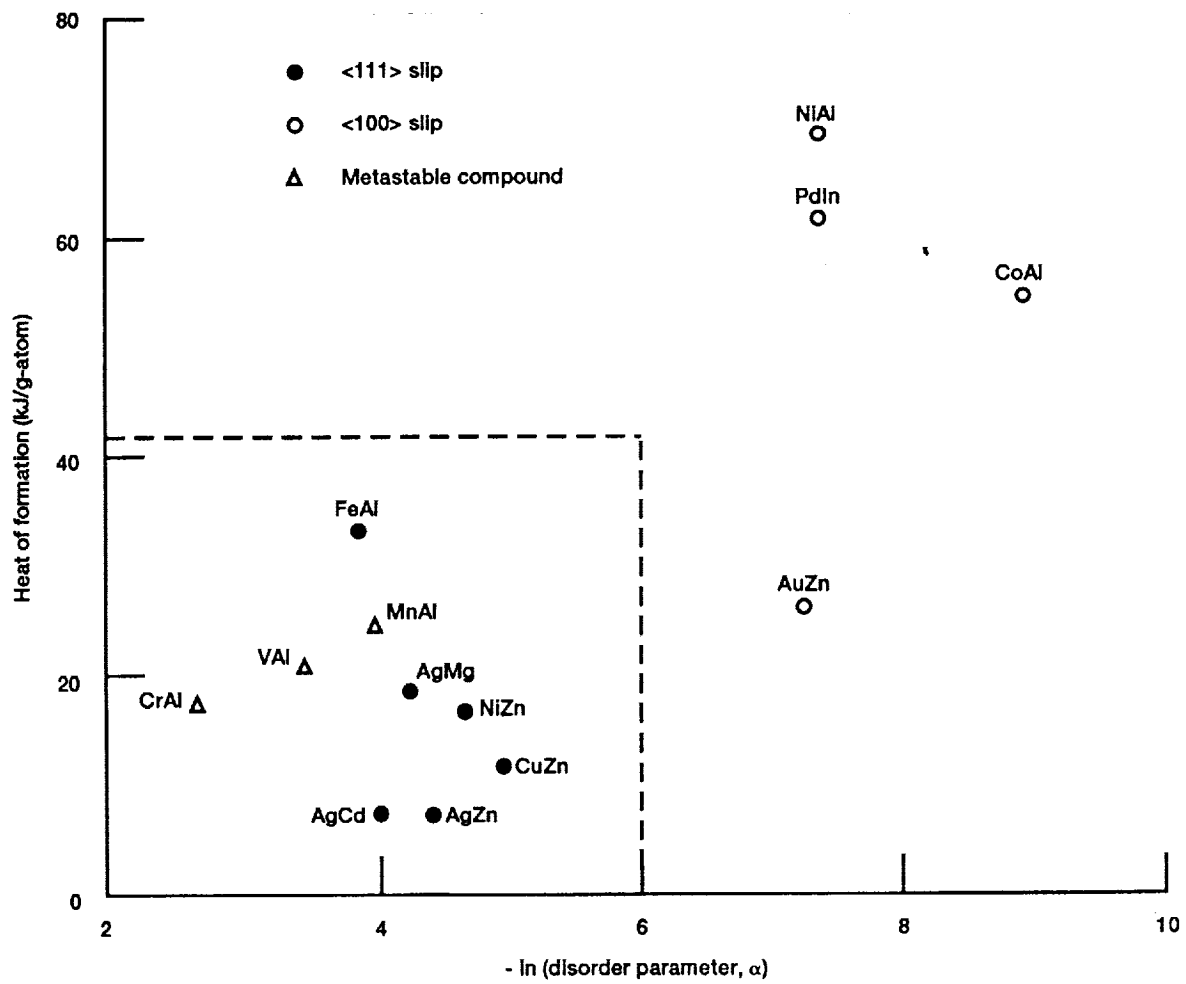
Figure 11.—The relationship between thermodynamic properties and operative slip systems in B2 compounds (ref. 199).
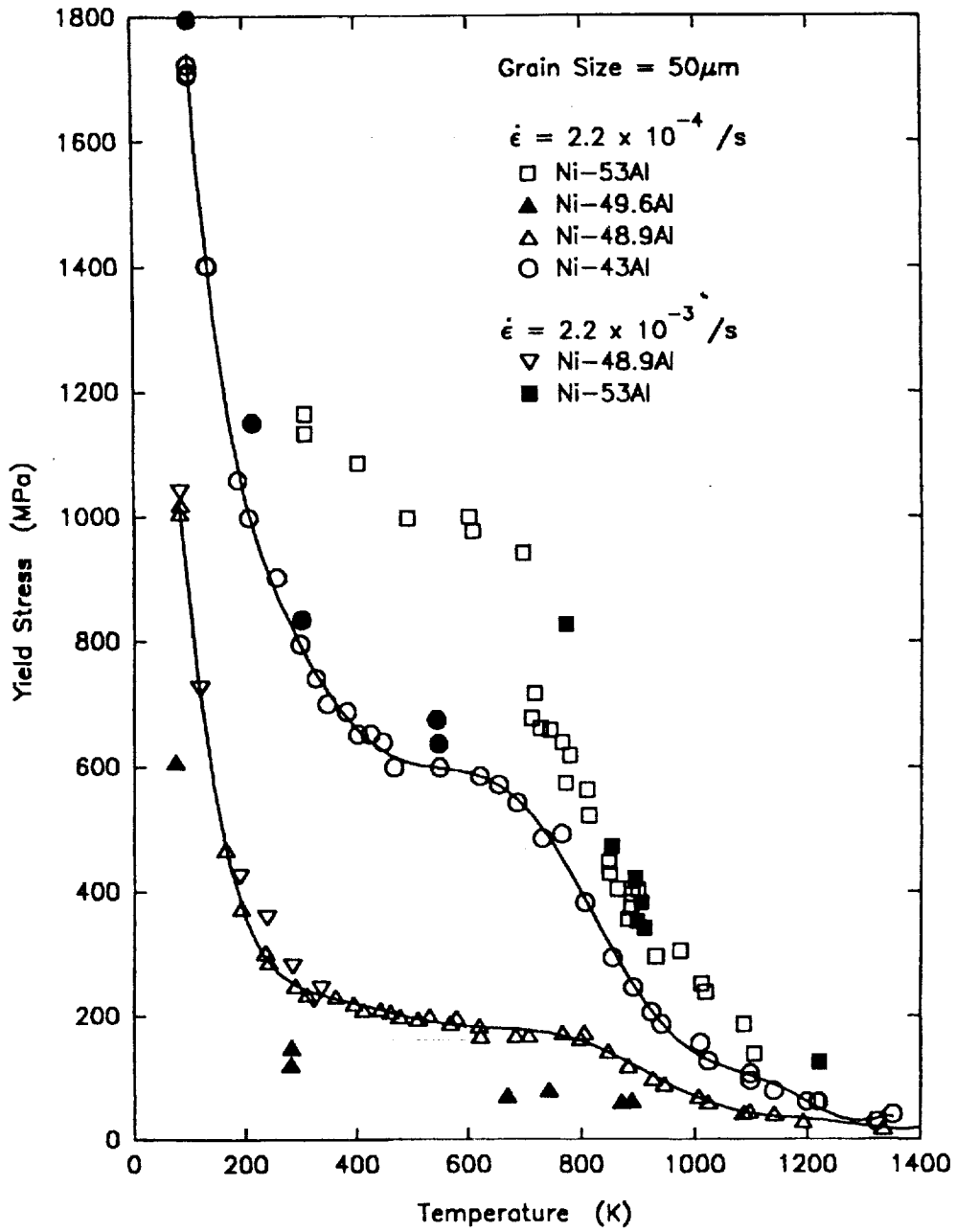
Figure 12.—Typical yield stress behavior as a function of temperature for polycrystalline NiAl (ref. 216).
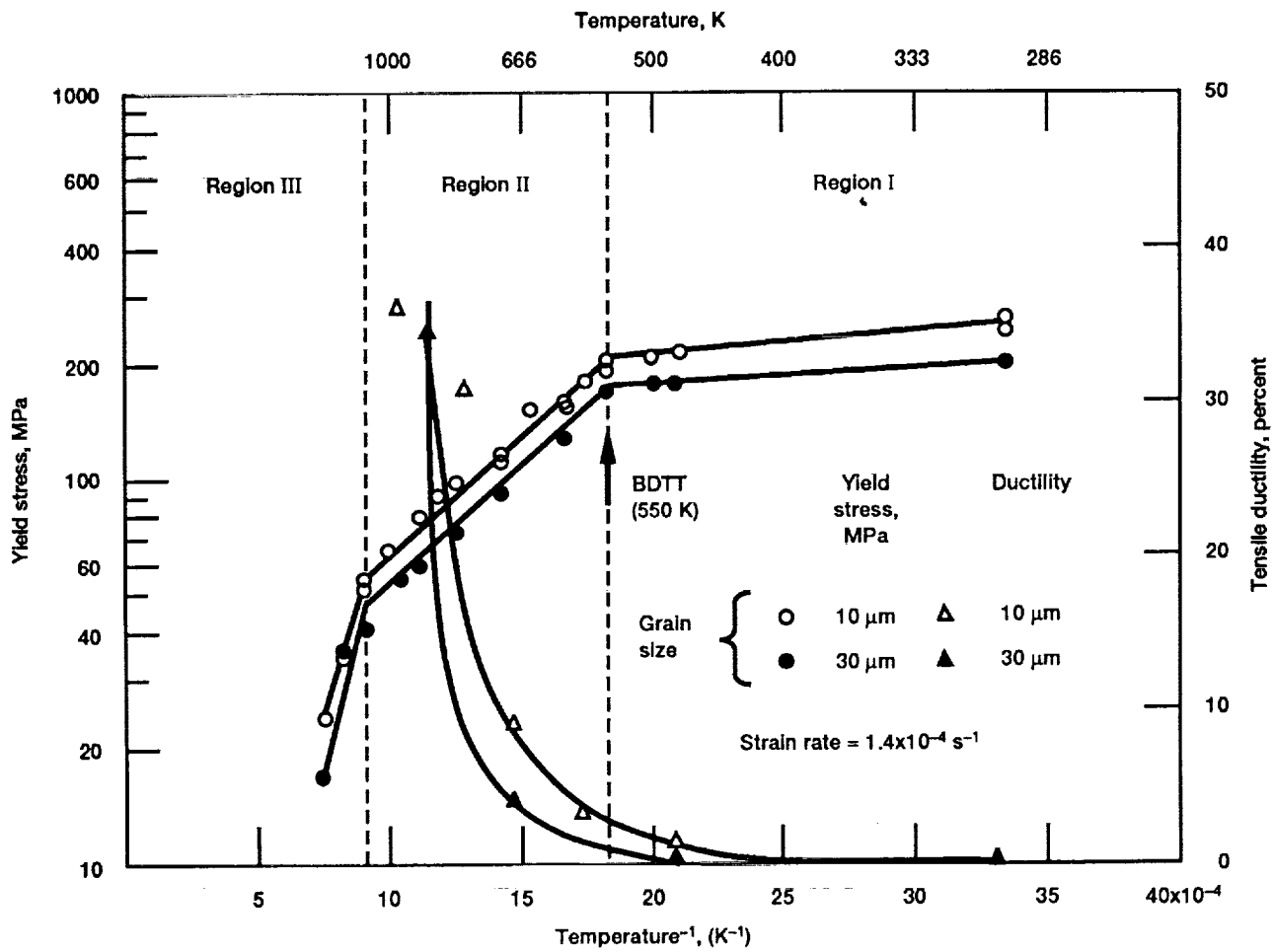
Figure 13.—Arrhenius representation of the yield stress of polycrystalline NiAl. The BDTT corresponds to a change in activation energy for plastic flow beginning at Region II (ref. 215).
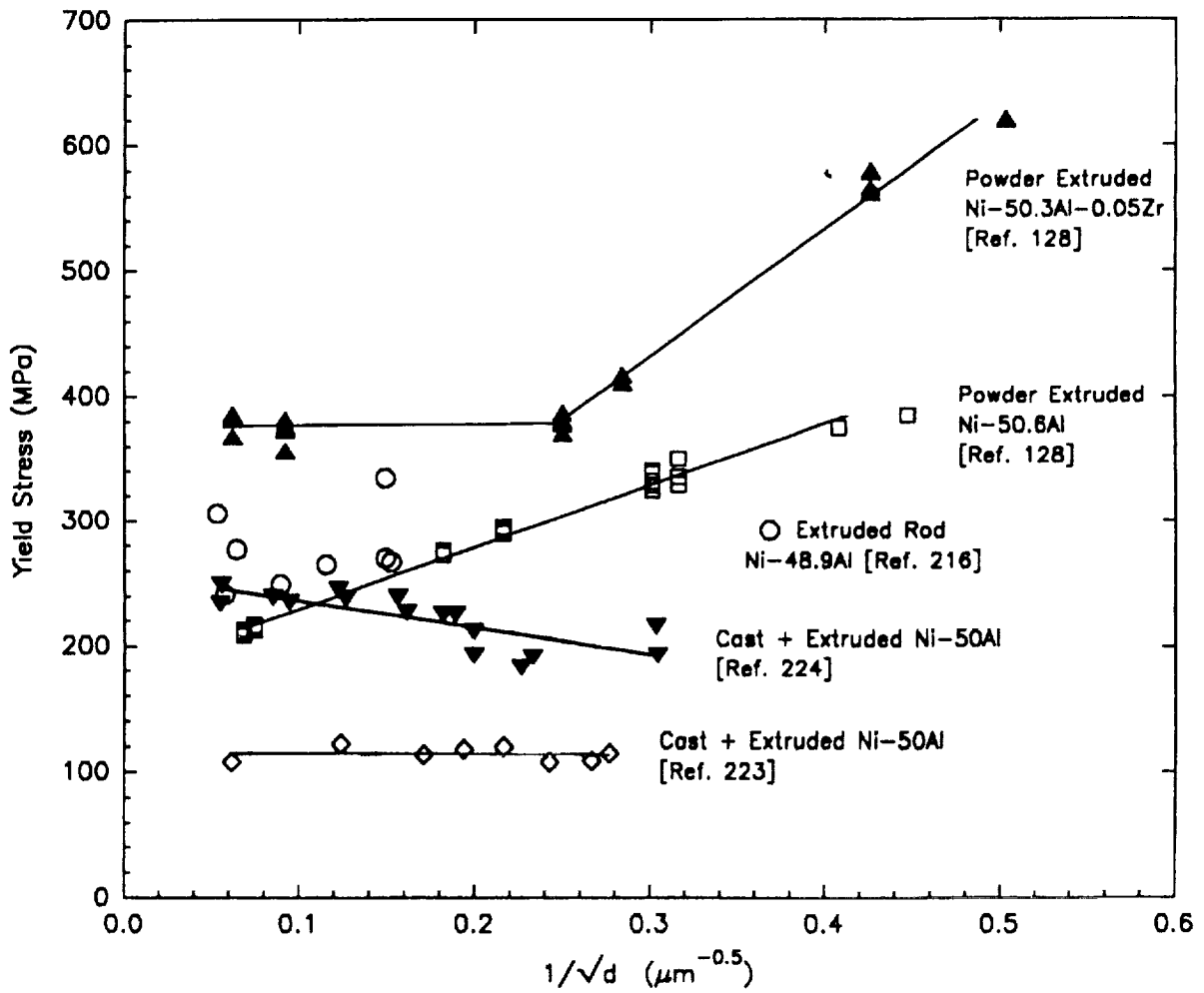
Figure 14.—The effect of grain size on the room temperature yield stress of NiAl.
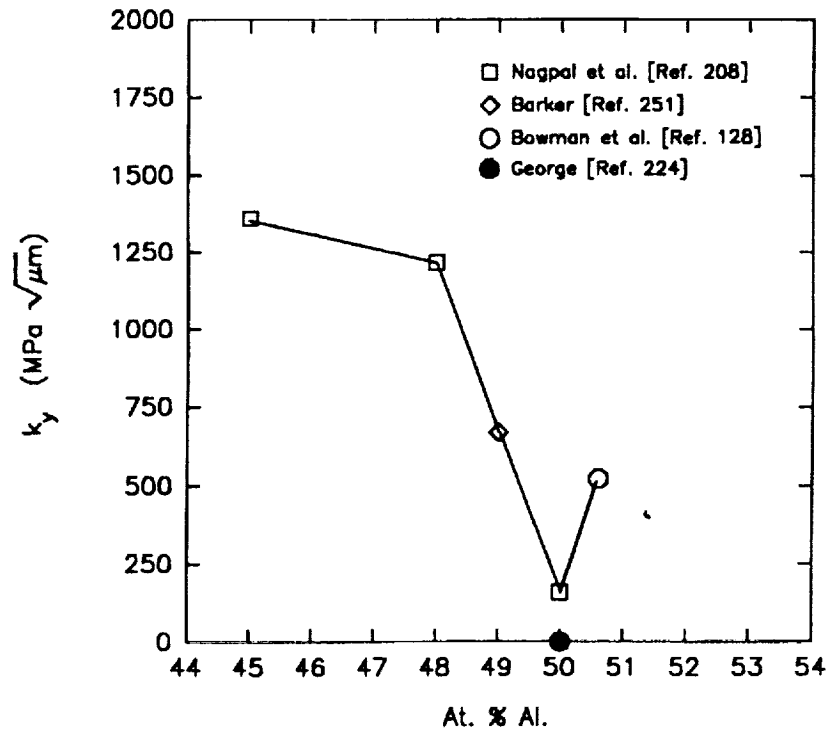
Figure 15.—The Hall-Petch slope for NiAl as a function of stoichiometry at room temperature.
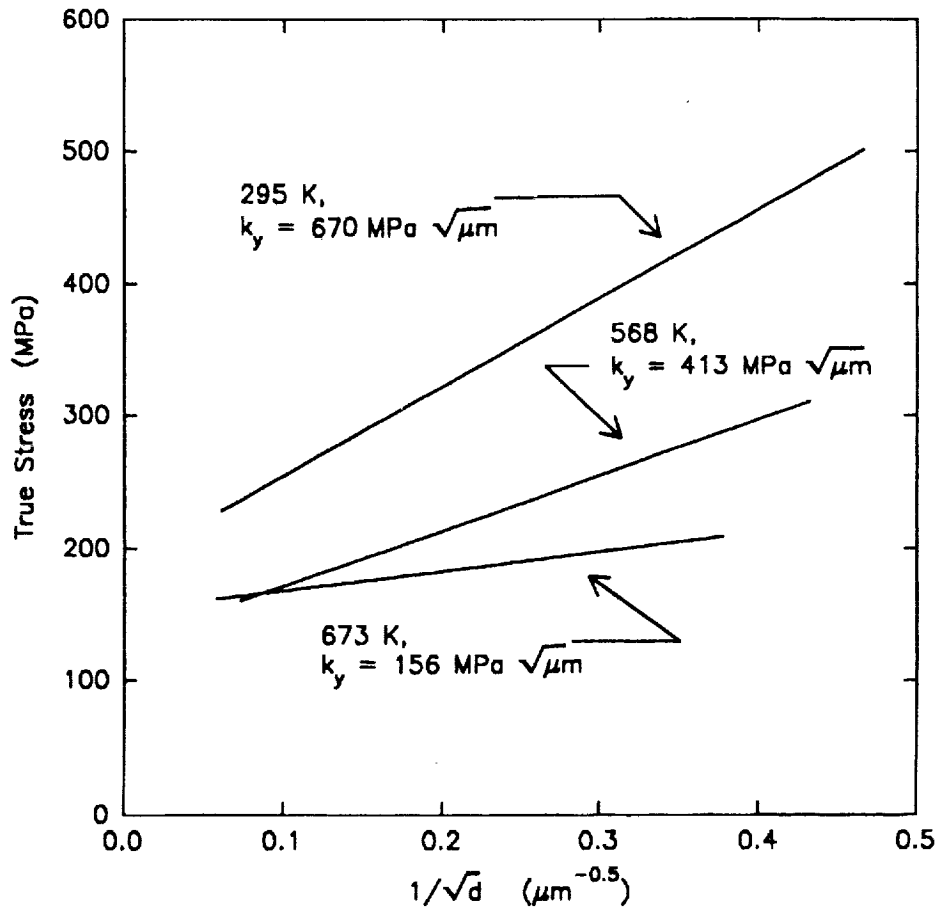
Figure 16.—The effect of temperature on the Hall-Petch slope of Ni-49Al-0.01Zr (ref. 251).

◇ Nagpal et al.., 300 K [208]
+ Hahn and Vedula, 873K [213]
▲ Graham thesis, 673 K [220]
■ Lautenschlager, 973 K [210]
O Pascoe, 600 K [216]
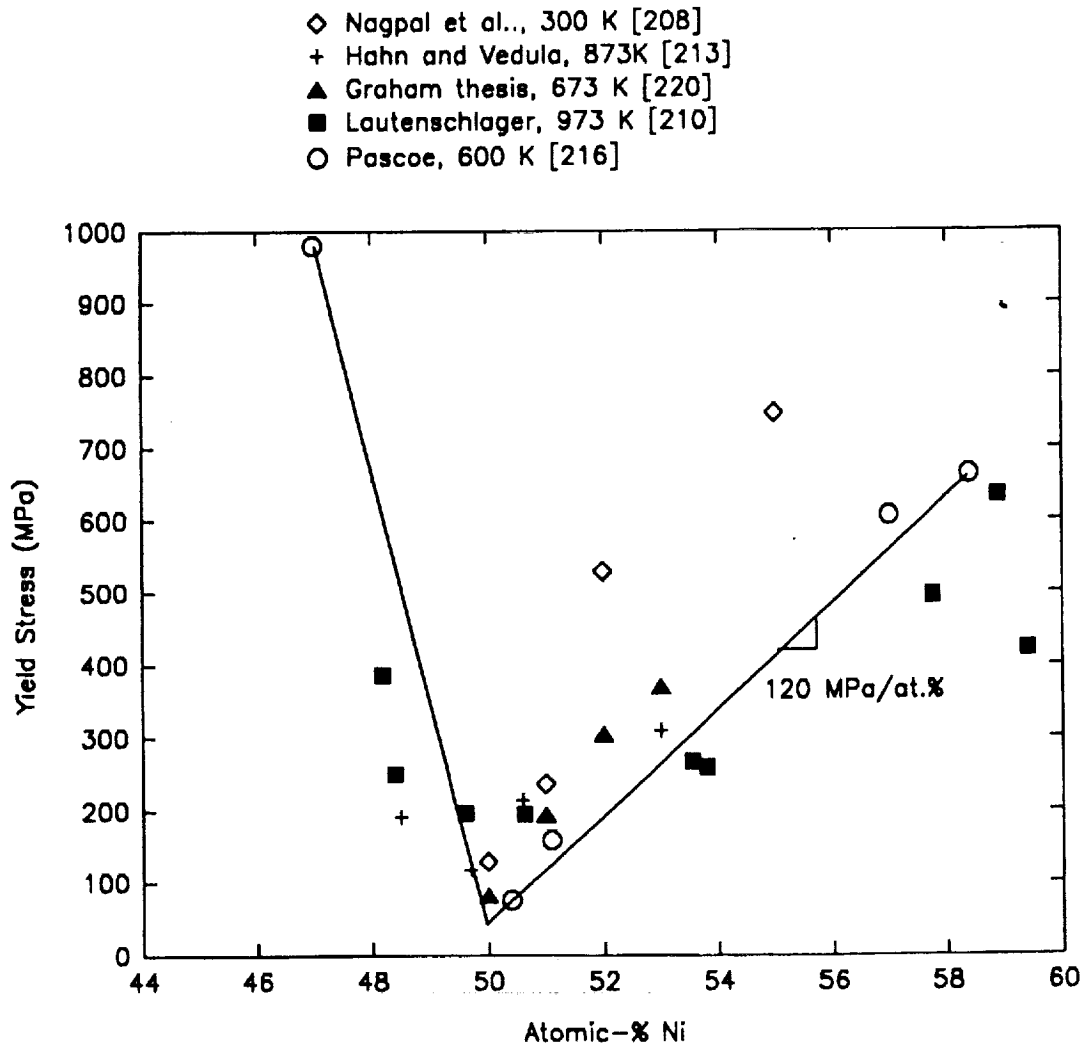
Figure 17.—Yield stress of NiAl as a function of stoichiometry.
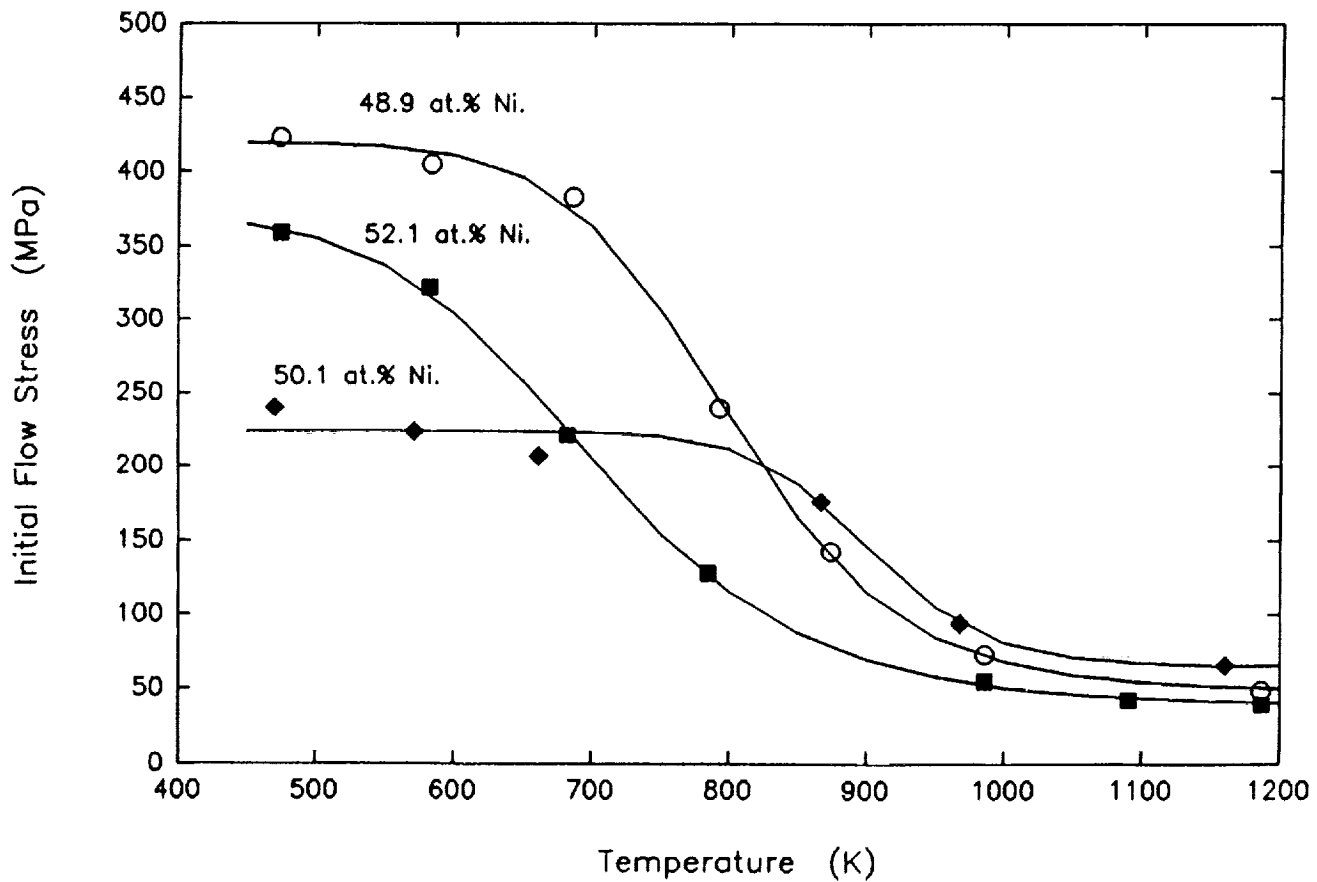
Figure 18.—The effect of composition and temperature on the yield strength of NiAl. Note the reversal in strength levels for stoichiometric and non stoichiometric compositions as temperature increases (ref. 182).

C : George and Liu [227]
     (lower limit)
Be : George and Liu [227]
B : George et al. [228]
Zr : Bowman et al. [128]
Cr : Cotton [189]
Mo : Graham, Stover
     [220,229]
Y : Graham [220]
La : Graham [220]
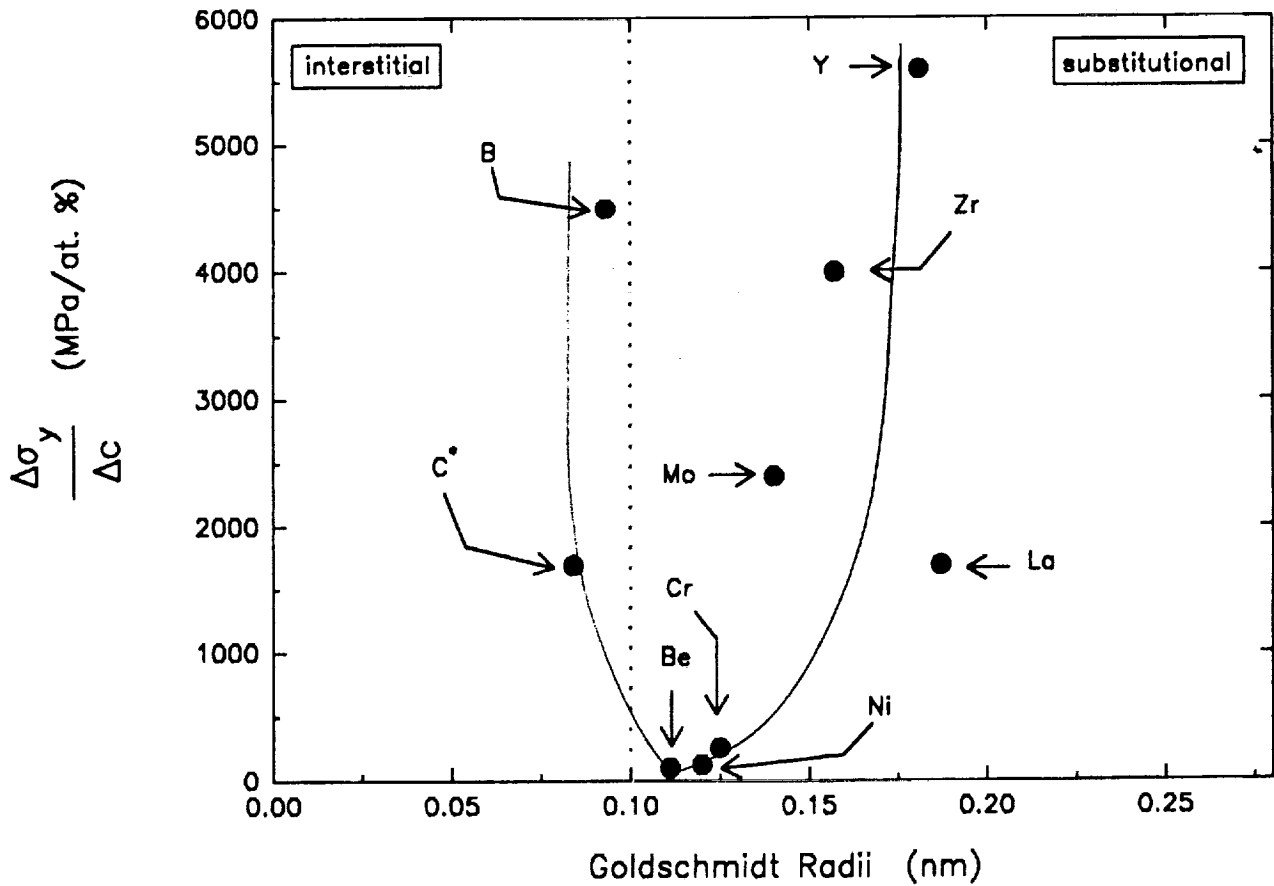
Figure 19.—The relationship between hardening rate and element size for various alloying elements in NiAl.

91
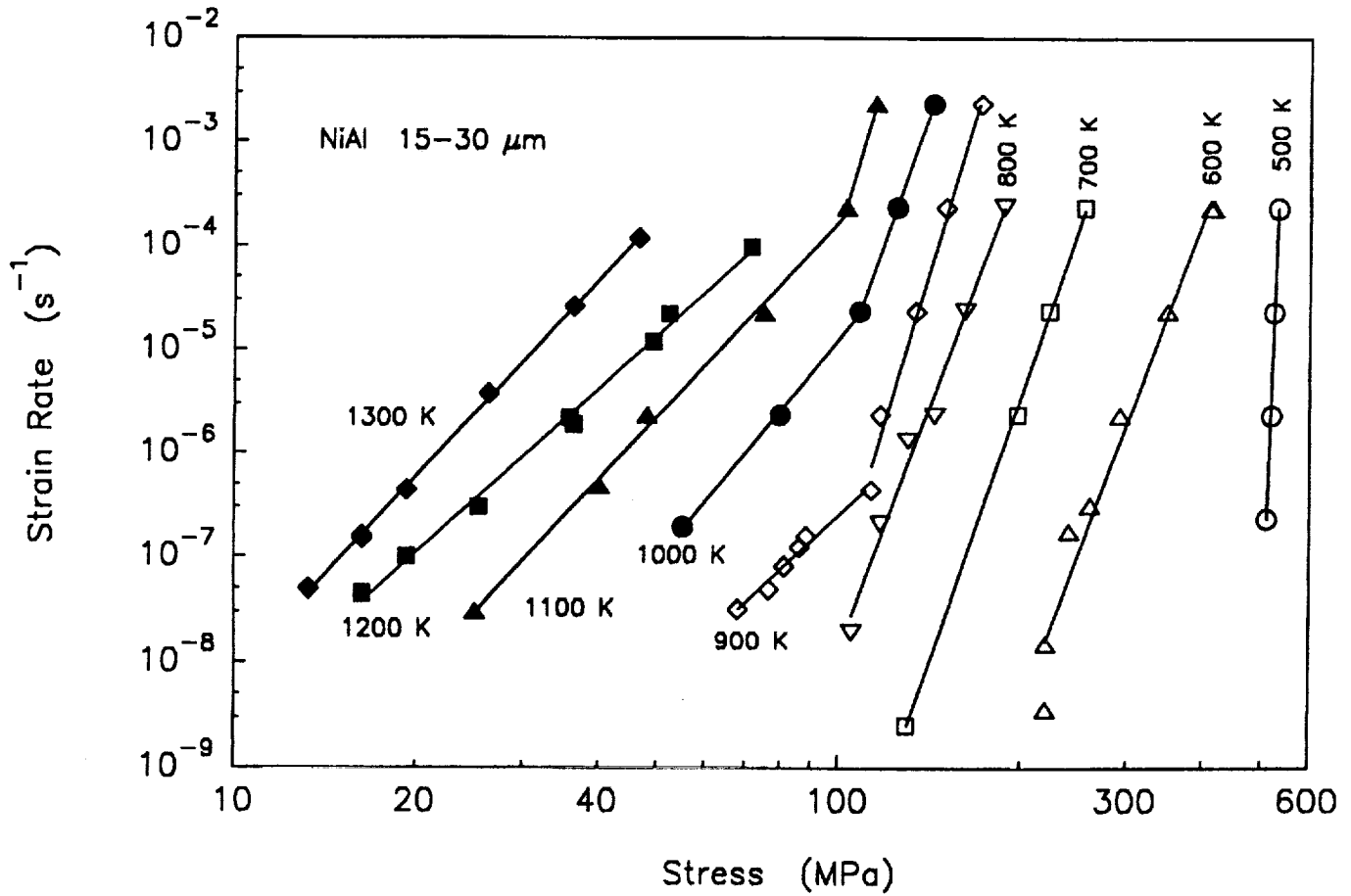
Figure 20.—The effect of strain rate on the yield strength of NiAl between 500 and 1300 K (ref. 128).
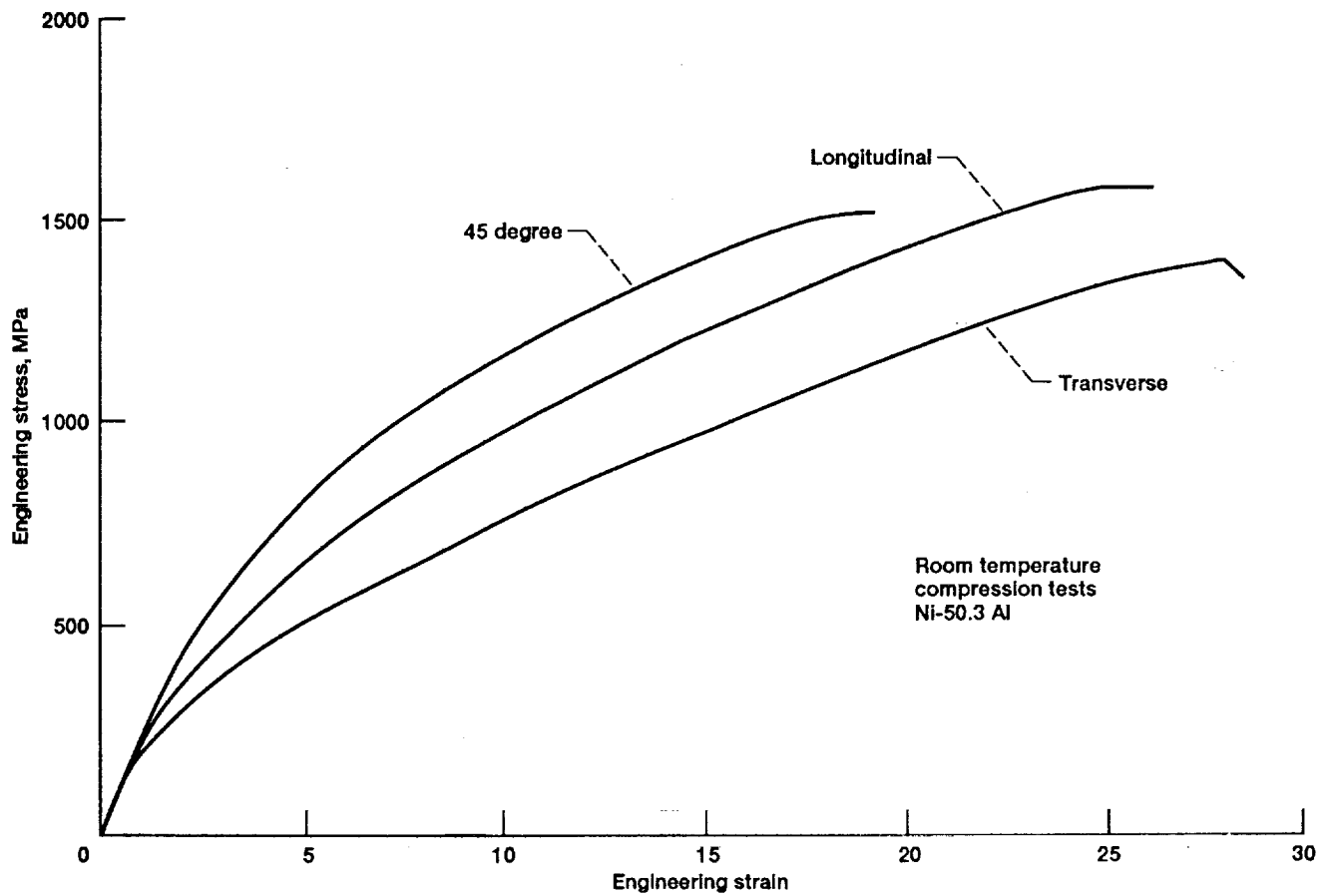
Figure 21.—The flow strength of extruded NiAl compression specimens taken from various orientations relative to the extrusion axis and tested at room temperature (ref. 178).
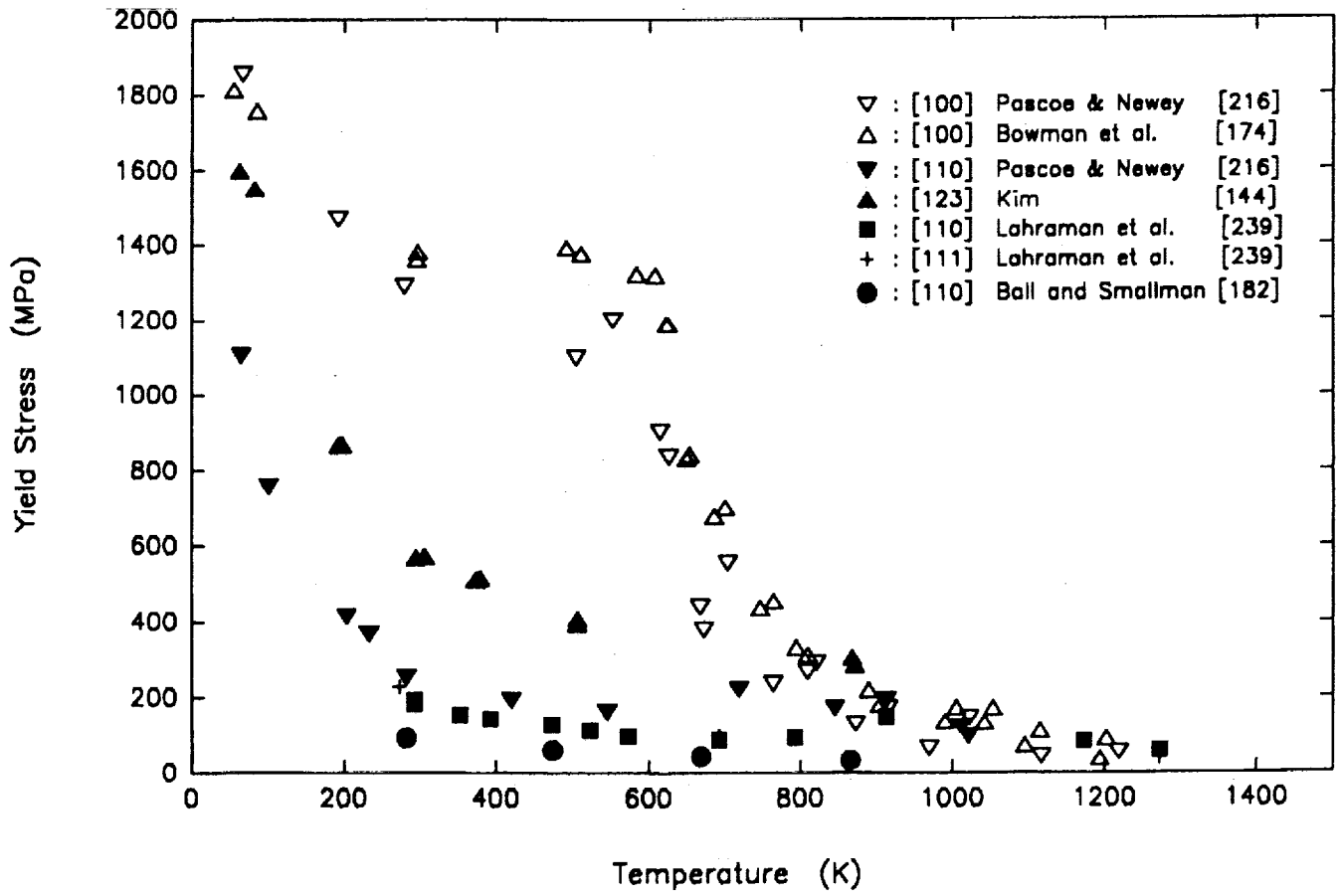
Figure 22.—Yield stress as a function of temperature for several different single crystal orientations.
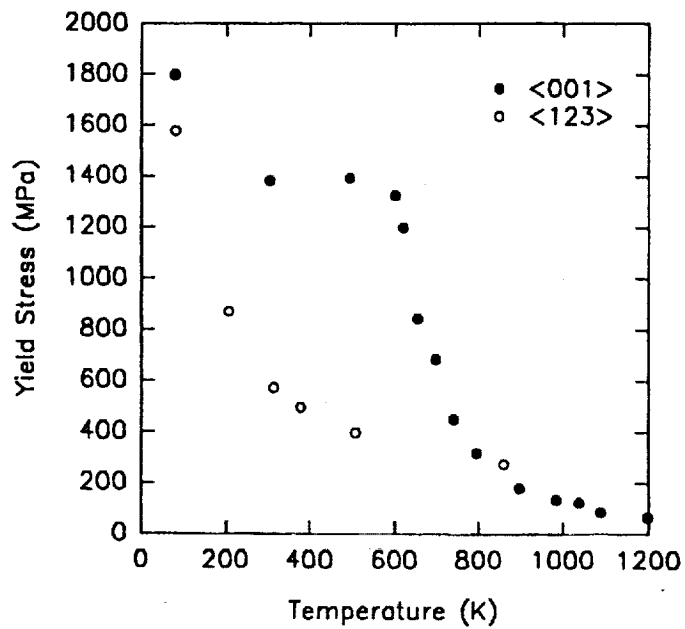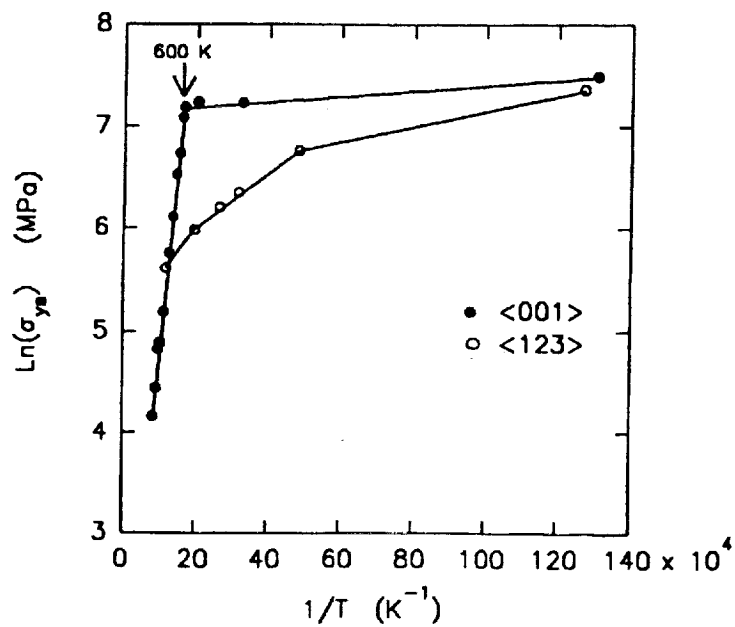
Figure 23.—(a) Compressive yield stress of [001] and [123] oriented NiAl single crystals and (b) Arrhenius representation of the yield stress for NiAl single crystals.
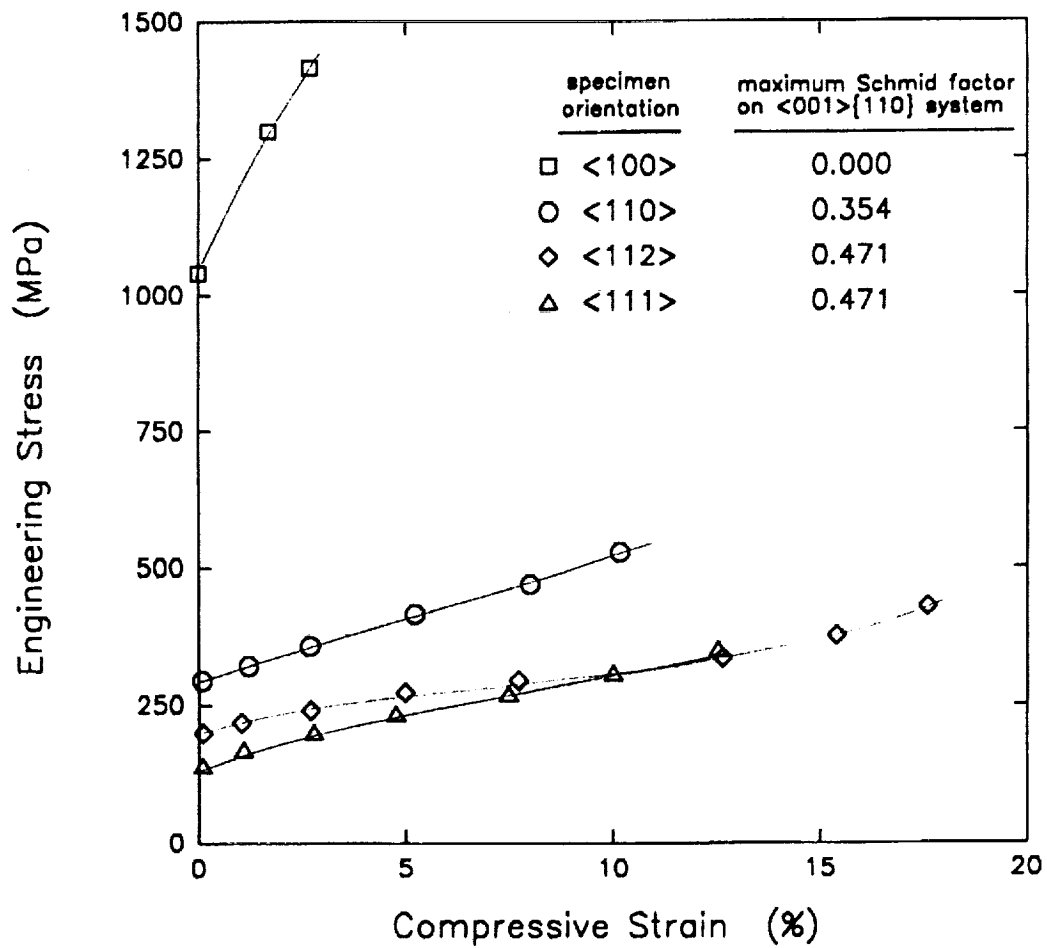
Figure 24.—The room temperature stress strain behavior of NiAl as a function of orientation (ref. 165).
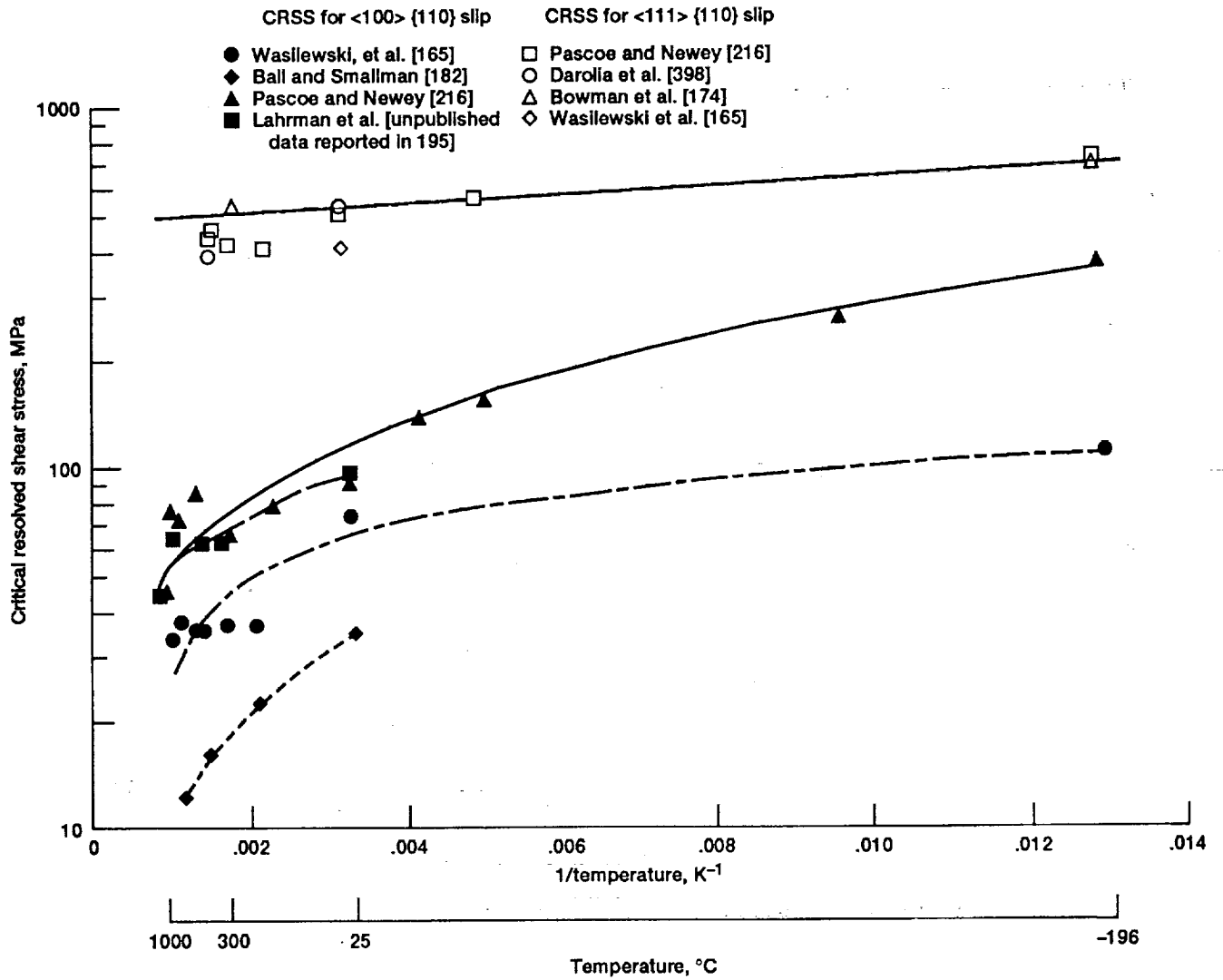
Figure 25.—The CRSS as a function of temperature for hard and soft orientations of single crystal NiAl (ref. 195).
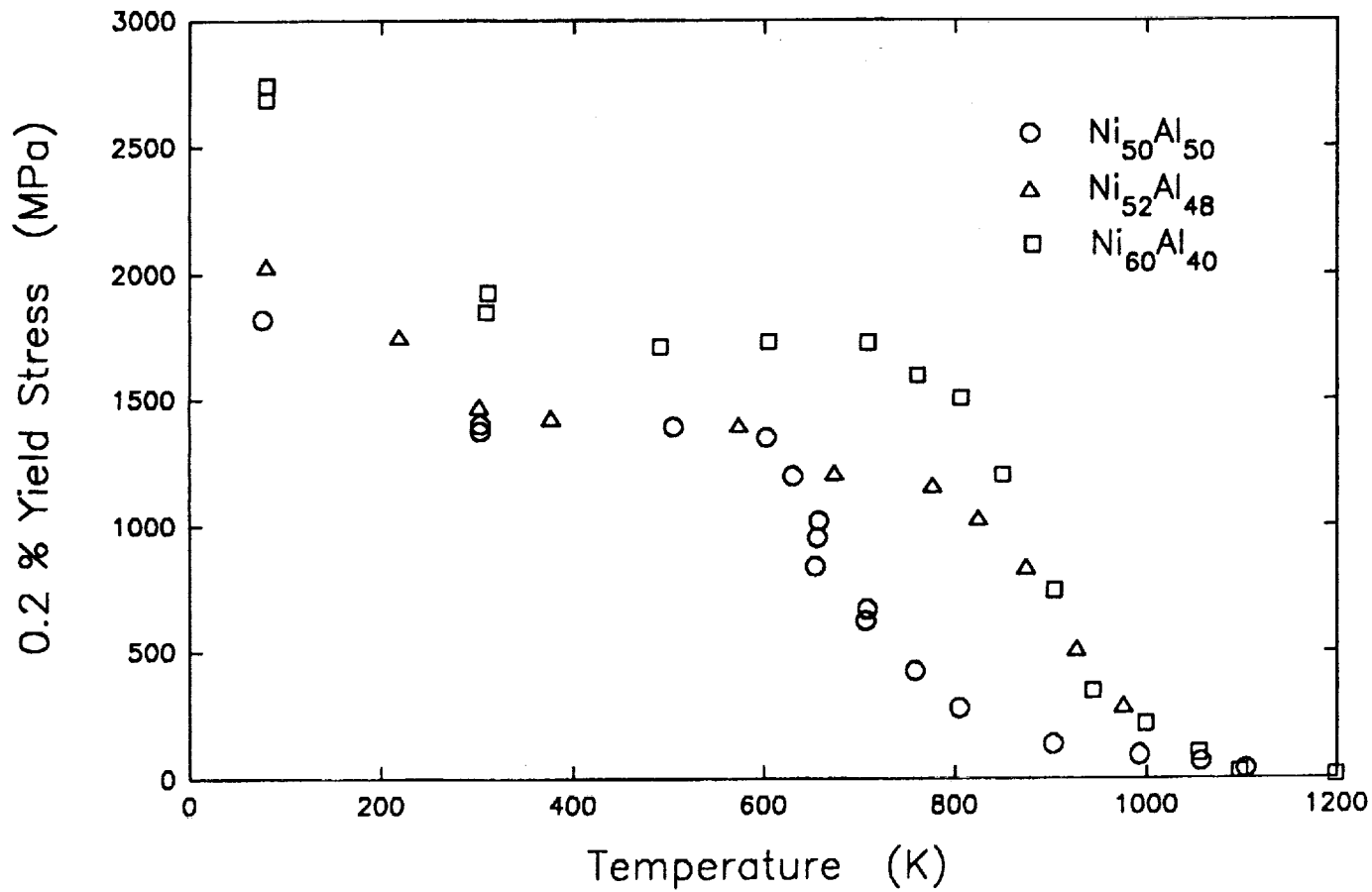
Figure 26.—The effect of alloy stoichiometry on the temperature dependent yield strength of [001] single crystal NiAl (ref. 149).
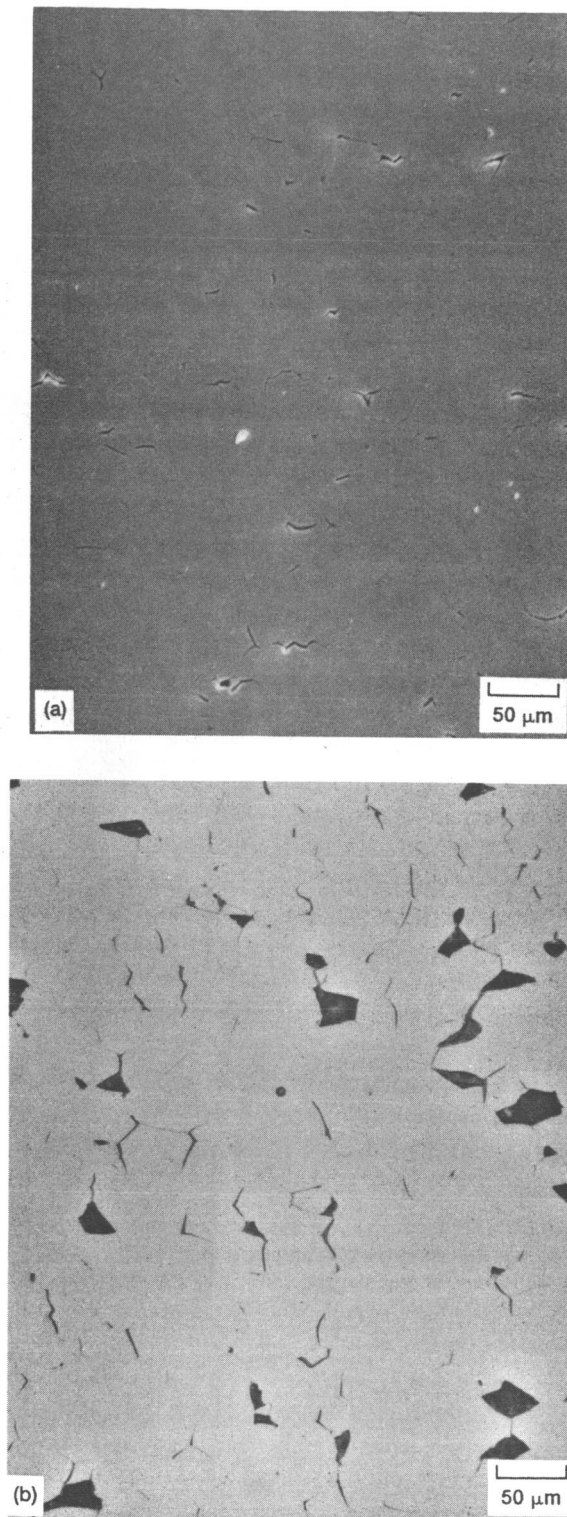
Figure 27.—Longitudinal sections of NiAl compression speci-
mens deformed to (a) 5 percent plastic strain and (b) 15 per-
cent plastic strain at room temperature illustrating the for-
mation of grain boundary cracks (ref. 128).
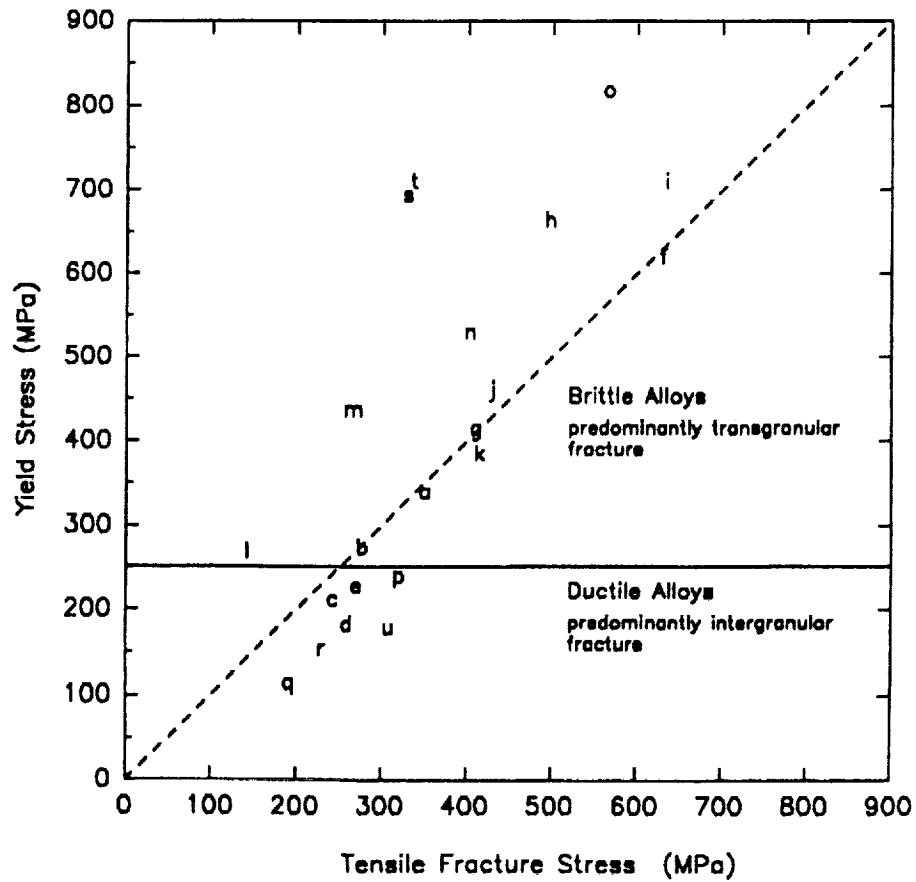
Figure 28.—Yield stress versus tensile fracture stress for a number of different NiAl alloys. From this plot two regions are apparent: a low yield strength region where plasticity precedes fracture and failure is mainly intergranular and a high yield strength region where all alloys fail in a brittle transgranular manner (ref. 250). A detailed legend for all alloys presented in this plot is summarized in Table V.
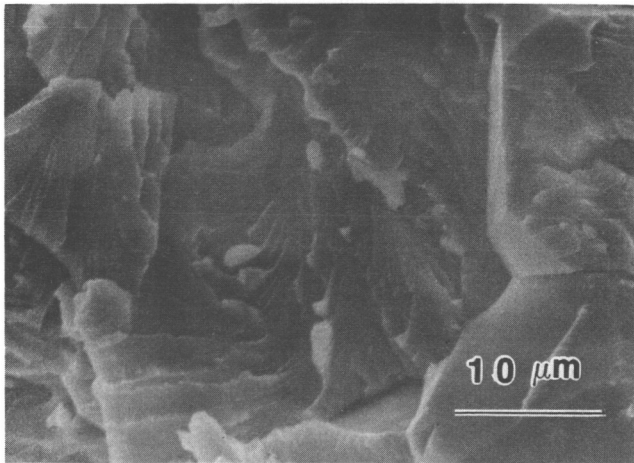
(a) Ni-42Al.
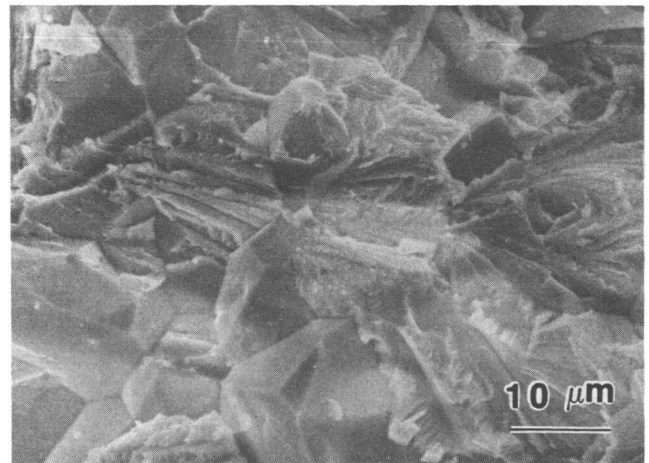
(b) Ni-45Al.
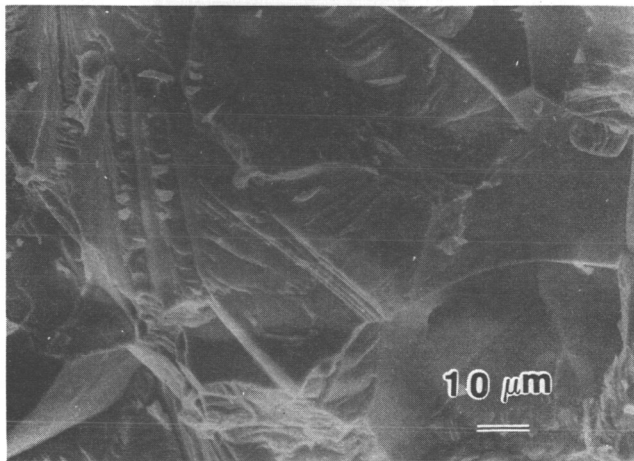
(c) Ni-48Al.
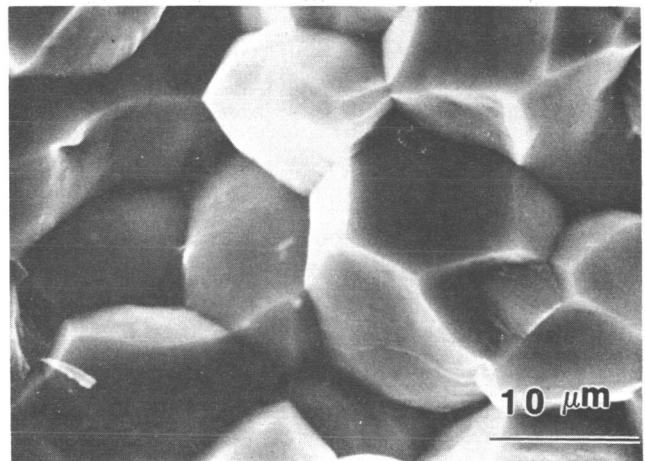
(d) Ni-50Al.

Figure 29.—Fracture behavior of NiAl as a function of stoichiometry. The fracture mode is predominantly transgrandular except for the stoichiometric alloy. (Figure courtesy of P. Nagpal and I. Baker).

101
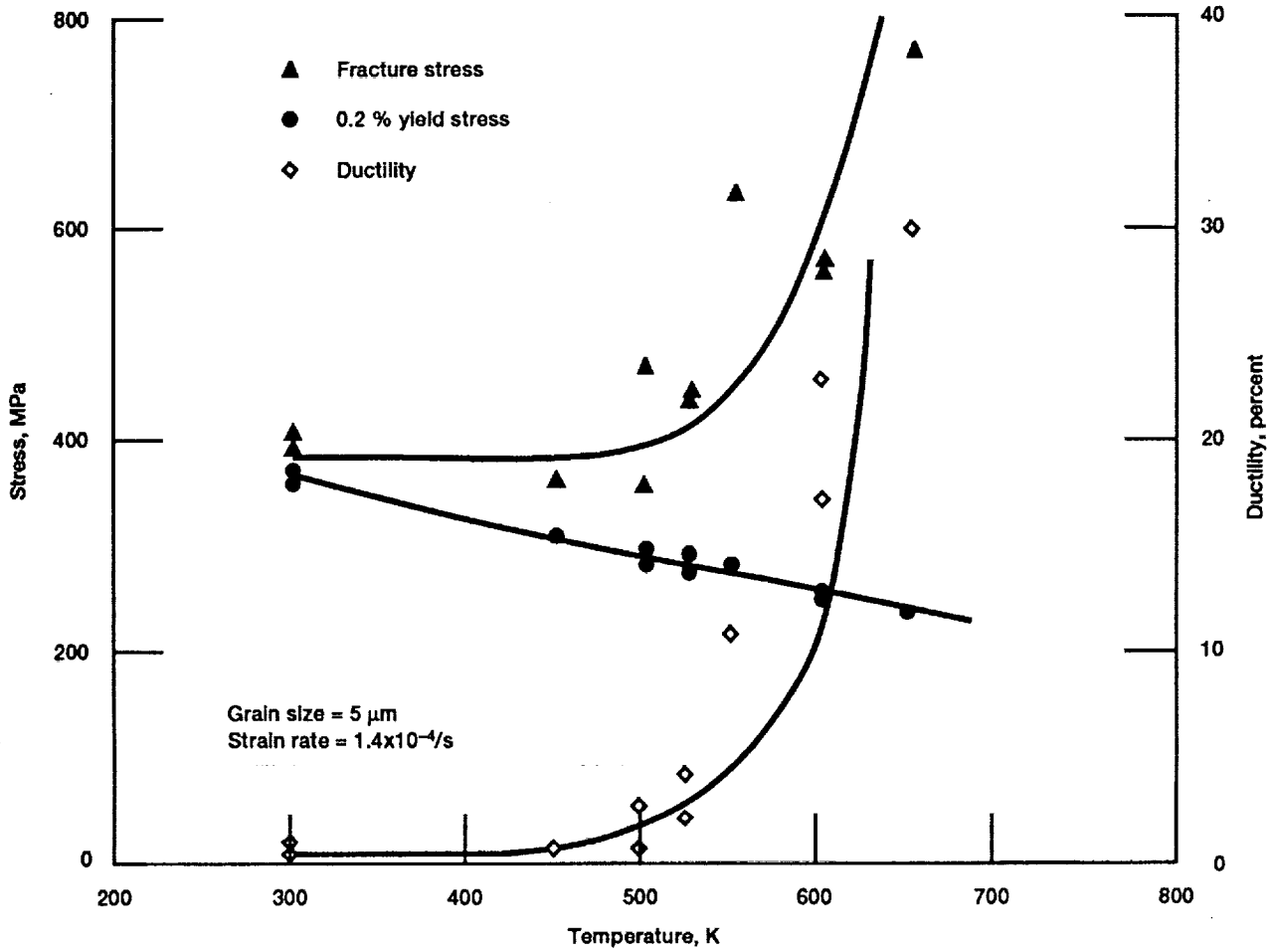
Figure 30.—The effect of temperature on the tensile properties of power extruded NiAl (ref. 215).
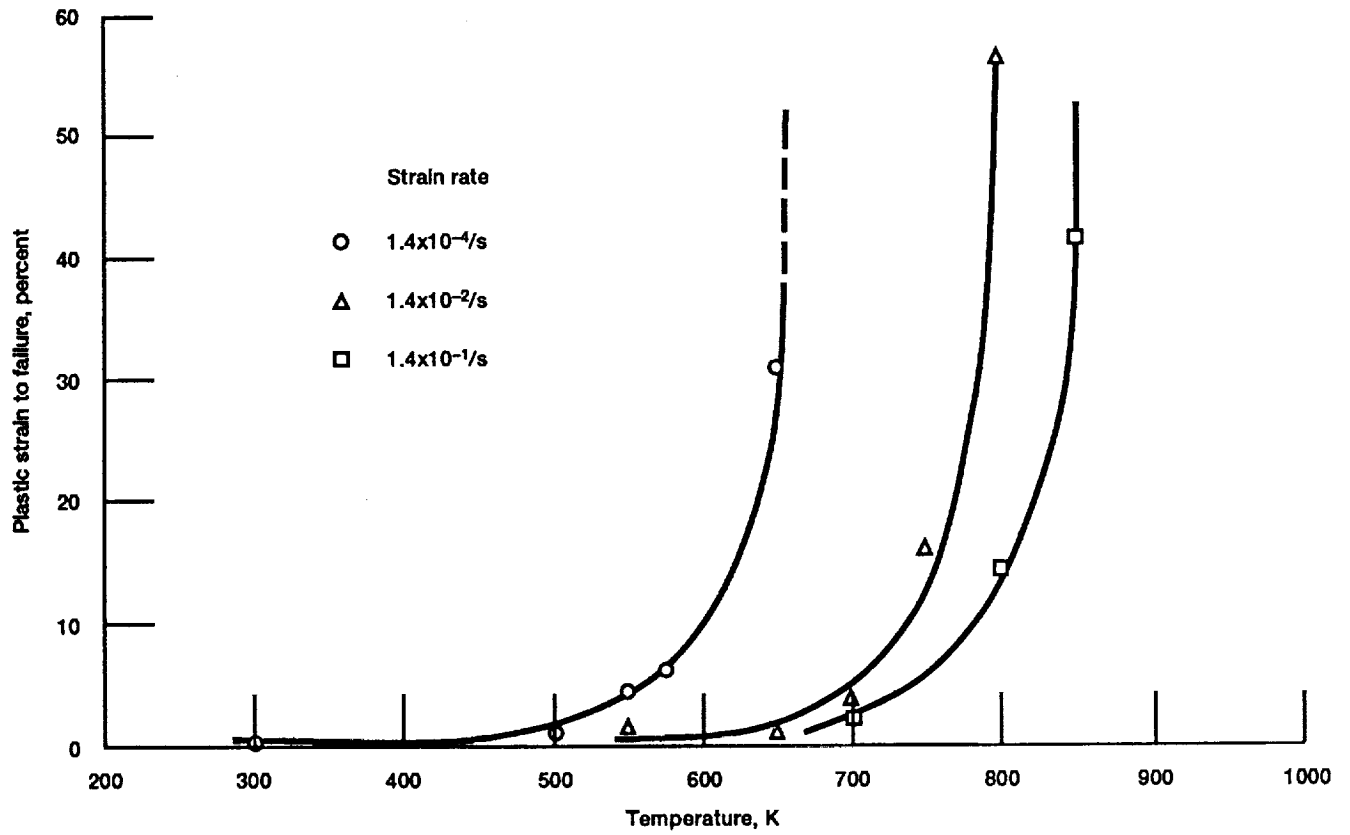
Figure 31.—The effect of strain rate on the tensile ductility and BDTT of cast and extruded NiAl (ref. 233).
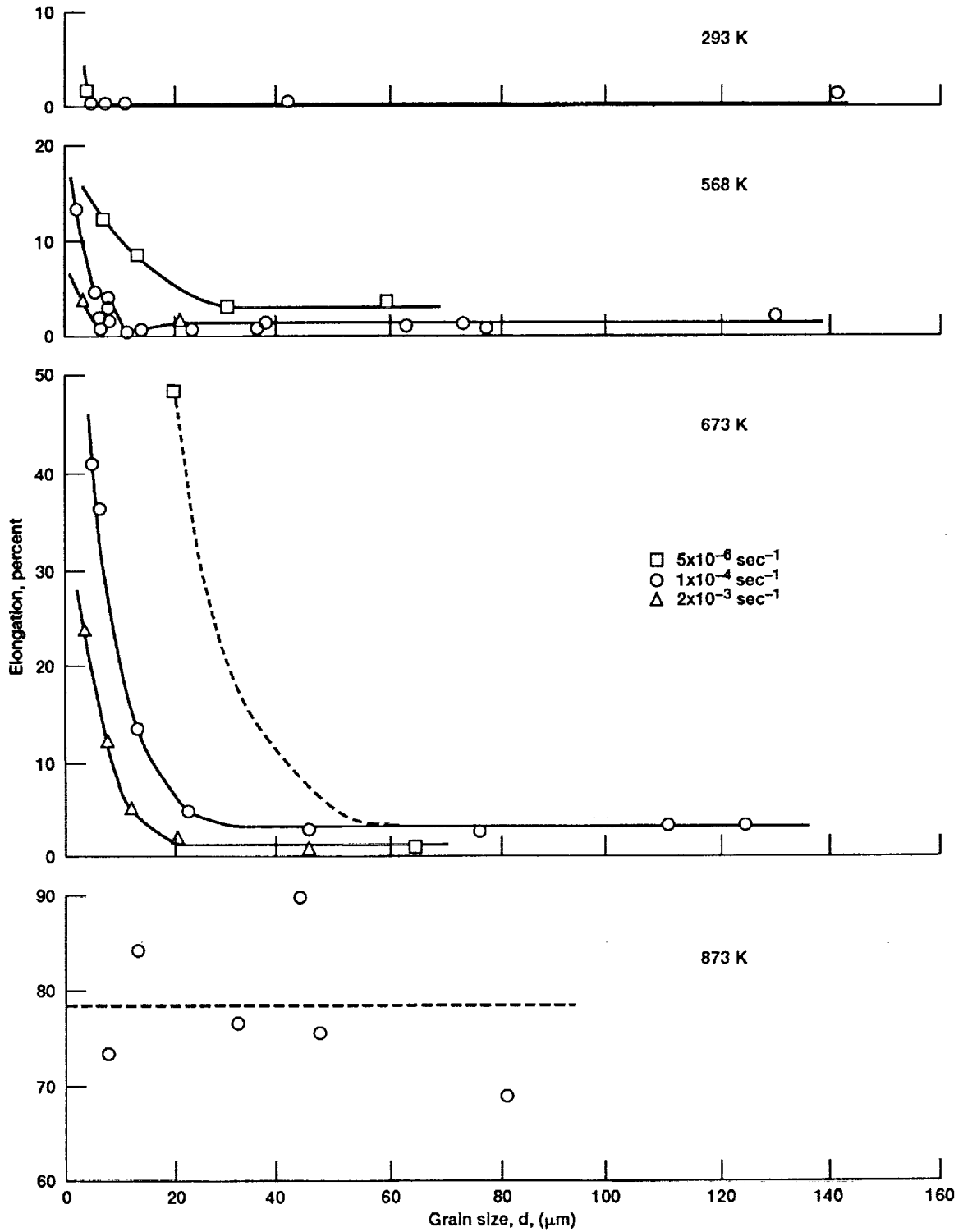
Figure 32.—Tensile elongation versus grain size for Ni-49Al at temperatures from 293 K to 873 K and strain rates from 5×10^{-6}/s to 2×10^{-3}/s (ref. 236).
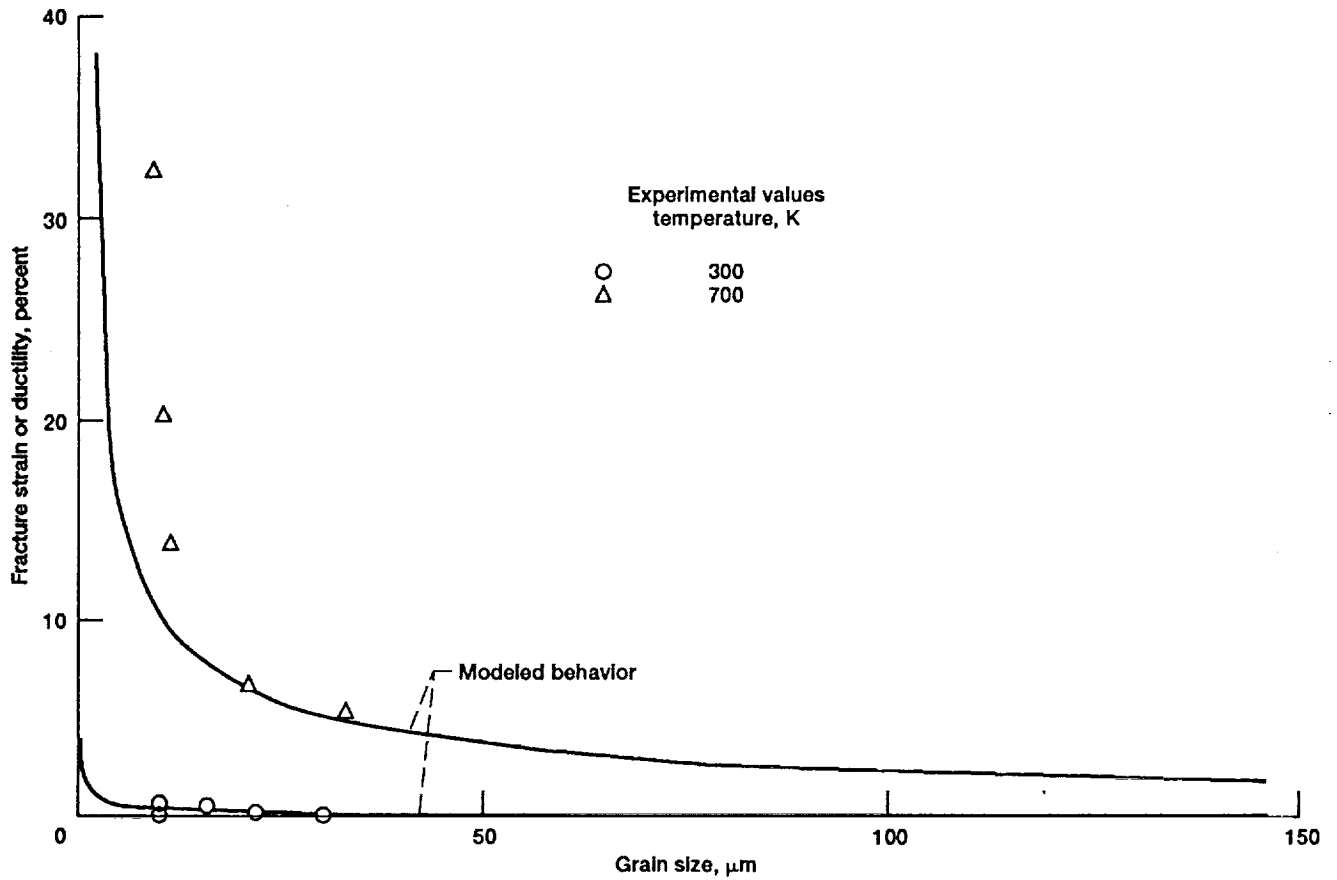
Figure 33.—Chan's model (ref. 258) for predicting tensile ductility of semibrittle materials as a function of grain size verified for NiAl (ref. 215). The figure shows experimental and theoretical ductility as a function of grain size for the alloy described in Table VIII.
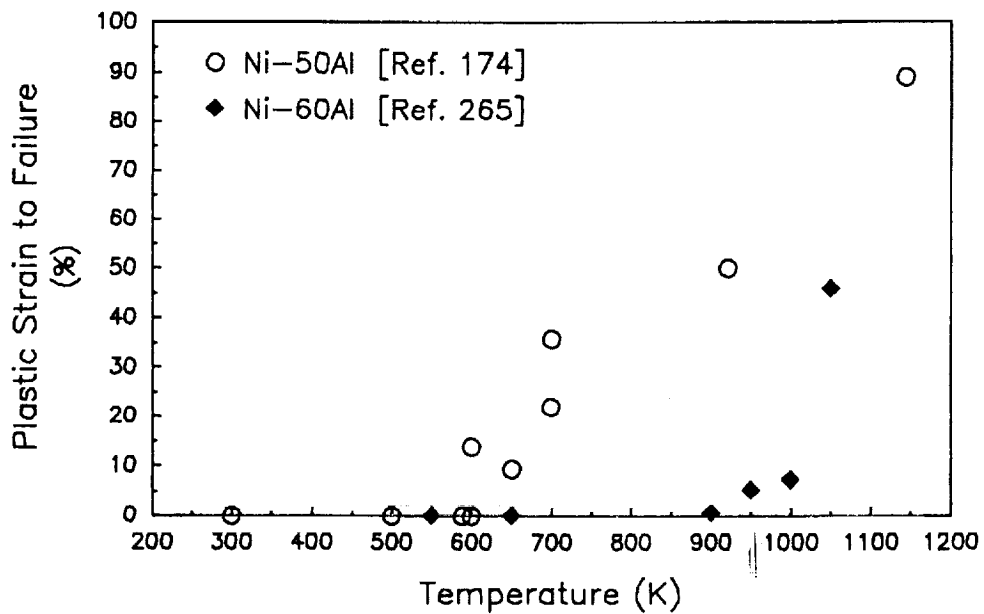
Figure 34.—Tensile ductility of [001] oriented Ni-50Al and Ni-60Al single crystals as a function of temperature.

105
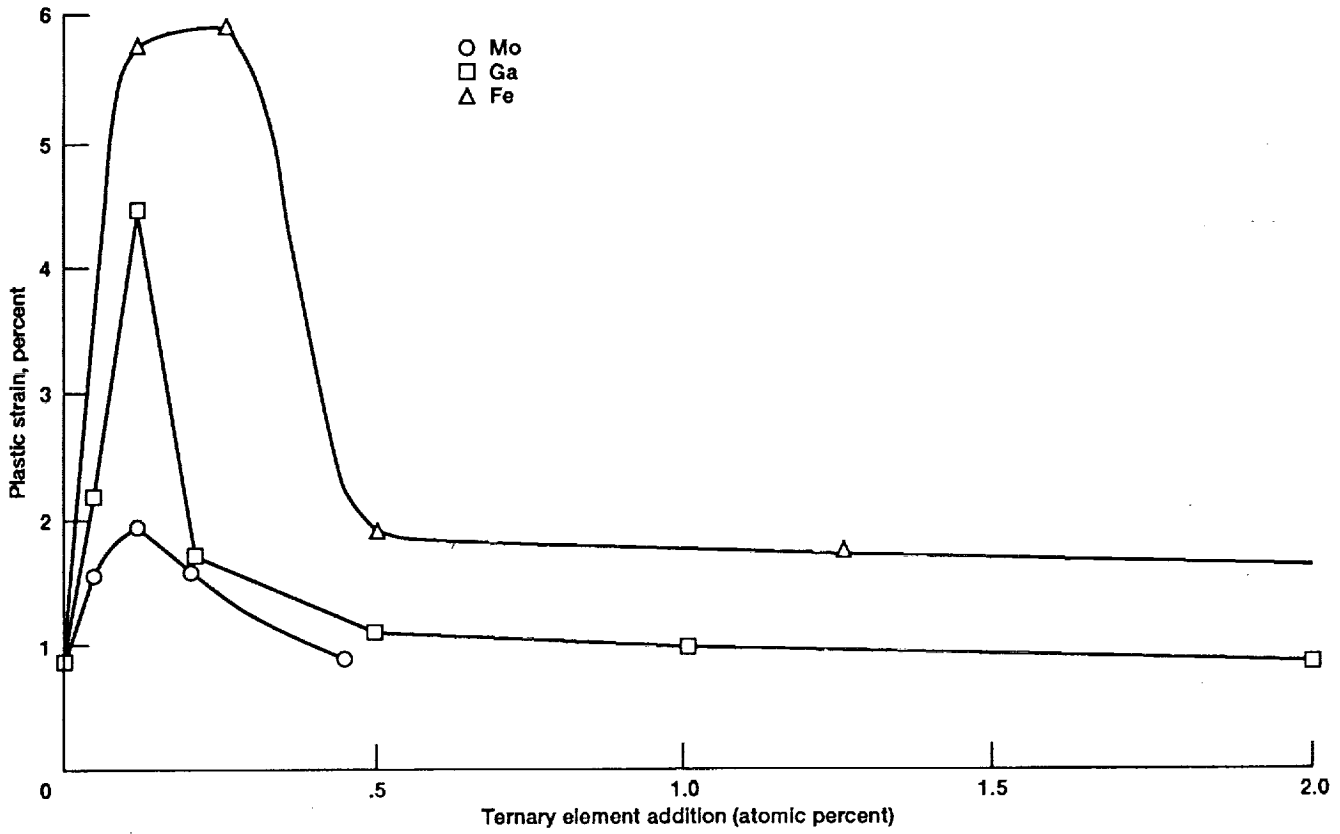
Figure 35.—Room temperature tensile ductility of <110> single crystal NiAl with microalloying additions of iron, gallium or molybdenum (ref. 62).
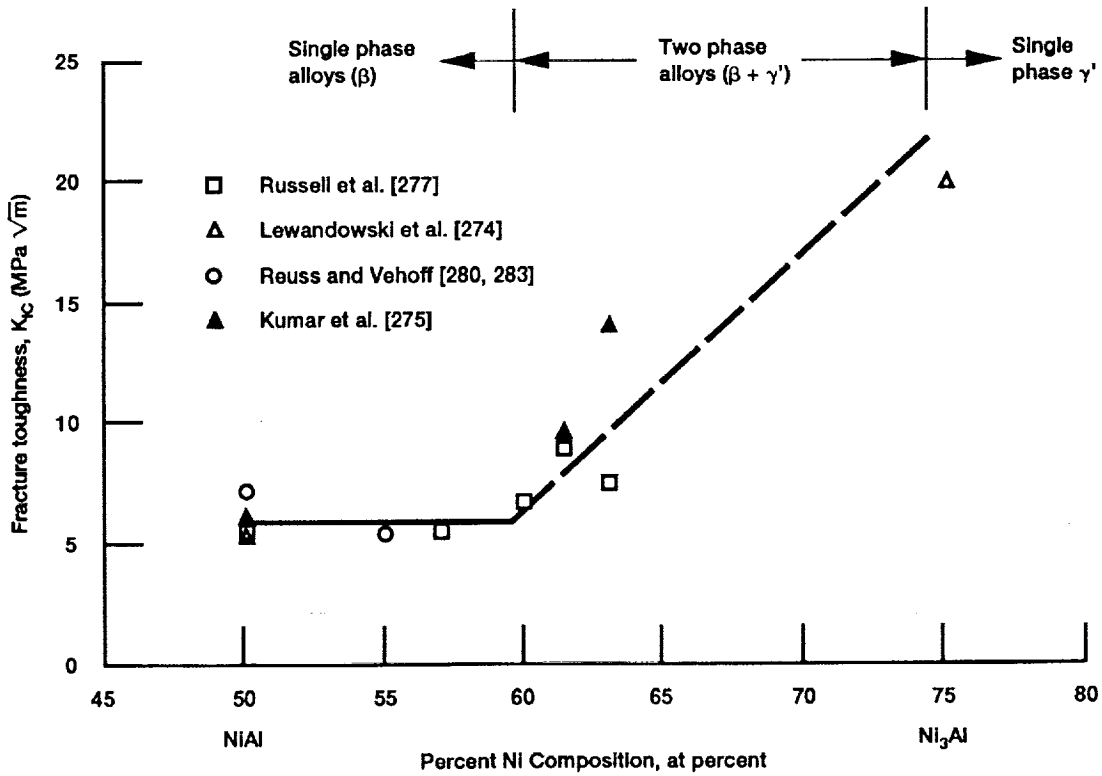
Figure 36.—Room temperature fracture toughness of NiAl alloys as a function of stoichiometry. An increase in toughness occurs as the percentage of γ' increases in the two phase β + γ' alloys.
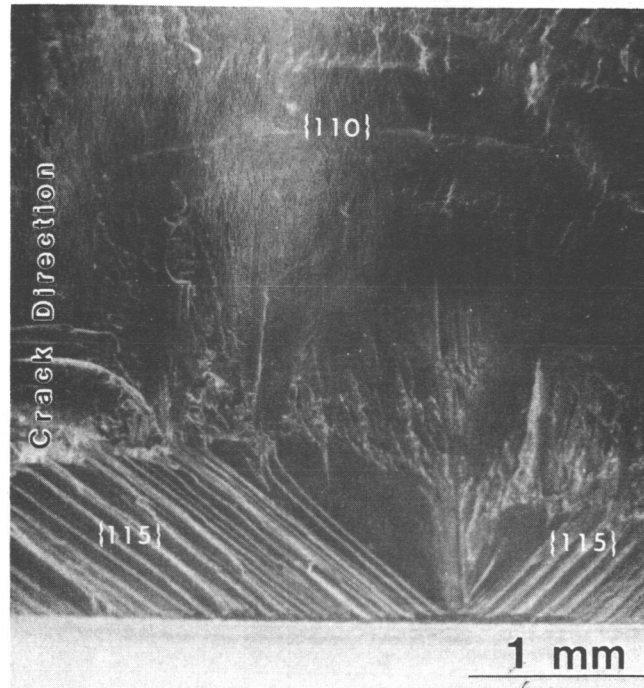
Figure 37.—Cleavage on transient fracture planes such as {115} or {117} occurs prior to final cleavage on {110} planes in single crystal NiAl. (Photo courtesy of R. Darolia, G. E. Aircraft Engines.)
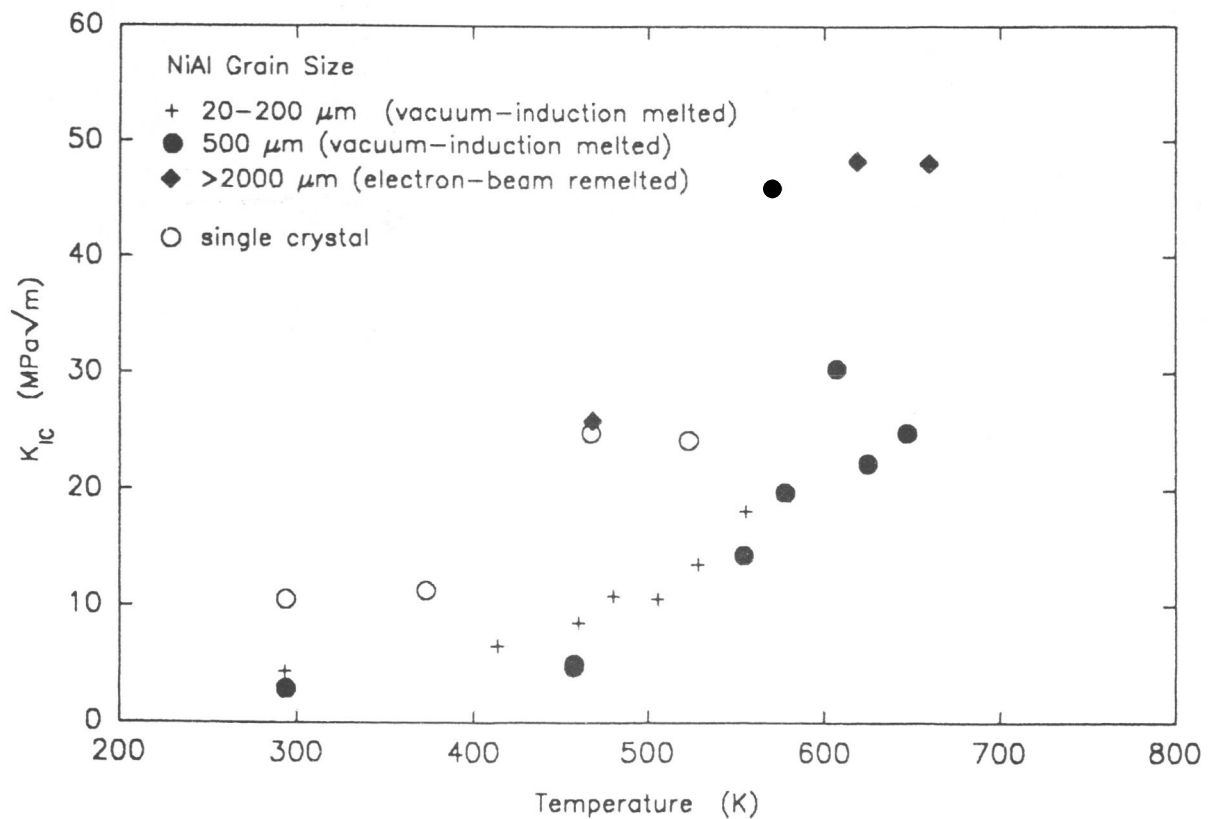
Figure 38.—Fracture toughness of NiAl alloys as a function of temperature. Alloys were produced by several different techniques resulting in material with a range of grain sizes (ref. 283).
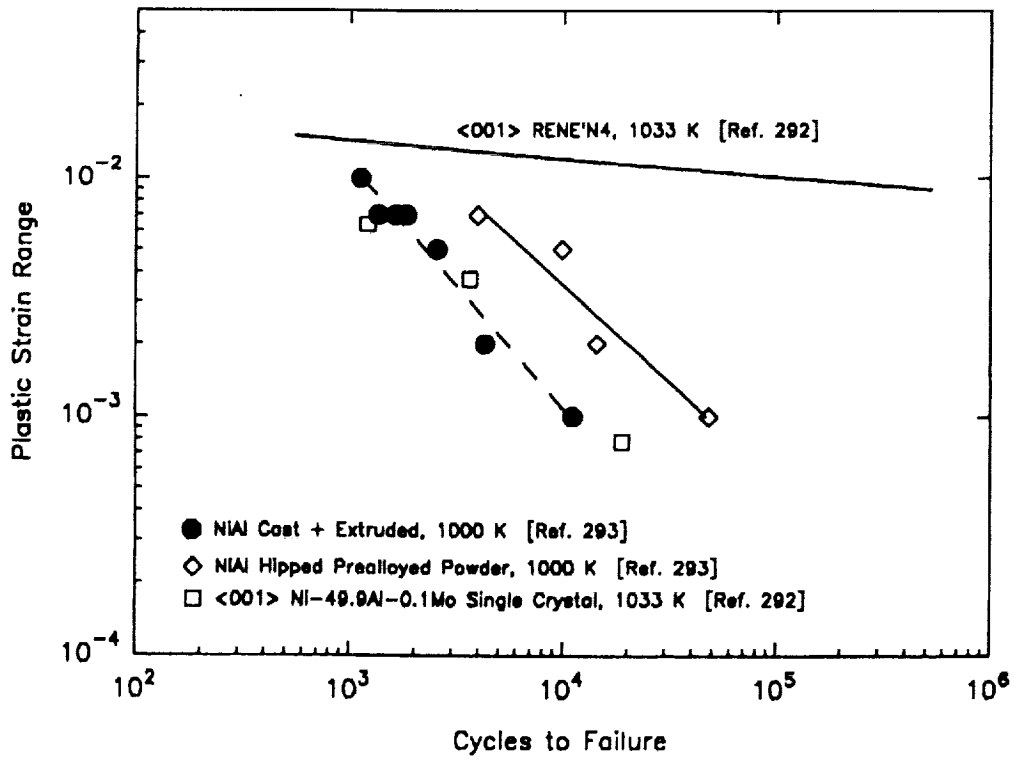
Figure 39.—The effect of processing conditions on the elevated temperature, low cycle fatigue lives of NiAl.
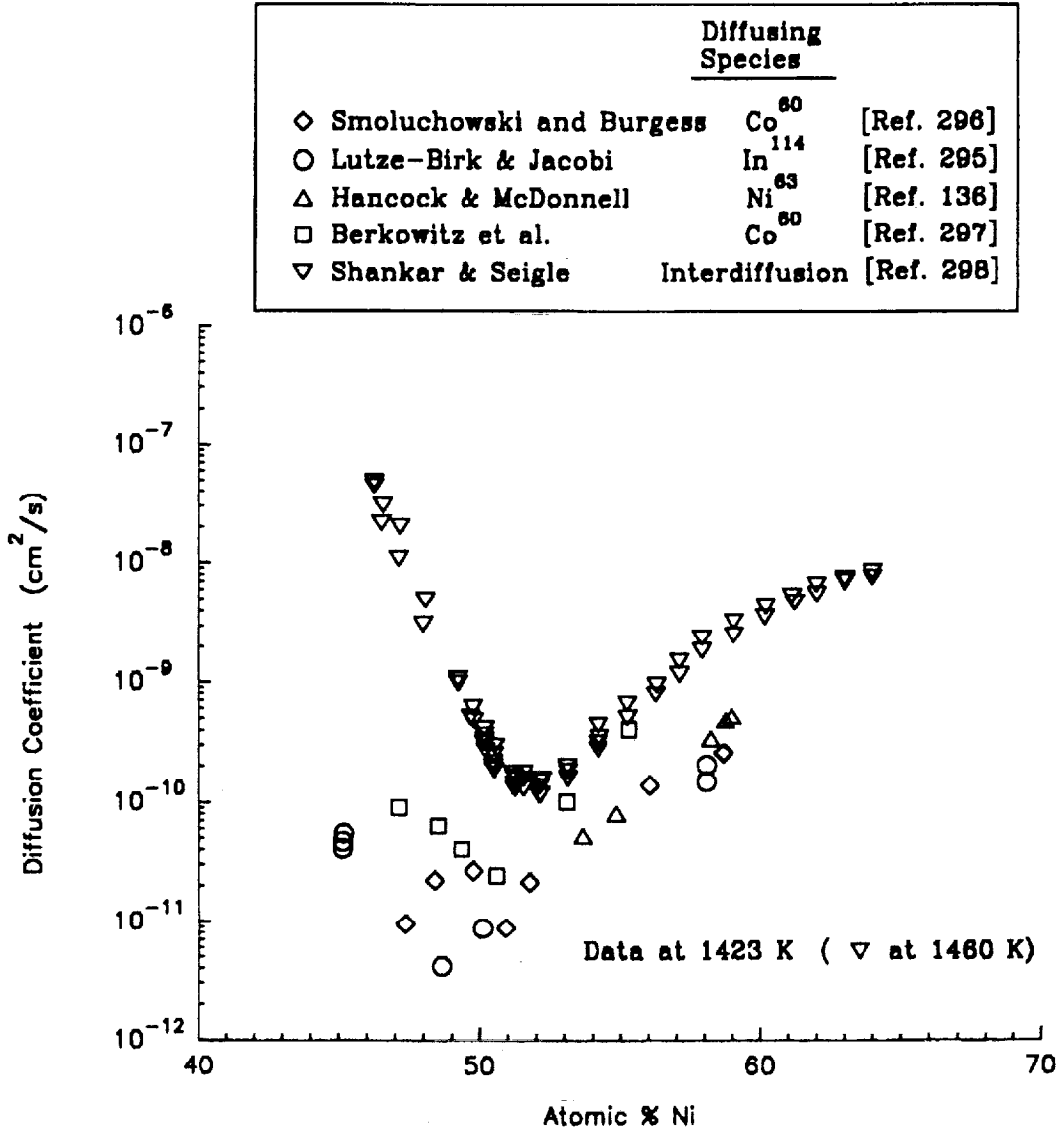
Figure 40.—Compilation of diffusion coefficients as a function of Ni content for single phase NiAl alloys at 1423 K.
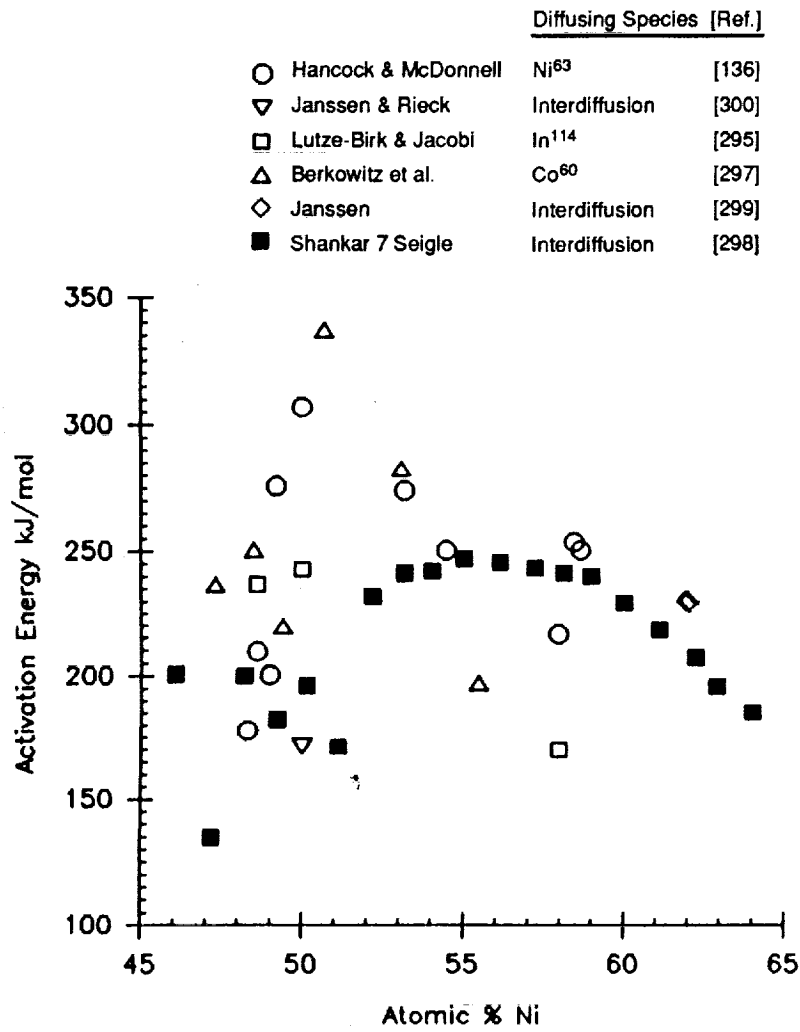
Figure 41.—The activation energy for diffusion of various species in NiAl as a function of stoichiometry.
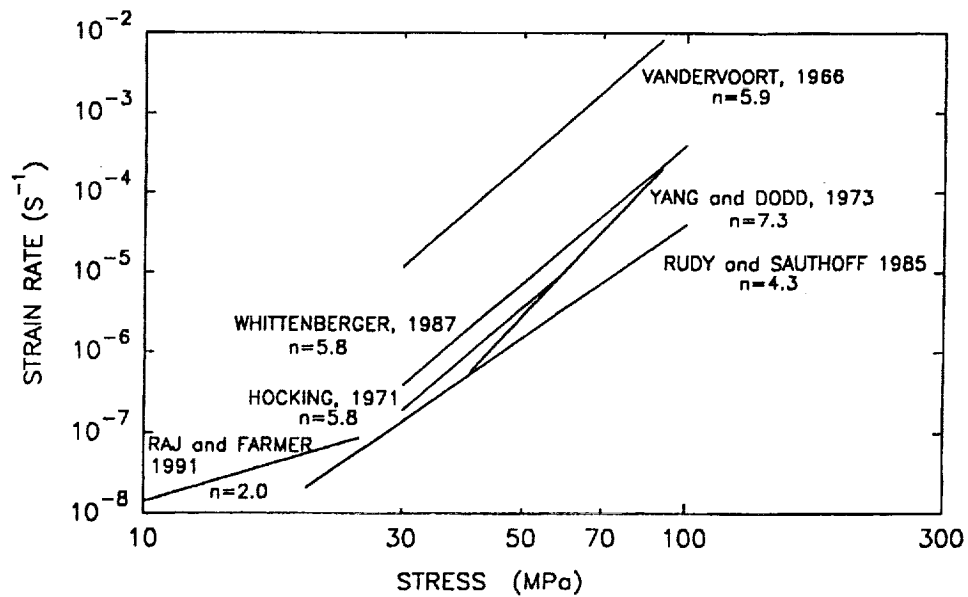
Figure 42.—Creep behavior of stoichiometric NiAl at 1175 K (refs. 235, 317, 319-321, 323).

110
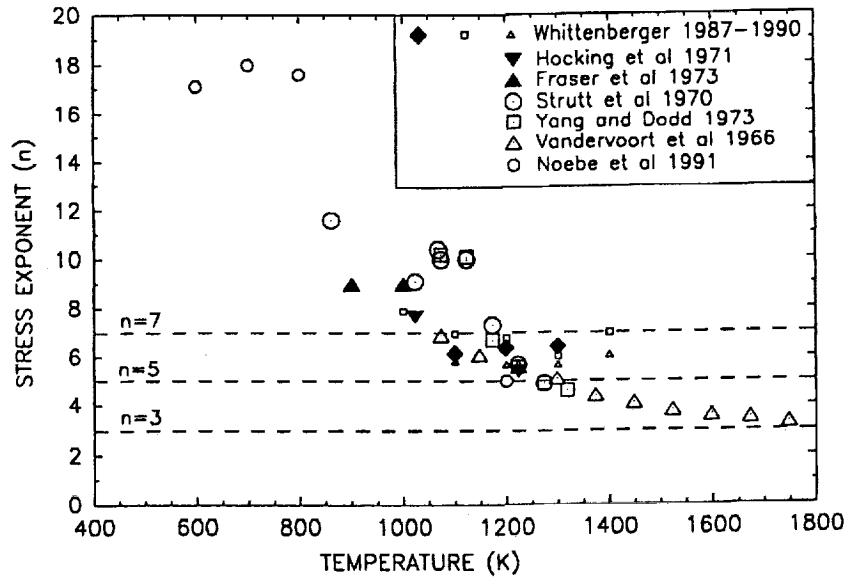
Figure 43.—The relationship between stress exponent and temperature for near stoichiometric NiAl as compiled from numerous studies (refs. 166, 170, 235, 316-319, 321, 322).
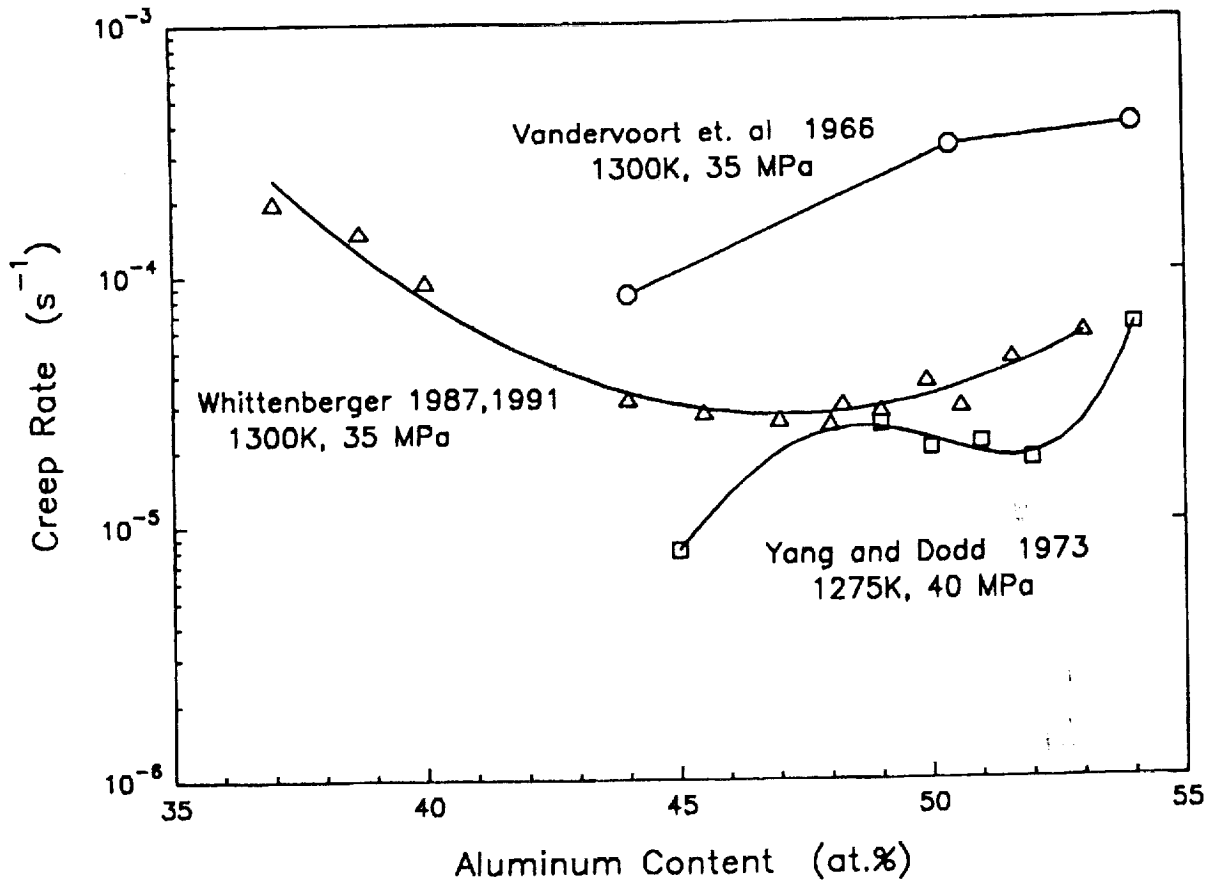
Figure 44.—The effect of stoichiometry on the compressive creep rate of NiAl (refs. 235, 317, 319, 327).
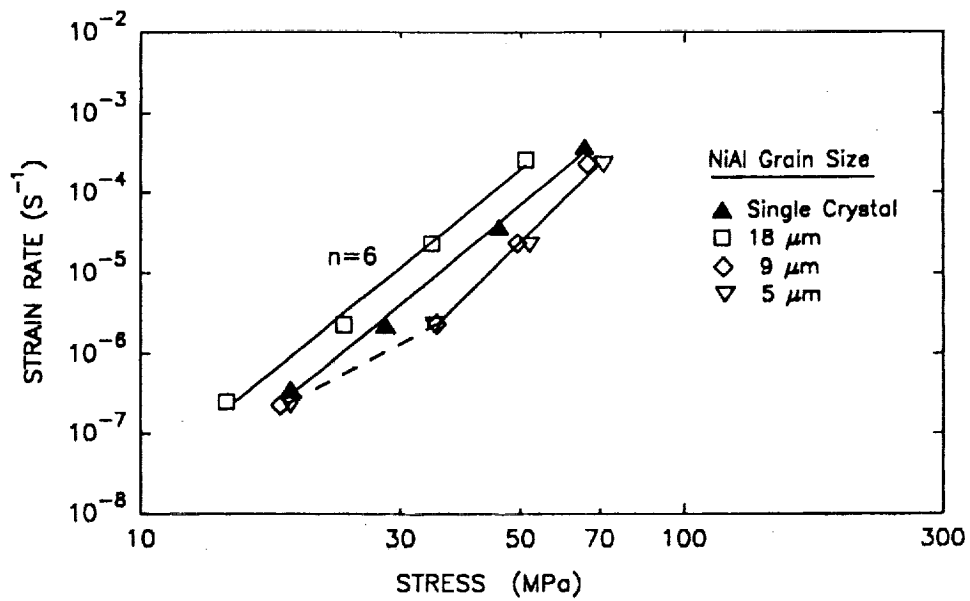
Figure 45.—The influence of grain size on the compressive creep strength of NiAl at 1300 K (refs. 316, 322).
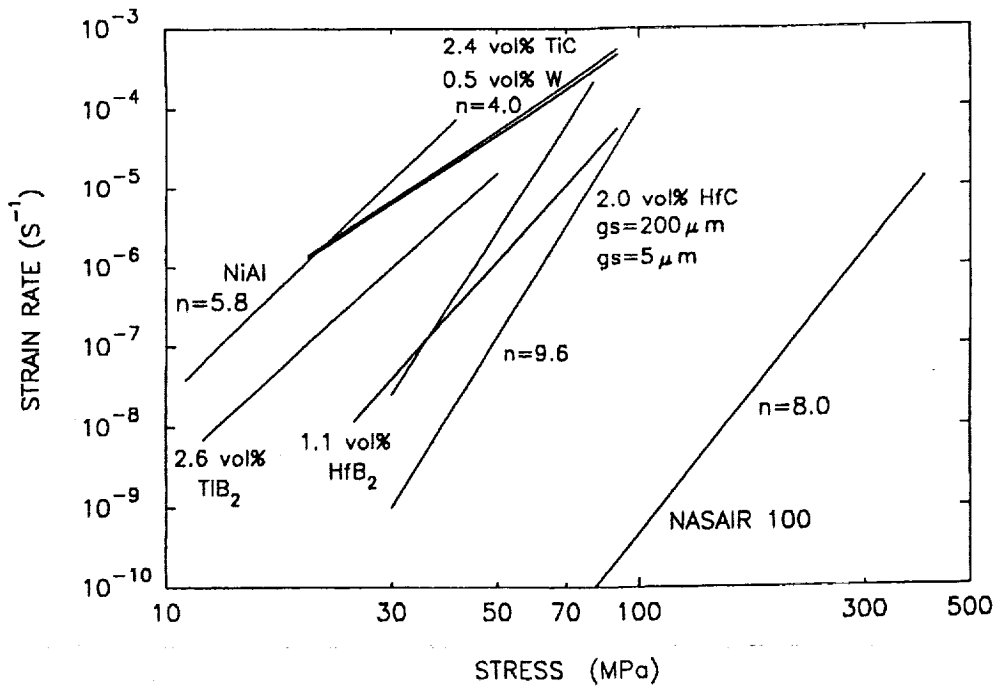
Figure 46.—Solid solution hardening of polycrystalline NiAl at 1200 K (refs. 317, 320, 322, 329, 330-332).
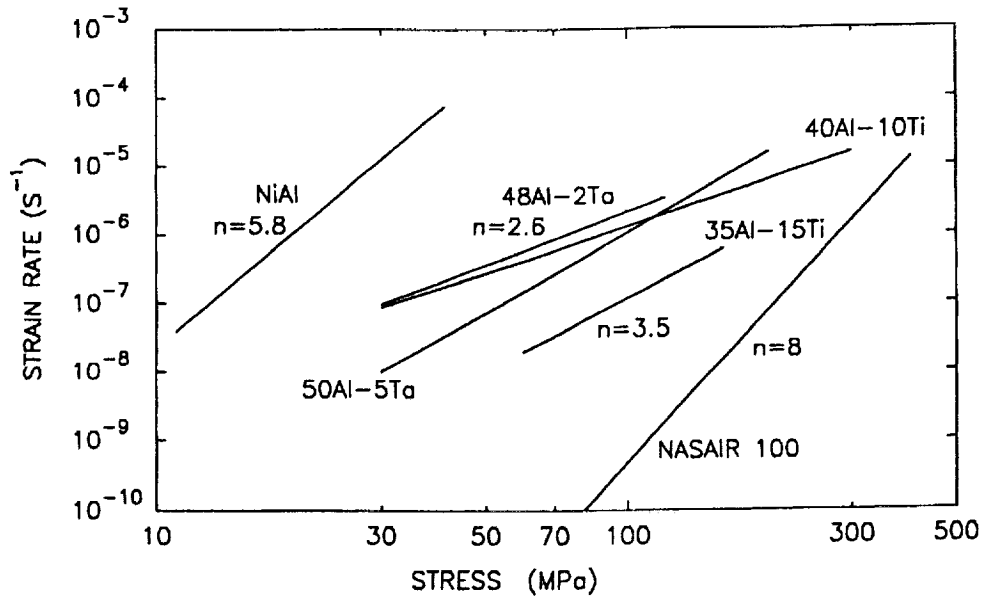
Figure 47.—Precipitation hardening by Heusler and Laves phases by the addition of Ti and Ta to NiAl (refs. 317, 330-332, 334).
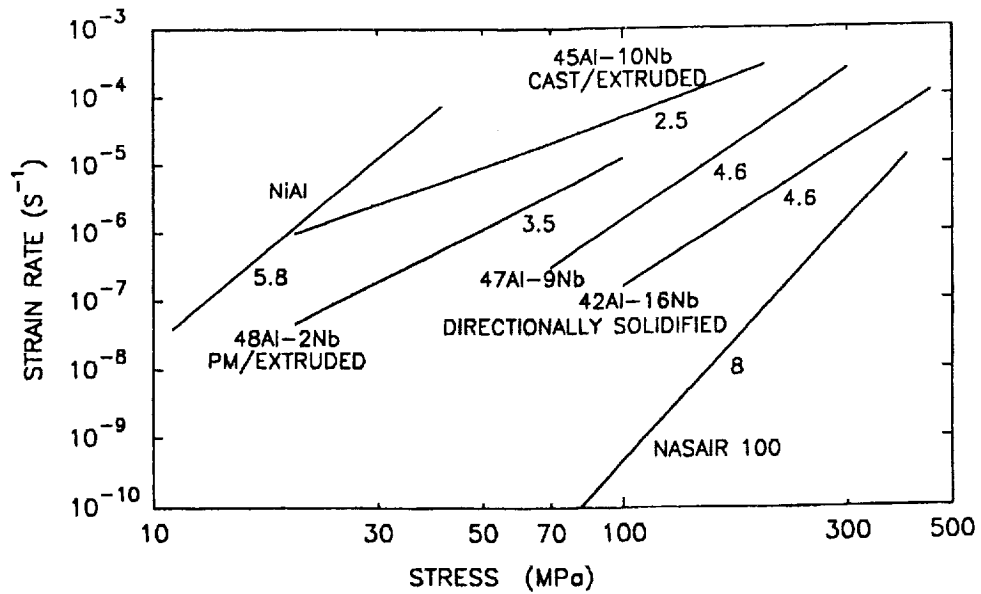
Figure 48.—Creep strengthening of NiAl by the NiAlNb Laves phase at 1300 K (refs. 317, 330, 332, 335, 336).
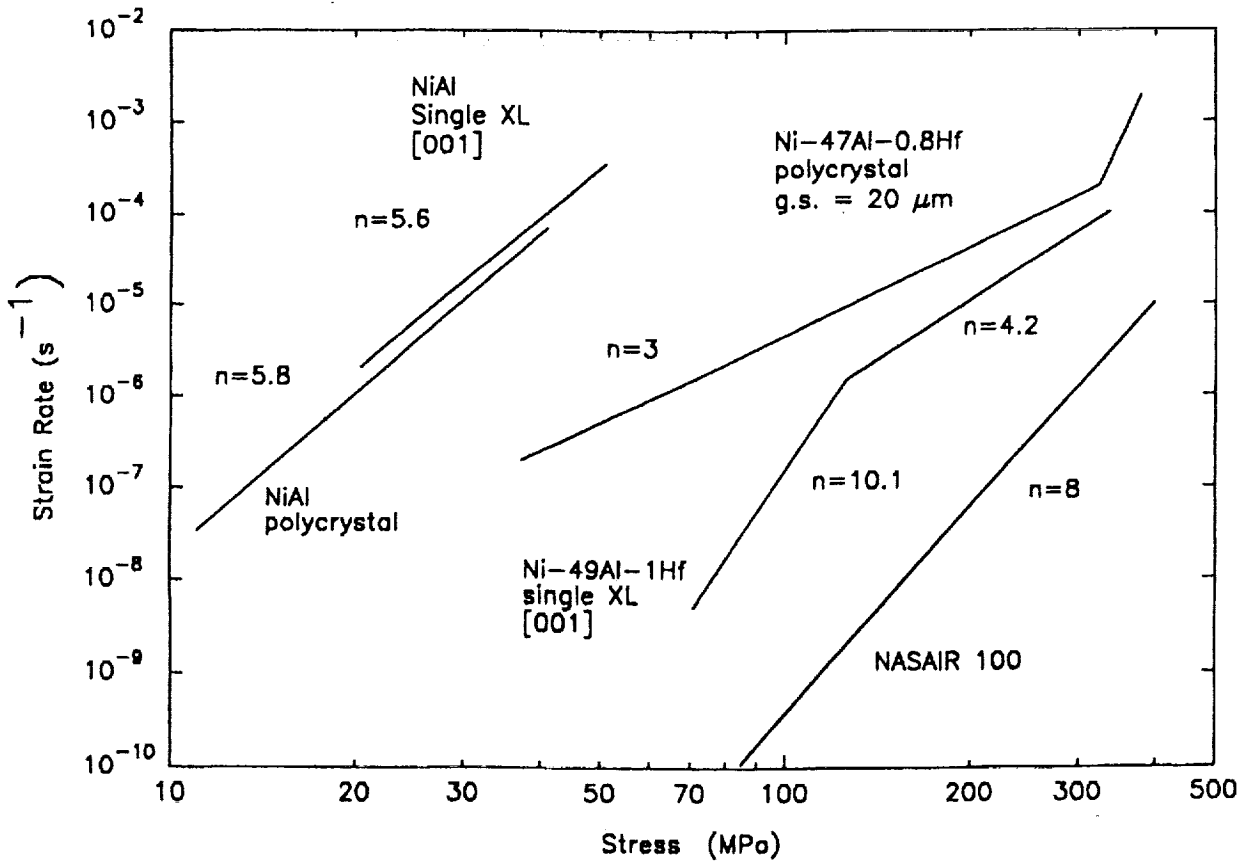
Figure 49.—A comparison of the creep response of NiAl +1Hf in both polycrystalline and single crystal form at 1300 K (refs. 317, 330, 337, 338).
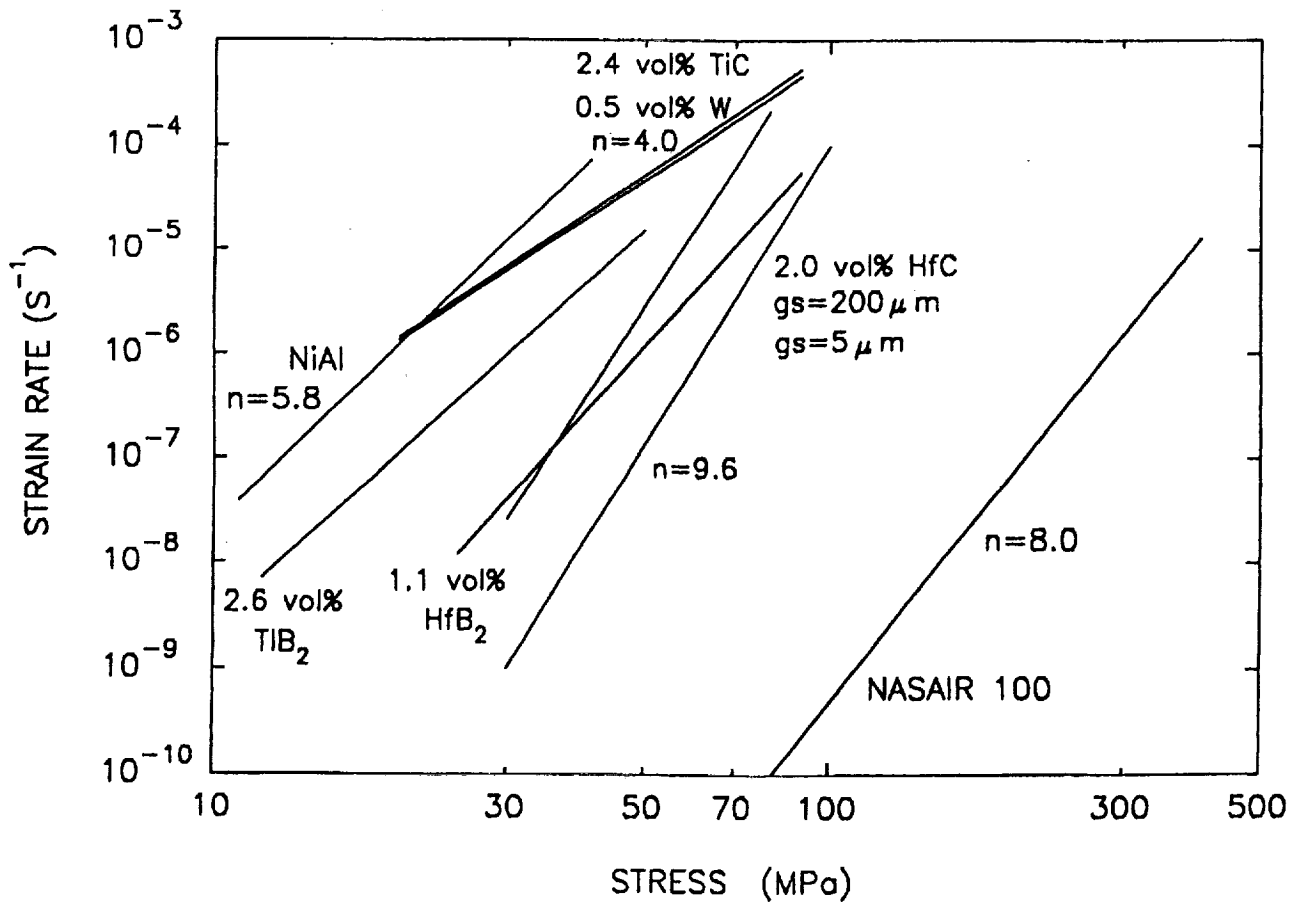
Figure 50.—The effect of dispersoids formed by rapid solidification on the 1300 K Creep strength of NiAl (refs. 310, 317, 330, 342-344).
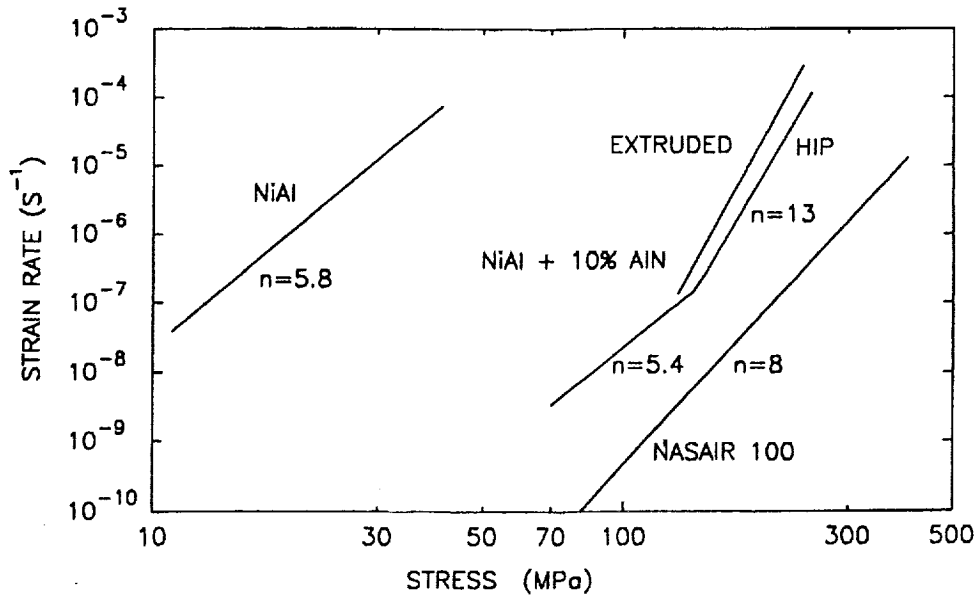
Figure 51.—The effect of AlN particles formed by reaction milling on the compressive creep strength of NiAl at 1300 K (refs. 317, 330, 347, 348).
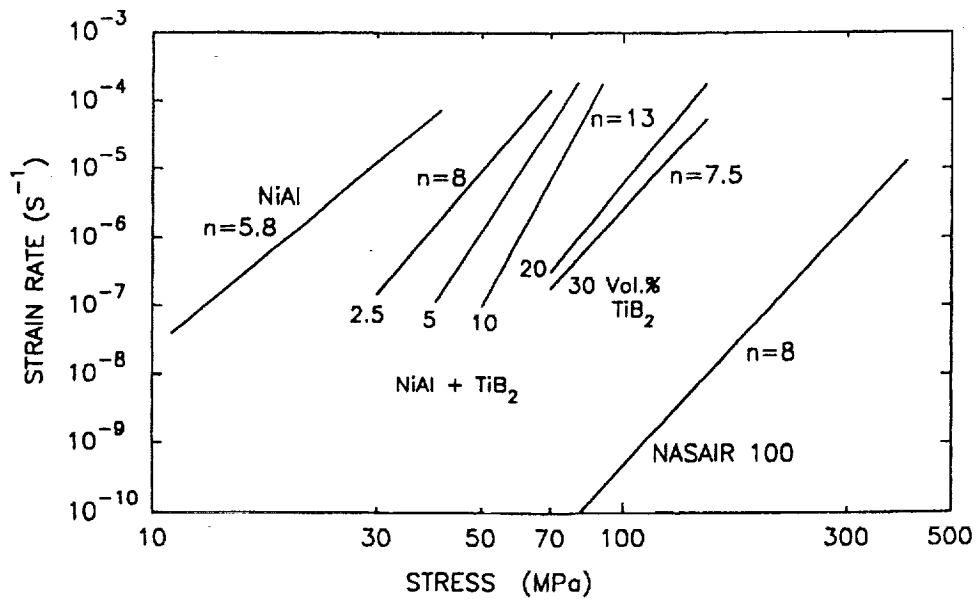
Figure 52.—Effect of TiB_2 particles added to NiAl by XD^{TM} processing on the 1300 K compressive creep strength of NiAl (refs. 317, 318, 330).
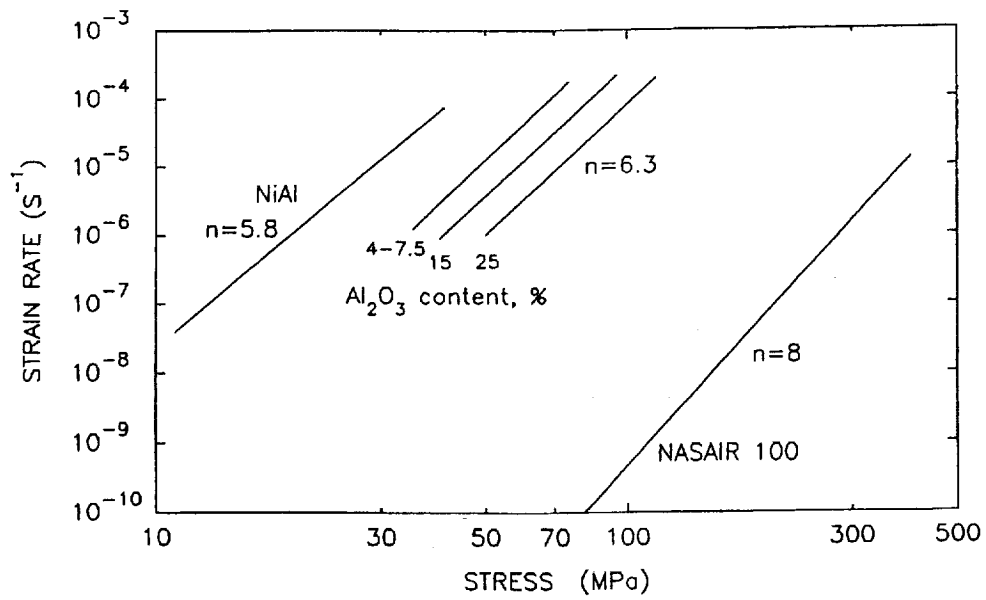
Figure 53.—The effect of Al_2O_3 whiskers added to NiAl by a powder blending process on the 1300 K compressive creep strength of NiAl (refs. 317, 330, 354).
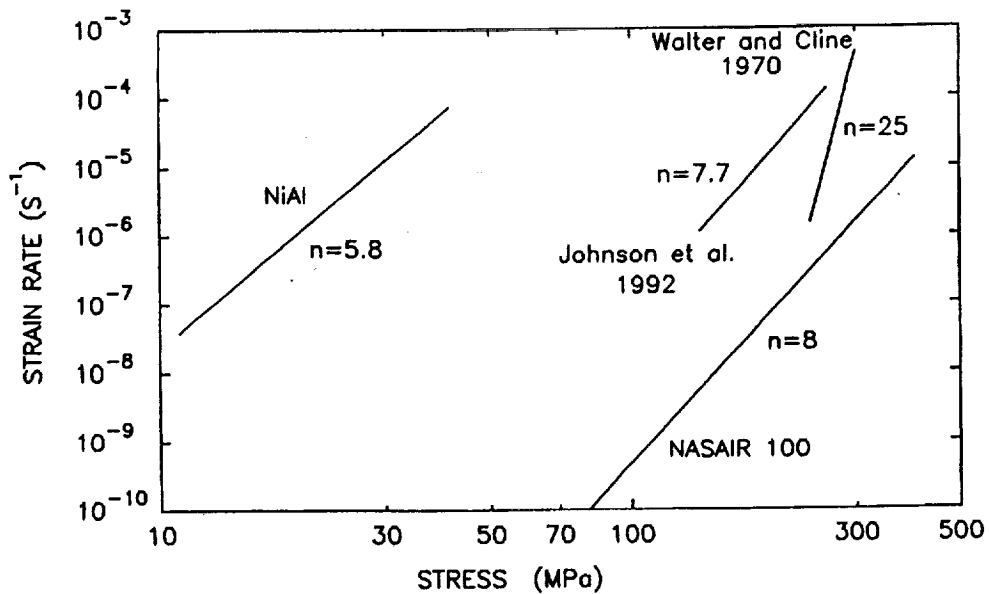

Figure 54.— Creep strength of directionally solidified NiAl-34 at.% Cr Eutectic at 1300 K (refs. 317, 330, 359, 360).
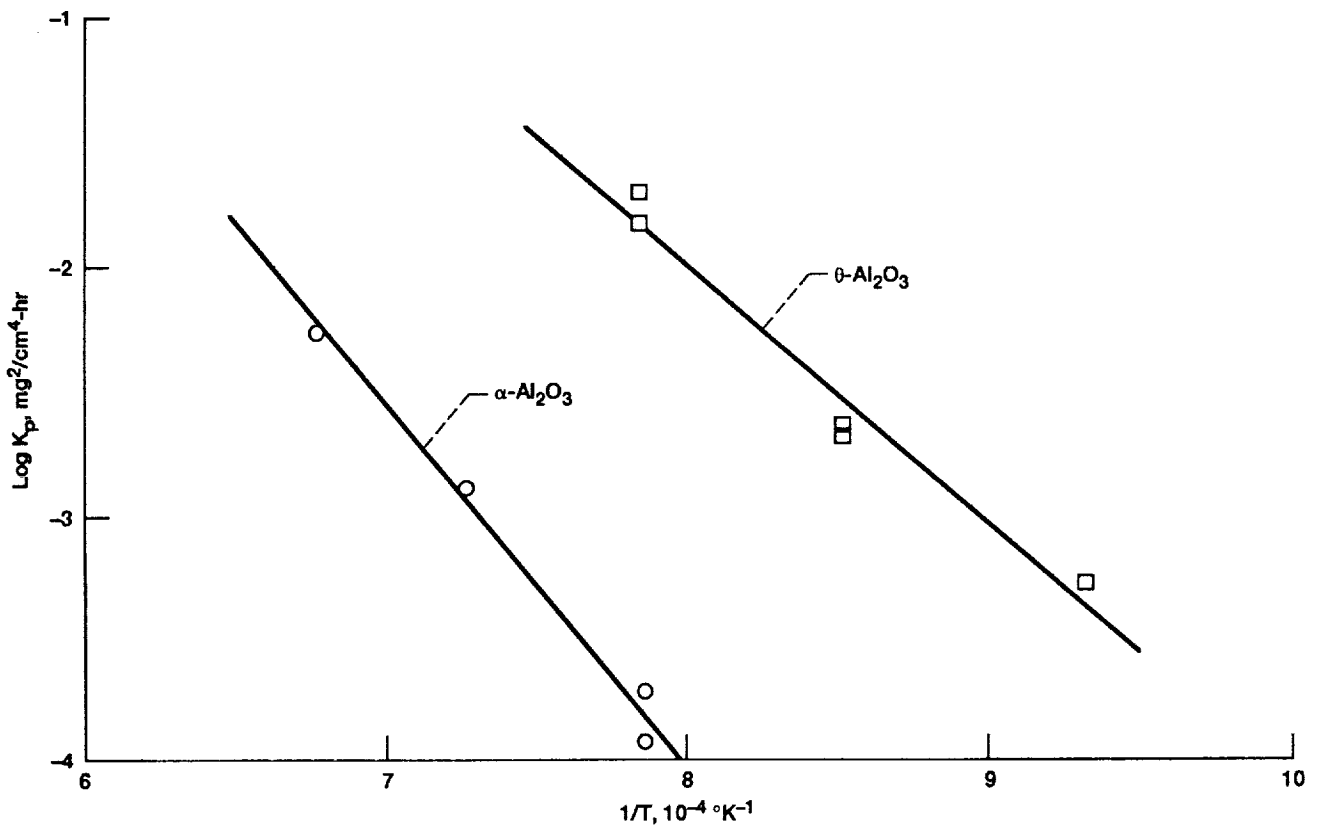
Figure 55.—Arrhenius plot of the growth rate constant, k_p, for transition θ-Al_2O_3 scales and mature α-Al_2O_3 scales formed on Zr-doped NiAl (ref. 373).

118
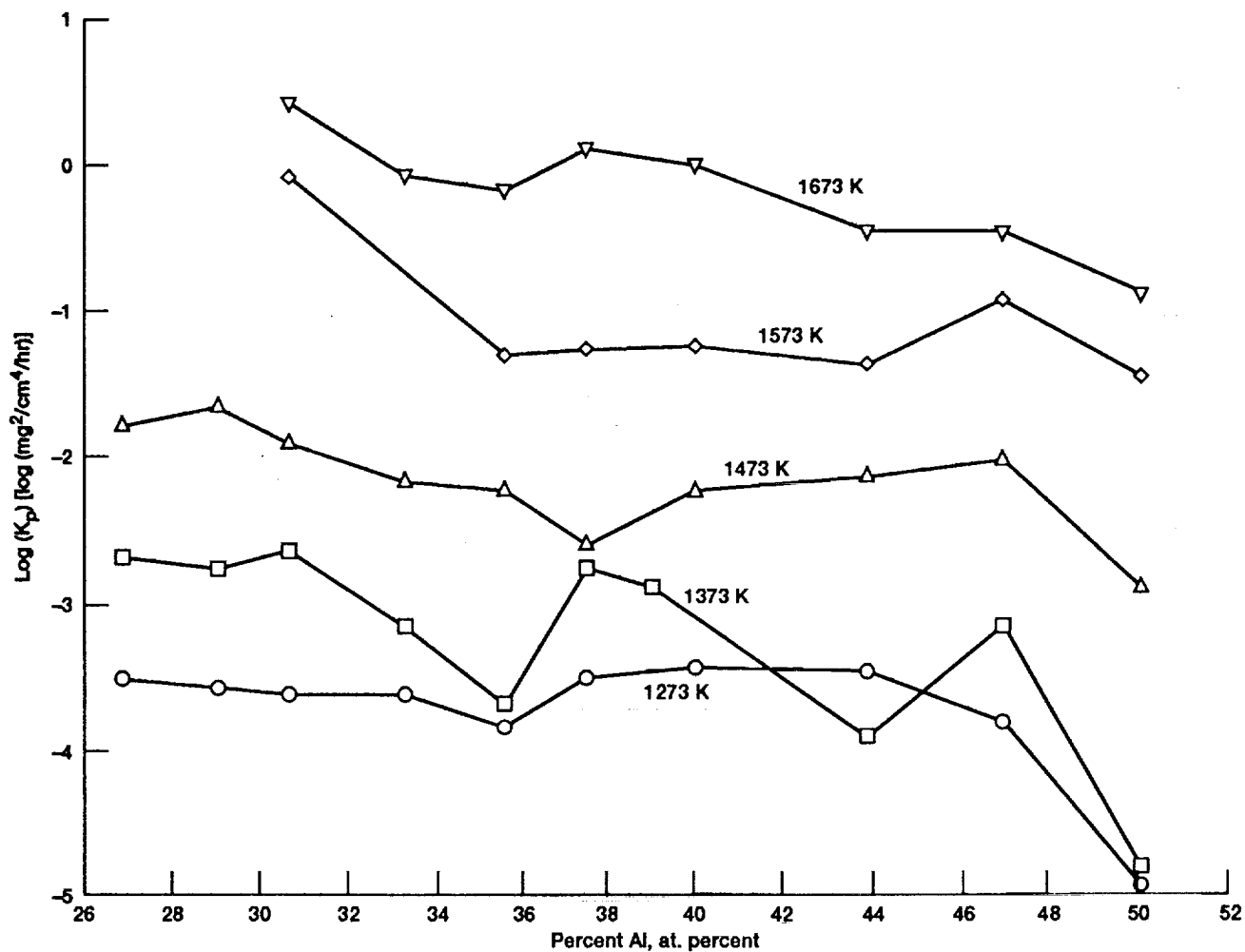
Figure 56.—Parabolic growth rate constants as a function of aluminum content for NiAl oxidized at 1273 to 1673 K (ref. 380).

119
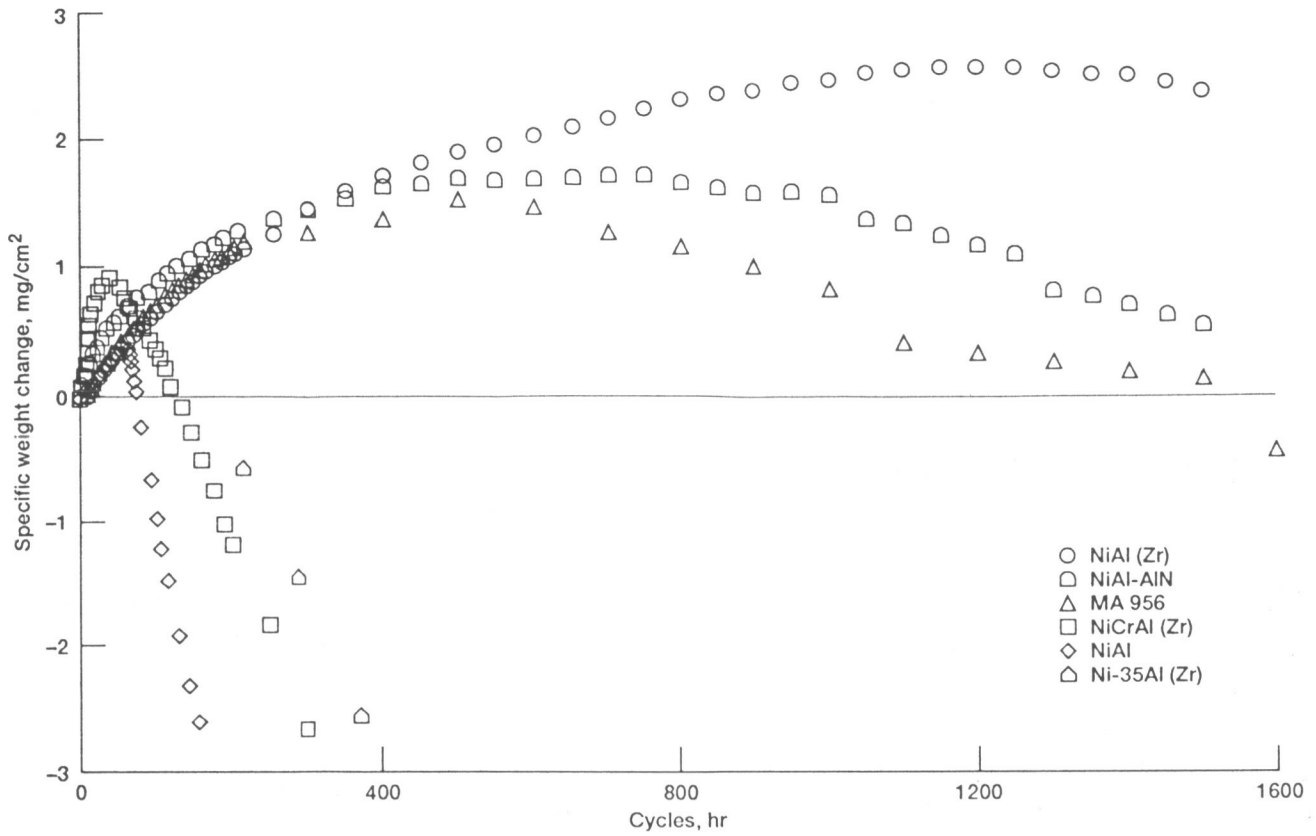
Figure 57.—The cyclic oxidation behavior of NiAl (Zr), cryomilled NiAl-AlN composites, NiAl, Ni-35Al (Zr), MA956 and NiCrAl (Zr). One hour cycles at 1473 K. (After Lowell et al. ref. 351).
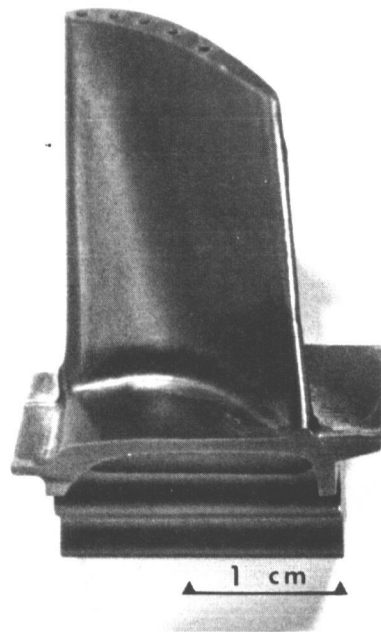

Figure 58.—A high pressure turbine blade machined from a single crystal NiAl ingot. (Photo courtesy of R. Darolia, G. E. Aircraft Engines.)

REPORT DOCUMENTATION PAGE

Form Approved
OMB No. 0704-0188

Public reporting burden for this collection of information is estimated to average 1 hour per response, including the time for reviewing instructions, searching existing data sources, gathering and maintaining the data needed, and completing and reviewing the collection of information. Send comments regarding this burden estimate or any other aspect of this collection of information, including suggestions for reducing this burden, to Washington Headquarters Services, Directorate for Information Operations and Reports, 1215 Jefferson Davis Highway, Suite 1204, Arlington, VA 22202-4302, and to the Office of Management and Budget, Paperwork Reduction Project (0704-0188), Washington, DC 20503.

1. AGENCY USE ONLY (Leave blank)	2. REPORT DATE	3. REPORT TYPE AND DATES COVERED
	April 1992	Technical Memorandum

4. TITLE AND SUBTITLE

Review of the Physical and Mechanical Properties and Potential Applications of the B2 Compound NiAl

(Unabridged Version of a Paper Published in International Materials Review)

5. FUNDING NUMBERS

WU–505–63–5A

6. AUTHOR(S)

Ronald D. Noebe, Randy R. Bowman, and Michael V. Nathal

7. PERFORMING ORGANIZATION NAME(S) AND ADDRESS(ES)

National Aeronautics and Space Administration
Lewis Research Center
Cleveland, Ohio 44135–3191

8. PERFORMING ORGANIZATION REPORT NUMBER

E–6925

9. SPONSORING/MONITORING AGENCY NAMES(S) AND ADDRESS(ES)

National Aeronautics and Space Administration
Washington, D.C. 20546–0001

10. SPONSORING/MONITORING AGENCY REPORT NUMBER

NASA TM–105598

11. SUPPLEMENTARY NOTES

Responsible person, Ronald D. Noebe, (216) 433–2093.

12a. DISTRIBUTION/AVAILABILITY STATEMENT

Unclassified - Unlimited
Subject Category 26

12b. DISTRIBUTION CODE

13. ABSTRACT (Maximum 200 words)

Considerable work has been performed on NiAl over the last three decades, with an extremely rapid growth in research on this intermetallic occurring in the last few years due to recent interest in this material for electronic and high temperature structural applications. However, many physical properties and the controlling fracture and deformation mechanisms over certain temperature regimes are still in question. Part of this problem lies in the incomplete characterization of many of the alloys previously investigated. Fragmentary data on processing conditions, chemistry, microstructure and the apparent difficulty in accurately measuring composition has made direct comparison between individual studies sometimes tenuous. Therefore, the purpose of this review is to summarize all available mechanical and pertinent physical properties on NiAl, stressing the most recent investigations, in an attempt to understand the behavior of NiAl and its alloys over a broad temperature range.

14. SUBJECT TERMS

Aluminides; Mechanical properties; Physical properties; Ni-Al nickel aluminide

15. NUMBER OF PAGES

120

16. PRICE CODE

A06

17. SECURITY CLASSIFICATION OF REPORT	18. SECURITY CLASSIFICATION OF THIS PAGE	19. SECURITY CLASSIFICATION OF ABSTRACT	20. LIMITATION OF ABSTRACT
Unclassified	Unclassified	Unclassified	